DISSERTATION

A contribution to the critical assessment of methodological prerequisites of atom-atom pair distribution function analysis

submitted by

Philipp Hans

performed at

X-Ray Center of TU Wien

supervised by

Klaudia Hradil

Berthold Stöger

Getreidemarkt 9, 1060 Wien, Österreich

Vienna, July 2018

Referees:

Reinhard B. Neder
(Friedrich-Alexander-Universität Erlangen-Nürnberg)

Matteo Leoni
(Università degli Studi di Trento)

20.08.2018
date

student's signature

Short description

Standard crystallographic approaches to structure solution rely on *periodicity* and in consequence *infinite extension*. If a material is structurally so strongly uncorrelated that the standard crystallographic methods fail, the *nano structure problem* arises. This is true for "nano-structured" materials such as crystalline nano-particles and amorphous structures. Up to now, despite intense research, no single agreed-on approach to solve the nano structure problem has been brought forward. The approaches range from atomistic simulations over various techniques of microscopy to the investigation of the atom pair distribution function (PDF) - which recently is experiencing an ever increasing publicity - and a combination of those approaches. A PDF is obtained by sine-Fourier transformation from corrected total scattering data of powders and contains information on all atom-to-atom distances in a material.

A big part of this work is dedicated to the critical assessment of experimental practices for gaining PDFs from total scattering data, i.e. data handling, data correction or detector image integration procedures. Furthermore, an examination of the capabilities of PDF analysis on materials with use in sustainable energy applications was performed. The first material is amorphous SiO_2 doped with TiO_2. Its intended application is technical catalysis of organic reactions. Simulations show a restructuring of the SiO_2 matrix around embedded TiO_2 particles. The other material is Si nano particles for anode materials in lithium ion batteries. A comparison of real and reciprocal space Rietveld refinements was performed and a procedure for the quantification of amorphous contents is provided.

Kurzbeschreibung

Die Standardmethoden der Kristallographie beruhen auf der Annahme einer *Periodizität* des atomaren Aufbaus des Materials und damit einhergehend dessen *unendlicher Ausdehnung*. In nano-strukturierten Materialien, wie Nanoteilchen oder amorphen Festkörpern, sind diese Voraussetzungen nicht erfüllt, weswegen das *Nanostrukturproblem* auftritt. In der Fachliteratur existiert kein einheitlicher Ansatz zur Lösung dieses Nanostrukturproblems. Von Stuktursimulationen über Mikroskopie bis zur Analyse der (Atom)paarverteilungsfunktion (PDF, engl.: pair distribution function), welcher in jüngerer Zeit eine zunehmende Bekanntheit zuteil wird. Es scheint unerlässlich zu sein, eine Kombination all dieser verfügbaren Verfahren zur Strukturfindung einzusetzen. - Eine PDF wird mittels Sinus-Fourier-Transformation aus Gesamtröntgenstreuungsdaten (total X-ray scattering data) gewonnen. Eine ideale PDF enthält Informationen über alle Atom-Atom-Abstände in einem Material.

Ein Teil dieser Dissertation ist der kritischen Untersuchung experimenteller Praktiken, die zum Erhalt einer PDF führen, gewidmet. Einen großen Anteil an der Arbeit ist eine Untersuchung der experimentellen Praktiken die zur PDF führen: Datenverarbeitung, Datenkorrektur und Integration von Detektorbildern. Zudem wurde eine Studie zur Praktikabilität der PDF-Analyse anhand von Besipielen von Materialien für nachhaltige Energieanwendungen angestellt: Ein Material ist amorphes SiO_2, das mit TiO_2 versetzt wurde, für den Einsatz in der technischen Katalyse von organischen Reaktionen. Simulationen zeigen eine Restrukturierung der SiO_2-Matrix um eingebettete TiO_2-Teilchen. Zum anderen wurden Si-Nanoteilchen für Anodenmaterialien in Lithiumionenbatterien untersucht. Im Rahmen der Analysen dieses Materials wurde ein Vergleich von Rietveldverfeinerungen im Realraum und im reziproken Raum angestellt. Außerdem wird eine Prozedur zur Bestimmung von amorphen Anteilen beschrieben.

Table of contents

List of Figures

List of Tables

Nomenclature

$\langle \quad \rangle$		symbol to indicate averaging
$*$		convolution operator
$f(Q)$		atomic form factor of atom i; it is dimensionless
$F(Q)$		The crystallographic structure factor. It is a complex quantity and its modulus is called the structure or scattering amplitude and the expression $\|F(\mathbf{Q})\|^2$ gives the intensity $I(\mathbf{Q})$
$F(Q)$		The reduced an normailsed structure function which is transformed into G(R) by sine-FT. Unfortunately it has he same notation as the crystallographic structure factor, $F(\mathbf{Q})$
FT		Abbreviation for: Fourier transformation
$\mathcal{F}$		Symbol for FT
$\mathcal{F}^{-1}$		Symbol for inverse FT
$\mathcal{F}_{\mathcal{S}}$		Symbol for sine FT
$G(r)$	[Å^{-2}]	PDF, pair distribution function; reduced radial distribution function. $G(r)$ can be seen as a derivative of $R(r)$
$I(Q)$		intensity of the scattered radiation at $\mathbf{Q}$ or Q
$\mathbf{k}_i$	[Å^{-1}]	the wave vector which describes the direction and properties of the incident photons
$\mathbf{k}_o$	[Å^{-1}]	the wave vector which describes the direction and properties of the scattered photons

λ	[Å]	wavelenght of the applied radiation
$P(\mathbf{r})$ or $P(r)$	[Å^{-1}]	density-density or auto-correlation function; it is also called (3D)Patterson function; it contains all interatomic vectors $\mathbf{r}$ or r but they are shifted to the origin of the Patterson map
$p(\mathbf{x})$	[Å^{-1}]	total distribution of atoms throughout the sample
Q_{broad}	$[r^{-1}]$	parameter asserted to account for the influences of the limited experimental resolution on the PDF
Q_{damp}	$[r^{-1}]$	parameter asserted to account for the influences of the limited experimental resolution on the PDF
Q_{max}	[Å^{-1}]	upper limit of the FT of the diffractogram to $G(r)$
Q_{min}	[Å^{-1}]	lower limit of the FT of the diffractogram to $G(r)$
$\mathbf{Q}$	[Å^{-1}]	Scattering vector; defined by the relation $\mathbf{Q} = 2\pi(\mathbf{K}_o - \mathbf{K}_i)$
Q or $\lvert\mathbf{Q}\rvert$	[Å^{-1}]	Modulus of the scattering vector $\mathbf{Q}$
ρ_0	[distances.Å^{-3}]	averaged auto-correlation; in literature tis quantity is also denoted be the term *atom number density* which defines the mean number of atoms per unit volume at large values of R
$\rho(r)$	[distances.Å^{-3}]	density-density correlation function C(R) from which the self reference of each atom is subtracted
$\mathbf{r}_{ij}$ or r_{ij}	[Å]	distance between two atoms $\mathbf{x}_j - \mathbf{x}_i$; it is also the Patterson vector; its magnitude is interpreted as a radius r

$S(Q)$	[au]	reduced total scattering structure function (in some literature given in terms of the classical scattering of one electron)
$S(r)$	[au]	Patterson self-correlation
θ	[rad]	scattering angle; the theoretically possible range is from 0 to 180; due to the experimental setup this can never be reached
$T_i(\mathbf{Q})$		Debye-Waller factor of atom i (see section 1.2.1)
$W(r)$		rectangle function the PDF is multiplied with in order to account for the measurement range (section 2.1.5)
$\mathbf{x}_i$	[Å]	position vector of atom i

Introduction

> "But finally, of course, small devices are more delicate! (And if they are not small, why bother?) Why do we want smaller devices? So that we can make many more of them, within a given system. That means it won't be enough to have the smaller devices as reliable as the larger ones. They have to be more reliable. [...]
> Pessimism is, unfortunately, unpopular. But excessive optimism can only cause a premature and excessive counter-reaction when the optimistic promises are not speedily fulfilled."
>
> — Rolf Landauer (1989), 'Nanostructure physics: fashion or depth'

The initial aim of this thesis was to characterise nano-particles for application in batteries by means of analysis of the pair distribution function (PDF) obtained from X-ray diffraction data. This task was part of a project whose aim was to develop a battery with all its components, the LixSi-project. The LixSi-project was a joint project between TU Wien, PLUS (Paris-Lodron-University Salzburg), CEST (Competence center for Electrochemical Surface Technology) and AIT (Austrian Institute of Technology). The main motivation for this project was that the amount of consumed (electrical) energy is increasing. This is due to the fact of an ever increasing number of electrical devices in use. One important facet of those devices are devices in connection with individual mobility. The importance of electricity driven devices for mobility is amplified by the required exchange of conventional combustion machines by alternatives. - While there is a general necessity of reducing the overall energy-consumption and building much more efficient devices, another point is to store unused energy as often energy that is produced is not immediately used. One logical consequence is

the development of cheap and green materials with long-time cycle stabilities, high energy storage capacities and little energy losses.

A big part of the project was dedicated to the development of a new anode material for use in rechargeable batteries made from Silicon and its structural characterization. Silicon was chosen because it forms an alloy with a theoretical mass storage capacity of lithium that is six times higher than that of graphite which is used nowadays in many battery-applications ($Li_{44}Si_{10}$ vs LiC_6; Tarascon and Armand (2001)). During formation of the Li_xSi-compound, a volume expansion of multiple times the initial volume can occur (Mukhopadhyay and Sheldon 2014). This renders batteries that apply this material mechanically unstable and thereby unusable. Going to "nano-structured" materials may present the following opportunities: They can be embedded in a compressible matrix that is able to buffer the volume expansion. Possibly they are amorphous or differently structured or small enough in order not to form thermodynamic stable or stoichiometric compounds (Bourderau et al. 1999). This allows charging/discharging without destruction of the battery. Owing to a too early end of the project and other obstacles, some results of this thesis are still connected to batteries indeed but its focus lies on instrumental and methodological aspects of X-ray methods connected with the analysis of "nano-materials" rather than on the process of finding a good material.

The method of PDF-analysis was chosen as it is marketed as a very promising method for investigation of amorphous materials and small particles. In a nutshell, an ideal pair-distribution-function (PDF) gives the 1D-projection of the total information of all bond distances occurring in a given sample under given physical conditions such as temperature, pressure, magnetic field, etc. It is a weighted distribution of all bond distances occurring in a material. Each distance is weighted with the number of electrons of the contributing atoms. The PDF is obtained by a (real-valued) sine Fourier transformation of corrected one-dimensional scattering data. This means a shift in domain from *reciprocal space* to *real space*. The pair-distribution-function can be compared with a model in order to find out which atomic arrangements suit the PDF best.

The thesis is written from the point of view that everything is an empirical finding. - Traditional approaches might state that it is only a careful preparation

of the sample that ensure high data quality, but calibration procedures, evaluation of instrumental parameters, data reduction and physical corrections are by no means less experimental than arriving at a "well prepared" sample. Some even might go as far as to say that even analysis and simulation are part of the experiment as they depend on a theoretician's expertise concerning the choice of parameters (Collins 1994; Godin and Gingras 2002; Kennefick 2000). - General aspects and peculiarities of the PDF-method are discussed in the chapters one and two. Theoretical and observed limitations give motivation for approaching a profound analysis of current practices, strengths and obstacles in data-handling in chapters three, four and five. A discussion of important aspects concerning the experimental procedures relevant to this work is given there, accompanied by remarks on data quality as well as data collection. As many materials are polyphasic like composites and contain amorphous contents to provide a proper matrix, the analysis of 'nano-structured' mixtures is given by a model system in chapter six. The thesis ends with an investigation of the capabilities of PDF-analysis of particles.

Vienna, August 2018
Philipp Hans

Chapter 1

The pair distribution function (PDF) and its relation to matter

1.1 Some important facts

In the last years, the abbreviation PDF could be established in the crystallographic community and beyond, next to other meanings, as the **p**air **d**istribution **f**unction for the real-space-analysis of structures. The (1D-)PDF, which this work focusses on, is a one-dimensional function and is extracted from X-ray total scattering data from powders. The PDF is a variation of the so called density-density-correlation function or *autocorrelation function* of a material (Chung and Thorpe 1997). It gives information on the totality of electron-electron distances in a probed specimen. Because in a one-dimensional description each distance-vector becomes a scalar, the distance distribution is referred to by a radius r. The PDF is often referred to as $G(r)$ (Neder and Proffen 2008, p. 43).

What should be mentioned at this point is that there are various definitions and correspondingly notations of radial distribution functions such as the PDF. They have their origin in different communities, such as people working with neutrons, x-rays or dealing with particular classes of structures, and one should know what is dealt with where, how to relate the functions and when which is useful (for details see Keen (2001)). This is a reason why the mathematical formalisms in this chapter are stated in a rather general way. In all cases, not

only in strongly dynamic systems like gases or liquids we deal with a time averaged quantity (see e.g. Van Hove 1958).

As this work is about analyses of PDFs gained from X-ray (total) scattering data, a definition of scattering and relevant terminology is given straight ahead. Scattering is the phenomenon of radiation (X-ray light, neutrons, electrons..) getting redistributed by an irradiated specimen (arrangement of atoms). The angular dependence of the scattered light is measured and the angle between the wave vectors of incident and scattered radiation, $\mathbf{k}_0$ and $\mathbf{k}$ respectively, is denominated 2θ. Equation 1.1 defines the scattering vector and parameter $\mathbf{Q}$ and Q. They are given in [Å^{-1}] and give the scattering angle normalised on λ to make scattering experiments, which were performed with different radiation, relatable. The choice of the parameter definition is dependent on the field of application and also community based. The parameter Q is widely used in the PDF-literature.

$$Q = |\mathbf{Q}| = 2\pi|\mathbf{k} - \mathbf{k_0}| = 2\pi \left(2\sin(\theta)\frac{1}{\lambda}\right) \tag{1.1}$$

Due to the atomic composition of matter it is legitimate to group locally dense arrangements of electrons into specific atoms a_i centered at positions $\mathbf{x}_i$. In consideration of the atomicity of matter, it is clear that (in addition to the internal structure of the atoms) some structural features must remain even in the most unordered or distorted arrangements of matter (i.e. gases). The distribution of atoms throughout the sample can be given in terms of the atom distribution function $p(\mathbf{x})$, which is defined in terms of an arbitrary origin. In our case, $p(\mathbf{x})$ is defined as a sum of Dirac-delta distributions convoluted with the electron densities of the individual atoms:

$$p(\mathbf{x}) = \sum_{\mathbf{x}_i} \delta(\mathbf{x} - \mathbf{x}_i) * a_i \tag{1.2}$$

$\delta(\mathbf{x})$ is defined such that $\int_V \delta(\mathbf{x})d\mathbf{x} = 1$ if $\mathbf{o} \in V$ and $\delta(\mathbf{x}) = 0$ for whenever $\mathbf{x} \neq \mathbf{o}$. The density-density correlation or auto correlation of $p(\mathbf{x})$ at the point $\mathbf{r}$,

$P(\mathbf{r})$, also known as Patterson function, is defined in equation 1.3. $\mathbf{r}_{ij} = \mathbf{x}_j - \mathbf{x}_i$ and $\langle \quad \rangle$ denotes a thermal and temporal average.

$$P(\mathbf{r}) = \left\langle \int p(\mathbf{x})p(\mathbf{r}+\mathbf{x})d\mathbf{x} \right\rangle = \sum_{\mathbf{r}_i} \sum_{\mathbf{r}_j} \langle w_{ij}(\mathbf{r})\delta(\mathbf{r}-\mathbf{r}_{ij})\rangle \tag{1.3}$$

$P(\mathbf{r})$ can be considered to be a vector map of all the pairwise interactions $\mathbf{r}_{ij}$ between the atoms in $p(\mathbf{x})$. The lengths and directions of the $\mathbf{r}_{ij}$ are preserved but they are translated to a mutual origin, $P(\mathbf{0})$. The weights of the vectors are proportional by to the product of the electron-densities $w_{ij}(\mathbf{r}) = Z_i Z_j$ at the tips of the vectors in $p(\mathbf{x})$ (Bricogne 2010; Chung and Thorpe 1997; Patterson 1935; Tong et al. 2010). The part of equation 1.3 containing the double sum should be interpreted only in qualitative terms because atoms have a spatial extension. In the case of other radiation applied the weighting scheme is analogous.

$P(\mathbf{r})$ can be split into two functions $R(\mathbf{r})$ and $S(\mathbf{r})$. $R(\mathbf{r})$ accounts for the interatomic vectors $\mathbf{r}$ corresponding to the vectors $\mathbf{r}_{ij}$ and $S(\mathbf{r})$ for the intraatomic vectors "within" the atoms, corresponding to all distances in the vicinity of $\mathbf{r}_{ii}$:

$$P(\mathbf{r}) = R(\mathbf{r}) + S(\mathbf{r}) \tag{1.4}$$

If the sample is orientationally averaged, the quantity $P(\mathbf{r})$ becomes a one-dimensional quantity $P(r)$. A sample is orientationally averaged if it is isotropic, e.g. a powder of crystals or nano-particles, or amorphous. Then there is a crystallite (structural element) with every orientation with equal probability. Because of this, the information of the vectors' orientations is not evaluable. In this case, also the vectors $\mathbf{r}$ and $\mathbf{Q}$ become scalars r and Q respectively. The same is true for the resulting measurable intensity $I(\mathbf{Q})$ which in turn becomes $I(Q)$.

Doing so, also $R(\mathbf{r})$ becomes a one-dimensional function: $R(r)$. In this representation $r = |\mathbf{r}|$ can be interpreted as a radius from the origin of the Patterson map. $R(r)$ can be interpreted then in terms of a radially averaged correlation function or radial distribution function (RDF). In principle, the notation for calculation of $R(r)$ being an orientational average (Neder and Proffen 2008) up to a maximum distance is given by equation 1.5. To eliminate the Q-dependence of the atomic form factors $f(Q)$ in the experimental data, the $f(Q)$ are divided by

an average atomic form factor $\langle f(Q)\rangle$. In the best case, the numbers of electrons Z per atom are resembled approximately then. This procedure will be discussed in more detail in section 2.1.4. In a modeling approach, this approximation should be accounted for.

$$R(r) = \frac{1}{N}\sum_{i}^{i\neq j}\sum_{j}[Z_i Z_j \delta(r - r_{ij})] \approx \frac{1}{N}\sum_{i}^{i\neq j}\sum_{j}\left[\frac{f_i(Q)f_j(Q)}{\langle f(Q)\rangle^2}\delta(r - r_{ij})\right] \tag{1.5}$$

This notation equals the total $R(r)$ being the sum of N partial RDFs $R_i(r)$, N being the number of atoms in the system. In other words is the total RDF the average of the partial RDFs over each atom taken at the origin (see e.g. Chung and Thorpe 1997; Farrow and Billinge 2009). To keep a rigorous treatment, note that $R(r)$ in equation 1.5 is linked with its definition in equation 1.4 by N as a scaling factor:

$$R(r) = \frac{1}{N}\sum_{i}^{N} R_i(r) \tag{1.6}$$

For a system composed of only one sort of atom, $R(r)$ is defined such that for an arbitrary atom i at the origin, $\int R_i(r)dr$ gives the number of atoms or atom pairs in a shell of thickness dr at a distance r from that atom. Literature is not uniform what such an integration gives.

At this point a quantity $\rho(r)$, which is called the *real-space pair density* (see e.g. Chung and Thorpe 1997; Farrow and Billinge 2009), is introduced, so that

$$R(r) = 4\pi r^2 \rho(r) \tag{1.7}$$

and that the integral over this pair density: $\int dr d\phi d\theta r^2 sin(\theta)\rho(r) = \int R(r)dr$. - In other interpretations, $\rho(r)$ is the number of atoms per unit volume at a distance r from the reference atom in Å^{-3} (see Klug and Alexander 1974, p. 794). This usage of the RDF or $\rho(r)$ is not helpful in systems composed of several types of atoms. This is due to the weighing of each distance with w_{ij}. An integration will never give a number of atoms contained in a shell, not even a number of pairs. It appears not necessary to introduce $\rho(r)$ as a new quantity since it is never really used alone.

It appears further to be the case that identification of features is better possible when the $R(r)$ is modified and reduced to a function that oscillates around zero. With increasing r the RDF tends to obscure the correlations between atoms due to its rapid growth (Chung and Thorpe 1997). The better suited function is the **reduced radial distribution function** $G(r)$ or PDF.

$$G(r) = 4\pi r[\rho(r) - \rho_0] = \frac{1}{r}[R(r) - 4\pi r^2\rho_0] \tag{1.8}$$

ρ_0 is handled as an average or atomic number density of the material. Since $\rho(r)$ is a pair distribution, it is debatable if ρ_0 should be measured in terms of an average number of atoms per unit volume. Anyway, since the average density is subtracted, $G(r)$ oscillates around zero and shows the correlations more clearly than the RDF does. Usually, it is this function to which the experimental data are transformed through the relation (Chung and Thorpe 1997).

Equation 1.9 gives the connection between a PDF $G(r)$ and the measured intensity distribution function $I(Q)$ by means of a sine-Fourier-transformation (sine FT, $\mathcal{F}_S$) in a very general way. $I(Q)$ must be corrected in several ways to $S(Q)$, the reduced structure function. $S(Q)$ gives the **unmodified scattering** (Zachariasen 1935) that ideally describes only the unpolarised, elastic and coherent contribution to **total scattering** from a sample, corrected for self scattering (stemming from interference of signals from the same origin). Detailed derivations are given in chapter 2.1.

$$G(r) \propto \int_{Q_{min}}^{Q_{max}} Q[S(Q) - 1]\sin(Qr)dQ = \mathcal{F}_S\{CorrScal[I(Q)]\} \tag{1.9}$$

1.2 The limits of classical crystallographic approaches and the nano-structure problem

1.2.1 A general expression for the scattering of X-rays in the elastic regime

There are a handful of theories that describe the process of scattering at different levels of sophistication, enabling us to calculate the angle-dependent resulting

and measurable intensities. Examples for those are the kinematic (Durbin 1995; Feil 1977) and the dynamic theory of scattering (Ekstein 1942; Ewald 1969) or the quantum integral (Compton 1923).

Due to its experimental convenience and mathematical simplicity, the kinematic theory or first Born approximation of scattering is used in many cases. It enables us to calculate via a plane-wave-approach the observed intensities $I(\mathbf{Q})$ at distances from the sample that are large compared to interatomic distances. It states that each measured photon stems from an elastic and coherent scattering process (a part of the total scattering (Waller and Hartree 1929)). For every deviation from this rules corrections are necessary (absorption, polarization, multiple scattering). Already Born (1926) speaks critical about the basic assumptions of this approximations[1]. - And already here, we should take into account that the alleged contributions of different scattering processes to the measurable total intensities have to be distinguished by special means.

The first Born approximation states that the coherent elastic component of the scattering, in units of the scattering of a free electron, is given by equation 1.10. It equals the square of the Fourier transformation of the electron distribution map over the specimen (Coppens 2010). The integration is done over the coordinates of all electrons. Due to the generality of the treatment at this point, all quantities are described in terms of vectors which are denoted as bold letters. The intensity is a real observable and the only quantity that is directly measurable in a scattering experiment. The intensity is proportional to the square of the structure amplitude. The structure amplitude is the modulus of the structure factor: $|F(\mathbf{Q})|$.

$$I_{coherent,elastic}(\mathbf{Q}) = |F(\mathbf{Q})|^2 = \left| \int \rho(\mathbf{x}) \exp(i\mathbf{Q} \cdot \mathbf{x}) d\mathbf{x} \right|^2 \tag{1.10}$$

Equation 1.10 results from equation 1.11 which is more general. Ψ is the n-electron space-wavefunction which is expressed in the 3n coordinates of the

[1] "Die Schwierigkeiten, die man bisher bei der Einführung des ‚Gespensterfeldes' in die Optik gefunden hat, scheinen mir zum Tell auf der stillschweigend gemachten Annahme zu beruhen, daß Wellenzentrum und emittierendes Partikel an demselben Ort sein müssen. Aber dies ist]a schon beim Comptoneffekt sicher nicht der Fall und wird wohl im allgemeinen niemals zutreffen" - Born 1926, p. 827

electrons and a complex quantity. The positions of the electrons are given by the vectors $\mathbf{r}_j$. The integration must be performed over all coordinates but those of the j[th] electron and the summation over all electrons.

$$I_{coherent,elastic}(\mathbf{Q}) = \left| \int \Psi_0^* \left| \sum_j \exp(i\mathbf{Q} \cdot \mathbf{x}_j) \right| \Psi_0 d\mathbf{x} \right|^2 \tag{1.11}$$

There are discrepancies in what different authors mean when they apply the terms elastic and inelastic as well as coherent and incoherent scattering (Frey et al. 2010). In a strict sense there is no incoherent scattering at all, since all scattering processes are correlated in space and time. Moreover, 'elastic' and 'inelastic' scattering are approximations in some sort. Pure inelastic scattering would take place if the momentum and the energy of a photon were transferred to a single scatterer. An elastic scattering process would demand a uniform exchange of momentum and energy with the whole crystal (Frey et al. 2010; see also Compton 1923).

Inelastic scattering is due to dynamical fluctuations or ionization processes and may become observable as a 'diffuse' contribution in a diffraction pattern (Frey et al. 2010). Thermal diffuse scattering (TDS) is one process in which the radiation is scattered inelastically, so that the incident X-ray photon (or neutron) exchanges one or more quanta of vibrational energy with the crystal. The vibrational quantum is known as a phonon, and the TDS can be distinguished as one-phonon (first-order), two-phonon (second-order), etc scattering according to the number of phonons exchanged (Alexandropoulos et al. 2006). Considering this, thermal diffuse scattering is intertwined with scattering processes that involve atomic motion. Most work on phonons has been done for the case of single-crystals (e.g. Xu and Chiang 2005).

Inelastic scattering can be detected with appropriate equipment (Alexandropoulos et al. 2006; Schülke 1989). Information on inelastic scattering can contribute much e.g. to our knowledge of structural transitions (Sinn et al. 1997). In order to distinguish and evaluate the coherent and incoherent contributions of the elastic and inelastic parts, comparative measurements have to be performed as the distinction is not possible in a conventional single experiment. Anyway, while "a separation of elastic from inelastic diffuse scattering is generally pos-

sible, [but] difficulties may result from small energy exchanges that cannot be resolved for experimental reasons. The latter is true for scattering of X-rays by phonons, which have energies of the order of 10^{-2}–10^{-3} eV, values which are considerably smaller than 10 keV, a typical value for X-ray quanta. Another equivalent explanation, frequently forwarded in the literature, is the high speed of X-ray photons, such that the rather slow motion of atoms cannot be 'observed' by them during diffraction. Hence, all movements appear as static displacement waves of atoms, and temperature diffuse scattering is pseudo-elastic for X-rays. This is not true in the case of thermal neutrons, which have energies comparable to those of phonons." (Frey et al. 2010) - To emphasize: for measuring phonons (correlated motion of atoms with their surrounding) we are interested in inelastically but coherently scattered photons (Willis 1969). For X-rays the differences are very small and are handled as neglectable.

As indicated in equation 1.10, $I(\mathbf{Q})$ is $|F(\mathbf{Q})|^2$, the square of the structure amplitude. The convolution theorem (equation 1.12) states that the FT of a convolution is the product of the single Fourier-transforms. $|F(\mathbf{Q})|^2$ clearly equals to $|F(\mathbf{Q})||F(\mathbf{Q})|$ or $F(\mathbf{Q})\overline{F(\mathbf{Q})}$, where the overline indicates the complex conjugate and $*$ is the convolution operator.

$$I(\mathbf{Q}) = |F(\mathbf{Q})||F(\mathbf{Q})| = \mathcal{F}[p(\mathbf{x})]\overline{\mathcal{F}[p(\mathbf{x})]} = \mathcal{F}[p(\mathbf{x}) * p(-\mathbf{x})] \tag{1.12}$$

$$\mathcal{F}[p(\mathbf{x}) * p(-\mathbf{x})] = \int\int p(\mathbf{x})p(\mathbf{r}+\mathbf{x})d\mathbf{x}\exp(i\mathbf{Q}\mathbf{r})d\mathbf{r} \tag{1.13}$$

What follows from the convolution theorem is that the inverse FT of $I(\mathbf{Q})$ yields the autocorrelation $P(\mathbf{r})$, which is the convolution of the electron density with the electron density that has been inverted at the origin, but not the electron density $p(\mathbf{x})$. $P(\mathbf{r})$ is also called the Patterson function (Bricogne 2010; Tong et al. 2010). For this reason and also because the PDF is some sort of Patterson function, in what follows will be focused only onto data which is derived from the measured intensities.

$$\mathcal{F}^{-1}[I(\mathbf{Q})] = \mathcal{F}^{-1}[\mathcal{F}[p(\mathbf{x}) * p(\overline{\mathbf{x}})]] = P(\mathbf{r}) \tag{1.14}$$

As a good approximation, the electron distribution can be represented by

atoms (isolated atom approximation), i.e. a (spherical) electron-distribution around a nucleus. The scattering behavior of a so defined atom can be expressed by an atom-specific, diffraction angle dependent scattering function $f(|\mathbf{Q}|)$ (also called: atomic form factor). Operating in terms of atoms, equation 1.15 then gives a general formulation for the intensity distribution resulting from an arbitrary arrangement of atoms.

$$I(\mathbf{Q}) = \sum_j f_j(\mathbf{Q}) \sum_k f_k(\mathbf{Q}) [\exp\left(i\mathbf{Q} \cdot (\mathbf{x}_j - \mathbf{x}_k)\right) T_j(\mathbf{Q}) T_k(\mathbf{Q})] \tag{1.15}$$

The quantities $T_j(\mathbf{Q})$ are called *Debye-Waller factors* (DWF): to take into account variations in the scattering intensities due to displacement of atoms from a mean position (static or dynamic) a correctional term can be introduced. The atom distribution is convoluted with a displacement function, thus the diffraction pattern can be multiplied with the FT of the displacement function which is the Debye-Waller factor $T_j(\mathbf{Q})$ of the jth atom (Trueblood et al. 1996). The DWF describe the reduction of Bragg intensities only but do not take into account that diffuse scattering appears which increases in intensity with increasing Q. The DWF can be isotropic or anisotropic and is resembled by a Gaussian function such as given in equation 1.16. $\mathbf{u}$ is an displacement vector of the atom from its center position and U is the related mean-square displacement (which resembles the case of isotropic displacement) given in [Å^2] (Trueblood et al. 1996). U is linked with the isotropic thermal coefficient B by $B = 8\pi^2 U$. It is possible to give much more complicated descriptions for atomic motion or displacement in general than is done by the isotropic $T_j(\mathbf{Q})$:

$$T_j(\mathbf{Q}) = \exp\left[-2\pi Q^2 \langle |\mathbf{u}|^2 \rangle\right] = \exp\left[-2\pi Q^2 U_j\right] \tag{1.16}$$

In this most general case of equation 1.15, the $T(\mathbf{Q})$ will account only for thermal motion because all atom positions are considered by the equation and therefore static displacement is already considered. In other formalisms, $T_j(\mathbf{Q})$ is applied to also describe static disorder.

In a diffraction experiment on a crystalline powder or nanoparticles it is assumed that the individual particles are randomly oriented. Under ideal sample preparation conditions this assumption will be reasonable well realized and the

sample can be treated as an isotropic sample. Amorphous materials like glasses or liquids are isotropic as well. Here the lack of long range periodicity usually implies isotropic behaviour. The magnitude of the scattering is dependent only on the diffraction angle then. The vector $\mathbf{Q}(hkl)$ becomes a scalar quantity $|\mathbf{Q}| = Q$. The same is valid for the vectors **r** in the auto-correlation function. $P(\mathbf{r})$ becomes $P(r)$.

1.2.2 Classical assumptions for quasi-periodic arrangements

Classical crystallography relies on the main assumption of periodicity, which leads to infinite extendedness of an atomic ensemble. A periodic structure can be described in multiples of a smallest unit, a *unit-cell*, then. In such cases, we can reduce the number of parameters needed for describing a structure drastically. The basis vectors **a**, **b**, **c** span a real lattice. A triple of coordinates (x_i, y_i, z_i) defines the positions of each atom in the unit cell in terms of the basis vectors so that $\mathbf{x_i} = (x\mathbf{a} + y\mathbf{b} + z\mathbf{c})$. — Having this condition of periodicity fulfilled, diffraction of X-rays can be described as if light was being reflected by planes. Reflection can only occur when the diffraction or reflection condition $n\lambda = 2dsin(\theta)$, i.e. Bragg's law, is fulfilled.

The corresponding measured intensities are concentrated to reflexes $I(\mathbf{Q}[hkl])$ ("Bragg-peaks") which are attributed to points in reciprocal space. These points are located on a reciprocal lattice spanned by the vectors $\mathbf{a}^*$, $\mathbf{b}^*$ and $\mathbf{c}^*$. The triples (h, k, l) define points of the reciprocal lattice where $\mathbf{Q}(hkl) = 2\pi(h\mathbf{a}^* + k\mathbf{b}^* + l\mathbf{c}^*)$; h, k and l are integers (equation 1.17).

$$I(\mathbf{Q}) = \sum_j \sum_k f_j(\mathbf{Q}) f_k(\mathbf{Q}) \exp\left(i\mathbf{Q}(hkl) \cdot [\mathbf{x}_j(x_j y_j z_j) - \mathbf{x}_k(x_k y_k z_k)]\right) \qquad (1.17)$$

1.2.3 Deviations from classical conditions

Any real crystal will contain *defects* such as missing or wrong atoms on an atomic site, interstitials, clusters, domains, stacking faults etc. Defects are deviations from the periodic ensemble which is characterizable by a direct lattice. Although many arrangements of atoms are in a good approximation indeed periodic (sufficiently large and sufficiently regular), this is nevertheless an approximation.

With increasing amount of defects, the unit-cell approach discussed in the previous section becomes increasingly insufficient and we therefore need a more refined treatment for the description of disordered structures.

Two limiting cases of disorder are:

.) Substances which are *disordered*. - The extreme cases of randomness are glasses and liquids ("X-ray amorphous") which are highly disordered. Amorphous substances may be built up of millions or more of atoms and do posses short-range-order (SRO)[2] only.

.) Small particles (e.g. nano-clusters which consist only of a few atoms). In principle, those can be seen as aperiodicities as well.

.) A combination of the two preceding points.

All defects lead to elastic scattering apart from the Bragg-peaks. This type of scattering has been named *diffuse scattering*. The complete experimentally observed scattering will consist of Bragg reflections and diffuse scattering and this combined signal is referred to as *total scattering*. The Bragg reflections by themselves then no longer contain the full information on the sample. - Dependent on the suspected complexity of disorder, two general modeling methods are proposed to build structure model to calculate the resulting total scattering from: small-box and big-box modeling (Keen and Goodwin 2015 - "'The crystallography of correlated disorder'"):

In small-box modeling, disorder is introduced into a unit-cell like construct, maybe also something which is a few unit cells in extension. Here, the introduction of an isotropic or anisotropic Debye-Waller factor $T_j(\mathbf{Q})$ which incorporates ADPs (anisotropic displacement parameters) can suffice to describe the inevitable thermal motion as well as static disorder (Trueblood et al. 1996). An occupancy-parameter for the accounting of occupancy (or substitution defects) can be introduced, if a crystallographic site happens to show this sort of structural defects. In molecular compounds, different molecular orientations and displacements can be considered. The diffraction patterns of layered structures

[2]Short-range-order is defined here as the atomic surrounding of each point up to a selectable distance. No periodic order as in crystalline materials (that goes along with the surrounding of each point being similar) must be found.

might be described by the statistical combination of the diffraction patterns of a few layers (Treacy et al. 1991).

In big-box modeling, a big supercell is built on the computer and atomic environments are locally altered. Up to now, this is a considerable effort in many cases and structures must be approximated via fragments often. (For details on strategies towards model building and refinement as well as further references like Monte-Carlo (MC) or Reverse-Monte-Carlo (RMC) simulations see Neder and Proffen (2008)). The transition line from the small box to the big box might be a fluid one.

As a last complication, there might be several structures which describe a diffractogram equally well (homometry; Klug and Alexander 1974, p. 837; Ravy 2013). In powders, we get an additional loss of information owing to projection of the scattering vector **Q** from a three-dimensional onto a one-dimensional space. The measured scattering at a given diffraction angle is the summed scattering of all crystallites in the sample that fulfill the reflection condition. When dealing with diffuse scattering, things become even more intricate in one but also in three dimensions. This heap of complex questions concerning structure solution has been titled *nano-structure-problem* recently. (See e.g. Cliffe et al. 2010 or Billinge 2010). For a nice example of attempting this "new" nano-structure problem on nano-particles see Petkov et al. (2014).

1.3 A case for the PDF?

Crystallographically challenging materials have of course been known for a long time and interpretation of diffuse scattering in single-crystals was done by analysis of the diffuse scattering (Neder et al. 1990, Welberry 2010; Welberry and Butler 1994; Keen and Goodwin 2015; Temleitner and Pusztai 2013). - The idea of analysing the distributions of interatomic distances is old nevertheless. The framework of pair distribution function analysis was worked out by Zernike and Prins (1927). The first usage of PDF-like-function analysis is ascribed to Debye and Menke (1931). Countless studies dealing with radial distributio -function (RDF) analysis have been performed since then. Back then it was used to analyse amorphous materials (also known as glasses; see for example

Wright 1988; Wright 1990; Wright 1994; Wright 2000a; Wright 2000b; Wright et al. 1991) or liquids and gasses (for examples see: Gingrich 1943; Gingrich and Heaton 1961). - With the advent of what was so prominently named the *nano structure problem*, speaking of the pair distribution function became more popular. Nowadays, not only amorphous and other strongly disordered substances exhibiting bulk properties, but also small systems such as small particles and clusters available as powders or dispersions (e.g. Zobel et al. 2015) are investigated in terms of *"real-space-studies"*.

Traditionally, working with real-space-data and thus PDF-analysis was considered as a method of last resort and to be used only if all other means of crystallographic analysis would fail. This impression arose due to broad peaks in the PDFs of such strongly disordered materials which are due to broad bond-distance distributions. This phenomenon was falsely interpreted as impreciseness ot the method itself. Further, a lack of well-suited correction procedures of raw data and experimental procedures in former times led to artefacts and spurious trends in the PDF-data (see Toby and Egami 1992).

The analysis of interatomic distances in a material, as is given through the PDF, appears to be well-suited in the cases mentioned above. When a strong lack of periodicity hinders the application of the standard concepts, Fourier-transformation of data can be helpful because it leads to a change of the information's representation. In doing so, it changes the weighting-scheme which is applied in the optimization of a structural model. To distinguish and characterize structures, comparisons or refinements of models against pronounced features (like bond distances) are preferred over broad and shallow diffraction curves from amorphous compounds. Careful considerations about structural units and their assembly may be done in the case of strongly disordered structures and could lead to a useful result.

Chapter 2

Technical details

As mentioned, there are many variations of radial distribution functions (Keen 2001). The form of the PDF chosen here is the **reduced radial distribution function** $G(r)$. $G_{calc}(r)$ (equation 2.1) is the PDF that can be derived from a structure model (Neder and Proffen 1997). $G_{exp}(r)$ (equation 2.2) is the PDF that can be obtained by real-valued sine Fourier transformation (see Kammler 2008, p 63, also: Rahman 2011, p. 11) of the reduced and normalised total (unmodified) scattering structure function $Q[S(Q)-1]$. Mathematical derivations, suitability considerations and discussion of computational aspects of the applied procedures will be given in this chapter.

$$G_{calc}(r) = \frac{1}{r}\sum_{i}^{i\neq j}\sum_{j}\left[\frac{f_i(Q)f_j(Q)}{\langle f(Q)\rangle^2}\delta(r-r_{ij})\right] - 4\pi r\rho_0 \tag{2.1}$$

$$G_{exp}(r) = 4\pi r[\rho(r)-\rho_0] = \frac{2}{\pi}\int_{Q_{min}}^{Q_{max}} Q(S(Q)-1)\sin(Qr)dQ \tag{2.2}$$

2.1 Total scattering, the Debye-function, and the PDF

2.1.1 Conceptual aspects of PDF-analysis

The PDF we get is intrinsically tied to the theory we decide to use for the description of the scattering process. Before we resume with the common derivation of the PDF for some cases, we must shortly discuss when it is valid.

An equation that permits the calculation of the *total scattering* of a configuration of scatterers with averaged distribution in space is the *Debye-Scattering-Equation* (equation 2.3; Debye 1930; Debye 1915). At the moment it is *the* equation which is used to derive the PDF from total scattering data after corrections and by mathematical transformations. As the name suggests, this formula goes back to Peter Debye who tried to give an explanation of diffraction phenomena and thereby models of the electronic structure[1] in atoms in 1915 (Debye 1915). Under the **assumption of randomly and uniformly distributed building units** one can obtain it *via radial integration over all orientations* (over solid angle) from the common equation for kinematic diffraction, equation 1.15. The Debye-formula is derived for an ensemble of isolated atoms (that is in principle: a gas - Grigson 1967) and the electron distribution between atoms (chemical bonding) is neglected (what is un-important if a sample consists of heavy atoms). Also it does not account for small angle scattering (SAS) effects (at least not very well due to computational issues and because SAS also emerges from interactions between particles [Gelisio and Scardi 2016]).

$$I(Q) = \sum_i \sum_j f_i f_j \frac{\sin(Q r_{ij})}{Q r_{ij}} = \sum_j f_j^2 + \sum_i^{i \neq j} \sum_j f_i f_j \frac{\sin(Q r_{ij})}{Q r_{ij}} \tag{2.3}$$

f_i are functions $f(Q)$ and called atomic scattering factors (or atomic form factors in classical X-ray crystallography). They show a decay with increasing Q. The single sum in the right part of the equation is also defined as *self-scattering*, because it involves only the same atom. - A tempting and plausible derivation of the "Debye-Formula" equation 2.3 from equation 1.15 is given by Gingrich (1943).

It is important to stress that we are entitled to use the theory based on the Debye-Scattering-Equation only straightforwardly if we are dealing with ensembles where structural elements are ideally averaged. An ideal powder is an ensemble of crystallites or particles that has a distribution of sizes and shapes that are statistically equally distributed and this is the theoretical presupposition, the equation has been derived for. We have to take care during

[1] Back then, before the advent of quantum mechanics he proposed a circular arrangements of electrons in the atom.

preparation that we arrive at that state (and unfortunately we cannot guarantee for that).

All things and effects not accounted for by this formalisation have to be accounted for by corrections afterwards or an adequate experimental setup making corrections unnecessary. The equation is valid for unpolarised, monochromatic, coherent radiation and each photon is scattered elastically (without remaining energy transfer). X-ray scattering is regarded as pseudo-elastic in principle. Photons are scattered only once by the specimen. Corrections are necessary for deviations from those assumptions like multiple scattering, absorption and polarization effects, inelastic scattering as Compton-scattering as well as for instrumental effects. By the fact that corrections for geometry dependent absorption or multiple scattering have to be applied one can already see that the theory of kinematic diffraction is an approximation, even if it is a good one.

It is an open question which information about the specimen is needed in which case in order to do corrections or mathematical transformation to the PDF in the correct manner. That implies that a user actually had to be acquainted with many physical effects and theoretical details. It might be the case that empirical absorption corrections work well in single-crystal-research and are an easy and efficient way to handle a problem. Actual developments in PDF-methodology, promising also very inexperienced users automated data handling (e.g. Juhás et al. 2013) obfuscate this need. Problems concerning empirical data-correction to the PDF which were found while working for this thesis are discussed in the next chapter.

2.1.2 Derivation of a PDF-equation for an extended (amorphous) ensemble with only one atom-species

In case of a compound consisting of N atoms of only one kind, equation 2.3 can be reduced to equation 2.4. The aim of the transformations is the separation of the atomic scattering factors from the atomic coordinates. (For space reasons the $f(Q)$-terms will be written simply as f in most of the occurrences.)

$$I(Q) = \sum_{N} f^2(Q) + f^2(Q) \sum_{i}^{i \neq j} \sum_{j} \frac{\sin(Q r_{ij})}{Q r_{ij}} \tag{2.4}$$

Under the assumption that there are many atoms, the second sum can be replaced by an integral over the volume of the sample. Assuming that the atom distribution is spherically homogeneous in average, we can introduce an averaged radial-pair-distribution function $R(r)$ as defined in equation 2.5 and rewrite equation 2.4 as 2.6. Since the integral is taken, the parameter r_{ij} is expressed as r.

$$R(r) = \frac{1}{N}\sum_{i}^{N} R_i(r) = 4\pi r^2 \rho(r) \tag{2.5}$$

$$I(Q) = Nf^2 + f^2 \sum_{i}^{i\neq j} \int_0^{R_{max}} R(r)\frac{\sin(Qr)}{Qr} dr \tag{2.6}$$

The formalism in equation 2.5 states that $R(r)$ is the totality of atomic pairs on the surface of a sphere that is defined by r. In the alternative formulation of $R(r) = 4\pi r\rho(r)$, $R(r)$ is built up in terms of a reduced radial distance-distribution $\rho(r)$ wich is also called pair density. Through integration of $\int 4\pi\rho(r)dr$, all distances in a spherical volume can be obtained. If we further suppose that the material's extension is orders of magnitude larger then the radial integration limit, surface effects can be neglected. The author wants to emphasize that the averaged quantity $R(r)$ is compiled by individual quantities $R_i(r)$ in modeling as well as in the physical reality.

$$I(Q) = Nf^2 + Nf^2 \int_0^{R_{max}} 4\pi r^2 \rho(r)\frac{\sin(Qr)}{Qr} dr \tag{2.7}$$

$$I(Q) = Nf^2 \left(1 + 4\pi \int_0^{R_{max}} r^2 \rho(r)\frac{\sin(Qr)}{Qr} dr\right) \tag{2.8}$$

Through rearrangement, equation 2.9 can be obtained, which defines the reduced and normalised total scattering structure function $F(Q)$.

$$Q\left(\frac{I(Q)}{Nf^2} - 1\right) = Q[S(Q) - 1] = F(Q) = 4\pi \int_0^{R_{max}} r\rho(r)\sin(Qr) dr \tag{2.9}$$

Since the right-hand side of equation 2.9 is a sine-Fourier transformation, we can arrive at the reduced radial distribution function $G(r)$ in equation 2.10 by an inverse sine-Fourier transformation of $F(Q)$.

$$G(r) = 4\pi r\rho(r) = \int_{Q_{min}}^{Q_{max}} Q\left(\frac{I(Q)}{Nf(Q)^2} - 1\right)\sin(Qr)dQ \tag{2.10}$$

Figure 2.1 shows the transformation steps from the experimental intensity distribution of a Si standard 640d from NIST $I(Q)$ by data correction to $S(Q)$ and $F(Q)$. Figure 2.2 shows the corresponding PDF.

2.1.3 Introduction and subtraction of a mean pair density to account for the small angle scattering (SAS) signal

The Debye-Scattering-Equation does not fully account for the SAS signal because interactions between domains are not included (Grigson 1967). Modeling such an ensemble will be extremely difficult. Using conventional setups, the SAS signal will not be experimentally measurable, because the SAS-signal will be located under a value of Q_{min}, e.g. in the primary beam. The coherence length of the probing radiation is another aspect which determines the amount of signal from particle-particle interactions.

Theoretically, the intensity can be split up into two parts: one F_{sas} that occurs only under and one (the rest) F_{was} above a minimal Q-value Q_{min}. Under the assumption that the SAS intensity from a large crystal or amorphous ensemble is identical to that from a solid with uniform (scalar) density ρ_0, it is suitable to account for the SAS signal in the following way: a) subtraction of ρ_0 from $\rho(r)$ that is described by the Debye-Scattering-Equation. b) Addition of a term that contains ρ_0 and which is integrated separately (equation 2.12).

$$F(Q) = F_{was} + F_{sas} \tag{2.11}$$

$$\frac{F(Q)}{4\pi} = \int_0^{R_{max}} r[\rho(r) - \rho_0]\sin(Qr)dr + \rho_0\int_0^{R_{max}} r\sin(Qr)dr \tag{2.12}$$

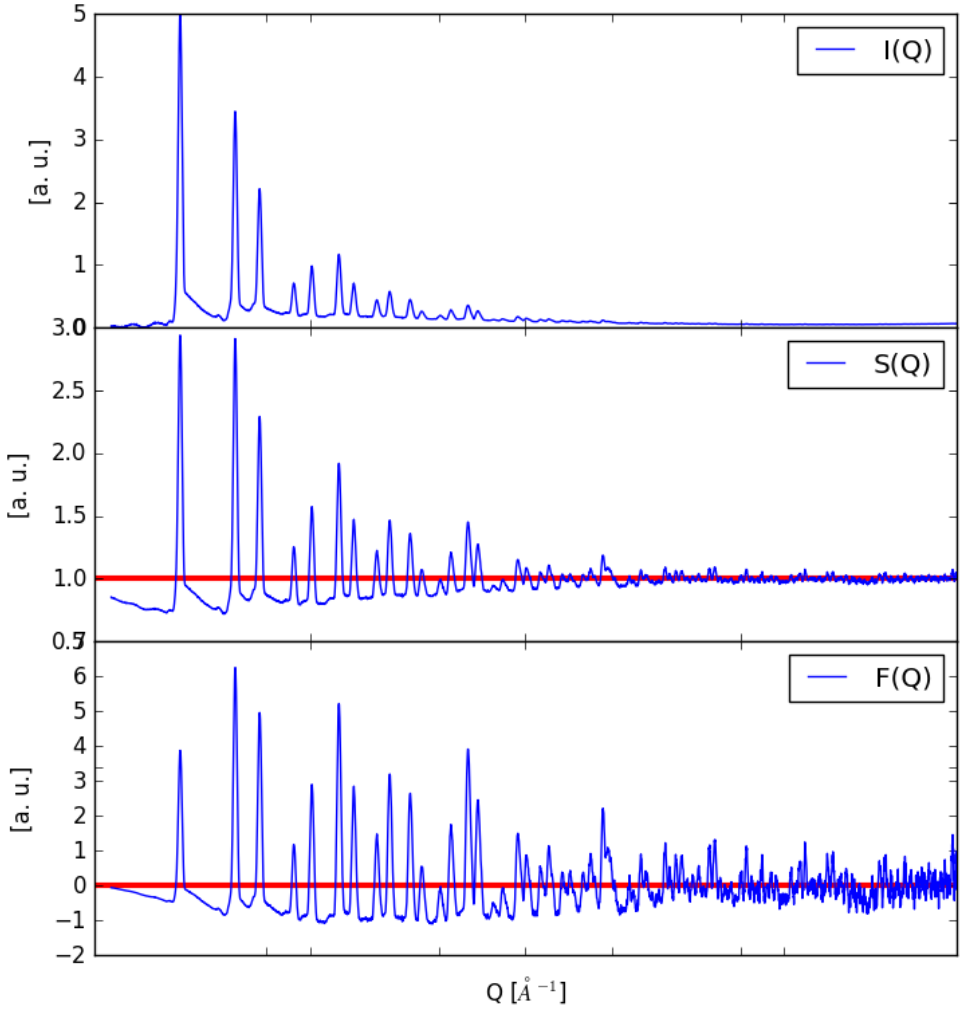

Figure 2.1: Data reduction steps exemplified by means of a Si-NIST 640d standard measured with Ag-radiation: $I(Q)$ (top) is the container-signal-corrected raw intensity-distribution. $S(Q)$ (middle is obtained by subtraction of "self-scattering" (see equation 2.3) from $I(Q)$. The resulting curve oscillates around 1. The data-correction was accomplished by means of an ad-hoc polynomial. (This method is discussed later, e.g. in sections 2.2.5 and 4.) $F(Q) = Q[S(Q) - 1]$ (bottom) oscillates around 0.

Integration of the second part gives equation 2.13.

$$\frac{F(Q)}{4\pi} = \int_0^{R_{max}} r[\rho(r) - \rho_0] \sin(Qr) dr + \rho_0 \frac{\sin(Qr) - rQ\cos(Qr)}{Q^2} \Big|_0^{R_{max}} \tag{2.13}$$

so that after integration $F(Q)$ and F_{sas} are

$$F(Q) = 4\pi \int_0^{R_{max}} r[\rho(r) - \rho_0] \sin(Qr) dr + F_{sas} \tag{2.14}$$

$$F_{sas} = 4\pi\rho_0 \frac{\sin(QR_{max}) - R_{max}Q\cos(QR_{max})}{Q^2} - 0 \tag{2.15}$$

For $r = 0$ the last term of F_{sas} is zero. For large R_{max} the function only gets big at very small Q and decays fast. As the model-assumption is based on an ensemble with large extension and therefore large values for R_{max}, the scattering stemming from the last term is rendered into a region not observable, namely into the region of the primary beam. In other cases, we actually had to correct or to account for the SAS-signal as it is not easy to take into account the SAS signal of ensembles by modeling via the Debye-Scattering-Equation. — This is the case for small objects (such as nanoparticles) which should be treated differently (Farrow and Billinge 2009). — By setting the F_{sas} to zero and proper rearrangement, equation 2.13 is transformed into the initial definition of $G(r)$ in equation 2.2.

$$G_{exp}(r) = 4\pi r[\rho(r) - \rho_0] = \frac{2}{\pi} \int_{Q_{min}}^{Q_{max}} F(Q) \sin(Qr) dQ \tag{2.2}$$

By introducing ρ_0 it seems that the PDF becomes a measure for the deviation of a structure from an averaged structure and not an absolute structural function. In the PDF-literature, ρ_0 is identified with the slope of the baseline of $G(r)$ (at least in region of low r; figure 2.2). $G(r)$ oscillates in this representation around zero for large distances. It turns out that this definition of a radial distribution function $G(r)$, is advantageous for the work with crystalline materials because it shows correlations more clearly (Chung and Thorpe 1997). Because the SAS-signal is not measured in many cases, it is often $G(r)$ which is obtained from the experimental scattering data.

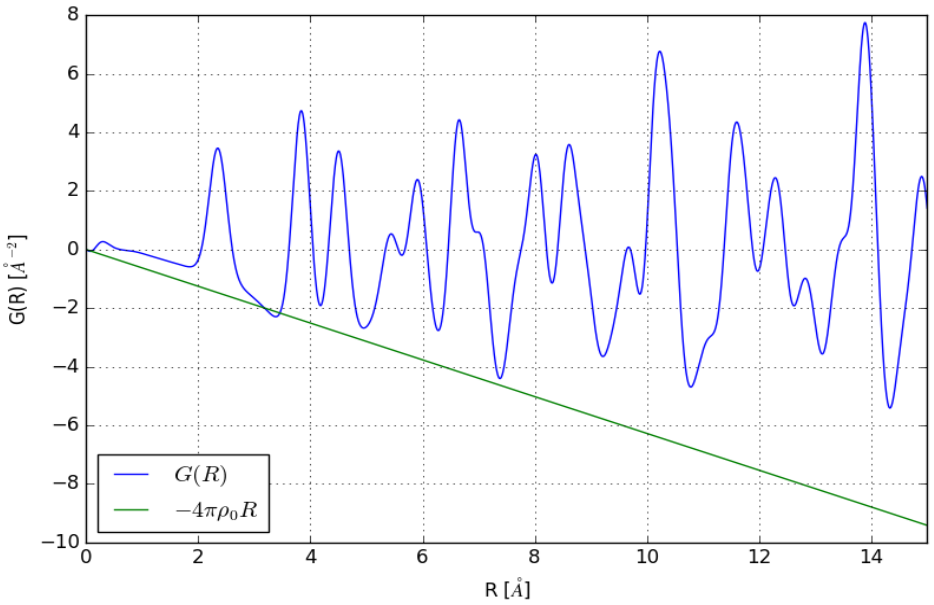

Figure 2.2: Theoretical $G(r)$ of Si obtained by sine-Fourier transformation of a calculated $F(Q)$ showing the progression of the baseline along $-4\pi r\rho_0$

2.1.4 Derivation for an extended (amorphous) ensemble with multiple atom-species

With equation 2.16, one can calculate the intensity of elastic scattered radiation from an ensemble of different atoms. As in section 2.1.2, the intensity is expressed in terms of a pair density $\rho(r)$, but in the case of multiple atom sorts, partial atom-distances-distribution functions $\rho_{ij}(r)$ have to be introduced, so that $\rho(r) = \sum \rho_{ij}(r)$. (With these partial distribution functions, it is possible to define theoretical partial structure factors $S_{ij}(Q)$ in reciprocal space - Enderby et al. 1966.) $\rho_j(r)$ denotes the radial distribution of distances to atoms j from an atom of type i.

$$I_{exp}(Q) = \sum_{i}^{N} f_i^2(Q) + \sum_{i,j} f_i(Q) f_j(Q) \int_0^{R_{max}} 4\pi r^2 \rho_{ij}(r) \frac{\sin(Qr)}{Qr} dr \qquad (2.16)$$

Because of their Q-dependence, we cannot remove the atomic form factors from the sum and therefore cannot disentangle them from the $\rho_{ij}(r)$-terms to obtain the radial distribution functions. Here lies the origin why the PDF

is weighted with the product of the single atoms' weights. In the case of different but similar atoms, the general mathematical procedure that is applied for data-transformation (e.g. in Juhás et al. (2013) and which is of course an approximation) is sketched. It goes without saying that the approximation is used independently of the sort of atoms that contribute to the diffraction pattern. — The approximation is often referred to as *Warren-Krutter-Morningstar approximation* (Warren et al. 1936). To get rid of the individual Q-dependences of the atomic scattering factors, it is approached to substitute the atomic scattering factors by the product of a scattering factor per electron and a corresponding multiplier K_m (equation 2.17).

To do so, a sum of all atomic scattering factors that correspond to stoichiometry is taken and divided by the number of electron corresponding to this stoichiometry (a sum of the atomic ordering numbers Z_i). Each atomic scattering factor is substituted then by the product of this "scattering factor per electron" f_e and an effective number of electrons per atom K_i. Note here that the K_is do not necessarily resemble the Z_is but could be other quantities. In the optimal case of course, $K_i = Z_i$ and the original scattering curve f_i is resembled well, but it might also result in something that looks different, so the division of f_i/f_e might give another number for K_i than Z_i. The quality of this approximation is dependent on the similarity of atomic scattering factors of the elements the sample contains. [On the other hand, the results of this approximation can be interpreted as a sharpening of the peaks in the Patterson function (Patterson 1935; Tong et al. 2010). The approximation can be refunctioned then to an empirical problem of finding the function that gives the sharpest PDF peaks.]

$$(a) \quad f_e(Q) = \left(\sum_i^N f_i(Q) \right) / \sum_i^N Z_i; \qquad (b) \quad K_i f_e(Q) = f_i(Q) \tag{2.17}$$

Approximation 2.17 (b) is introduced into equation 2.16, giving equation 2.18 which gives equation 2.19.

$$I_{exp}(Q) = \sum_i f_i^2(Q) + \frac{1}{f_e^2(Q)} \sum_{i,j} f_i(Q) f_j(Q) \int_0^{R_{max}} 4\pi r^2 \rho_{ij}(r) \frac{\sin(Qr)}{Qr} dr \tag{2.18}$$

$$I_{exp}(Q) = \sum_{i}^{N} f_i^2 + 4\pi \sum_{i,j} K_i K_j \int_0^{R_{max}} r\rho_{ij}(r) \frac{\sin(Qr)}{Q} dr \tag{2.19}$$

With the term $i(Q)$ defined as a reduced scattering function in equation 2.20, equation 2.19 is rearranged to equation 2.21.

$$i(Q) = I_{exp}(Q) - \sum_i f_i^2 = I_{exp}(Q) - \sum_i K_i^2 f_e^2 = \frac{I_{exp}(Q)}{\sum_i K_i^2 f_e^2} - 1 \tag{2.20}$$

$$Qi(Q) = 4\pi \sum_{i,j} K_i K_j \int_0^{R_{max}} r\rho_{ij}(r) \sin(Qr) dr \tag{2.21}$$

What we get in the case of a structure which is constituted of different kinds of atoms is the sum of approximated, species dependent (weighted) partial PDFs (i.e. the sum of different atomic environments or in other words the sum of the partial PDFs where the atoms of species "A" are in the center, atoms of species "B" are in the center...).

$$G(r) = 4\pi r \sum_{i,j} K_i K_j \rho_{ij}(r) = \frac{2}{\pi} \int_{Q_{min}}^{Q_{max}} Qi(Q) \sin(Qr) dQ \tag{2.22}$$

The further procedure of introducing the ρ_0-term is done as discussed above. The terms $\rho_{ij}(r)$ are regularly substituted by the expression $[\rho_{ij}(r) - \rho_{0e}]$ for this purpose, where ρ_{0e} is an average pair density suitable for the one-electron-scattering-approximation.

However there are different formalisms, some dividing everything by the mean electron-scattering approximation, some dividing through a mean atomic form factor. Knowledge about the reduction and simulation procedures is highly advised. Besides artefacts due to the approximation, this will result in differences that call for scaling factors which must be applied to the calculated or experimental PDFs. - Further details on even more refined methods can be found in Warren (1990), which nevertheless are also approximations. Possible choices of parameters and approximating functions are discussed in Korsunskiy and Neder (2005). Klug and Alexander (1974, p. 824) mention Finbak et al. (1949a) and Finbak et al. (1949b), who elucidated an *electronic distribution*

function which apparently is much less prone to artefacts in then the functions discussed above.

2.1.5 Influences of the integration limits in the FT

$G(r)$ is obtained via an integral formula from experimental intensities. In this section, it is shown that it is crucial to apply suitable integration limits.

The experimental $G(r)$ is the "real" (calculated) $G(r)$ superimposed with *termination ripples* (Toby and Egami 1992). The broadness and amplitude of those ripples depend on the choice of Q_{min} and Q_{max}, the lower and upper integration limits of the FT. If a low value is chosen fo Q_{min}, low frequency oscillations are superimposed on the diffractogram. In the literature, they are considered to be negligible. Breaking at Q_{max} causes high frequency ripples which are bothersome artefacts and could be confused with bond-distances. - Moreover, the experimental PDF shows peak broadening compared to an idealistic $G(r)$ that is dependent on the measurement range. The real PDF is convoluted with $W(r)$ (equation 2.23) which is the Fourier transform of a rectangular function $W(r)$ which describes the measurement range. This leads to an r-dependent broadening of the PDF-peaks (Neder and Proffen 2008).

$$W(r) = \frac{sin(Q_{max}r)}{r} \tag{2.23}$$

Both effects have to be considered when calculating a PDF from a structural model (see also section 2.3.1). — Figures 2.3 to 2.6 give comparisons af the PDFs for a model of crystalline Si ($Fd\bar{3}m$, $U = 0.016$ Å^2), all calculated for different values of Q_{max}. The models have been calculated with the software pdfgui (Farrow et al. 2007). As no value for Q_{min} could be defined, it was assumed that this one is set to 0 by the program. The comparison shows that it is essential to carry out measurements with radiation of high energy and collect data up to high Q-values (at least 17 Å^{-1} [Lab-Mo], better 22 Å^{-1} [Lab-Ag] or 30 Å^{-1} [synchrotron]). The improvements by application of radiation of energies approaching 40 Å^{-1} is marginal compared to Ag and seems to be not necessary for the achievement of highly resolved PDFs (figure 2.6). It should be mentioned that significant differences are to be expected for larger U-values.

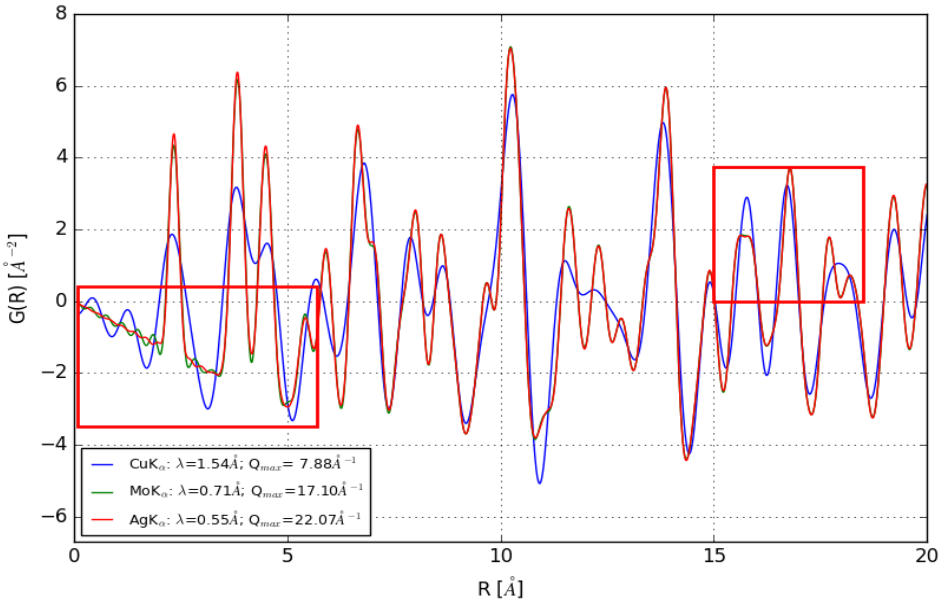

Figure 2.3: Comparison of three PDFs of crystalline Si modeled for different Q_{max}-values which are experimentally attainable with Cu, Mo- and Ag-radiation. Two regions, which will be analysed in magnification in the following figures, are marked by red squares. It can be seen that peaks are ever better defined when radiation with smaller wavelengths is applied. A Q_{max} from at least Mo-radiation should be chosen for measurements and as upper FT-limit, what is also discussed in the text.

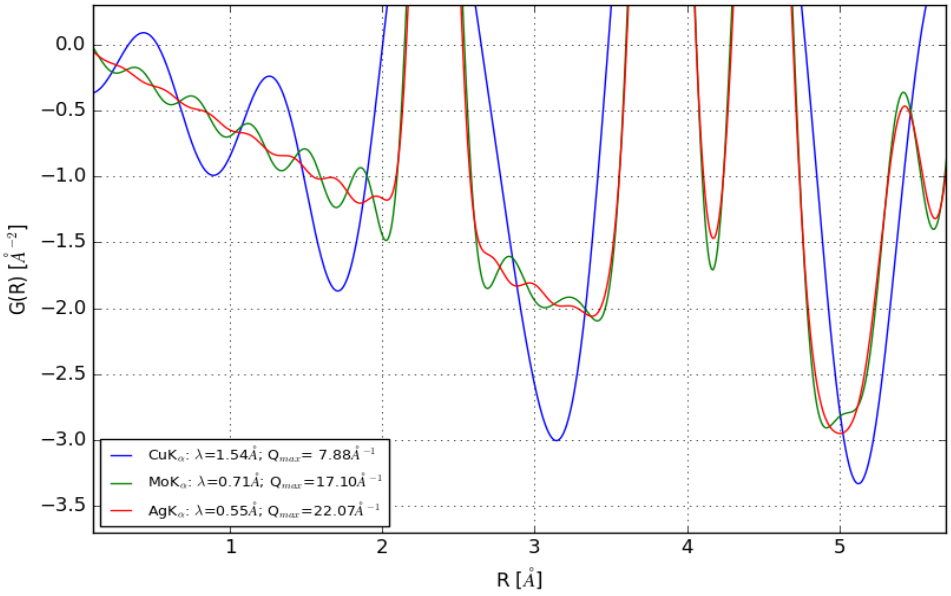

Figure 2.4: Zoom of the comparison in figure 2.3 shows a comparison of termination ripples and peak-widths from scattering data collected with various radiations.

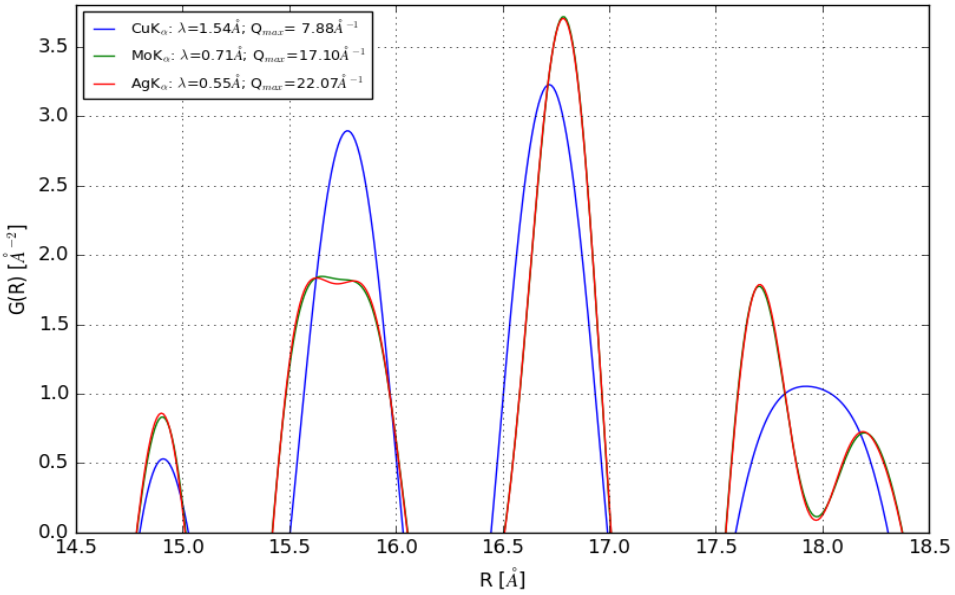

Figure 2.5: Zoom of the comparison in figure 2.3 shows that PDFs created from scattering data exhibiting Q_{max} from Cu-radiation are not capable of resolving peaks and therefore structural features.

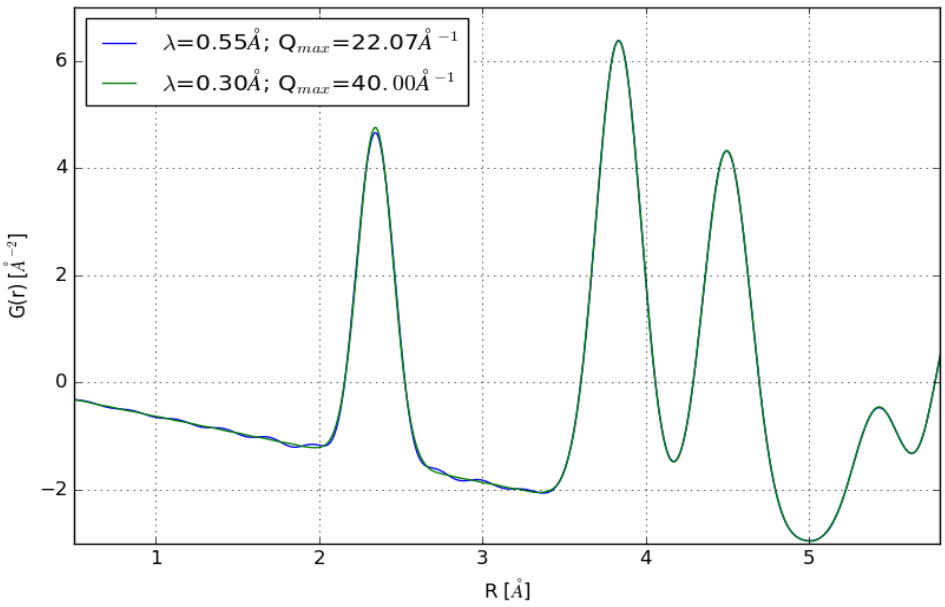

Figure 2.6: Comparison of $G(r)$s calculated for Q_{max} of Ag at 22 Å^{-1} and 40 Å^{-1}. The differences in termination ripples appear negligible. Of course, analysis largely depends on the features of the specimen, anyway, already by applying Ag-radiation the first PDF-peak is only little affected by termination ripples so that a source of error is excluded.

2.2 Developments of PDF-methodology according to literature

2.2.1 Quality criteria for PDF-creation and refinements

As structural investigation by PDF-analysis is increasingly applied, corresponding literature on its advances is published: "'Advances in total scattering analysis'" (Proffen and Kim 2009) or "'Advances in Pair Distribution Profile Fitting in Alloys in Local Structure from Diffraction'" (Thorpe 1998). Going along with this, first tips on PDF-refinement strategies came to be published ('Structural analysis of complex materials using the atomic pair distribution function—A practical guide' - Proffen et al. 2003), which already exist for the analysis of scattering data from crystalline powders e.g. in the form of the "'Rietveld refinement guidelines'" (McCusker et al. 1999). Toby and Billinge (2004) performed some work on the "'Determination of standard uncertainties in fits to pair distribution functions'" and Peterson et al. (2003) also "'Improved measures of quality for the atomic pair distribution function'".

2.2.2 PDF for unique structure identification

The possibility of identifying or distinguishing different (amorphous) compounds has already been mentioned in Klug and Alexander (1974, p. 847) with a short discussion of general drawbacks of this method. The tenor in some actual literature is that the PDF is suitable for fingerprinting (Billinge et al. 2010; Davis 2011; Dykhne et al. 2011). As fingerprints are in principle unique, those statements are interpreted that identification is possible in every case. Following this interpretation, it becomes unclear if these authors took into account the phenomenon of homometry (Ravy 2013). Further, Klug and Alexander (1974, p. 851) documented cases where substances could not be distinguished by means of the PDF but via the reduced scattering function $S(Q)$. They report that *this apparently anomalous phenomenon appears to result from the fact that small structural modifications tend to produce differences localized in one part of the intensity curve, which make them more obvious.*.

2.2.3 Intermolecular interactions

Going further, Prill et al. (2015), Rademacher et al. (2012) and Thorpe et al. (2002) published on analyses of molecular compounds and about describing intermolecular interactions. Besides that some reciprocal space approaches for elucidation of intermolecular interactions are proposed (Mou et al. 2015).

2.2.4 Nanoparticles and amorphous structures - estimating the baseline of the PDF

For usual PDF-simulations of an infinitely extended (very large) material the assumption of a homogeneous density, where features are averaged out at large distances from the summation-center, works to obtain an appropriate PDF-baseline. A (nano-)particle does not satisfy this condition. There are no large interatomic distances. That means that incorporating a term similar to $-4\pi r\rho_0$ is not useful.

Great work has been done by Harrington et al. 2012; Korsunskiy and Neder 2005; Korsunskiy et al. 2003; Korsunskiy et al. 2007; Neder and Korsunskiy 2005 which applied a seemingly robust approach for baseline approximation (shown in figure 2.7). A polynomial is fitted into the coarse slope of the experimental PDF. This polynomial is subtracted from the calculated PDF to approximate the correct baseline (see some discussion of that also in Farrow and Billinge 2009). Another approach is to multiply bulk-PDFs with a shape function (see e.g. Page et al. 2011).

A further difficult task connected with PDF-simulation are conglomerates of objects with little extension. Farrow and Billinge (2009) tried to get estimates from the small angle scattering signal.

2.2.5 Recent approaches to data correction for inelastic scattering

"*In many diffraction studies, it is necessary to correct the intensities of the Bragg peaks for a variety of inelastic scattering processes. Compton scattering is only one of the incoherent processes although the term is often used loosely*

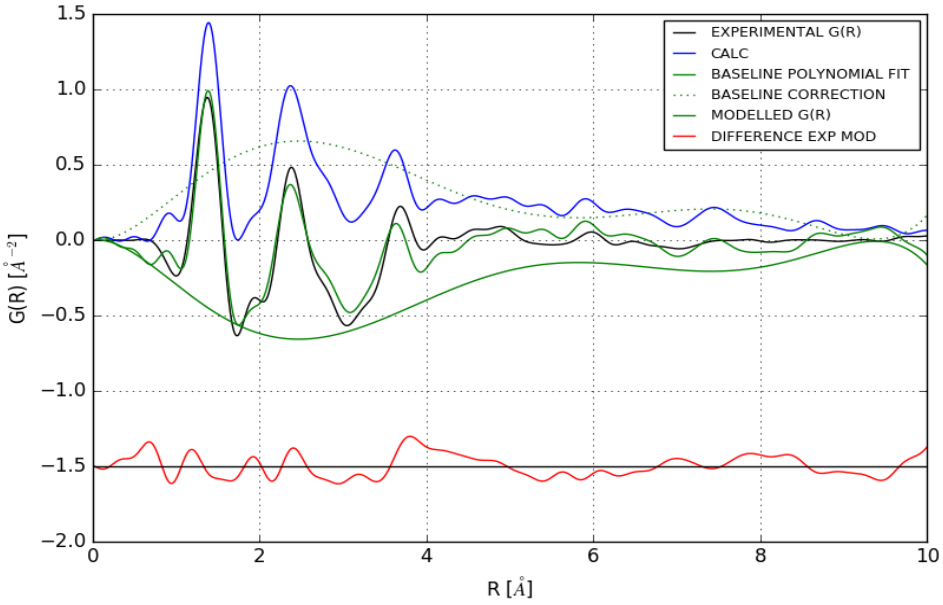

Figure 2.7: Example for the estimation of the baseline of a material with weak long-range correlation (here: amorphous organic solid). A polynomial fit (green line) through the experimental PDF is performed. The polynomial is inverted (dotted line) and subtracted from the calculated PDF to obtain the modeled PDF. The red line at the bottom is the difference curve between the final PDF and the measured one.

to include plasmon, Raman, and resonant Raman scattering all of which may occur in addition to the more familiar fluorescence radiation and thermal diffuse scattering [...] the dominance of each interaction is characterized by the energy and momentum transfer and the relevant binding energy." (Alexandropoulos et al. 2006)

In a very recent software for data correction all necessary data correction steps are handled by an user-defined ad-hoc polynomial (Billinge and Farrow 2013; Juhás et al. 2013. This possibility was already outlined by Klug and Alexander (1974)). It is declared to be a robust procedure giving stable results. This is justified by showing the good agreement of the data obtained with older procedures. It is an interesting question if showing similarities can be a proof. The program is written in order of easy operation for laymen and other novice users. — Using an ad-hoc polynomial itself is justified by claiming the slow and continuous change of non-sample related signals in the raw-intensities. It should be considered that "*With the exception of thermal diffuse scattering, which is known to peak at the reciprocal-lattice points, the incoherent background varies smoothly through reciprocal space. It can be removed with a linear interpolation under the sharp Bragg peaks and without any energy analysis.* ***On the other hand, in non-crystalline material, the elastic scattering is also diffused throughout reciprocal space; the point-by-point correction is consequently larger and without energy analysis it cannot be made empirically; it must be calculated. These calculations are [mostly] imprecise*** [...]" (Alexandropoulos et al. 2006)

Therefore, things would ease if energy dispersive detectors could be used as inelastic scattering must be subtracted and how is not necessarily known. In addition, collecting purely elastic scattering apparently is only possible in very unusual experiments and a sharp collection of only elastically scattered photons is difficult (Toby and Egami 1992).

2.2.6 Influences of the instrumental setup on the PDF

There have been some investigations on the effects of peak shapes and similar on the PDF (see e.g. Qiu et al. 2004 or Jeong et al. 2005). As instrumental effects

are not taken into account by corrections in most cases, some parameters have to be introduced to account for those effects. Toby and Egami (1992) state that because of the limited angular resolution, the experimental PDF is multiplied with a Gaussian damping $exp[-\frac{1}{2}r^2\sigma_Q^2]$. Secondly, an r-dependent broadening of the PDF-peaks, also stemming from limited instrumental Q-resolution, should be accounted for with the expression $\alpha^2 r_{ij}^2$ (Neder and Proffen 2008). Farrow et al. (2007) state that this broadening stems from increased noise at high Q. Sometimes the variables σ_Q and α are also referred to as Q_{damp} and Q_{broad}. In section 2.3.1 the incorporation of those parameters into the calculated PDF will be discussed.

Some postulate that instrumental effects are not influencing the PDF or that influences are at least not crucial to it (Egami and Billinge 2003, p. 173). Others simply propose using an instrument which shows a minimal amount of such effects in the measured data (Bordet 2015, p. 9).

2.3 Modeling and refinement

To extract structural details, a model has to be generated and refined. In this section, aspects concerning PDF-generation and structure solution are discussed. — The approach common to all modeling procedures is to calculate the PDF for an ensemble of atoms. In order to do so, all interatomic distances must be computed which results in a distribution. Each interatomic distance is weighted by the $f_i(Q)$ for each atom as discussed in the derivaton of the PDF further above. There are two options then to proceed from this distribution - PDF-creation by altering this distribution with parameters or calculating a diffractogram from it and yielding the PDF via FT from it - which will be discussed below.

The parametrization (e.g. the choice of displacement parameters) can be dependent on the choice of the model's size (big box modeling where displaced atoms are modified by a parameter for thermal motion or not at all if the box is very big vs. small box modeling where such a displacement parameter might describe also static disorder).

2.3.1 Traditional approach to PDF-modeling: altering the pair distribution

- incorporating thermal motion and correlation

To incorporate the broadening effects of PDF-peaks due to thermal motion, mostly one of the following approaches is applied: a) creation of a model with a large number of atoms where each atom is given random displacements to account for (static displacement and) thermal motion (big box). b) the PDF from a relatively small model is convoluted with a Gaussian broadening function after computation of the distribution.

Method b for the PDF-modeling (of crystalline materials) is a computational less demanding simulation method. Further, it eases analysis because local distortions are not masked by random displacements that should simulate thermal displacements.

The choice of the best method to model thermal motion appears to be an empirical. For the convolution approach, the delta function in equation 2.1 is replaced by a Gaussian $T_{ij}(r)$ so that equation 2.24 is obtained. This is discussed in more depth in Neder and Proffen (2008, p. 45) or Thorpe et al. (2002).

$$G_{calc}(r) = \frac{1}{r}\sum_{i}^{i\neq j}\sum_{j}\left[\frac{f_i(Q)f_j(Q)}{\langle f(Q)\rangle^2}T_{ij}(r)\right] - 4\pi r\rho_0 \tag{2.24}$$

$$T_{ij}(r) = \frac{1}{\sqrt{2\pi}\sigma_{ij}(r)}\exp\left[-\frac{(r-r_{ij})^2}{2\sigma_{ij}^2(r)}\right] \tag{2.25}$$

The width of the function $T_{ij}(r)$ is given by the atomic displacement parameters, U, of atoms i and j. In the formalism, the expression $\sigma_{ij}(r) = \sqrt{\sigma_{ij}'^2 - \frac{\delta}{r_{ij}^2} - \frac{\gamma}{r_{ij}}}$ also accounts for correlated motion of atoms (which is r-dependent) via the parameters γ and δ. It is possible, that the first neighbour-peaks sharpen if they are vibrating in phase. It is not fully clear from literature when to apply γ or δ or both, it is mostly advised to take the parameter that gives the best fit. Sometimes, the choice of γ or δ is related to the Debye-temperature of the material, so that δ is used if the measurement happened at a temperature below and γ if it happened above the Debye temperature (Jeong et al. (2003) and

Jeong et al. (1999) try to elaborate on this). It is possible to sophisticate those expressions at will and some expression are given in Jeong et al. (2003), Neder and Proffen (2008) and Thorpe et al. (2002).

- instrumental effects

In terms of a PDF, Toby and Egami (1992) write that firstly, because of the limited angular resolution, the experimental PDF experiences a damping which is resembled by the expression $exp[-\frac{1}{2}r^2\sigma_Q^2]$. Secondly, a broadening of the PDF-peaks stemming from limited instrumental resolution in Q-space is said to be accounted for within the expression for thermal motion $\sigma_{ij}(r) = \sqrt{\sigma_{ij}'^2 + \alpha^2 r_{ij}^2}$ (Neder and Proffen 2008).

- measurement range

The calculated PDF is convoluted with $W(r)$, the sine-transformed of the step function for consideration of the integration limits. Further, termination ripples have to be accounted for. (See section 2.1.5 for both.)

- baseline of the PDF

A discussion on the factors influencing the baseline of the PDF can be found in section 2.2.4.

2.3.2 PDF-creation by FT of a calculated diffractogram

Direct calculation of the PDF has often been the method of choice, since it is a relatively fast process. In the second variant, Calculating a diffraction pattern is a computational expensive task and also FT takes time.

But since, of course, the PDF is determined by the scattering curve, using a diffractogram has some benefits, because some features need not to be accounted for. Further, recent approaches (see e.g. Cervellino et al. (2006)) give an example of optimising data handling and faster calculation of diffraction patterns according to the Debye formula. Also calculations on GPUs are an option (Gelisio et al. 2010). (See also Leonardi and Bish (2016)).

- benefits of this method of PDF-creation

A benefit of FTing reciprocal space data is the automatic incorporation of termination ripples and broadening due to the extension of the measurement range.

As data are often interpolated from an equidistant 2θ-grid to an equidistant Q-grid, effects from this procedure could be incorporated into a PDF. The practice of interpolation of the Q-axis to get an evenly spaced interval which is needed for certain mathematical treatments such as FFT (fast Fourier transformation) is discussed in section 5.1.1. Also, effects stemming from data corrections and modifications as well as noise might be incorporated easier by the "FT-approach" than directly adding them to the PDF. If the small angle signal is correctly incorporated, no algorithm for baseline-estimation is necessary.

Eventually, instrumental effects can be considered easily. Zuev (2006) and Ida and Toraya (2002) give procedures for calculating and convolving or deconvoluting instrumental profiles from powder-scattering data.

As the PDF is obtained by FT from a diffractogram, effects stemming from temperature or "disorder" have to be accounted before the diffractogram is calculated.

- incorporation of thermal motion into diffractograms

Thermal diffuse scattering (TDS) in X-ray powder-diffraction patterns produces a non-uniform background, as in the single-crystal case. To great amount, it peaks sharply at the positions of the Bragg reflections (one-phonon scattering by the acoustic modes) and because of this concentration around the Bragg-peaks a large part of the TDS cannot be corrected easily for. TDS often contributes 10% or more, also less, depending on the chosen instrumental setup (big contribution by selection of the primary radiation) and sample at hand (Alexandropoulos et al. 2006; Beyerlein et al. 2012) to the overall intensity.

A rough approach for accounting TDS from thermal motion of atoms is adding a term (1 - DWF) (see e.g. Lipkin (2004)) given by equation 2.26. It should be noted that static disorder is not intended to be modeled in this case as static disorder should already be sufficiently well described by the model. As,

especially in case of disorder, the thermal motion can be an directional quantity for each atom, this DWF description (which usually accounts for static and dynamic effects) is an approximation which might be strongly imperfect.

$$\mathrm{TDS}(Q) = 1 - \exp^{-Q^2\langle|\mathbf{u}|^2\rangle} = 1 - \exp^{-Q^2U} = 1 - \mathrm{DWF}(Q) \tag{2.26}$$

$$S(Q) = \frac{I(Q)}{f_0^2(Q)} \frac{\sum(\mathrm{DWF}(Q)Q)}{\sum\left(\frac{I(Q)}{f_0^2(Q)}Q\right)} + \mathrm{TDS}(Q) \tag{2.27}$$

u is a displacement vector and U is an isotropic mean-square displacement given in [Å^2] (Trueblood et al. 1996). U is linked with the isotropic thermal coefficient B by $B = 8\pi^2U$. The term TDS in equation 2.26 describes the broadly distributed part of thermal diffuse scattering. This equation does not describe the peaked phonon scattering. Thus it is no surprise that there are no sharp peaks in $F(Q)$ (figure 2.8)! Thus, also the PDFs in figure 2.8 show little effects of the TDS. This approximation is a very basic one and should be applied only if the influences of the TDS are very mild. This conforms to the findings of Beyerlein et al. (2012), who analysed the suitability of the DWF-approximation in nano-materials.

2.3.3 Structure refinement by aid of the PDF (PDF-refinement)

In many cases it is necessary to achieve a model via a refinement routine. There are numerous programs to do so. In principle, all approaches which alter coordinates of atoms in a structural model can be applied in PDF-refinements. The difficulty is to find a suitable modeling approach and to apply the refinement algorithm in a proper way to get models with physical meaning. - The optimization process in PDF-refinements is driven by comparison and minimization of the differences between calculated and experimental properties ($G_{calc}(r)$ against $G_{exp}(r)$). It is possible to refine different quantities with one model in addition, such as the XAFS (X-ray absorption fine structure), electronic DOS (density of states) or vibrational spectroscopy spectra.

Some example of modeling approaches are: something that has been named real-space-Rietveld refinement, which optimizes structural parameters in a

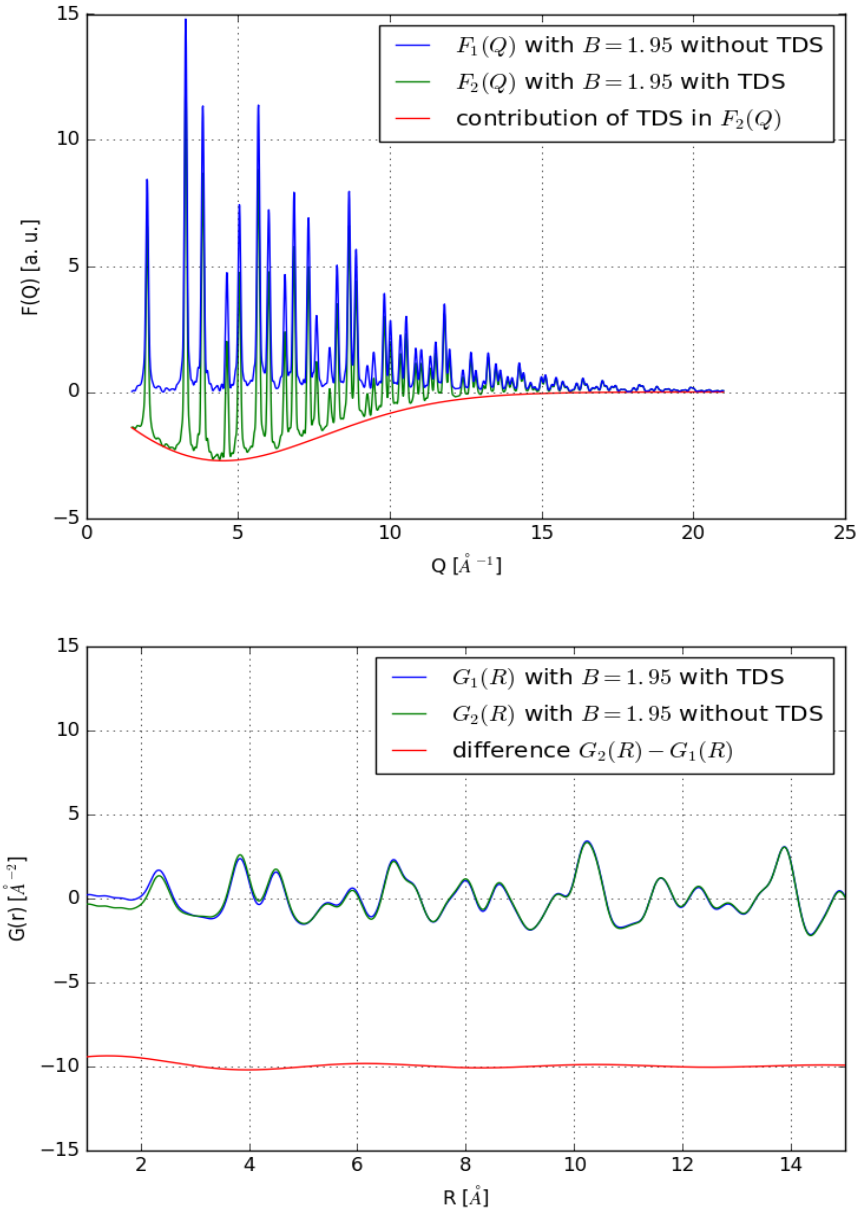

Figure 2.8: Comparison of thermal diffuse scattering in $F(Q)$ and $G(r)$ by the DWF approximation: In the lower figure the pair of curves on top gives a comparison of $G(r)$ calculated with and without TDS with $B = 1.95$, where $B = 8\pi^2 U$. The corresponding difference curve is drawn below. The effects introduced by this approximation are so mild that they could be confused with termination ripples caused by Q_{min}.

least-squares algorithm. Differential-evolutionary algorithms as implemented in DIFFEV in the DISCUS_SUITE are used for systematic alteration of structural models on a larger scope and potential parameter space. Also empirical-potential-based refinements, molecular dynamics (MD), Monte Carlo (MC) reverse Monte Carlo (RMC), density-functional-theory (DFT) can be used for structural evolution in the model. (See e.g. Young and Goodwin 2011, Neder and Proffen 1997, Juhás et al. 2006; Juhás et al. 2008; Juhas et al. 2010, Cliffe and Goodwin 2013). As one can imagine, not all methods are applicable for each question at hand. Some, e.g. MD, DFT or empirical potentials for structural relaxation, might be used as separate techniques or applied locally to correct structural properties in a specified step of a refinement cycle.

2.4 Critical remarks related to PDF-methodology

Unfortunately, only few articles are concerned with the general limits of extraction of structure information via the PDF-method. - What has been done up to now to "prove" the suitability of the "PDF-method" and the corrections applied, is comparisons of RDF-data of simple substances, like fcc-Ni, which has one kind of atom and is strictly ordered (eg Juhás et al. 2013).

From what is presented and communicated, the impression emerges that the PDF is a robust tool for probing and getting exact information on local environments (Billinge 2013; Billinge and Kwei 1996; Billinge et al. 2000a; Billinge et al. 2000b; Proffen and Billinge 2002). But the PDF can at most give the information that the total-raw-scattering data themselves can give, which is average information from the probed volume. - Modulo artefacts from Fourier transformation and alterations caused by data corrections and a baseline of the F(Q)-curve that does not converge to 0. - Also we do not know if we measure a sample with a representative distribution of building units. (As a tool for really probing local environment, one could use a HRTEM (high-resolution transmission electron microscopy) or related, as done in Yang et al. (2002).)

2.4.1 General assertions about PDF-analysis in literature

More and more authors claim to be able not only to extract qualitative information (which is a difficult task by itself) such as analysis of thin films without geometrical corrections (Jensen et al. 2015) but also quantitative (e.g. Abeykoon et al. 2012; Davis et al. 2013; Farrow et al. 2010; Masadeh et al. 2007; Paglia et al. 2006) by analysis of total-scattering data and their RDF-derivatives. Also polyphasic materials such as a zeolite with CdSe inclusions in Abeykoon et al. (2008) are treated. Also, the PDF has been presented as **the** means of choice for investigating nano-particles of all sorts (Billinge 2013 - "'Materials science: Nanoparticle structures served up on a tray'").

Sometimes, difficulties in distinguishing the origin of certain signal are mentioned while nevertheless stating that the method is capable of solving all issues. See for example Proffen et al. (2005) who state that "One problem, however, especially in more complex systems is to answer the question *if certain features observed in the PDF indeed point to an amorphous contribution or [if they are] in fact related to disorder in the crystalline phase*". They continues that "[...]Finally [they] like to draw the readers attention to *the fact that total scattering or the PDF technique provide a method to unravel the atomic structure of materials ranging from liquids, over glasses to disordered crystalline materials as well as mixtures.*

Despite continued research on diverse topics concerning the quality and reliability of the PDF-method as was discussed in section 2.2, some authors assert that "*G(r) is barely influenced by diffraction optics and experimental factors since these are accounted for in the step of extracting the coherent intensities from the raw diffraction data. This renders the PDF a structure-dependent quantity only.*"(Saravanan and Rani (2011)).

2.4.2 Assertions about phonons in (1D-)PDF-literature

Even though this section focuses on the one-dimensional PDF, some of the arguments also apply to classical (three-dimensional diffraction pattern) crystallography.

In important PDF-literature (Egami and Billinge 2003, p. 32) it is stated that "*this term* [rem: 1 - DWF] *approximately "describes the diffuse inelastic scattering intensity due to phonons.* They write further that *a significant proportion of the total integrated intensity [...] and is too often disregarded.* Further "*[t]he Debye-Waller factor reduces the intensities of the Bragg scattering but where does the lost intensity go? It appears in between the Bragg peaks and becomes what is called diffuse scattering.*" This last, very general statement might be true, anyway, Beyerlein et al. (2012) state that it is difficult to account for the TDS which often shows directional dependence in reciprocal space. This implies that a DWF does not suffice.

It is not mentioned that it is only elastic and quasi-elastic scattering we should use for creating a diffractogram which is normalised to a Q-grid. TDS is "pseudo-elastic" only in the X-ray case and this practice is prohibited e.g. for conventional neutron scattering. Additionally, we have no guarantee if the treatment for the separation of the Q-dependent atomic form factors to obtain $\rho(r)$ is valid for the scattering from phonons.

In another publication it is asserted that corrections for thermal effects have not been performed, because: it contains valuable information (Thorpe (1998, p. 162)). In addition, it should be noted, they are also not corrected for, because to correct for them would mean to know how the contributions look like and then much of the phonons is already known. - And in the single crystal case it is even possible to evaluate a correction factor for the TDS. But to calculate properly the phonons' contributions, we require a knowledge of the lattice dynamics of the crystal and not just its elastic properties and this we don't get from powder data. This is one reason why relatively little progress has been made in calculating the X-ray correction factor for (and information on phonons from) powders (Alexandropoulos et al. 2006, p. 657).

2.4.3 Issues concerning the extraction of information

As due to instrumental restrictions low-Q-data are often missing, concepts for estimating those are discussed in literature (Olds et al. 2015). Leadbetter and Wright (1972), Pusztai et al. (2008), Wright et al. (2001) and Wright (1993)

evaluated obstacles to structure extraction from scattering and PDF data. Soper (2007) and Soper (2013) investigated "'On the uniqueness of structure extracted from diffraction experiments on liquids and glasses'" and "'The radial distribution functions of water as derived from radiation total scattering experiments: is there anything we can say for sure?'". Hamad and Mansoori (1989) and Mansoori (1993) about radial distribution function methodology related to mixtures of liquids.

Problems concerning the accuracy of the methods discussed are occurring already in simulation of simple liquids and some discussion on where those could emerge from is gven in Van Houteghem et al. (2014) ('Critical analysis of the accuracy of models predicting or extracting liquid structure information'). They "tried to highlight the origin of errors by a detailed comparison of the experimental data with accurate ab initio MD." Their "*conclusion is that the experimentally derived properties are prone to large artifacts*" and that in order "*to improve the reliability of the experimentally derived properties, we need an unbiased model-independent intermolecular total SF without the help of interatomic potentials. The lack of such a bias free quantity hinders a fully reliable comparison with theory.*"

Beyerlein (2013) "[...]demonstrated that the technique of Debye function analysis [rem: and therefore PDF-analysis?] is best suited for systems with only a few possible atomic arrangements." Further important aspects are discussed for example in Gibson (2007) - "'Understanding the limits of pair-distribution functions for nanoscale correlation function measurement'".

2.4.4 PDF for multiphasic materials?

Proffen et al. (2005), for example, did some analysis of an amorphous phase within an engineering material which had different composition. As experienced researchers, they may be aware when the PDF method can be applied. - In general, the PDF method is not valid for the analysis of polyphasic materials. An exception might be made for polymorphic phases that exhibit the same composition, although here the question arises how the baseline-estimation should be performed.

In general, in phase-mixtures intensities from the phases are additive in reciprocal space but stem from independent domains. Any reduction procedure must transform the intensities. As it is impossible to separate intensities without prior knowledge of their origin, no correct treatment can be performed before information of the sample's structure has been elucidated. The potential error that emerges from wrong treatment of intensities cannot be estimated. Currently, verificative calculations concerning the amounts of error in treating polyphasic materials are attempted.

2.5 Conclusions

What we can recognise up to now is that data transformation and maybe also correction can be quite tricky and prone to errors. For example, strong approximations are made in data treatment, if atoms with (strongly) differing scattering behavior are contained in a sample. - An important result might be the remark that we could get rid of potential artefacts that are introduced in PDF creation from raw data if we use a different approach of modeling: calculated scattering which that are reduced in the same way as the raw data and then sine-Fourier transformed to a PDF. This would assure having the same artefacts in the experimentally derived and calculated curves. What is then left is to correctly interpret structural features.

To end this chapter, it remains to say that up to now, it is an important question which status the interpretation of PDFs should be assigned to. Is it quantitative information one gets or is one stuck with purely qualitative information about changes and occurrence of interatomic distances in a given specimen? — If we are dealing with ensembles of particles, a bundle of interesting questions arises, for example: How to account for all this objects. What if different objects express a different density and what if different objects exhibit different absorption behavior. Many propositions in the PDF-literature appear like mere statements of opinions. It is to be seen if that is the beginning of a trend of overestimation of the capabilities of a method and if critical voices will be considered.

If it turns out in the end that the PDF really can be a suitable crystallographic tool, it might be better to use the following formula for $G(r)$. It is $G(r)$, defined as the reduced and normalised radial distribution function which is yielded by sine-Fourier transformation of a scattering function $i(Q)$, as introduced by equations 2.20 and 2.21. It is no necessary to artificially create a function $S(Q) - 1$ for the sake of satisfying the equation for the one-atom case. If calculated, $i(Q)$ is a diffraction pattern which describes the full intensity in the measurement range (maybe even including the SAS-signal) and is reduced and sine-transformed to the PDF in the same was as the experimental data are. -

$$G(r) = 4\pi r\rho(r)_{direct} = \frac{2}{\pi}\int_{Q_{min}}^{Q_{max}} Qi(Q)\sin(Qr)dQ \tag{2.28}$$

By such a method, no need for introducing a density ρ_0 remains and also mathematical artefacts will be directly included. Further, no need for evaluating a suitable baseline emerges because the shape of the baseline will readily be defined by the FT. In parallel, we then also should consider a different scheme of correcting data.

Chapter 3

Investigation of non sample related information

What follows is an overview of theoretical and practical aspects concerning creation and evaluation of PDFs. Although ample literature on direct-space-approaches has been published, calculating PDFs from scattering data seems to be highly subjective. It is not only corrections for well-understood effects (such as Compton-scattering, angle dependent polarisation, absorption and geometrical corrections) that have to be considered. Other influences, such as scattering by phonons, sample misalignment, and influences of the intensity-value at Q_{max} are not easily determinable or not determinable at all such as noise, stray radiation, complex absorption effects that cannot be accounted for by a (simple) algorithm.

- details on exemplary calculations in this chapter

For the theoretical investigations, PDFs were created by FT of a calculated diffraction pattern. A Si-supercell consisting of 10x10x10 unit-cells of crystalline silicon was chosen as a model system (using the formalism in section 2.3.2). Integration limits have been taken from 1.5 to 21.0 Å^{-1}. 21 Å^{-1} were chosen as the upper limit because it is a high value experimentally achievable with Ag-radiation and a routinge measurement up to $2\theta = 150°$. 1.5 Å^{-1} was chosen as the lower limit because the Debye scattering equation is not well suited for the calculation of small angle scattering signal of a realistic system as it leaves out interaction between particles and because this is the lower experimental limit in many cases.

3.1 Influences owing to the experimental setup

Literature usually gives the impression that effects owing to the instrumental setup can be neglected or accounted via some damping or broadening terms in PDF analysis, e.g. Q_{damp} or Q_{broad}. Only few authors talk about them at all (Bordet 2015; Egami and Billinge 2003; Toby and Egami 1992) or made investigations (Jeong et al. 2005). General discussions of those effects in scattering data is given by Cervellino et al. (2005) or Ida and Toraya (2002).

Figure 3.1 shows a refinement of the diffractogram of a silicon sample with GSAS-II (Toby and Von Dreele 2013). It was measured with a PANalytical Empyrean laboratory diffractometer located using Ag-radiation. The radiation was filtered with a Rh-foil to remove a large amount of K_β radiation. A long tail of Bremsstrahlung that could not be removed by the filter is located around every peak and the profile-parameters could not be evaluated satisfactorily. The crucial point here is not to "satisfactorily" evaluate the Caglioti UVW-parameters. What it shows is that the calculated diffractogram differs from the experimental and that the theory applied is not sufficient for a full description. We must account e.g. for peaktails and parameters influencing peak-shapes. The current practice is to evaluate a Q_{damp} and Q_{broad} that damp and broaden the experimental PDF (see section 2.2.6). Up to now, we have no convincing reason to believe that the influence of instrumental effects on extractable structural information from PDF will behave differently, i.e. less complex, than from scattering data since the PDF is derived from the scattering data. Therefore, we have to investigate models and where the effects in real space are precisely found.

Firstly, comparisons concerning influences of the instrumental profile and disorder were performed to determine if they can be differentiated. To introduce disorder into a 10x10x10-Si-supercell, all atoms were given small random displacements from their initial position, which were in the limit of the atoms' U-values. An instrumental profile was superimposed by invoking the following commands in the powder-menu of the DISCUS software: set profile, pseudo (setting the peak profile as pseudo-Voigt); set profile, eta, 0.634 (setting the ratio of Gaussian and Lorentzian contribution for each peak); set profile, uvw, 0, 0, 0.015 (defining Cagliotti UVW parameters); set profile, asym, 0.015, 0.001, 0.0055, 0.0 (defining an asymmetric peak shape)

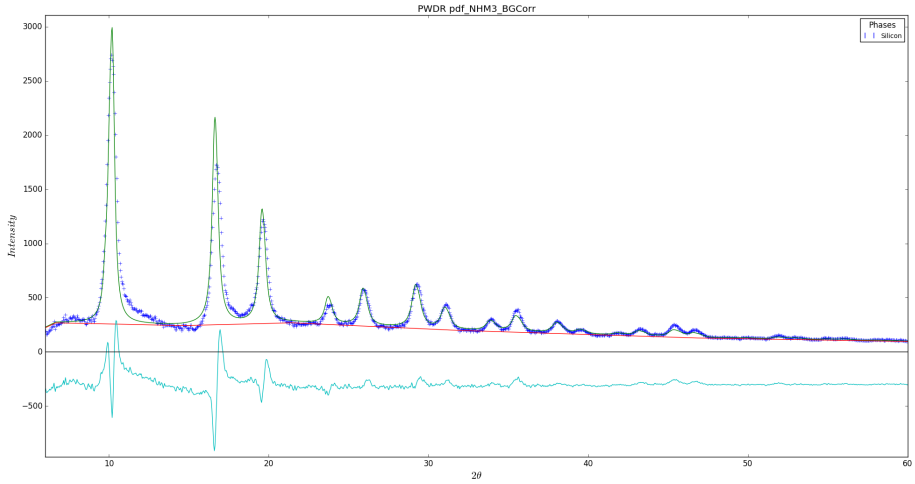

Figure 3.1: Rietveld-refinement to obtain the UVW-parameters for a laboratory device from a Si-sample with the GSASII-software. The profile is not fit well in reciprocal space with the parameters U, V, W and it is expected that 2 parameters (Q_{broad} and Q_{damp}) for a refinement in real-space will be also insufficient.

Figure 3.2 shows the diffractograms for an undistorted and a distorded Si-supercells, where each diffractogram was modified by an instrumental function in addition, thus resulting in four diffractograms. Figure 3.3 gives pairwise comparisons of the PDFs obtained from these the diffractograms. It suggests that the effects of the instrumental function are more than just a broadening and dampening, as visible e.g. in the first comparison in the region from 5 to 6.5 Å. There the curve with an instrumental effect added (red) has a bigger amplitude tan the unmodified PDF (blue). In a refinement this might lead e.g. to an ordered material being mistaken as disordered. The correct evaluation of the impact of the instrumental setup on the shape of the PDF remains a question to be solved. This finding opposes Qiu et al. (2004), who note that the Q *dependence of the instrument resolution is expected to result in an r-dependent broadening in the PDF peaks as well as a loss of intensity at high r* (Leoni M., Hans P. (2018) in preparation).

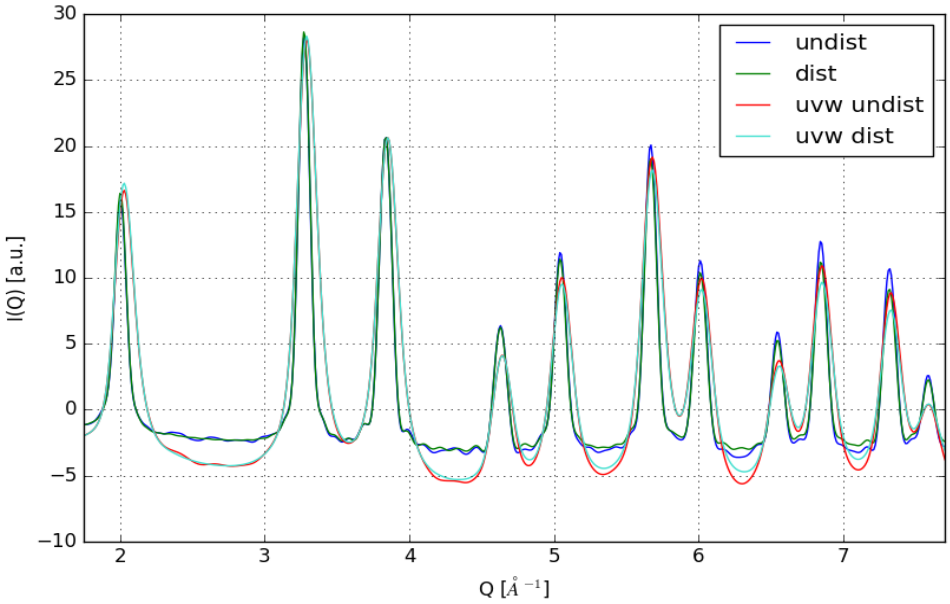

Figure 3.2: Comparison of four diffractograms for 10x10x10 Si-supercells. a) undistorted, b) distorted, c) undistorted with and altered by an instrumental profile function, d) distorted with and altered by an instrumental profile function.

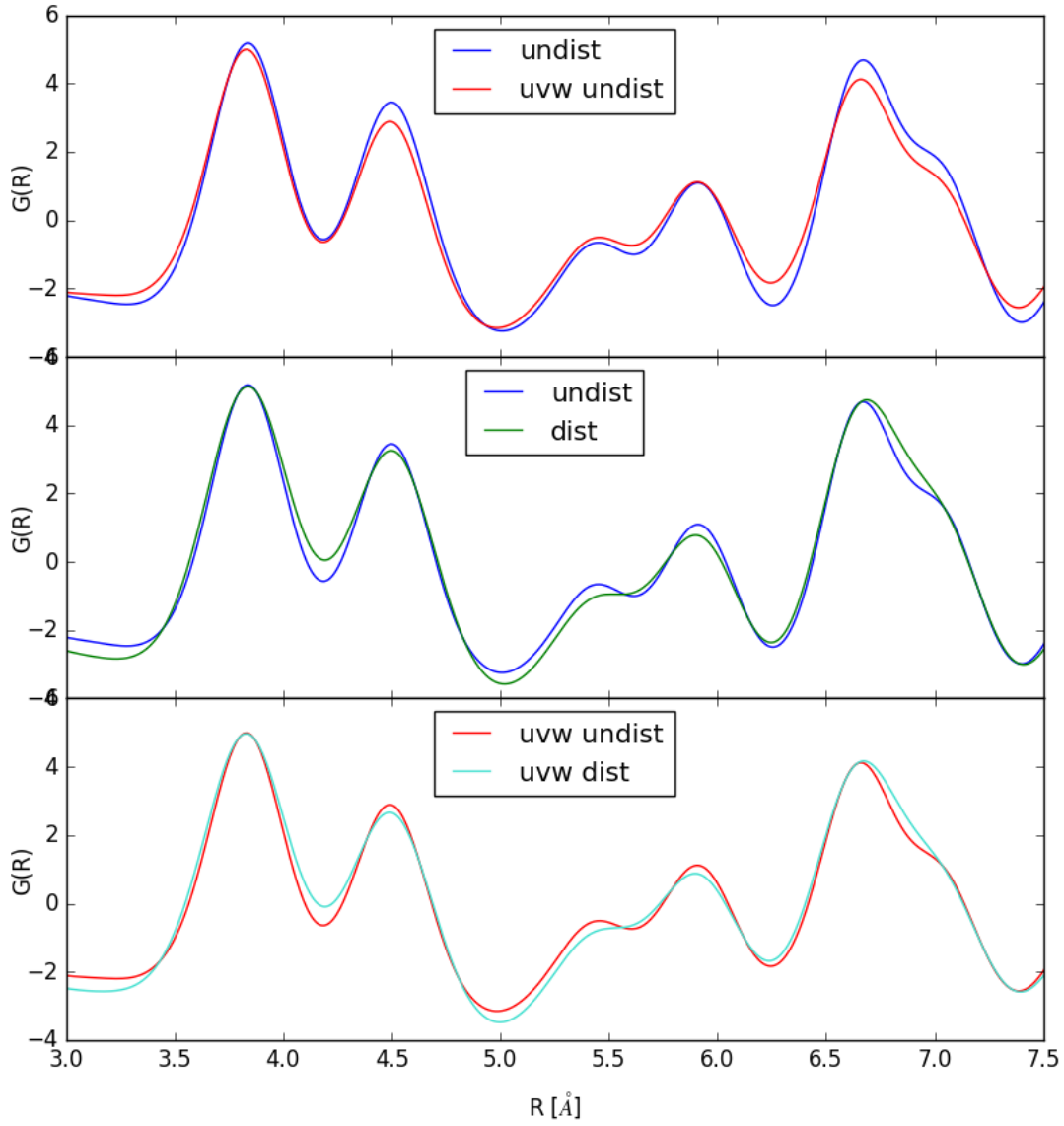

Figure 3.3: $G(R)$**-curves resulting from figure 3.2.**

3.2 Effects of non-monochromaticity

Secondly, the influences of deviations from monochromatic radiation on $G(R)$ were investigated. In many laboratory diffractometers we do not have pure $K_{\alpha 1}$-radiation. Filtered radiation still contains $K_{\alpha 2}$ radiation, often Bremsstrahlung, maybe K_{β}.

An experimental diffractogram versus 2θ collected with polychromatic radiation ($K_{\alpha 1} \approx 55.5\%$, $K_{\alpha 2} \approx 27.7\%$, $K_{\beta} \approx 16.6\%$) was simulated. Figure 3.4 shows the corresponding $S(Q)$ curves where the 2θ-scale has been transformed to the Q-scale by using $K_{\alpha 1}$ and a comparison with an $S(Q)$ from monochromatic radiation.

Figure 3.5 shows the corresponding PDFs obtained from scattering data with a monochromatic radiation and strongly polychromatic. Deviations from monochromaticity apparently shift peak maxima, further they introduce artefacts into the PDF in form of altered peak shapes and possible additional peaks. Soper and Barney (2011) studied the extraction of PDF-data from scattering data obtained with white-beam-radiation.

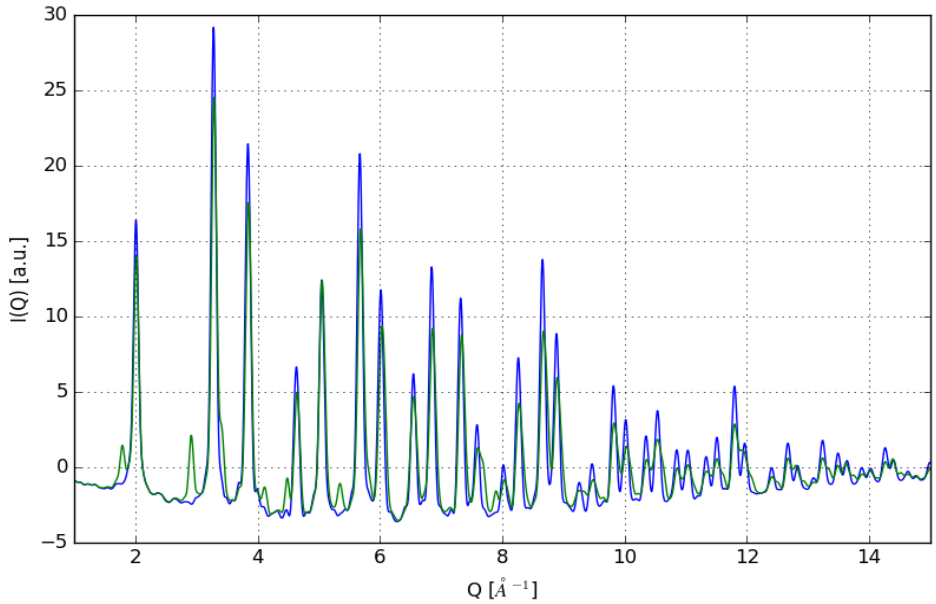

Figure 3.4: A comparison of the modeled F(Q)-curves for monochromatic and polychromatic raw-intensities obtained from scattering of Ag-radiation by Si. F(Q) mono was calculated with pure $K_{\alpha 1}$. For the non-monochromatic radiation a model composition of $K_{\alpha 1} \approx 55.5\%$, $K_{\alpha 2} \approx 27.7\%$, $K_{\beta} \approx 16.6\%$ was chosen.

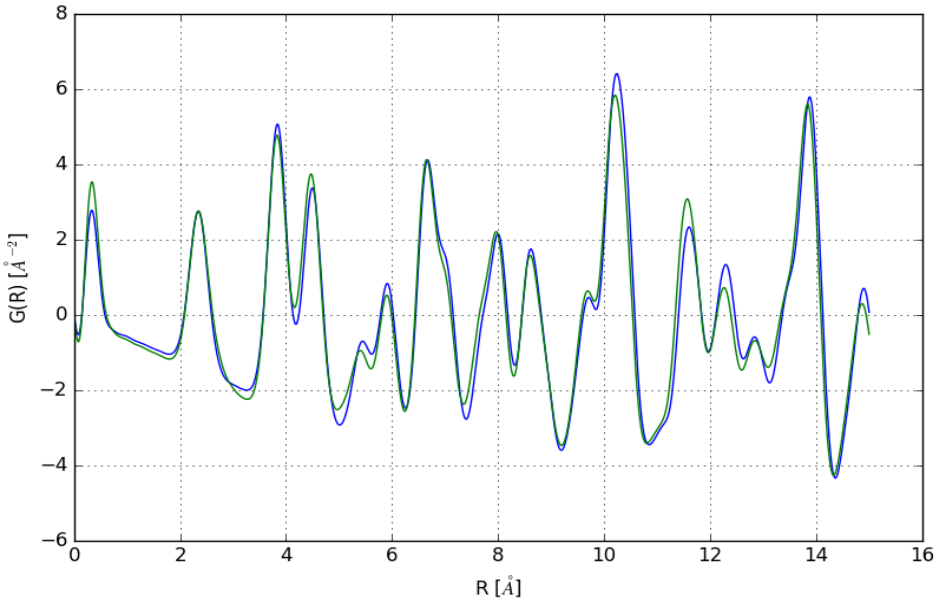

Figure 3.5: Comparison of FTs of monochromatic and non-monochromatic $F(Q)$s. Obviously, non-monochromaticity of the radiation has effects that should be considered in analysis

3.3 Influence of noise

Thirdly, a study on the influence of noise (electronic and thermal fluctuations) was done by means of theoretical data. For taking into account noise we can start from ideal, monochromatic scattering data that do not contain noise.

Raw intensities have positive contributions only and also noise can lead only to a positive detector response. Going along with the angle-dependent decay of scattering, noise in the diffractogram increases. The noise is related to detector counting statistics. It should be a Poisson noise but the Gaussian models it pretty well for sufficiently high counts. The noise level in this example was chosen to be 0.05 % of the maximum intensity of $I(Q)$.

For the study, a function ζ_n was created by taking the absolute of a Gaussian noise multiplied with the reciprocal of the mean atomic scattering factor so that $\zeta_n = |noise| * 1/f^2_{0\_Si}$. To account for the alteration of the baseline due to the additional contribution of the noise, a second function $\zeta_s = 0.5 * 1/f^2_{0\_Si}$ was defined. The noise-functions ζ_n and ζ_s were added to the raw intensities $I(Q)$ to obtain functions $I_n(Q)$ and $I_s(Q)$. If ζ_s is subtracted from the noisy diffractogram $I_n(Q)$, the resulting diffractogram $I_{ns}(Q)$ oscillates around zero at high scattering angles. From the modified raw intensites, the respective $F(Q)$s were calculated.

Figure 3.6 shows the modeled functions $F(Q)$, $F_n(Q)$ and $F_s(Q)$ of the Si-supercell. Figure 3.7 shows $F_n(Q)$ and $F_{ns}(Q)$ (the curve of the noisy diffractogram minus the slope of the noise). By the transformation from $I(Q)$ to $F(Q)$ the noise is strongly amplified.

Figure 3.8 shows the PDFs corresponding to figure 3.7. As can be seen, there is a strong effect in $G_n(r)$ that is characterized by very pronounced ripples in the front region and continuously smaller ripples with increasing r. A similar effect is present in $G_s(r)$ but not in $G_{ns}(r)$. This is evidence that, in sufficiently low amounts, not the noise but the deviation from the baseline of $F(Q)$ is negatively influencing $G(r)$. After subtraction of the "slope" of the noise in reciprocal space, the effects of noise, although prominent in the scattering-signal, are almost eliminated. The difference curve between $G_{ns}(r)$ and $G(r)$ emphasizes this. The

investigation shows that subtraction of a well suited function (best done after physical meaningful data correction) could give improvements to PDFs.

Figure 3.9 shows a $G_{ns}(r)$ calculated for a Q_{max} of 40 Å^{-1} that shows strong alteration compared to an ideal PDF without noise. The PDF's quality was higher for an Q_{max} of 21 Å^{-1}.

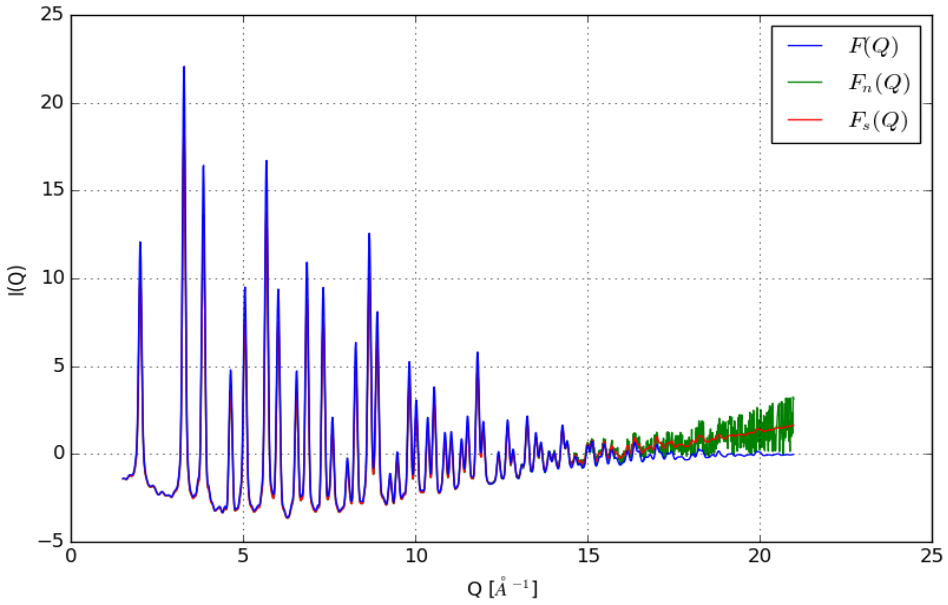

Figure 3.6: Illustration of noise in $F(Q)$ calculated from a Si-supercell-model. $F(Q)$: ideal scattering curve. $F_n(Q)$: a modified Gaussian noise ζ_n was added to $F(Q)$. $F_s(Q)$: only the slope of the noise ζ_s was added to $F(Q)$.

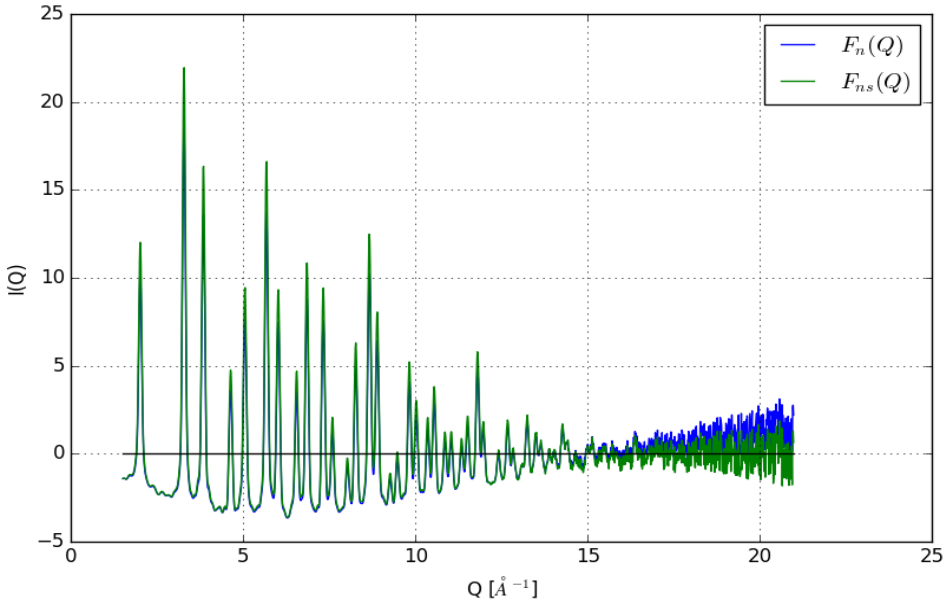

Figure 3.7: $F_n(Q)$ from figure 3.6 and $F_n(Q)$ with the slope of the noise ζ_s subtracted resulting in $F_{ns}(Q)$. $F_{ns}(Q)$ oscillates around zero.

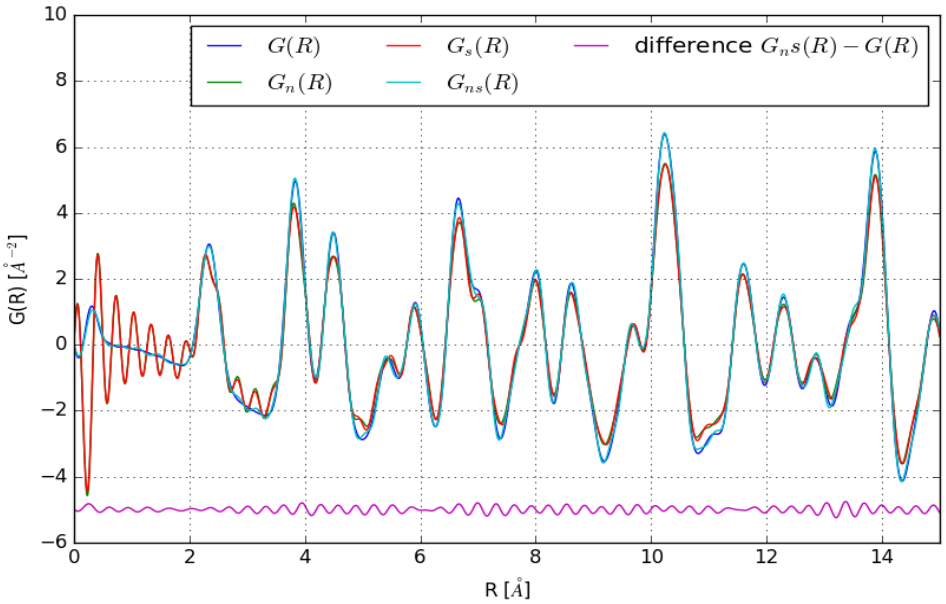

Figure 3.8: Comparison of the PDFs obtained from the different $F(Q)$-curves. The most remarkable result is that the differences between the PDF of the dataset of the ideal structure and the PDF of the noisy and slope-corrected dataset are already very similar.

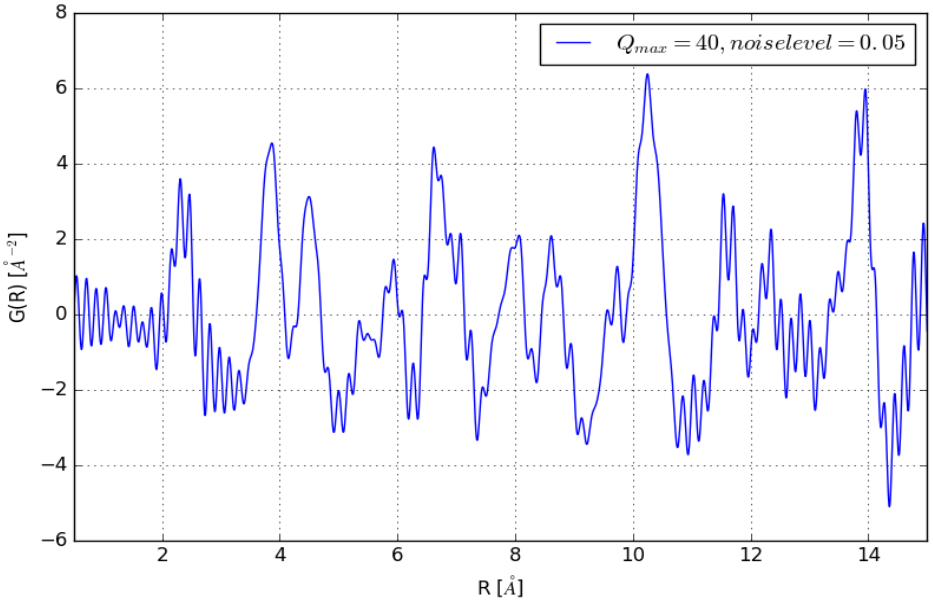

Figure 3.9: PDF obtained from the data up to 40 Å^{-1} and a noise level of 0.05 % of the maximum of the primary intensity. This is a good example that a high value for Q_{max} is not a guarantee for a useful PDF.

3.4 Remarks on scattering by the container and absorption related phenomena

For optimal subtraction of unwanted scattering, it is important to keep in mind that in a scattering experiment the total scattering can be understood as the sum of individual contributions: the empty device (presumably mostly gas) (a), the container (b) and from the sample in the container (c). Then the scattering of the empty container in theory is $d = b - a$ and the scattering from the sample in the container $e = c - a$. The difference of the scattering by the sample and the container, and the scattering by the container $e - d$ gives the scattering of the sample alone. The procedure is defined this way because it is possible that the contributions of the single components to the total scattering in the system (air + container) and in the system (air + container + sample) differ so that scaling of each single contributions must be performed. So the best practice for background subtraction should be a separated subtraction of all separable contributions to the integral scattering from the total scattering as defined above.

Figure 3.10 shows the results of an in-house laboratory experiment: the dataset from the empty device's measurement contains signal that is not present in the other measurements. The intensity data were collected under the same settings as the other measurements. It could not yet be explained where it comes from and if absorption effects cause it to not show up in the empty capillary's diffractogram.

What can be seen in figure 3.11 is a measurement of an Si-sample in a Kapton (R) capillary. The scattering by the container in the measurement of the filled capillary appears to differ from the scattering of the capillary measured empty. Moreover, the measurements of two different empty capillaries show different intensity profiles. It can only be speculated whether this difference origins in a slightly different shape and thickness of each capillary or in a different positioning (what can merely be improved over a certain level) and which effects the precessing of capillaries has.

Another important observation is presented in figure 3.12: Diffractograms of

a mixture of silicon and fused silica, and pure fused silica were recorded. The diffractograms appear to be composed only of a strong contribution due to air scattering at low scattering angles, and of the specimens' scattering over the remaining range. — The diffractogram of the mixture exhibits higher intensities than the pure fused silica between 5 - 20° 2θ. As the materials exhibited grain sizes of several μm, it is unlikely to be small angle scattering. A viable alternative explanation is that pure fused silica shows stronger absorption behavior than the mixture. From this it can be inferred that prior to any combination of scattering data, proper correction of data should be performed, incorporating information on all samples. Obtaining those might require an iterated correction procedure, which incorporates and refines detailed sample information in order to find a physically correct solution.

The observation made might also be crucial in for difference modeling where a PDFs is subtracted from another. Background subtraction can be called the prototype of all difference modeling. One might say that those effects do not really matter, because the PDF-method is an insensitive method with many approximations. In any case, insufficiently treated scattering by the container is prone to influence quantitative and maybe even qualitative interpretations and our practices should be characterized by striving for the best result possible.

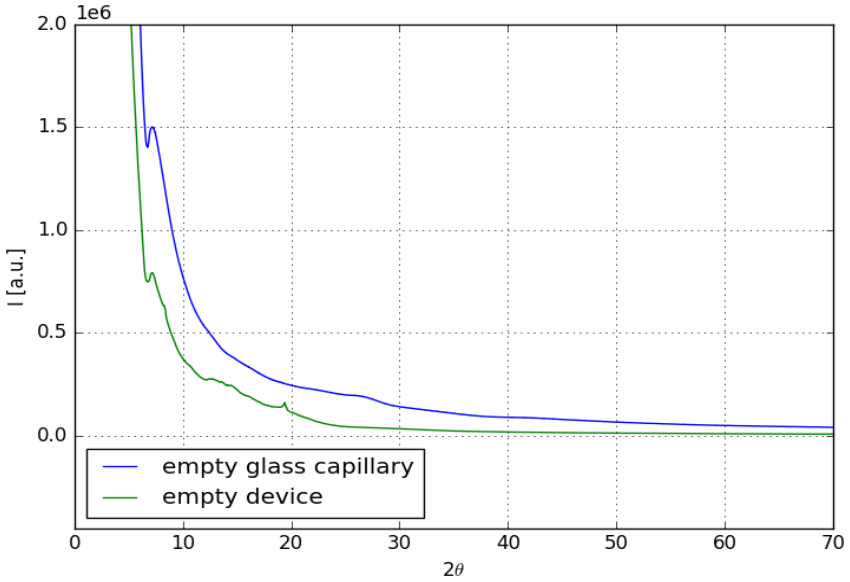

Figure 3.10: A comparison of the diffractograms of a container and the empty device in a laboratory-diffractometer. The dataset of the empty device clearly shows features (reproducible) that is not similar to the data curve of the empty capillary. The reason could not be elucidated up to now. The empty device should show less features than anything else.

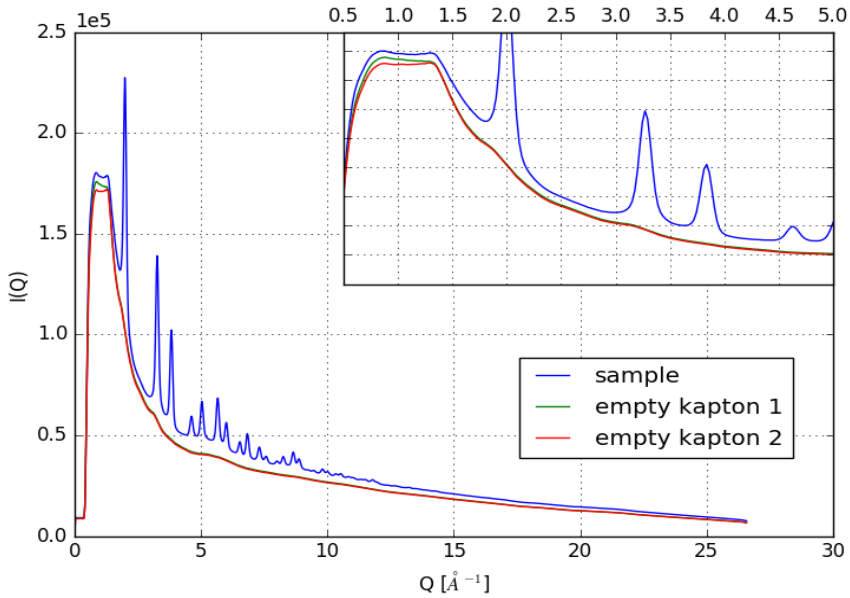

Figure 3.11: Data from container measurements do not exactly overlap

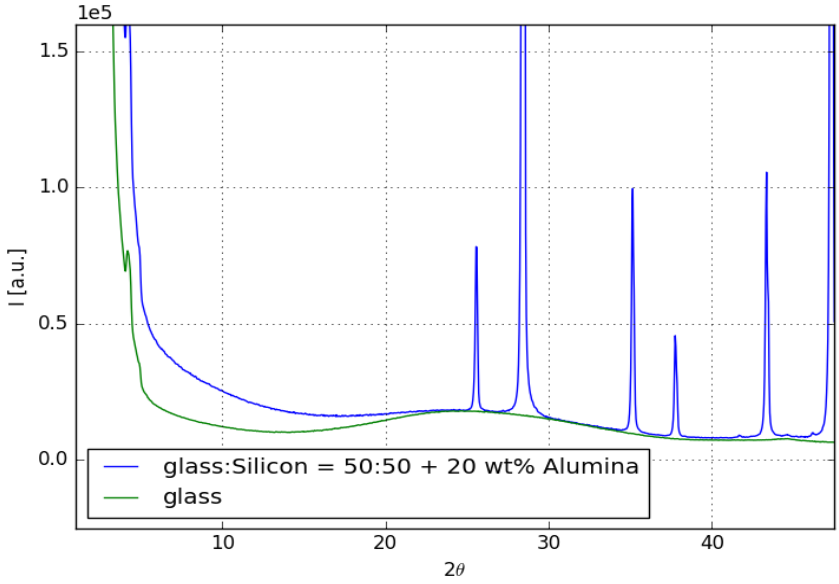

Figure 3.12: Comparison of X-ray absorption behavior of pure fused silica and a mixture of silicon/fused silica. The curve at low angular region and the artefacts differ in intensity. This might be an indicator for absorption effects at this region. In order to eliminate all non-sample signal via subtraction, a correction appropriate to the causes appears indicated.

3.5 Conclusions

We should not always rely that our experimental setup gives directly useable raw-data. As pointed out, more refined practices than applied at present might have to be introduced in order to reach higher qualities of data analysis. The most important conclusion from this chapter is that features owing to the instrumental setup, radiation properties, noise, and background subtractions can introduce artefacts. This must be considered in PDF analysis.

Either we get rid of them via deconvolution (Ida and Toraya 2002) or incorporation via convolution (Cervellino et al. 2005), which is an easier way.

By subtraction of a polynomial resembling the mean deviation of $F(Q)$ due to noise at high diffraction angles it is possible to reduce large ripples in the PDF. The strong contribution of noise is due to the deviation of the signal from zero at large Q, thus avoiding the demanded convergence. A corrective polynomial in the diffraction pattern might be a very effective correction. Anyway, for reliable correction of scattering data a reliable routine for achieving such a polynomial has to be developed. The choice of the highest Q_{max} possible does not guarantee a "smooth" PDF as noise or other artefacts can show influence. Instrumental effects feature the PDF.

A certainly tedious and virtually unexplored, but nevertheless promising option could be the simulation of the whole measurement setup including the container. By doing so, errors from data corrections might be circumvented. As the container consists of an amorphous material in most cases, a demand for the simulation and quantification of amorphous structures arises. Iterative procedures with parallel refinement in reciprocal and real space should be considered. Further, correct data collection and reduction strategies must be adopted.

Chapter 4

Critical assessment of ad-hoc data correction procedures in recent literature

Because, as Juhás et al. (2013) frame it, of the "*myriad of options available to users as well as the esoteric nature of many of the corrections (Egami & Billinge, 2013), PDF generation requires considerable user input and expertise in arcane details of the technique.*" An older software [pdfgetX2] "*[...]has a graphical user interface, [but] it is a time-consuming process to carry out the corrections, with many possibilities for input errors, and the process cannot be easily automated for high throughput of many data sets.*" This is why an ad-hoc correction approach by means of subtraction of a polynomial was suggested instead of physical meaningful corrections (Billinge and Farrow 2013). A corresponding software *pdfgetx3*, which does data correction and subsequent PDF-generation via an FFT algorithm, was published recently (Juhás et al. 2013).

4.1 Description of the correction algorithm

Concerning the proposed correction procedure, firstly, it has to be mentioned that multiple interpolations are made by the software. If the diffractogram is not provided on a regular Q-grid it is transformed and interpolated onto a regular Q-

grid, the step size being the distance between first and second data points. Then, the container intensities are interpolated onto the same Q-grid as the raw data in order to make possible proper non-sample-signal-subtraction (described in the pdfgetx3-publication). Usually, it appears to be the best to record the scattering by the container under the same condition as the scattering by the sample. Data mapped on an equidistant Q-grid apparently should give constant weights in Q-dependent fitting (what might be also true for Q-dependent corrections).

According to theory, the reduced structure function $S(Q) - 1 = I(Q)/ < f >^2 - < f^2 > / < f >^2$ should oscillate around zero (and approach zero at some point). To achieve so, the background-corrected raw intensities are scaled by a least-squares procedure so the formula fulfills the demanded conditions. We thereby can sidestep the task of evaluating the amount of sample employed in the measurement, what would be necessary for ordinary data reduction otherwise.

Then the function $Q[S(Q) - 1] = F(Q)$ is formed and a polynomial is subtracted. The correction polynomial is defined in equation 4.1. The polynomial has $(n + 1)$ nodes, which are equidistantly distributed between 0 and $Q_{maxinst}$. r_{poly} and $Q_{maxinst}$ are adjustable parameters and must be defined by a user.

$$n_{poly}\pi = r_{poly}Q_{maxinst} \tag{4.1}$$

The subtraction of the corrective polynomial results in a corrected function $F_{corr}(Q)$ which is not perfectly corrected. A difference function $\Delta F(Q)$ remains and its Fourier transform is a function $\Delta G(r)$ that is interpreted as an error so that:

$$F_{"real"}(Q) = F_{corr}(Q) + \Delta F[Q] \qquad \Delta G(r) = \mathcal{F}[\Delta F(Q)] \tag{4.2}$$

There should be no impact of $\Delta G(r)$ on the "real" PDF in the physical meaningful region, i.e. the region below the first interatomic distance. An impact emerges owning to the frequency of changes of $\Delta F(Q)$) from positive to negative sign. To prevent so, r_{poly} must be chosen that it is smaller than the first interatomic distance and equation 4.1 must be tuned to achieve a suited value for n_{poly} (which defines the number transitions from negative to positive).

Further, as it is likely that n_{poly} will not be integral, an adaptation procedure is performed, to make the polynomial's degree integer. The real-valued n_{poly} integer floor and ceiling are taken and polynomials are obtained for both values. The weighted sum of the polynomials obtained with those floor and ceiling values is taken. Weighting is done according to the respective distances of floor and ceiling to the real-valued n_{poly} lying in between them. Figure 4.1 shows a correction-polynomial, the corresponding $F(Q)$-curve and the $S(Q)$-curve calculated from $F(Q)$ of an amorphous, organic solid.

As the number of data-points in $G(R)$ directly obtained by FT is equal to the number of points in the scattering curve additional interpolation is applied before FFT is done. A shift of the limits Q_{min} and Q_{max} is done and then a partition of the range between the limits. The Q-grid is set and $F(Q)$ is interpolated to be appropriate for the desired step size and number of data points in R.

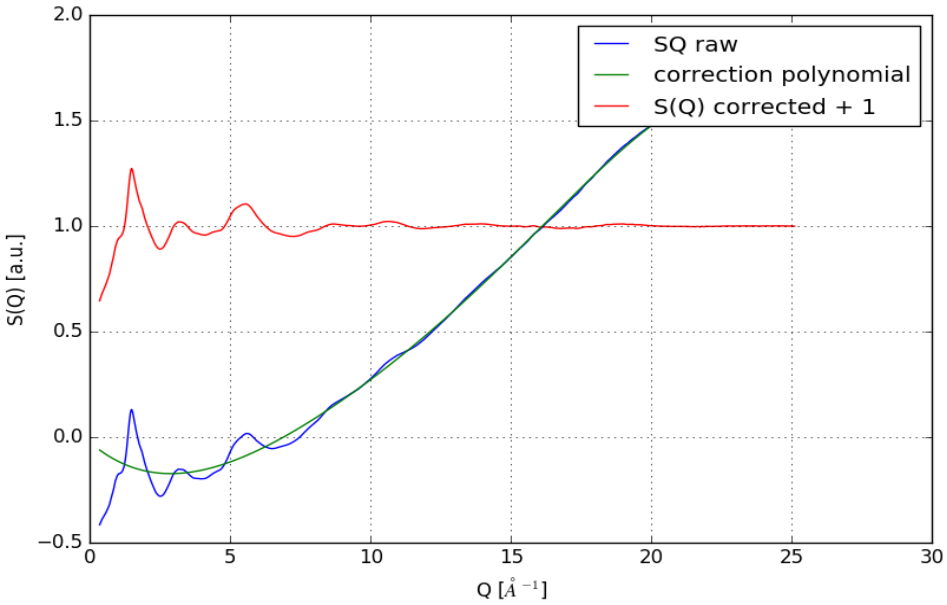

Figure 4.1: $F(Q)$-curve with ad-hoc correction polynomial and calculated $S(Q)$ curve thereof.

4.2 Analysis of some artefacts obtainable with the ad-hoc method

In the following, some tuning experiments have been performed, to show what novices are prone to perform. Figure 4.2 shows an exemplary series of achievable polynomials for an unchanged dataset. Figure 4.3 gives closer comparison of the obtained $F(Q)$-curves. Figure 4.4 documents the $G(R)$-curves obtained from the datasets from figure 4.3. Figure 4.5 gives a zoomed-in comparison of the short-range region from figure 4.4.

There is not much to comment. For five sets of parameters five sets of PDF-functions are obtained, which considerably differ. - The curve, which will be chosen for analyses or refinements, completely depends on a person's subjective criteria. - Unfortunately, so it seems, adopting an ad-hoc procedure that make the work easy for laypersons, renders data correction arcana to «numerical alchemy»(and also for experts as we have no reasonable criterion at hand to select the parameters). Even the qualitative information we can get is prone

to "tuning". But exactly quantification via the PDF method is what is desired and what authors connected to the authors of pdfgetx3 claim to have achieved quantification (Abeykoon et al. 2012). The same group published a software to extract the "real" peaks from a PDF and that was tested on approximately 20 datasets (Granlund et al. 2015). — Applying a correction procedure of such kind, demands prior knowledge of the correct PDF, otherwise no distinction between real and superficial maxima, peak-shapes and distance distributions can be is possible (Hans P., Leoni M. (2018) in preparation).

Another obstacle concerning data-extraction from PDFs was encountered during the analyses of solid phase catalysts in modulation experiments at the synchrotron (Diamond Lightsoure, beamline I15). In this case, time-dependent experiments of repeated reaction-cycles were performed. The solid phase catalyst Co_3O_4 was heated under defined temperature and in alternating reducing (H2 / CO / He) and oxidizing (O2 / He) atmosphere. Diffractograms were recorded with a flat plate detector in intervals of 5 seconds. The idea in the case at hand was to apply a demodulation algorithm (such as performed by Beek et al. 2012 on X-ray diffraction data) by using PDFs to time-resolve changes of SRO and phase composition in relation to the reaction start (Föttinger K., Lukashuk L., Yigit N., Leoni M., Hans P. (2018) in preparation).

Figure 4.6 shows three graphs: the top graph is an overlay of all $F(Q)$s, which were recorded during the reduction reaction of a reaction cycle. The difference-curves between each diffractogram and the first one are depicted in the bottom graph. A defined relationship between the first diffractogram and all other exists, and this relationship depends on the reaction time. Here, a phase transition takes place under reducing conditions (which is reversible under oxidizing conditions), so the corresponding peaks appear and disappear in the difference curves. The graph in the middle gives information on a mathematical phase relationship and correlation across the datasets of the cycle, but is irrelevant for the discussion at this point. It is simply contained in the output of the software for analysis.

In figure 4.7 the differences between the PDF of the first dataset and each other has been taken and drawn in the same manner as above. The clear relationship, which can be seen in the $F(Q)$ curves in figure 4.6 is lost in the

third graph. What should be seen is a selective appearing and disappearing of bond-distances as the reaction progresses thus indicating the formation dynamics of the phases and change in the SRO.

What remains to do is a detailed analysis of the reasons this correlation between datasets is lost in real-space (Hans P., Leoni M. (2018) in preparation). In the following only a few attempts to explanations are given:

One reason for the failure of extracting information on the correlation of phase occurrence and SRO with reaction time compared to the initial structure might be that the pdfgetx3-output is not normalized and not given per incident intensity or per number of scatterers.

As the reactions occurred under reducing or oxidizing atmospheres, the oxygen contents vary. Correct data correction is dependent on the stoichiometry to separate $\rho(r)$ from the atomic form factors.

The Warren-Krutter-Morningstar approximation (section 2.1.4), which appears to result in artefacts for samples containing atoms with strongly differing form factors, is applied. Anyway, this reason seems odd, because this information is already used to achieve the $F(Q)$-curves where the trend can be seen.

Another explanation could be related to particle size and shape and growth during the reaction: as the baseline of the PDF is determined by particle size and shape, direct correlation between PDFs or selected peaks of PDFs might not be possible so that models must be compared.

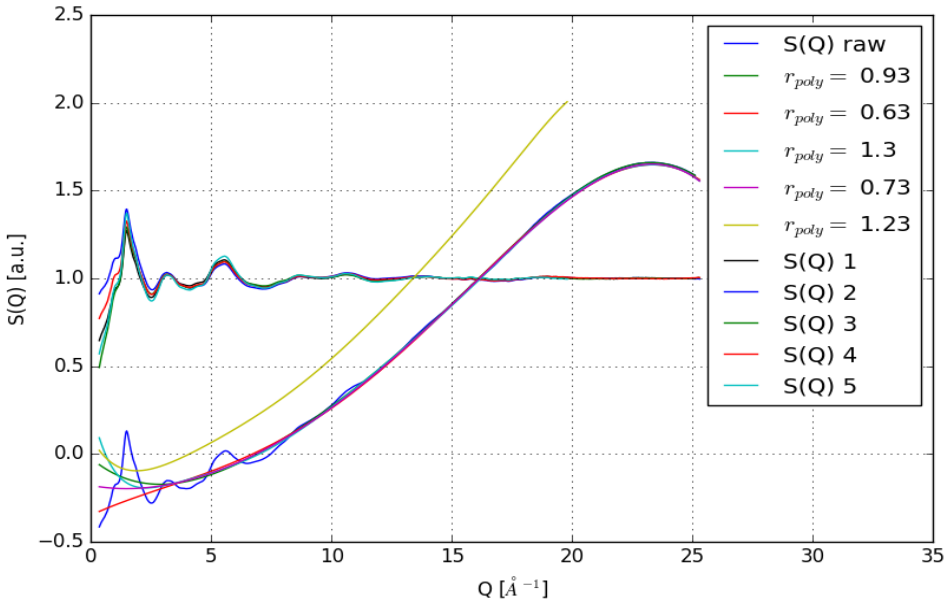

Figure 4.2: A comparison of several polynomials, which were obtained from the same dataset of an amorphous-organic solid, giving PDFs without severe ripples and corresponding $S(Q)$-curves.

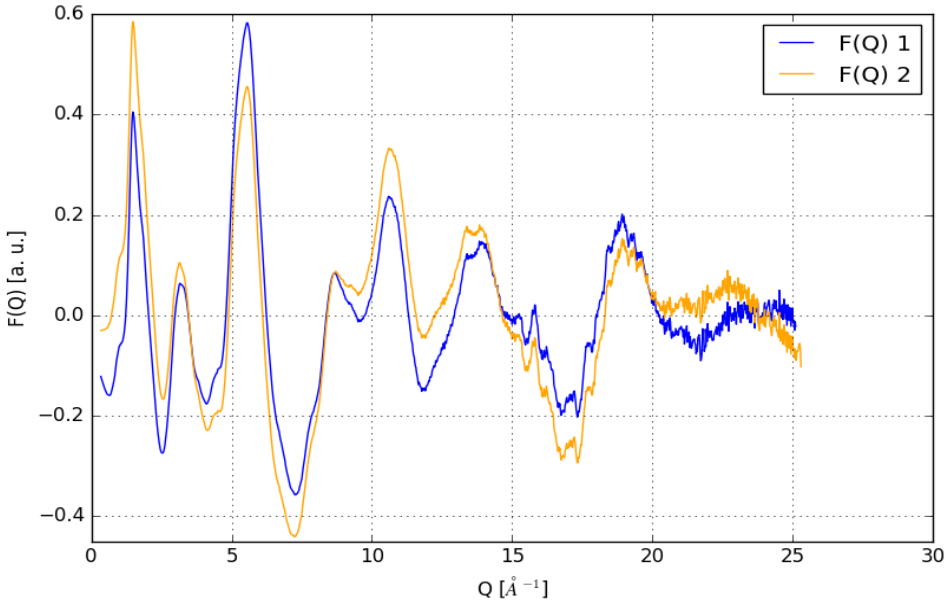

Figure 4.3: Detailed comparison of two $F(Q)$-curves constructed with the ad-hoc correction method.

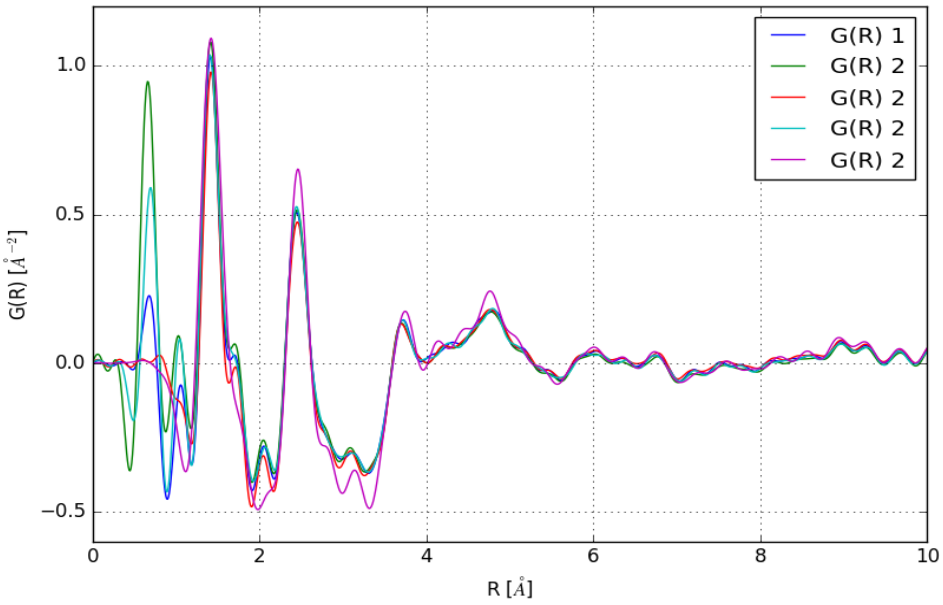

Figure 4.4: A set of PDFs all obtainable from a single set of raw data.

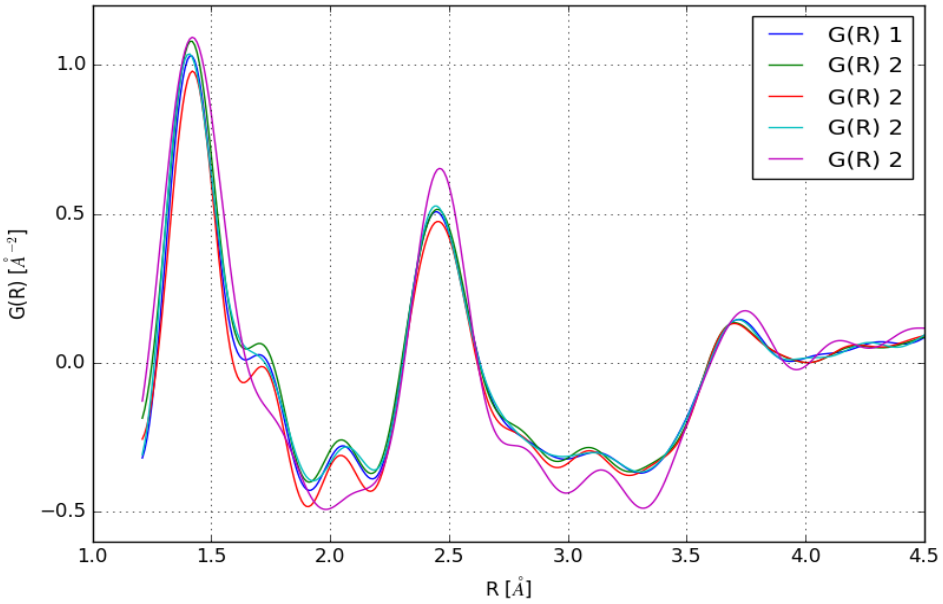

Figure 4.5: Zoomed region from figure 4.4. No criterion for the distinction of real bond distances from artefacts could be established.

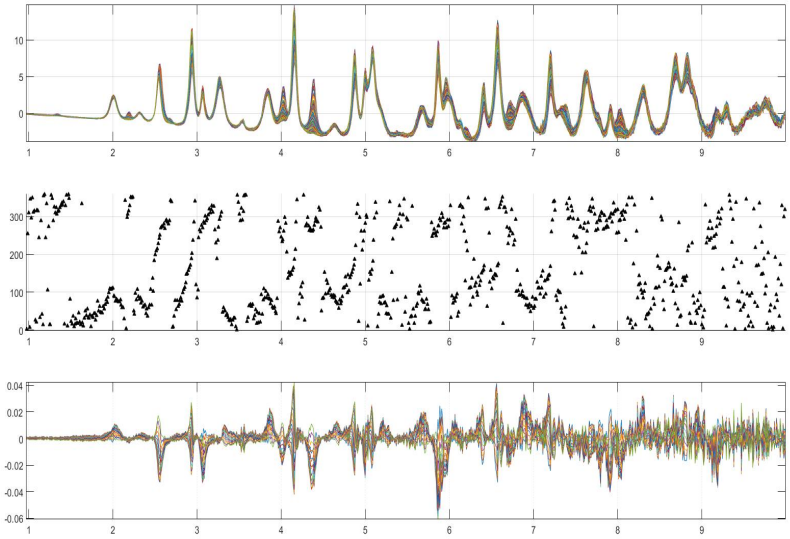

Figure 4.6: $F(Q)$-curves from modulation-experiments on solid-phase catalysts at Diamond I15. A continuous relationship between first and subsequent diffractograms can be seen in the difference-curve (bottom).

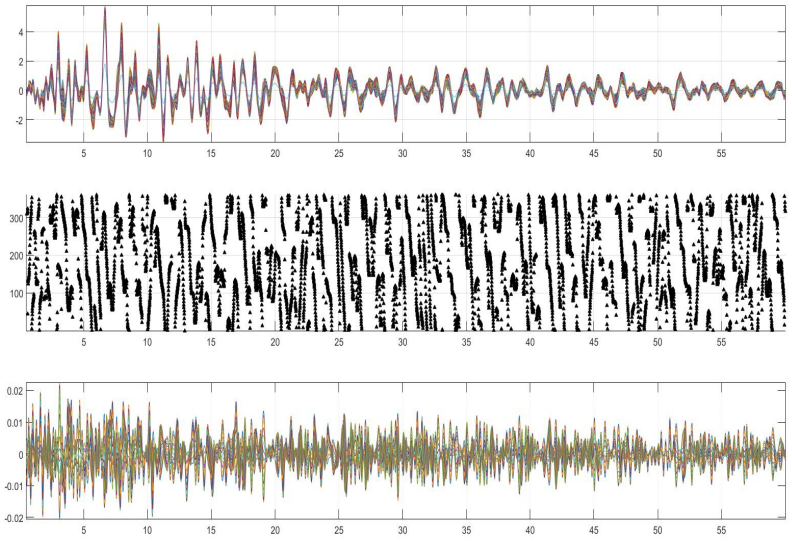

Figure 4.7: PDFs calculated from figure 4.6. No continuous relationship between the first and subsequent PDFs appears to exist.

Chapter 5

Remarks on data acquisition and data handling

The total scattering data, which are ultimately corrected and transformed to a PDF, are usually containing intensities mapped either onto a 2θ or a Q-grid. Data collection can happen in various ways. Here, data have been collected either by: a) collection of a 1D-diffractogram with a point-detector or b) simultaneous collection using a 2D-plate detector and reduction to 1D. In the process of data reduction, many steps such as interpolations or integration are executed. Those procedures are analysed in the following chapter.

5.1 Handling 1D-datasets - remarks concerning data sampling and interpolation

5.1.1 Interpolation of 1D-diffractograms and its effect on $G(r)$

A recommendation concerning the reduction of 2D-detector images can be found in Yang et al. (2014, p. 1282), namely *the use of a non-pixel-splitting integration algorithm and integrating data directly onto the final one-dimensional grid that will be modeled or further processed*. This is recommended because *reliable statistical uncertainties on points in a one-dimensional powder diffraction pattern obtained from widely used two-dimensional integrating detectors* can be

determined not easily or not at all. (See section 5.2.3 concerning pixel-splitting connected with the integration of 2D-detector images.) Juhás et al. (2013) write that *resampling introduces error correlations between points, which can be minimized if the data are azimuthally integrated from two dimensions directly onto a constant-Q grid*. Anyway, it is to be questioned if the recommendation of directly integrating onto an equidistant Q-grid is realizable. Most likely, it is not possible to do an integration without pixel-splitting or without interpolation, which results on an equidistantly spaced Q-grid. The detector's pixel array does not allow for evenly spaced intervals in Q. On the other hand FFT-algorithms cannot be applied on datasets that are unevenly spaced in Q so interpolation appears to be necessary if one wants to apply FFT.

Figure 5.1 gives a comparison of two curves: One curve shows the $F(Q)$ of Si that has been calculated onto an equidistantly spaced 2θ-grid with a step size of 0.01 and was directly transformed to the corresponding Q-grid. The diffractogram has been calculated up to a Q_{max} of approx 40 Å^{-1}. For the other curve, the diffractogram was interpolated onto an equidistantly spaced Q-grid containing the same number of points as the 2θ-grid. Figure 5.2 shows the corresponding $G(r)$-curves and the difference between the two is minimal. Figure 5.3 shows the strongly magnified difference curve, which exhibits a reverse dampening. This means that the $G(r)$ otained from the interpolated diffractogram exhibits a damping-envelope in comparison to the non-interpolated diffractogram. It is hard on this basis to estimate if the introduction of the above mentioned statistical error correlations between points is crucial with respect to 1D-resampling or if there it is only a special type of interpolation that introduces such error correlations. Figure 5.4 shows the same example with a noise level of 0.025 % of the maximum intensity in $I(Q)$. There are slight differences between the PDFs, but by comparison with the example free from noise, it is concluded that artefacts introduced by noise can be influential whereas the differences stemming from interpolation are negligible.

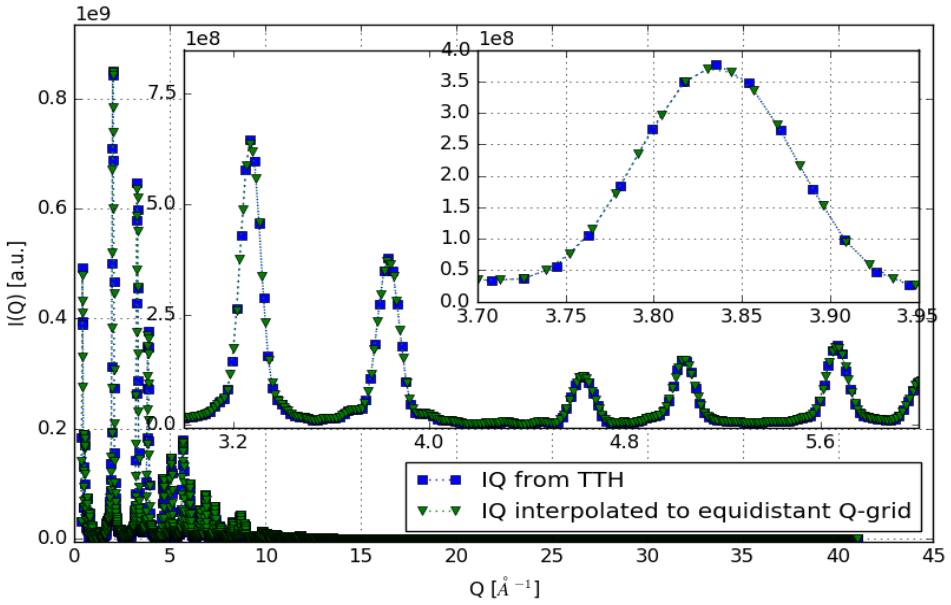

Figure 5.1: Comparison of interpolation effects in $I(Q)$ calculated for an Si-model. Effects seem to mild for data-points spaced closely enough

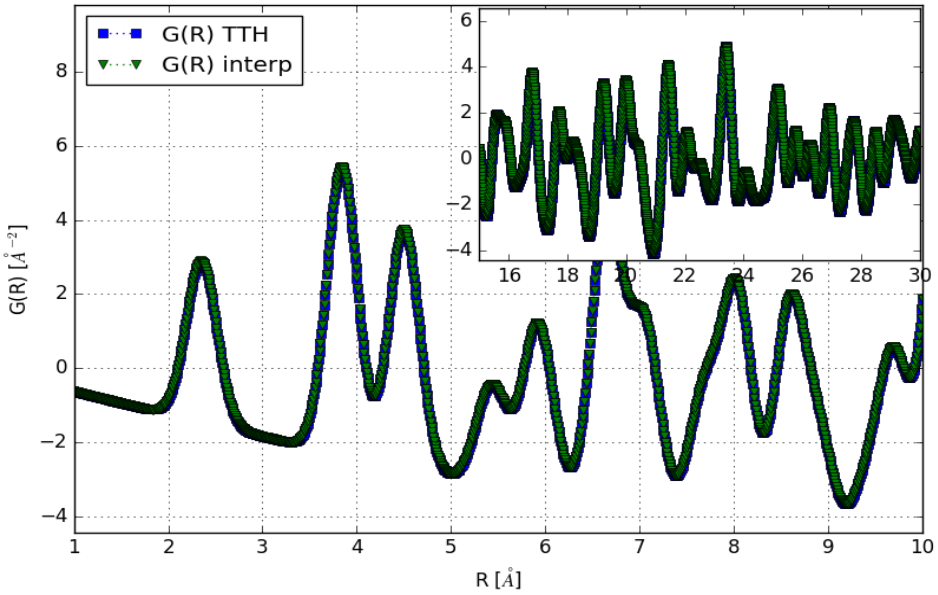

Figure 5.2: $G(r)$-curves obtained by FT from $F(Q)$s in figure 5.2. With the bare eye the curves are indistinguishable. The difference curve is shown in figure 5.3.

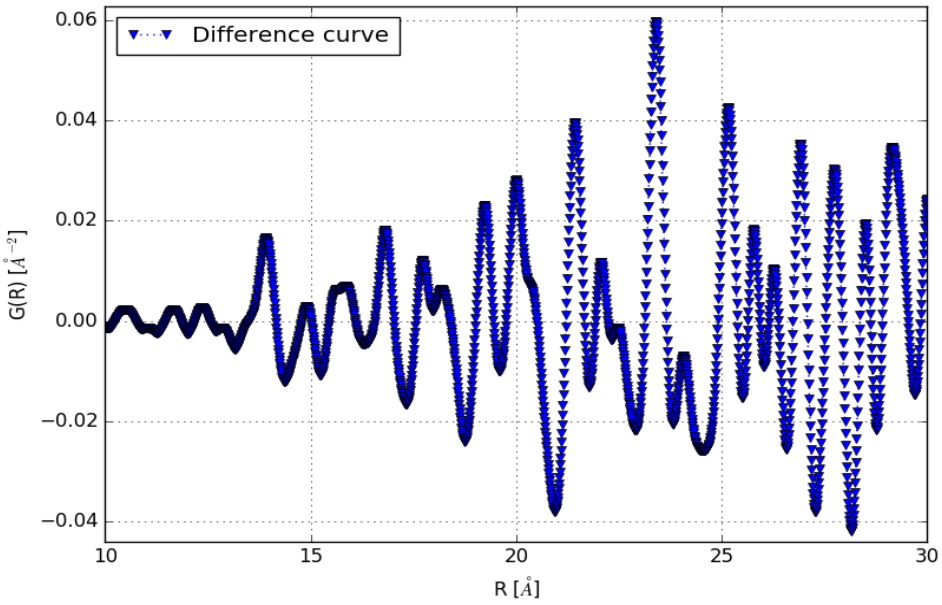

Figure 5.3: Differences between PDFs obtained by FT from ideal data, once interpolated to an equidistant Q-grid, once taken as is from their 2θ-scale.

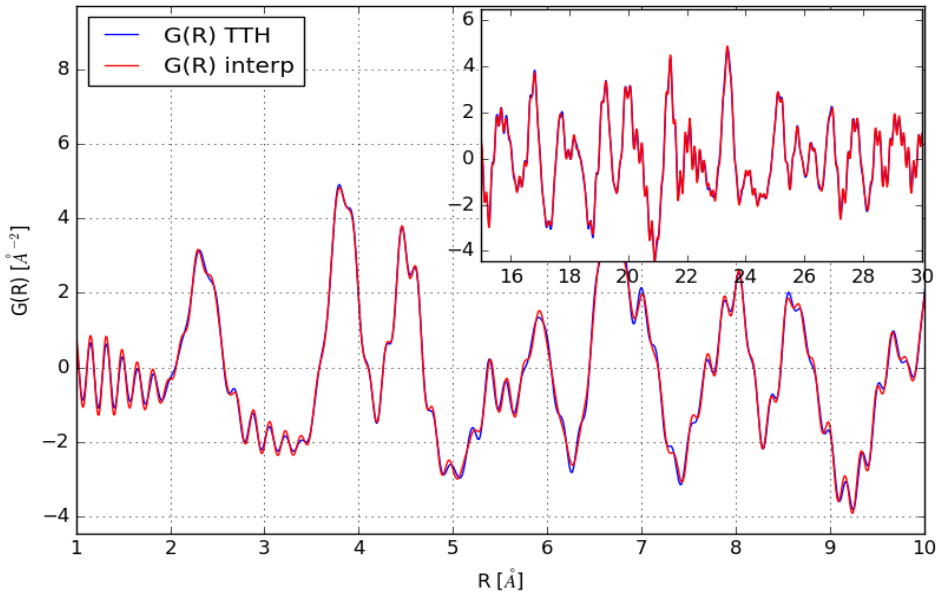

Figure 5.4: Comparison of $G(r)$ with noise and effect of interpolation.

5.1.2 Data collection strategies and possible obstacles

Diffractometer mechanics as well as pixels from 2D detectors are designed in a way to scan Q-space in (often equidistant) steps. No detailed survey concerning devices available for doing scans with equidistant steps in Q was performed, but none of the well known diffractometer companies advertise for such a thing. For modern pixel array detectors it seems unlikely that sampling is possible in arbitrarily varying Q-steps or in Q-steps at all. For moveable detectors it might be possible to do data sampling on a Q-grid by oversampling (collecting more data points than one would need) and selecting those which represent a Q-point. Which points in Q are collected depends on the energy of the applied probing radiation.

To improve the signal-to-noise (S/N) ratio in a dataset, it is common to perform measurement of intervals with different scan speeds (figure 5.5). Subsequently, the datasets have to be scaled and merged. It is wise to measure intervals so that overlaps exist: if the data acquisition times of the intervals are not known, a point wise comparison of overlapping regions and scaling by a mean scaling factor can be performed. If the data collection times are known then scaling the sections accordingly and discarding overlaps with the worse S/N ratio can be performed.

The software of PANalytical diffractometers, which were used for data collection in the investigations presented herein, sets the starting point of the measurements differently than specified by a user. Altered starting points of the collected diffractograms results in a not perfect overlap of data points in different intervals, in most cases. To accomplish the necessary scaling and merging of the intervals to a single diffractogram, a script was applied that performs interpolation of all segments to a common grid, and scaling and combination of the segments subsequently. The script was written in the python3 language and is documented in the APPENDIX. (The PANalytical software for data processing introduced steps between the sections, which render the diffractograms unusable.)

In the following different approaches for data merging are discussed and compared with a complete dataset that was recorded in one measurement: Figure 5.6

gives a comparison of three different diffractograms of the Si-NIST standard 640d. The reference curve was measured in one scan without pause. A second was created by merging three sections (figure 5.5), which were interpolated to an equidistant grid and scaled by the intensity-ratios of overlapping points prior. The third curve was also created by merging. Here, scaling was performed according to te known measurements times of each interval. Finally, it was interpolated onto the same grid as the two other curves for consistency. If, then linear interpolation was chosen. Compared to the complete and not interpolated dataset, slightly smoothed out maxima are observed.In acquiring data for PDF analyses of samples intrinsically giving broad diffraction features it should be negligible. What can be seen in addition and is most striking is that curve 2 shows an obvious deviation of the slope of curves 1 and 3.

Figure 5.7 shows the corresponding $F(Q)$-curves obtained by processing with pdfgetx3. For each curve the same correction parameters r_{poly} an $Q_maxinst$ parameters have been chosen. It is possible to tune the parameters for curve 2 (interpolated, scaled, merged) to obtain a PDF of Si but it deviates from the two other curves strongly nonetheless. Figure 5.8 shows the resultant $G(r)$s. It is concluded from the investigations that interpolation between data with strongly different S/N-ratios results in prominent artefacts.

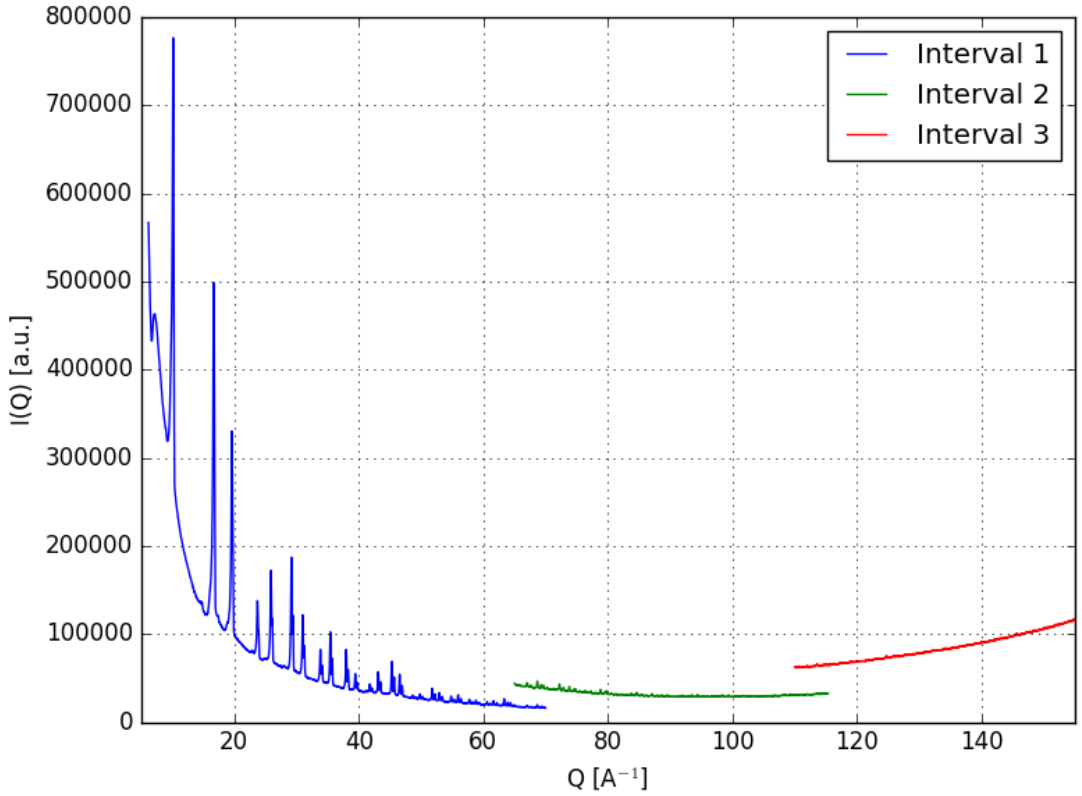

Figure 5.5: Measurement strategy for increasing the S/N-ratio.

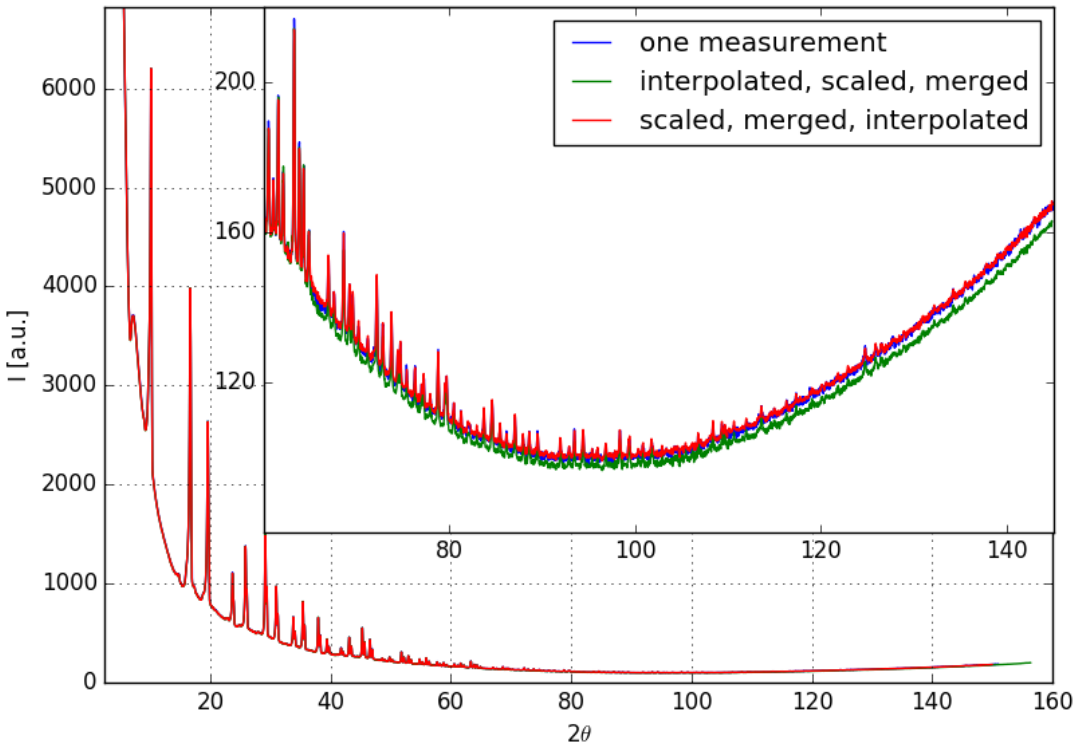

Figure 5.6: Comparison of interpolation strategies by means of measured data: Curve 1 was measured as a whole. Curve 2 was interpolated to equal step size and scaled by the mean ratios of each overlapping point. Curve 3 was scaled according to the (in this case known) measurement times of each interval and merged by adding the segments whilst discarding the overlaps with worse S/N-ratio. Interpolation was done in order to keep procedures similar and to obtain the same step size for each curve.

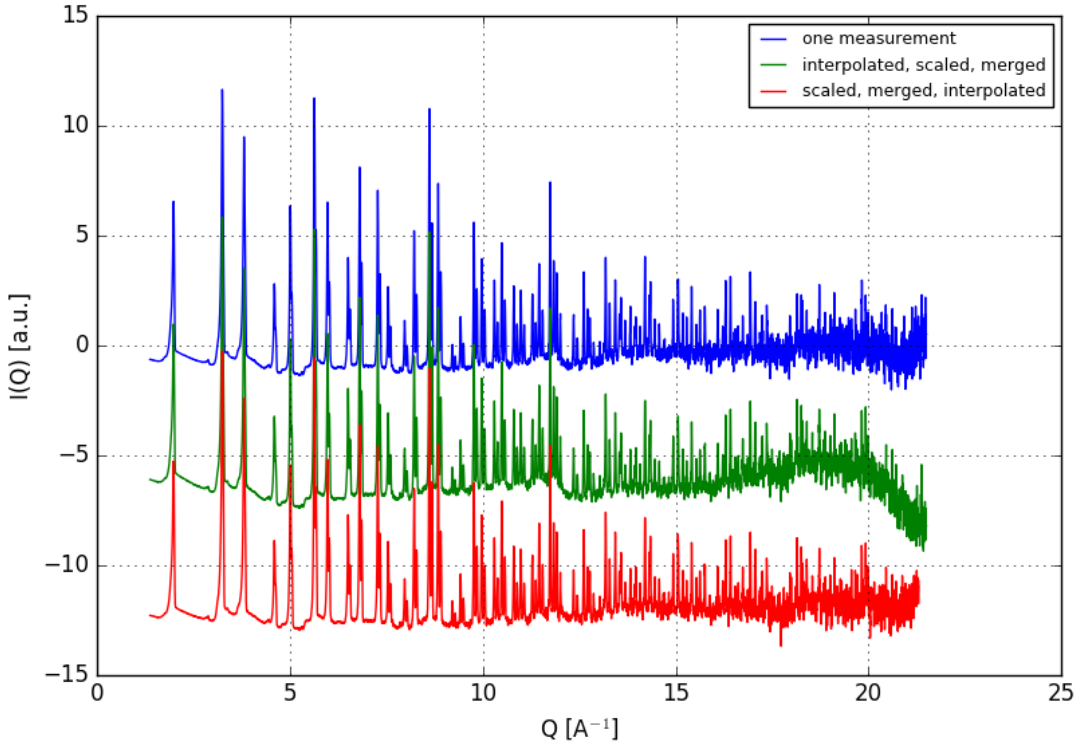

Figure 5.7: The $F(Q)$-curves obtained by correction of the curves in figure 5.6. Curve 2 results from the curve shifted in the high-Q region. Here, adjustment of the segments was done by scaling of overlapping regions and it clearly shows a different behavior. All curves have been processed applying the same parameters. The differences in S/N-ratio are detrimental to proper scaling.

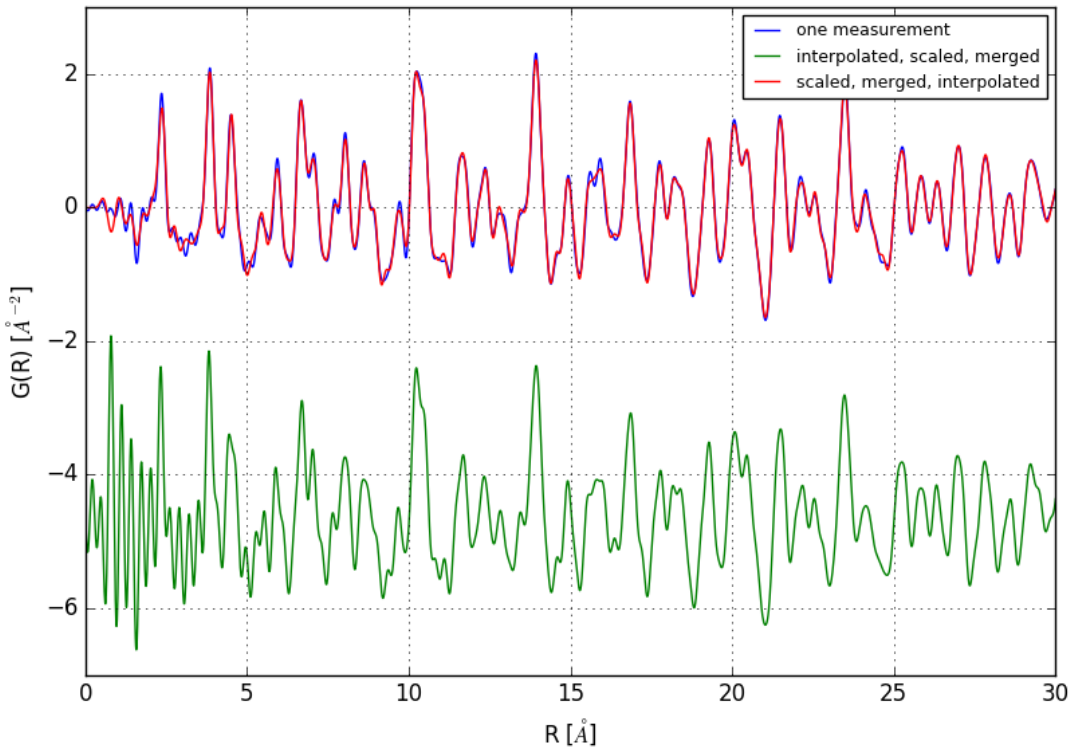

Figure 5.8: $G(r)$s from figure 5.7

5.2 Handling and reducing 2D-datasets - remarks on artefacts in context with data-correction masking

For calibration and integration of datasets, DAWN was used (Filik et al. 2017). Examples for other, easy available packages are GSAS-II (Toby and Von Dreele 2013), FIT2D (Hammersley et al. 1996) or DIOPTAS (Prescher and Prakapenka 2015).

5.2.1 The reason for using 2D-flat-plate-detectors

1D-diffractograms are a vertical cut through all diffraction cones (i.e. a plane going through radiation source, sample, and detector). In the case of statistically oriented (ideal) powder samples, the profile of the recorded diffractogram is independent from the sample orientation. The detector images of sufficiently large 2D flat plate detectors are conic sections through the Debye-Scherrer-cones. If the sample is ideal, it is justified to merge the signal by radial integration along the conic sections. Thereby, the amount of collected intensity is distinctly increased in comparison to a 1D-measurement and the signal-to-noise-ratio can be improved.

5.2.2 Procession steps: Calibration, masking and integration

Calibration (with an optional correction procedure), masking and integration are the three main steps in reduction of 2D-data to 1D-data.

The common procedure for obtaining a moveable 2D flat plate detectors' geometrical parameters (distance from the sample, tilting, rotation) is to calibrate with a very well defined and characterized substance, such as a NIST-standard. After evaluation of rotation and distance with this well-known standard-substance, which has well-defined structural parameters, radial integration of all images is performed . Note that of course there is no guarantee that each sample is equally aligned (which is often mounted in a capillary for PDF-measurements).

Artefacts would occur if malfunctioning pixels are included in data reduction. These pixels are called faulty pixels and are masked so they are not accounted for during azimuthal integration. Usually, faulty pixels either do not give a signal (i.e. 0 or a defined negative number) or they are constantly giving the same and unvaried signal. Some pixels respond differently dependent on their stimulation.

Prior to radial integration, correction steps can be performed such as X-ray polarization correction (Detlefs et al. 2012), corrections for influences by the sample geometry, correction for angle dependent pixel response (although apparently not developed for synchrotron application; see He (2009)), etc. – Some discussion on the achievement of "good" data from 2D-detectors is given by Skinner et al. (2012).

5.2.3 Pixel splitting in 2D-detector-image integration

During azimuthal integration, each pixel is assigned to a bin in the one-dimensional pattern. According to the position of the pixel along 2θ, the whole or a part of it is assigned to a one-dimensional bin. Depending on the algorithm deployed, the intensity in the corresponding bin is calculated as an average or weighted average of the intensities of pixels overlapping that bin (concerning general aspects see: Hammersley et al. 1996 and He 2009; concerning statistical measures: Yang et al. 2014).

Figure 5.9 shows a comparison of a CeO_2-standard measured at the ESRF synchrotron facility (beamline ID31, $\lambda = 0.175939$ Å ($70.47\ keV$) with an detector-to-sample distance of approximately $200\ mm$), once integrated with pixel-splitting and once without. - The diffractograms differ slightly and the result from non-pixel-splitting has slightly better resolved peaks. Avoiding pixel-splitting leads to distinctly stronger visibility of noise in the low Q-region (in this example up to 4 Å^{-1}; no plot is given). The noise is part of the recorded data and if it vanishes due to a mathematical procedure one should be cautious if also other information is altered. By smoothing noisy data one does not gain additional information nor improves one the S/N ratio.

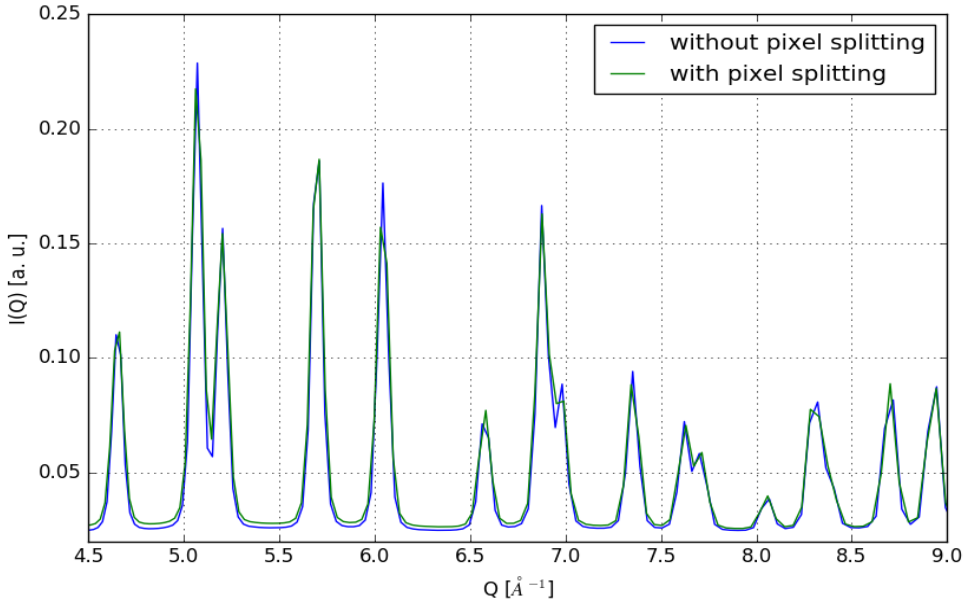

Figure 5.9: Comparison of the integrated 2D-detector-image of a CeO_2-sample invoking and not invoking pixel splitting. Not invoking pixel splitting lead to better resolved maxima and apparently better resolution. The data-points are not evenly distributed along Q which renders the data unsuitable for an FFT-algorithm.

5.2.4 Discussion of artefacts and conditions under which they can arise

As Hammersley et al. (1996) (the authors of FIT2D) write that "*it is better to account for the distortions within scientific analysis software, but often it is more practical to correct the distortions to produce 'idealised' data*". No polarization correction has been performed here, as the assumption was made that polarization correction can be done post-integration on the 1D-data. In addition, there was not information available on how inelastic scattering is influenced by the optional correction procedures during integration.

What was surprising in this context can be seen in figure 5.10. Here the integrated curve of a 2D-detector-image of an amorphous organic solid S2 is depicted. The synchrotron-data exhibit two broad peaks (marked with arrows) and the origins of those have not been able to rationalize. (In fact the detector image did not contain areas of intensities that are identifiable by eye as clearly differing.) Figure 5.11 shows the corresponding PDF that has high-oscillation ripples superimposed. To visualize and quantify the effects of such atrefacts, small peaks were introduced into a very simple simulated curve (figure 5.12) and the FTs to the corresponding $G(r)$s were taken (figure 5.13). As expected, the FT of artefactuous peaks in $I(Q)$ are ripples of corresponding frequency in real space. They can be the origin of disturbing features in $G(r)$, which do not contain structure information.

Inspired by those artefacts, a test-procedure was developed. An investigation of integration algorithm and masking was carried out (to test if artefacts are introduced e.g. by the integration algorithm at the borders of the mask). The mask's task is to remove faulty pixels so an undisturbed picture is obtained and to avoid artefacts. Therefore an "artificial detector image" was generated. The program is documented in the APPENDIX.

Figure 5.14 shows the unmasked dummy-image, and the same image with two different masks, which were applied for real data. Finally the integration results and the curve as it was intended are plotted which coincide in shape and differ only by a scaling factor. This schows that the integration procedures as well as masking apparently do not introduce artefacts.

What remains to do at this point is to search for the origin of the spikes in intensity differences between pixels, i.e. differences that are not easy to detect: To begin, figure 5.15 gives a comparison of the $F(Q)$-transformed integrated data-sets of substance S2, both applying and not-applying a polarization correction. It can be seen that the artefacts from the data not corrected for polarization effects vanish. Figure 5.16 depicts the $G(r)$-curves obtained from figure 5.15. The data seem improved, a discussion is given in the description of figure 5.16.

It is puzzling that polarization-correction should be the reason for eliminating (influencing) signal of this sort. A dedicated investigation is still outstanding. There is no reason to assume that polarization of light introduces peaks into a signal. Polarisation of X-rays should happen through a continuous change in intensity with angular region. Application of polarization-correction diminished the spikes observed. Nonetheless, this does not mean that it corrects the problems rooted somewhere else.

5.2.5 Remarks on masking and data correction strategies and how to influence the integration result thereby

While masking was successful in the case discussed, other cases seem more reluctant to an easy solution via careful inspection of raw data. In this section, it is examined if masking different regions of 2D-images effects shows effects in the integration result. The most simple approach is to apply a threshold mask to discriminate all pixels giving a signal below or above a user-defined threshold. Applying a threshold mask is insufficient for sophisticated masking problems: while it would be possible to locally account for wrongly responding pixels with an intensity-threshold, this is not possible globally as the primary beam and diffraction peaks usually exhibit high intensities. An evaluation-algorithm that compares the captured intensity of a given pixel with the captured intensities of adjacent pixels and sorts out pixels by means of a criterion would be very suitable. The FIT2D-software has a function to compare a pixel with adjacent pixels but it is very slow and it is unclear how it operates. - The DAWN-software has a built in outlier mask function, which works fast. Note that a user defined value for the selectivity of the outlier detection must be specified nevertheless.

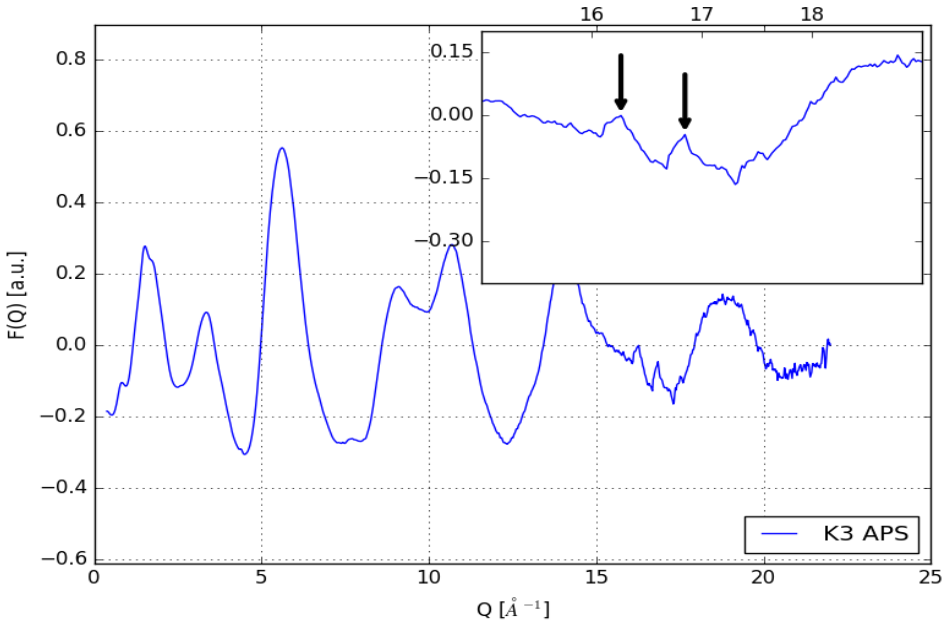

Figure 5.10: $F(Q)$ curve from the measured intensities of sample S2, obtained by azimuthal integration from a 2D-detector image and corrected with an ad-hoc polynomial, exhibits two big peaks (marked with arrows) at high Q-values, which must be a measurement artefact.

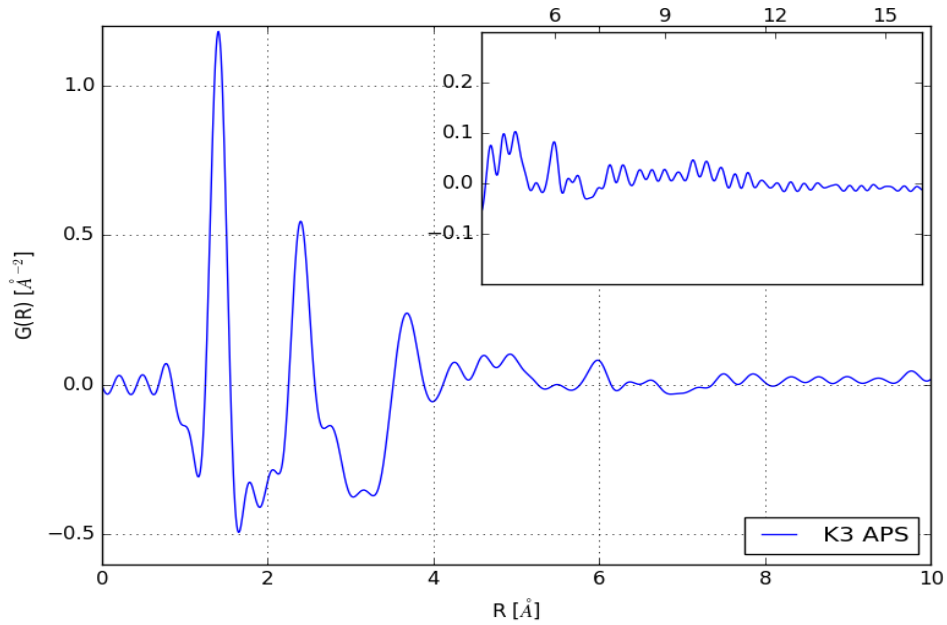

Figure 5.11: $G(r)$ curves from measured and corrected intensities in figure 5.10 exhibit strong oscillations which superimpose structural features.

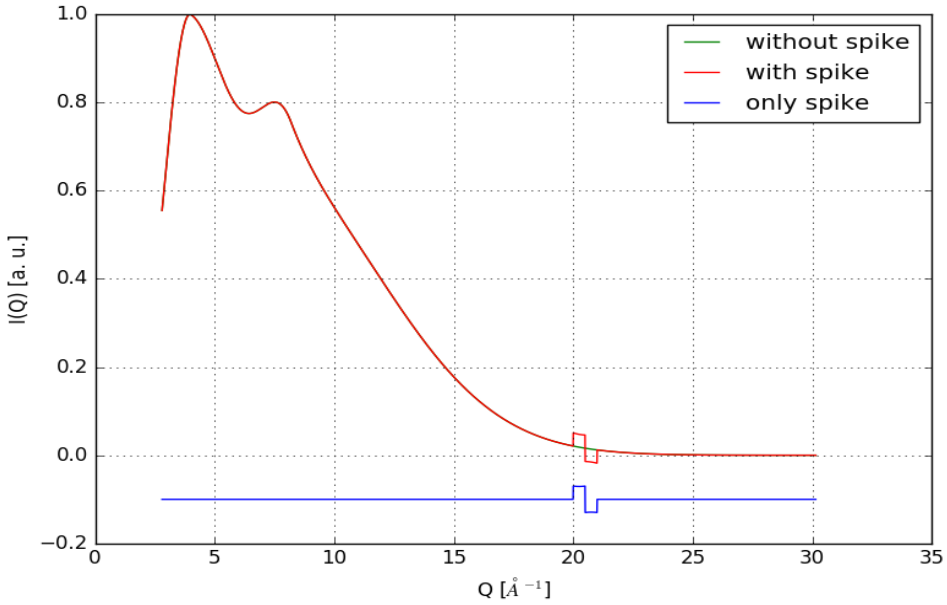

Figure 5.12: A theoretical model curve with a smooth slope was created and spiked with some ripples. The comparison shows both curves.

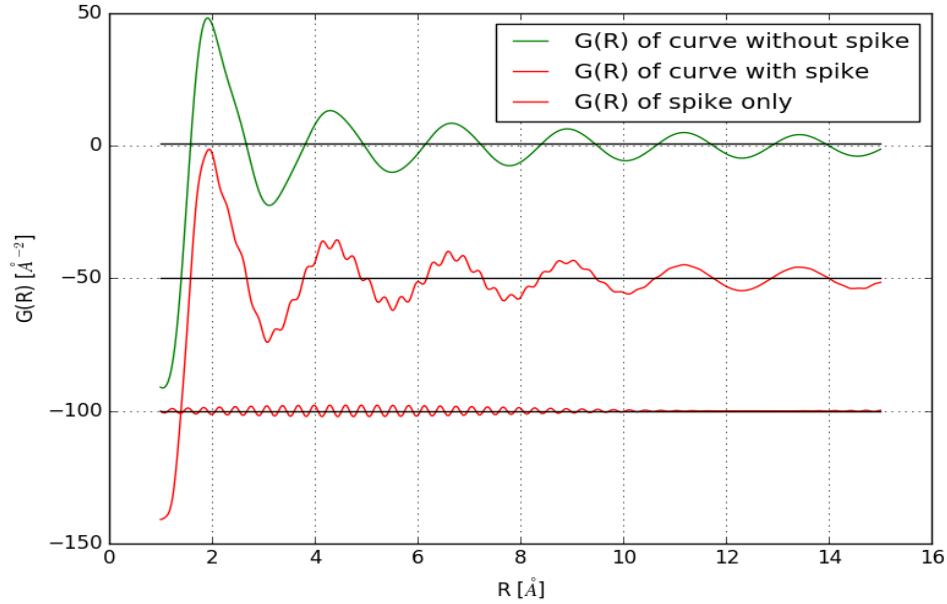

Figure 5.13: $G(r)$s of the theoretical curves from figure 5.12 obtained by FT. The FT of the "spiked curve" shows additional ripples, which stem from the addition of a sinc-function.

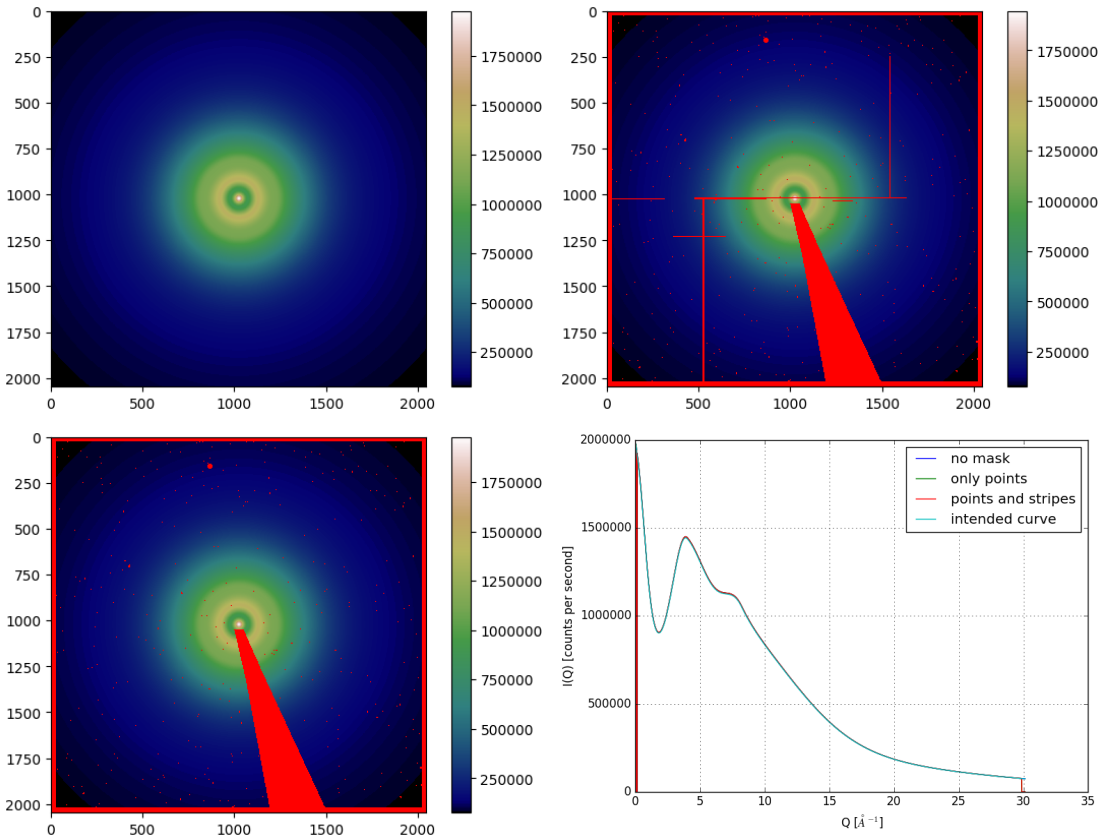

Figure 5.14: A "dummy image" has been integrated under three different circumstances. Firstly without a mask (upper left). Secondly considering masking only visible defect spots (lower left). Thirdly with visible defect spots and boundaries between detector panels masked (upper right). In the lower right the integrated curves are depicted. There is no difference between those curves, verifying that the integration procedures are working correctly. GSAS-II (Toby and Von Dreele 2013), FIT2D (Hammersley et al. 1996) or DIOPTAS (Prescher and Prakapenka 2015) give very similar results. Some of the other programs superpose a slope in order of resemblance the LP-effect found in conventional diffractometer-data. The exact procedure of this superimposition was not examined.

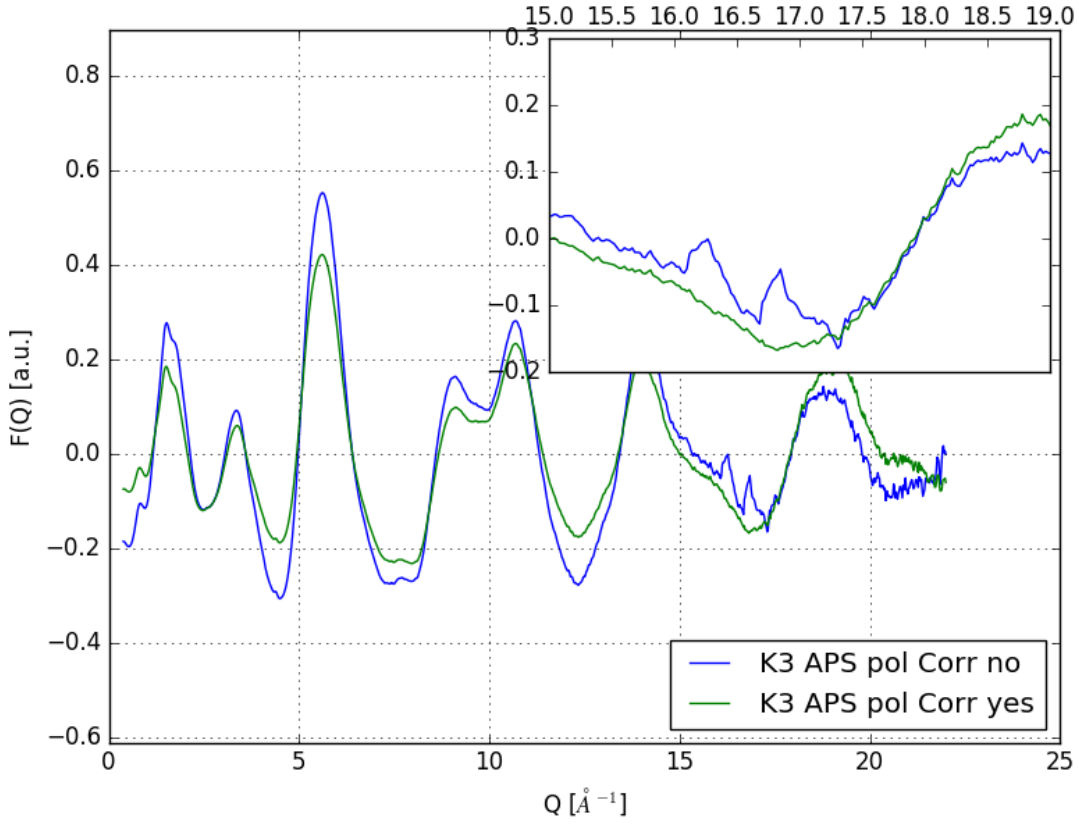

Figure 5.15: Comparison of $F(Q)$s of S2 resulting from correction of raw intensities obtained by integration of 2D-detector-images of an organic amorphous substance applying and not applying polarization correction. The points-and-stripes-mask from figure 5.14 was applied for masking faulty regions. The spike vanished in the polarization corrected sample.

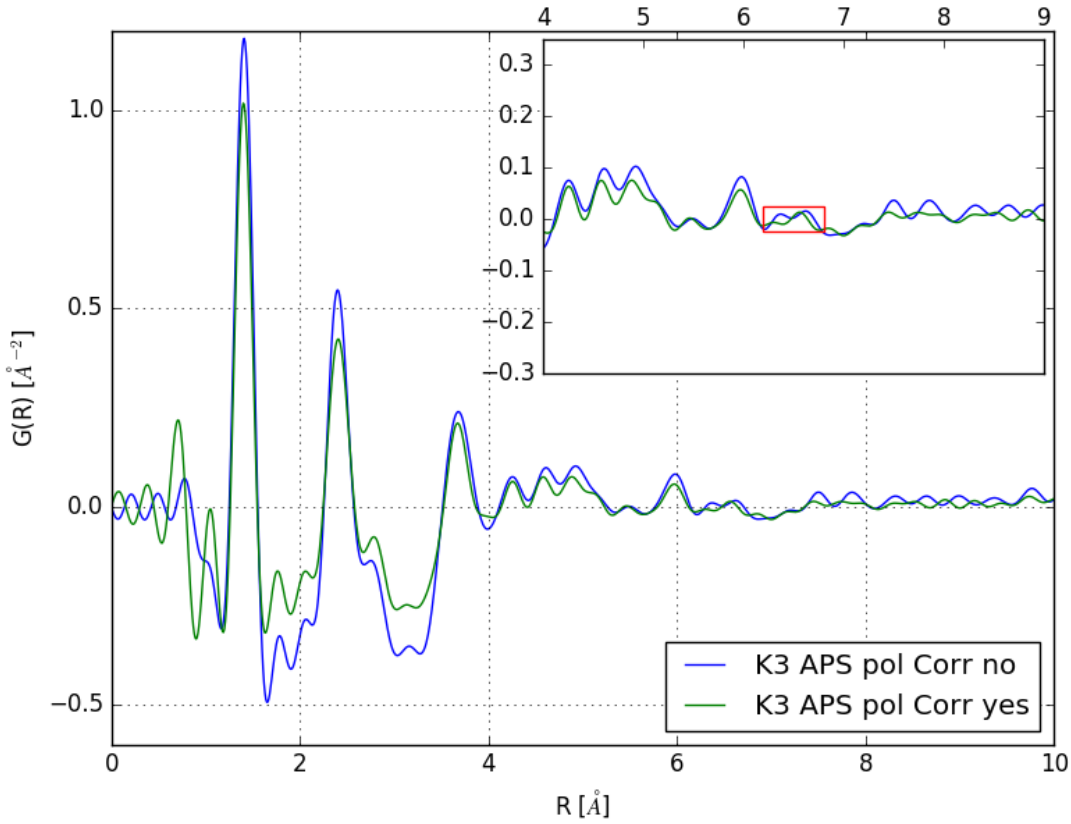

Figure 5.16: Comparison of resulting PDFs from 2D-detector-images integrated applying and not applying polarization correction using S2 (see page 84) as example. The comparison, e.g. in the area marked by the red square, shows quite plainly that slightest variations in the data processing steps can give differences. High quality comparisons as done in Petkov et al. (2009) (who used 1D synchrotron detector data) might be rendered impossible. A data reduction procedure should be traceable, reproduceable and unique. It is still under investigation whether the main artefacts in the $G(r)$ curve stem only from details in 2D-integration or also on the data transformation procedures used in pdfgetX3 in this case. Possibly it is a mixture of both. As figures 5.12 and 5.13 suggest, non-structural artefacts alter the PDF on their own. Also, we can keep in mind that, even if an ad-hoc polynomial is applied in the pdfgetX3-software, this does not remove sharp features as spikes. They become that obvious because of the weighting with Q in $Q[S(Q)-1]$. See also in the more recent Hansen et al. (2018) who identified the allegedly contribution of an amorphous phase in the layered compound $CrTe_3$.

Figure 5.17 gives a comparison of the outlier-masks S1-M1 (left) and S2-M1 (right), which were determined with DAWN after polarization corrections have been performed, of the 2D-data sets of two different substances, S1 and S2 (see page 84). Figure 5.18 shows the outlier-mask of S2 (S2-M2) taken before polarization correction. There is much difference between the masks S2-M1 and S2-M2 but also an appreciable difference between S1-M1 and S2-M1, which were obtained after corrections with the same parameters applied.

Figure 5.19 gives the $F(Q)$ curves of polarization corrected S2 after integration with different masks (points, points-stripes, outlier-before-polarization-correction, outlier-after-polarization-correction). Figure 5.20 shows the respective $G(r)$ curves: The differences are small in this case, nevertheless they fall into the same order of magnitude as differences in $G(r)$s found in examples cited in the review article of Young and Goodwin (2011).

5.2.6 Do we need more sophisticated data-calibration and correction techniques?

It is clear that we can only do our best to rule out errors. In the light of the observations concerning the limits of masking and intensity corrections it seems advisable to reconsider the current practices from manipulating 2D-detector images up to integration. In what follows an alternative calibration routine is proposed. It is more sophisticated but also more complicated than the established existing ones.

- Take the 2D-diffractogram of a well known ideal powder like a NIST standard (state of the art)
- As in the current routine, evaluate detector tilt and rotation
- Calculate a 2D-pattern by means of a model that incorporates container, specimen orientation, polarization state of incoming light etc
- Make very sure that you accounted for every known aspect
- Consider that pixels might respond differently according to exposure time. (This might justify the application of an additional outlier-mask on the

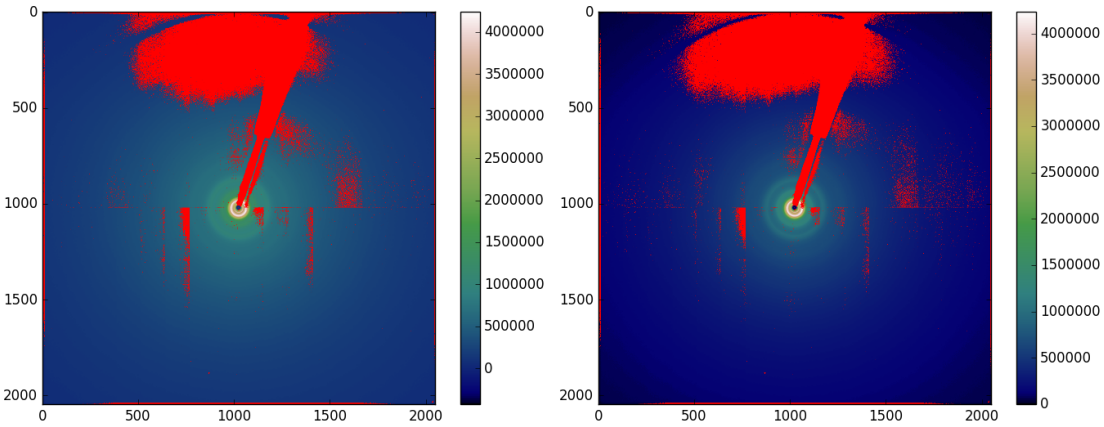

Figure 5.17: Comparison of the outlier-masks S1-M1 and S2-M1 of the 2D-diffraction patterns of two substances S1 (left) and S2 (right), which were taken after polarization correction for the same detector. Even with an outliermask, no definite solution concerning the faulty pixels is obtained (the choice of the threshold is subjective).

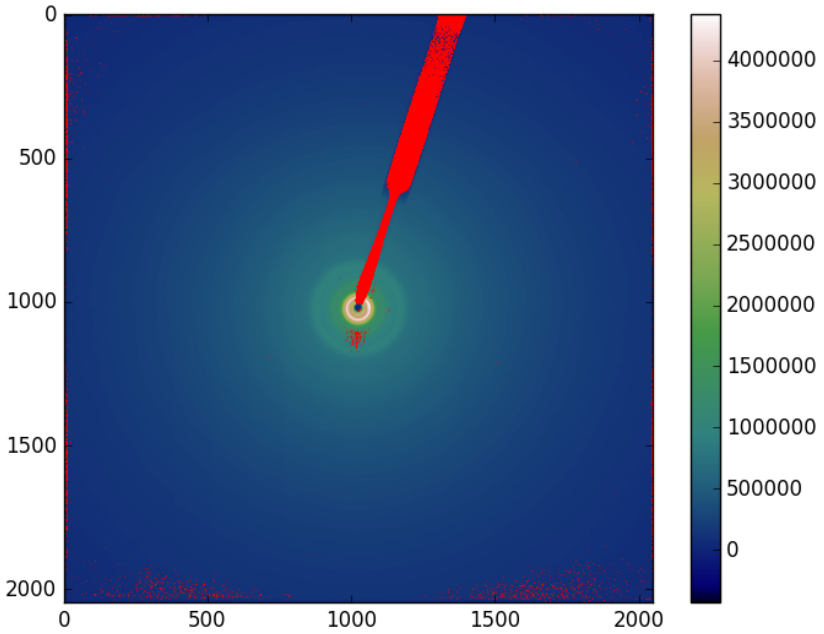

Figure 5.18: Outlier-mask S2-M2 on the dataset of S2 before polarization correction. In comparison to S2-M1 a very decent area of the image is masked.

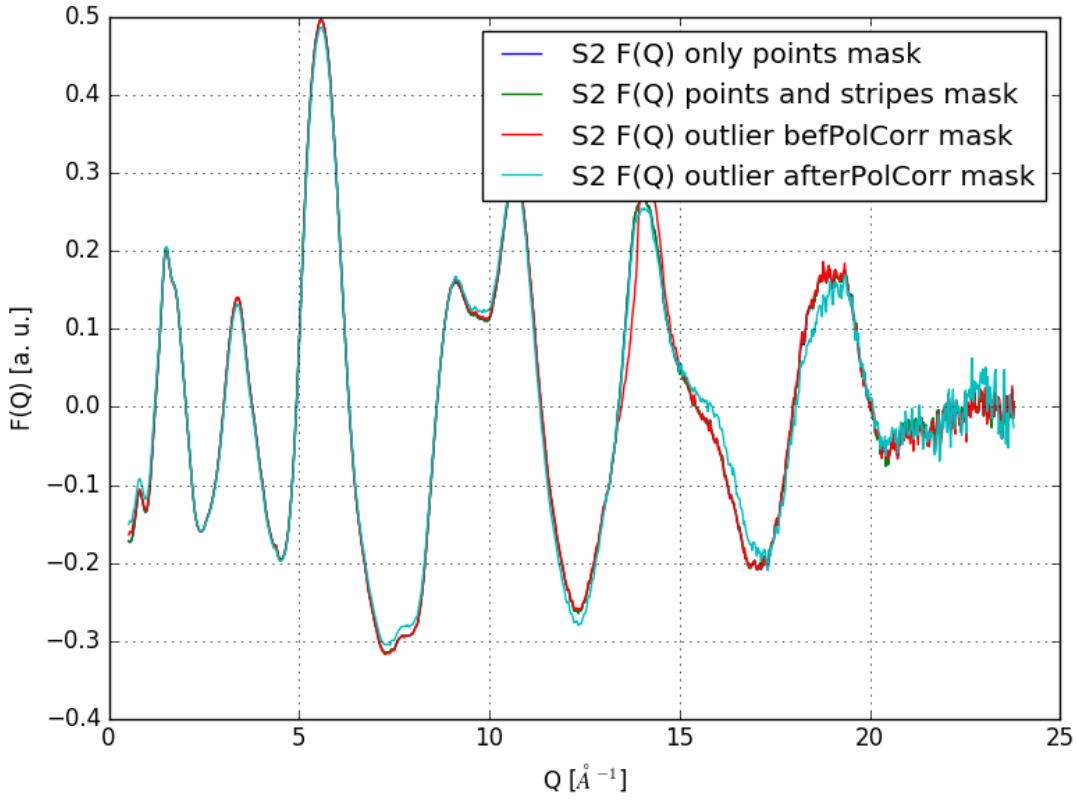

Figure 5.19: $F(Q)$s calculated with identical values for correction parameters from S2 integrated with polarization corrections but with different masks. - An ad-hoc polynomial correction has been applied . As the differences seen are not continuous, it is asserted that the differences are already contained in the raw intensities and therefore due to the differences in the integration procedure and not subsequent to data correction.

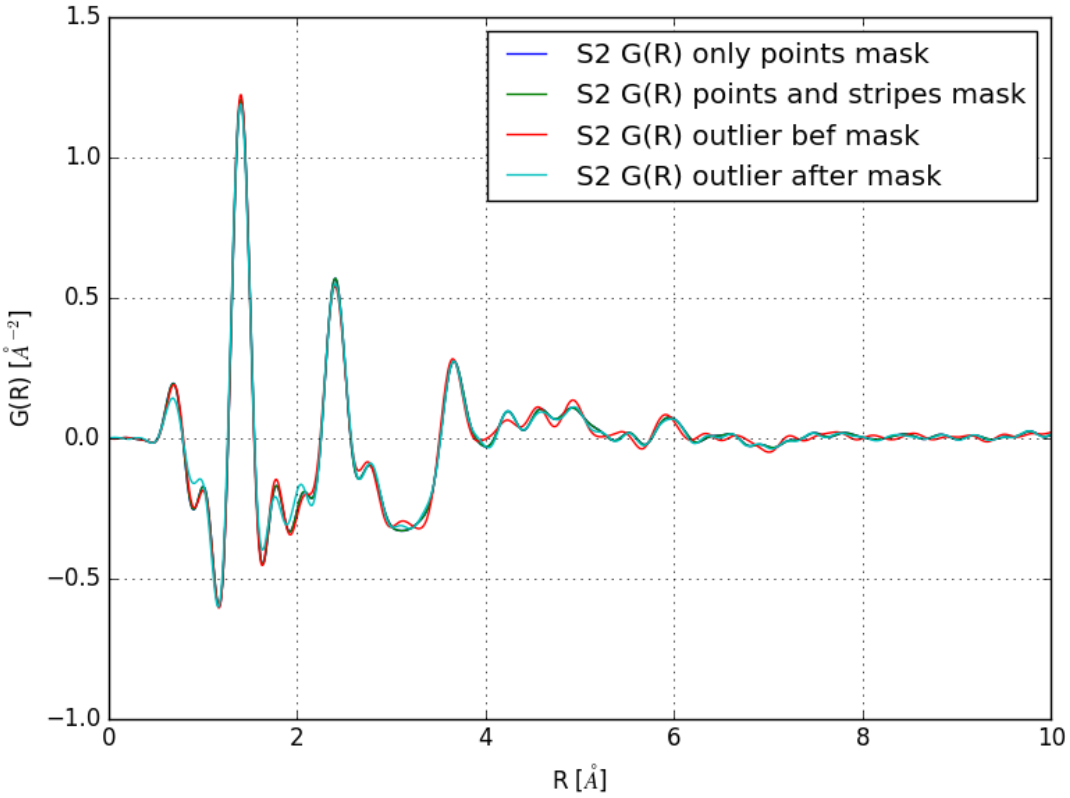

Figure 5.20: $G(r)$s of S2 calculated with identical values for the PDF-correction parameters from the $I(Q)$s in figure 5.19 which were integrated with polarization corrections but with different masks. - Slight difference are seen. The PDF is sensitive to shifts of peaks along R due to variations of bond-distances. Depending on the aim of analyses, the differences here might not be neglected.

other experimental patterns. The detector could also be evaluated by means of substances with different scattering powers. A data extraction approach to find a statistical model of the location of faulty pixels could be applied on a set of images.)

- Do a normalisation of each pixel due to a comparison of measured and calculated model
- Get a scaling matrix containing the ratios measured/model-calculation of every pixel
- Define a mask
- Use the scaling-matrix for correction of each other experimental pattern.
- Do all other corrections if really necessary before integration
- Integrate. Take into account that signal stemming from an inelastic scattering process might call for special treatment or correction.

5.3 Conclusions

Interpolation for rebinning was found to be neglectable, even under the presence of noise in the raw data. Interpolation in data merging procedures might have unwanted side effects and are not fully understood.

In processing data from 2D-detectors, masking is an important part. It determines from which pixels intensities are azimuthally integrated to a 1D-diffractogram. The 2D intensity distribution and which pixels must be masked out is influenced by data correction procedures such as polarization correction. Depending on the sequence of data reduction steps the integration results can be vary, sometimes containing artefacts the origin could not yet be rationalized. The questions how the elucidated effects in data handling and correction-methods might be treated best and if it is always clear how to distinguish «real features» from «artefacts» wait to be answered as well. Additional research is necessary.

Chapter 6

Capabilities of PDF-analysis in investigating quasi-amorphous materials

- details on refinements and data reduction

PDF-refinements were performed with the DISCUS-SUITE (Neder and Proffen 1997), which is a feature-rich, flexible and efficient program. It is possible to refine amorphous structures with this software if an initial-model is available. There are also other programs dedicated to the building and refinement of amorphous or strongly disordered supercells (RMCPOT Gereben and Pusztai (2012) or RMCPROFILE Tucker et al. (2007)).

1D-data correction and PDF-creation was done using the pdfgetX3-software (Juhás et al. 2013).

Values for Q_{damp} and Q_{broad} were obtained in a refinement against the PDF of a CeO_2 sample with an R_{max} of 60 Å.

In the refinements, all data points below the first interatomic distance were down-weighted by a factor of $1/10000$, because this is the region below r_{poly}, which does not contain meaningful information. The concept of r_{poly} is discussed in section 4. This gives the weighted R-values in this study and the weighted R-values will simply be called R-values in this chapter.

- details on data collection and reduction

Measurements were performed at the APS synchrotron facility (beamline 11 ID B, $\lambda = 0.21140$ Å with an detector-to-sample distance of approximately $162\ mm$; Argonne, U.S.A.).

Data handling was done with DAWN2 (Filik et al. 2017). Detector calibration was done by means of a CeO_2-standard. Radial integration of 2D-patterns was done without geometrical correction or polarization correction (Juhás et al. (2013) assert that correction for instrumental effects is not necessary with pdfgetx3).

6.1 The difficulties of describing glasses and creating initial models

Simulation of disorder in crystalline compounds is possible by (systematically) altering a sufficiently sized model (see e.g. Neder and Proffen 2008). Glasses (amorphous substances) mostly are also simulated by means of large cells but often the treatment must be different and already arriving at at sufficient initial model can be a task, which is no given by clear building instructions. - A comprehensive overview is given by Zallen (1985).

A proper starting structure is crucial for any simulation. Such initial models can be further refined and analysed. In the case that the material is built of units that are in turn built of multiple atoms and which exhibit SRO, the material can be built through arrangement of those building units. Dependent on the interactions between the building units different approaches might be chosen. As a rough classification, there appear to be two possibilities for creating initial models of an amorphous material: A molecular glass without covalent interactions might be an example for the first kind of amorphous solids, which are similar to a molecular liquid. Alterations at the position of one molecule might only slightly impact surrounding molecules. Network glasses as exhibited in amorphous SiO_2 are taken as an example for the second kind of amorphous solids. There, the building units are interconnected covalently and share atoms at their "points of connection". It appears that movements of a unit in those structures impacts surrounding units stronger as is the case in molecular amorphous solids.

Notably, modelling glasses is a problem of filling (packing; tiling) a space with atoms in an appropriate manner but due to the geometric peculiarities, i.e. mostly lack in periodicity, it is not clear which rules must be abided (Aste and Weaire 2008).

Extensive studies and discussion on network glasses have been performed by Djordjević et al. (1995), Wooten and Weaire (1984), Wooten and Weaire (1987b) and Wooten et al. (1985), more recent Barkema and Mousseau (2000), Barkema and Mousseau (1996), Mousseau and Barkema (2001), Pandey et al. (2016), Sava and Popescu (2011) and Tu et al. (1998). Many of them deal with tetrahedral networks but in any case of modeling it is preferred to achieve a set of basic goals:

- Compatibility with periodic boundary conditions. - This is important because we want to avoid finite-size and surface effects and yet obtain reasonable coordinations of all atoms.
- The method must be practical for samples of at least several hundred atoms.
- A flexible, efficient and comprehensible algorithm should be available.
- Good agreement with the observed radial distribution functions (which is not sufficient, as e.g. Treacy and Borisenko 2012 show), angular distribution function and ring statistics should be achieved. There might be more or other criteria, depending on the structure at hand.

Known ways to create networks with tetrahedrally coordinated species in software (Wooten and Weaire 1987a) are:

- **Accretion**. A cluster is grown by progressive addition of atoms. This is attractive mostly when surface properties or the kinetics of a deposition process are of interest. Moreover, chemical and geometrical constraints have to be taken into consideration as well as mechanisms for preventing infinite loops due to not satisfiable (surface) geometries. In the case of packing isolated, intraconnected systems such as molecules to amorphous

supercells, a packing problem must be solved. Research has been done on that by Martínez et al. (2009) and for example the program PACKMOL (Martínez et al. 2009) can fill space with objects by calculating the objects' envelopes and trying to fill a given volume as dense as possible (or specified) given those envelopes.

- **Molecular dynamics**. Examples for this are the in-silico "melting" of quartz to get a silica-glass (Lee et al. 2006). One also has to consider the possibility of multiple local minima (Soules 1990).

- **Randomization and relaxation**. By means of this procedure highly random structures can be created and then relaxed towards a low-energy structure which is so disordered that on average all long range correlation is lost but SRO preserved. This method can use very simple interatomic potentials and restrict covalent bonding to a given type. It works within a restricted space of bonding possibilities. More and more precise interatomic potentials are published to generate e.g. tetrahedral bonding (Pedone et al. 2006; Shan et al. 2010). The rules and potentials may be rather arbitrary and "unphysical" (in other terms empirical).
  An example for this is the rule to only switch parallel (approximately) second-neighbor bonds in the generation of amorphous Silicon (Wooten and Weaire 1987a, p. 15). But the procedure can be fast and simple and can give reasonable models. This exemplary procedure is also referred to as Winer-Weaire-Wooten (WWW) algorithm. - Implementing of such a modified WWW algorithm for the creation of amorphous SiO_2 (as proposed by Barkema and Mousseau 2000) into DISCUS for this work, was not (yet) successful, due to limited resources.

As a literature research revealed, a reverse-monte-carlo (RMC) refinement is well suited for creating amorphous Si with tetrahedrally coordinated Si. Given some constraints concerning the coordination and center-to-center distances, a configuration with the desired properties can be created out of a random configuration of atoms.

Concerning silica-glasses, which are the subject of this chapter, much research has been done, beginning with the general insights (Zachariasen 1932) over the

SRO of the building units (e.g. Warren et al. 1936) to the atomic arrangement at large scales (Bowron 2008; Lorch 1969; Marians and Burdett 1990; Wright 1994; Wright et al. 1991).

6.2 Analysis of amorphous networks with the stoichiometry $(SiO_2)_x(TiO_2)_y$ for use as catalysts

In 1983, Taramasso et al. filed a patent (Taramasso et al. 1983) concerning the zeolithe TS-1 (titanium-silicalite), which exhibits catalytic activity (phenol hydroxylation, olefin epoxidation, alkane oxidation, oxidation of ammonia to hydroxylamine, ammoxidation of cyclohexanone and hydroxyacetophenones, and oxidation of secondary alcoholes to ketones; see Henry et al. 2001). Its parent structure is silicalite-1. Being a highly porous substance, TS-1 has a high surface area and a large amount of active sites is therefore available.

An important, controversial question concerns the coordination number of the Ti-atoms with respect to oxygen. No study of total scattering data is documented in literature. Extensive studies (Rietveld analyses and neutron scattering using isotope substitution) have been performed on TS-1 to gain information about the crystallographic sites preferentially occupied by Ti (see Henry et al. 2001).

Li et al. (2001) state that a 4-fold coordination of Ti-atoms by substitution of bulk Si from SiO_2 is the reason for the material's catalytic properties with respect to e.g. epoxidation reactions of polypropylene in presence of H_2O_2. They report three kinds of species composed from Ti and O, which are distinguishable in spectroscopic analyses. One is anatase, which is capable of the oxidation reaction of H_2O_2 alone and is therefore unwanted. The second species species also exhibits sixfold coordination of Ti by O atoms and is removeable by washing with HCl, and third is Ti in fourfold coordination by O. In catalysts without anatase but the other species with sixfoldly coordinated Ti-atoms, only the epoxidation reaction takes place. After washing with HCl, the catalytic activity is preserved as well as the Ti on fourfold coordinated sites, but the species exhibiting sixfold coordination vanished, as IR-spectroscopy reveals. - From these experiments, it is inferred that the catalytically active site is Ti-atoms

which substituted Si-atoms in the SiO_2-network. It is argued that this Ti species is relatively instable, because the ratio of the atom radii Ti^{4+}/O^2 in TiO_4-tetrahedra exceeds the range where a tetrahedral configuration is stable. Nevertheless, this instability is required for the epoxidation reaction to take place but it is also difficult for Ti atoms to enter the framework and occupy Si-positions. This substitution happens only when low Ti amount are present during synthesis, otherwise clustering to 6-fold species occurs.

Some Rietveld-studies indicate that tetrahedrally coordinated Ti at Si-positions in TS-1 is consistent with the diffraction pattern and therefore Ti is fairly distributed in the network (Lamberti et al. 1999). Yang et al. (2008) state that TS-1 is a material, which exhibits multiple kinds of defects that are effective in proton transfer reactions connected with catalytic activity. Also Henry et al. (2001) report Si-vacancies and above this the systematic distribution of vacancies ans Ti atoms in the framework.

No consensus appears to be found yet on the coordination or exact position of Ti in TS-1 in literature and therefore also not on the origin of the catalytic activity. It should be emphasised that there appear to be many routines for preparation of TS-1 with different Ti-amounts. It might therefore be difficult to speak of a unique TS-1 and even more difficult to make a valid statement concerning the actual structure of "real" TS-1.

Porous and amorphous materials with the stoichiometry $(SiO_2)_x(TiO_2)_y$ and Ti in the required 4-fold coordination are said to be desirable from a technological point of view, because they exhibit improved mechanical stability compared to TS-1 and comparable catalytic activity. With increasing amount of Ti during synthesis of these new materials, an elevated probability of elements with sixfold coordination of Ti by O atoms, which form agglomerates with the characteristics of an anatase unit cell is declared. This is supported by spectroscopic analyses (EXAFS, UV-VIS, IR) (Flaig et al. 2014). As TS-1 is crystalline and periodic, strong deviations from the mean atomic positions should be visible in the diffraction pattern. On the other hand, nano-crystalline or amorphous structural elements, which show very broad diffraction patterns, might be lost in the background in a Rietveld refinement, especially in low concentrations. It is uncear, if clustering of O, Ti and vacancies can fake 4-fold coordination of Ti by O in EXAFS or other

spectroscopic measurements. Keeping the potential variability of the substances and influences of the synthesis route in mind, a PDF-study is performed in the following.

6.2.1 Samples and characterizations by XRF and SAXS

Two kinds of $(SiO_2)_x(TiO_2)_y$ samples with the names SF154 and SF155 were investigated. Their nominal TiO_2-contents are $y/x = 1/36$ and $1/6$. The samples were synthesized by sol-gel-processes by S. Flaig according to Flaig et al. (2014).

X-ray fluorescence analyses (XRF) have been performed on a home-built device (by Peter Wobrauschek from Atominstitut/TU Wien) and the obtained compositions under the assumption of stoichiometric oxides are shown in table 6.1.

Small-angle-X-ray-scattering (SAXS) measurements indicate elongated pores in the substances with approximately hexagonal arrangement, spaced by 10 nm. In the sample with higher Ti-content, this arrangement is lost. Th slope of the curve could be explained by inclusions in the material in the nm-range. Fused silica shows none of those features (figure 6.1).

Although interesting, no satisfactory investigations via TEM could be performed because electrostatic charging of the samples made focusing impossible.

6.2.2 PDF-refinements and discussion

Figure 6.2 gives a comparison between the diffractograms and the PDFs of fused silica, SF154 and SF155. The PDF of SF155 exhibits a shoulder at approximately 1.9 Å. A comparison with the partial PDFs of Ti-O from crystal-structures that

Table 6.1: Composition of the $(SiO_2)_x(TiO_2)_y$-samples according to XRF measurements

sample	Transition	Si as SiO_2 [wt%]	Ti as TiO_2 [wt%]	Si [mol%]	Ti [mol%]
SF154 XRF	Ka	92.86	7.14	94.5	5.5
SF155 XRF	Ka	70.36	29,64	75.9	24.1

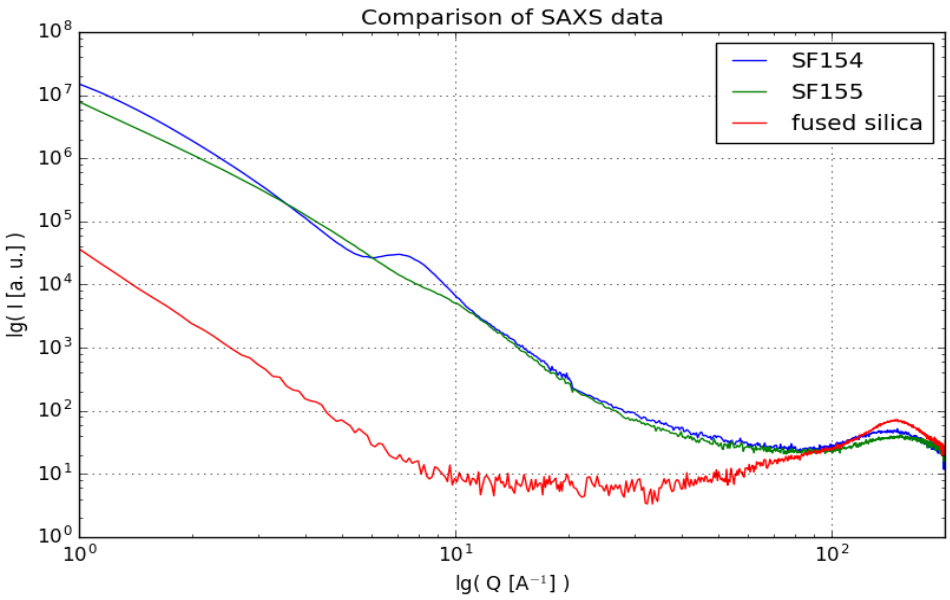

Figure 6.1: SAXS measurements of the Ti-containing SiO2 samples. Many thanks to Herwig Peterlik from University of Vienna for measurements and interpretation.

contain units of TiO_4 (Ba_2TiO_4 and TS-1) is given in figure 6.3. It can be seen that none of the structures help to explain the shoulder. This indicates that there are Ti-O distances that do not correspond to tetrahedrally coordinated Ti.

The difference curve between SF154 and fused silica shows a decent alternating behavior in the regions at approx 4, 5.5 and 7 Å (figure 6.4). This could be described by a dampened oscillation of the form $sin[\pi(x/\lambda - \varphi)]exp[-(x-pos)^2/\sigma_{as}^2]$ where $\sigma_{as} = \sigma/asym$ if $x < pos$ and $\sigma_{as} = \sigma * asym$ if $x > pos$. The distinction of cases is incorporated in order to introduce an asymmetry. The fitted function is drawn in turquoise and named "wave". A wave of this form was added to the refinement in figure 6.5 and helps decreasing the R-value.

Investigation of SF155 shows that a fit of the PDF of fused silica and the PDF of a spherical cut from a supercell of rutile can explain the features well (figure 6.6). Also in this case, the difference curve shows a dampened oscillation.

A refinement of the PDFs of fused silica, spherical Rutile-particles and the dampened oscillation to SF155 gives an reasonable fit as shown by the weigthed R-value in figure 6.9. A refinement including the PDF of rutileand the PDF of

SF154 (instead of fused silica and the dampened oscillation) gives a reasonable fit as well, but the R-value is slightly higher (figure 6.8).

To justify the application of rutile in the initial model, anatase was ruled out. This was done by refinements of the PDF of SF154 (= fused silica + dampened oscillation) together with a spherical cut from a supercell of anatase against SF155. The R-value is not as low as the R-value of the refinements invoking rutile and the refinement is shown in figure 6.7

A final refinement of fused silica, rutile and a dampened harmonic oscillation against SF154 shows that incorporating rutile even helps lowering the R-value (6.10). This could be an indication that, also in the material with low amounts of Ti, no incorporation of Ti into the SiO_2-network happens but formation of precipitates containing Ti and O atoms.

The refinements show that for SF154 and SF155, a model of fused silica and titanium-oxide in the rutile modification together with a dampened harmonic oscillation against the experimental PDFs gives reasonable fits. - In the original publication (Flaig et al. (2014)) no such features were reported but on the other hand they were not sought for. It is unlikely that the material altered because the material's porous structure remained stable also after long periods as SAXS measurements showed.

It is an interesting question what the origin of the central two peak feature is. Is it the same in SF154 and SF155 or does it appear for two different reasons: as in both refinements incorporation of a Rutile-PDF helps lowering the weighted R-value it seems sound to suppose that both materials contain small precipitates of Ti-O in the Rutile-modification in different concentrations. The dampened wave can be interpreted as restructuring of the amorphous matrix around the TiO-particles. Such interpretations are accepted in the literature dealing with colloids and other liquid-solid-dispersions (Zobel et al. 2015). Accordingly, it would be interesting to do RMC-modeling of such small particles embedded in the amorphous SiO_2-matrix. Nowadays, interfaces of heterogeneous materials are claimed to be modelable (Tu et al. 1998). Anyway, a low R-value is not everything and strict attention must be paid to distinguish termination ripples, artefacts owing to noise and data correction, and baseline differences, which all can counterfeit structural features. More research is called for.

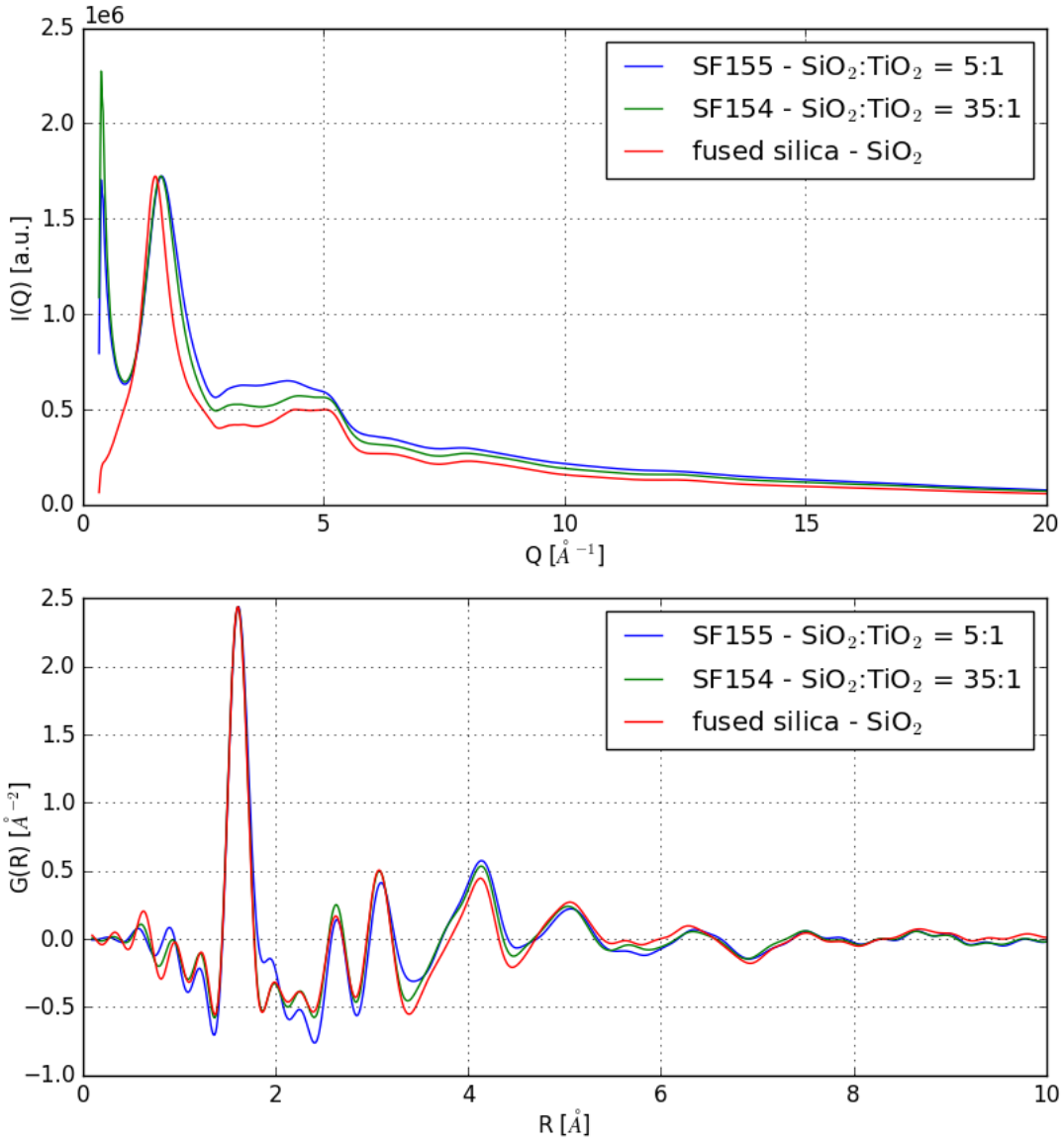

Figure 6.2: Comparisons of the diffractograms and PDFs of fused silica, SF154 and SF155. The PDFs of fused silica and SF154 look very similar but SF155 exhibits a shoulder around 2 Å.

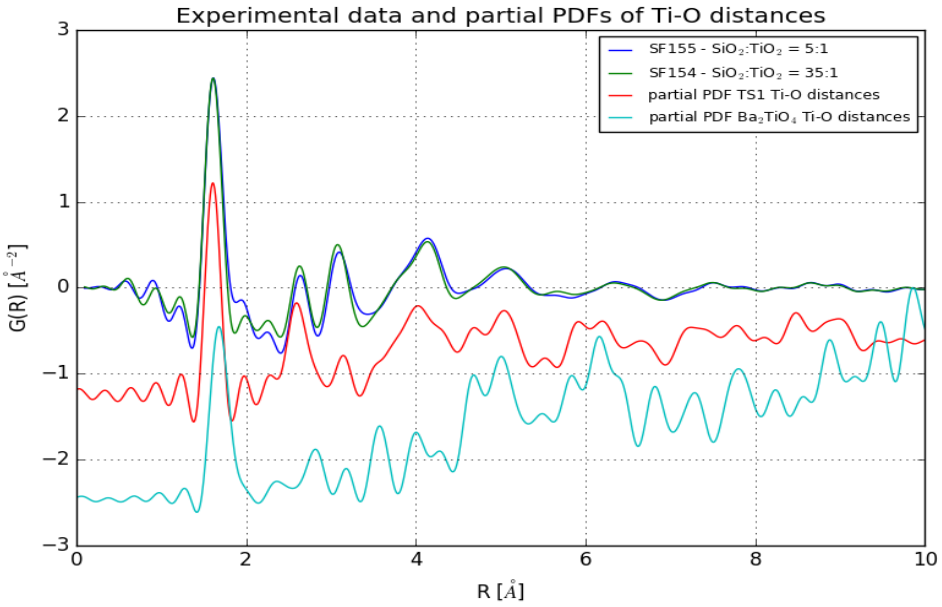

Figure 6.3: Comparisons of the PDFs of SF154 and SF155 with the partial PDFs of all distances between the Ti and/or O atoms in TS-1 and Ba_2TiO_4. - Concerning the comparison with TS-1 there could be a bias because the documented structure presupposes that Ti occurs on tertrahedrally coordinated Si-sites. The tetrahedra in Ba_2TiO_4 are no perfect tetrahedra. A comparison with the partial PDF can only be suitable at short distances because the long range order in the crystalline structure strongly differs from the atomic arrangement in the glass. - Comparisons should be taken with precaution because of termination ripples, artefacts owing to noise and data correction, and baseline differences.

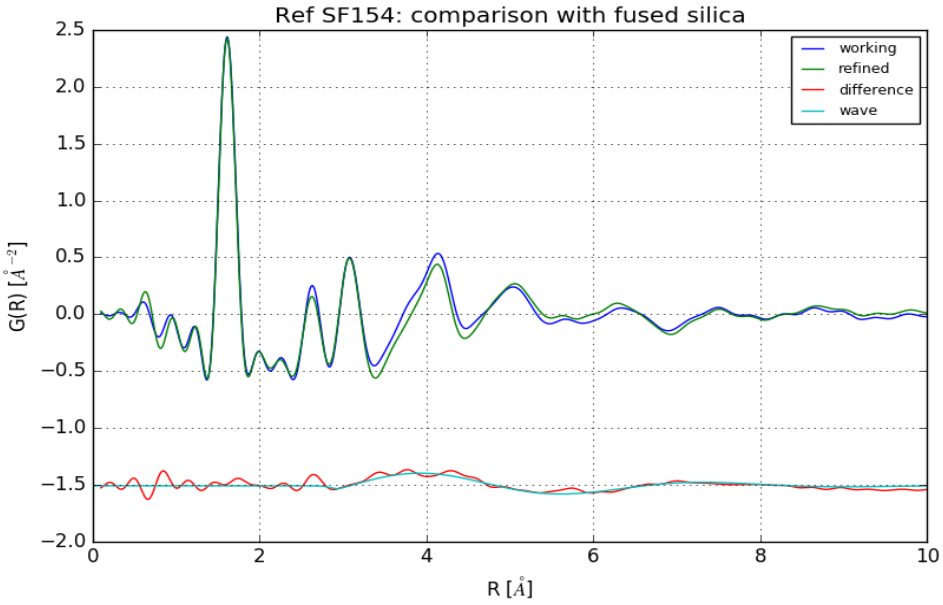

Figure 6.4: The PDF of fused silica was scaled to the PDF of SF154. The difference curve shows an dampened oscillatory behavior which is indicated by the fit "wave" to the difference curve; weighted R-value: 0.1339

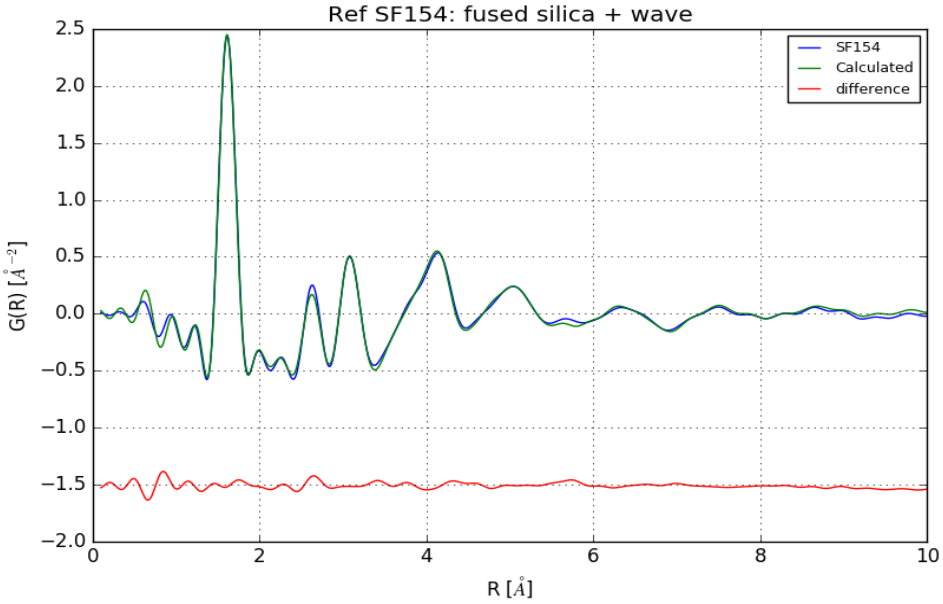

Figure 6.5: Refinement of the PDF of fused silica and a dampened oscillation such as seen in 6.4 against the PDF of SF154; weighted R-value: 0.0604

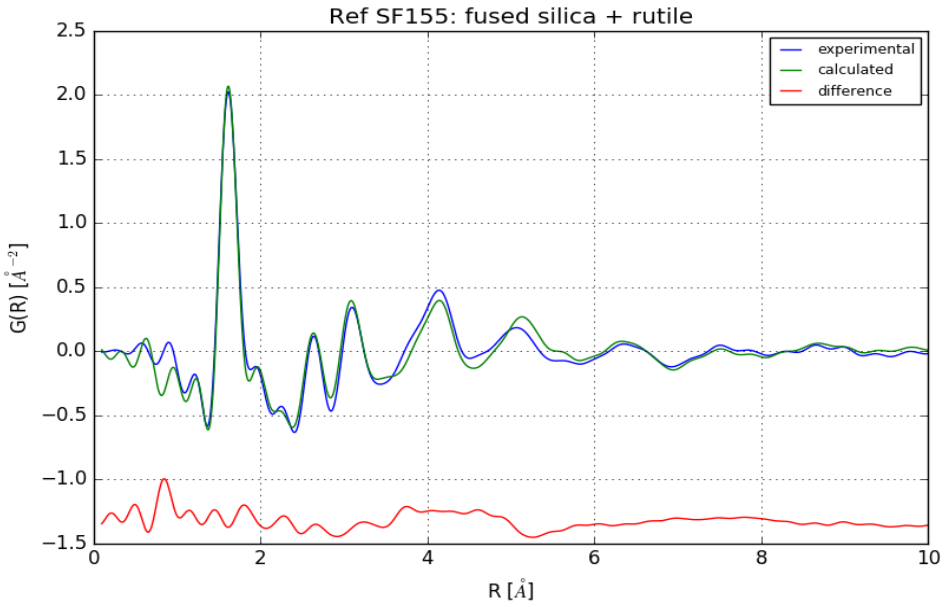

Figure 6.6: Refinement of rutile and fused silica against the PDF of SF155: also here, the difference curve shows an alternating behavior; weighted R-value: 0.1587

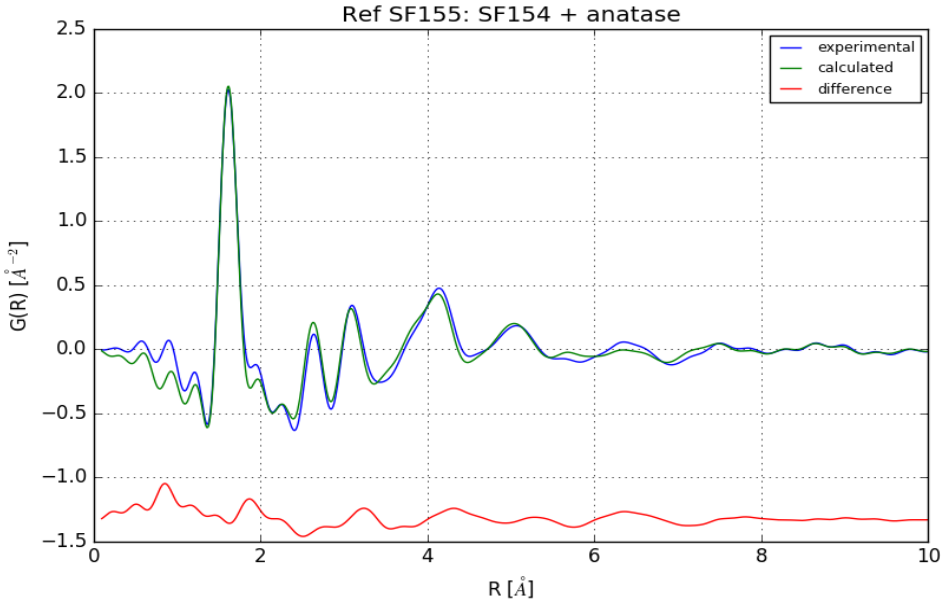

Figure 6.7: Refinement of the PDFs of anatase and SF154 (which ressembles the PDF of fused silica combined with a dampened oscillation) against SF155; weighted R-value: 0.2237

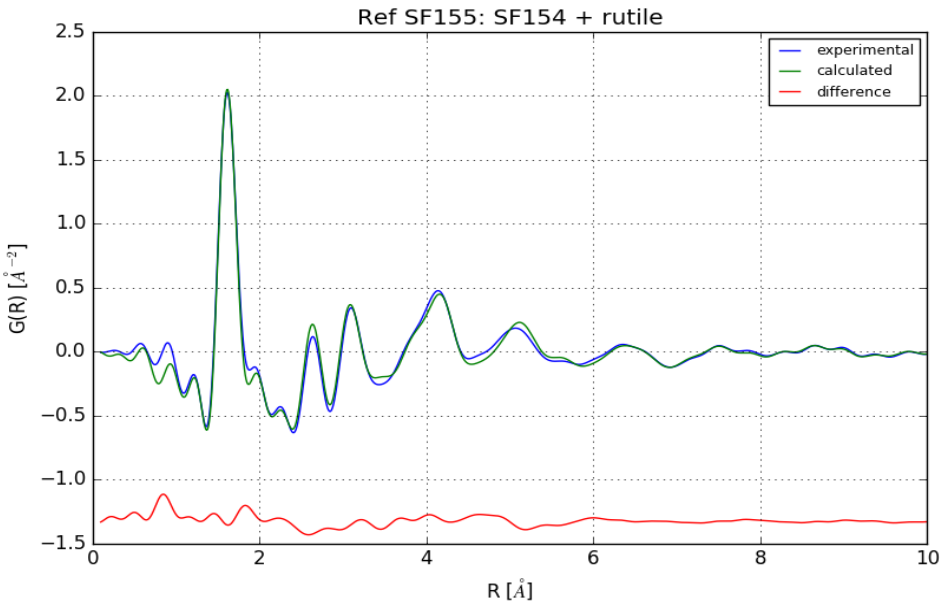

Figure 6.8: Refinement of the PDFs of rutile and SF154 (contains the wave) against SF155; weighted R-value: 0.1031

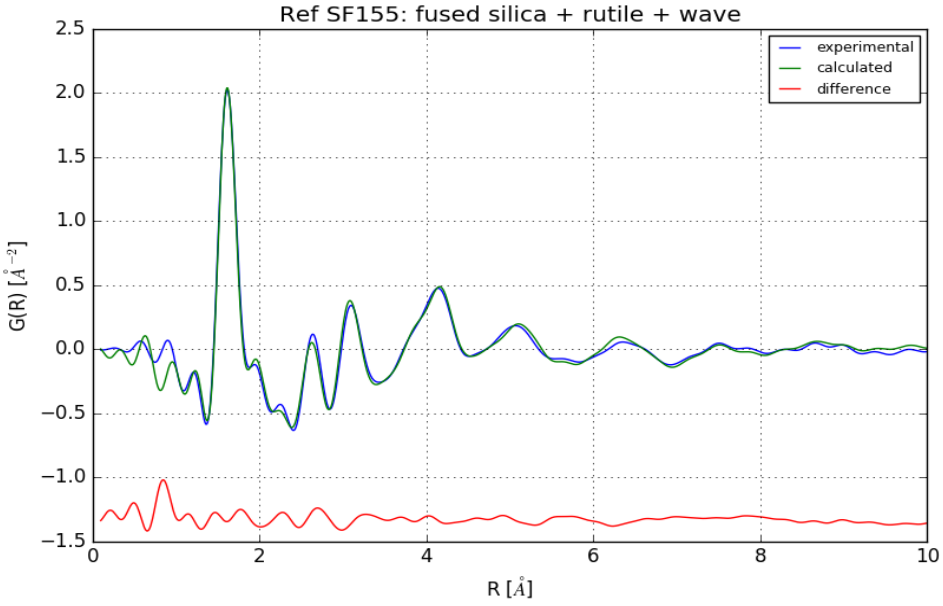

Figure 6.9: Refinement of the PDFs of rutile with fused silica and a wave against the PDF of SF155; weighted R-value: 0.0926

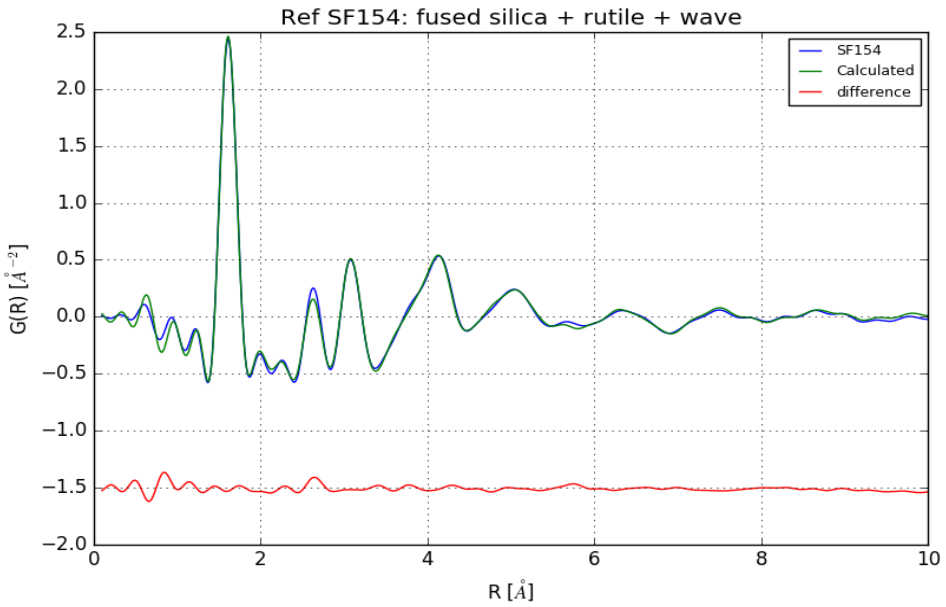

Figure 6.10: Refinement of the PDF of SF154 by aid of fused silica, rutile and dampened oscillation; weighted R-value: 0.0534

6.3 Conclusions

The PDFs of two amorphous mixed oxides with the stoichiometry $(SiO_2)_x(TiO_2)_y$, intended to mimic the catalytic properties of the zeolite TS-1 were analyzed. The experimental PDF could be modeled with a contribution by amorphous SiO_2 and small spherically shaped crystalline TiO_2-particles in the rutile modification, i.e. Ti in six-fold coordination. A model based on a pure glass phase with Si partially substituted by Ti in four fold coodination did not result in as good an agreement. The features in the difference PDF indicate interaction between the particles and the surrounding matrix. The PDF of fused silica plus a damped oscillation and of the particles lead to a very good fit of the experimental data.

This is also interesting as in literature concerning TS-1 only the occurrence of TiO_2 in the anatase-modification at high Ti-contents during synthesis in mentioned. In parallel, different literature asserted clustering of Ti and O atoms as well as Si vacancies in the SiO_2-matrix. At no point rutile was discussed or taken into consideration. It is documented that embedded particles can alter the properties of a material such as its glass-transition temperature (Berriot

et al. 2002). It might be possible that this is valid also for catalytic properties in this "derivatives" of TS-1.

TEM and SAXS measurements indicate a structure of elongated pores, but due to electrostatic charging in the TEM no magnification sufficient for the detection of the small TiO_2 particles could be achieved.

Chapter 7

Capabilities of PDF-analysis in investigating partly crystalline materials

- details on instrument settings and data collection

Measurements for obtaining data suitable for PDF-analyses were performed on a PANalytical Empyrean diffractometer in Debye-Scherrer setting. Table 7.2 contains the instrumental parameters and details on the measurements. Diffractograms were created with Ag-radiation because information on disorder was of interest too.

Measurements for the quantification of amorphous contents were performed on a PANalytical XPert2-Pro diffractometer in BB-geometry. Table 7.1 contains the corresponding instrumental parameters.

- details on refinements and data treatment

Rietveld refinements were performed with Topas 4.2 (Coelho 2008). For the Rietveld-refinements, no background subtraction (capillary, air-scattering,...) was performed.

PDF-refinements of crystalline contents were performed with PDFgui, a "real space" Rietveld program (Farrow et al. 2007). Its capability were exhausted with being able to simulate crystalline phases. It was not possible to account for

Table 7.1: Instrumental parameters for BB-measurements

Instrument	PANalytical XPERT-PRO
Radiation	Copper $K_{\alpha 1/\alpha 2}$: $\lambda_{\alpha 1}$ = 1.5405980 Å; $\lambda_{\alpha 2}2$ = 1.5444260 Å BBHD-Mirror to remove other radiation
Scattering geometry	Line focus (length/height: 20mm/1mm)
Distance source/sample	200 mm
Entrance slit	15 mm
Soller slits primary	0.04 rad
Divergence slit	½°
Distance sample/detector	200 mm
Soller slits secundary	0.04 rad
Anti-scatter slit	height 5.5 mm
Detector	X'Celerator (scanning line detector); continuous mode, active len

Table 7.2: Instrumental parameters and measurement strategy for PDF-measurements

Instrument	PANalytical Empyrean			
Radiation	Silver $K_{\alpha 1/\alpha 2}$: $\lambda_{\alpha 1}$ = 0.559421 Å; $\lambda_{\alpha 2}2$ = 0.563812 Å Rhodium foil (K_β-filter; thickness: 0.05 mm); line focus			
Scattering geometry	Line focus (length/height: 20mm/1mm)			
Sample	Powder within Quartz capillary (diam 1mm)			
Distance source/sample	140 mm			
Entrance slit	15 mm			
Soller slits primary	0.04 rad			
Exit slit	½° Tantalum slit			
Distance sample/detector	240 mm			
Soller slits secundary	0.04 rad			
Anti- scatter slit	height 2 mm			
Detector slit	height 2 mm			
Detector	Scintillation detector (point detector); continuous mode			
Measured range in Q	0.8 Å^{-1} < Q < 21.5 Å^{-1}			
Measuring time	Angle °2θ	Step °2θ	time s/Step	No. repetitions
	2.0 – 40.0	0.04	6	2
	38.0 – 75.0	0.04	6	8
	73.0 – 100.0	0.04	6	16
	98.0 – 115.0	0.04	6	24
	113.0 – 150.0	0.04	6	32

amorphous contents in the refinement by adding e.g. a strongly dampened PDF of quartz.

Data processing to obtain PDFs was done using the pdfgetX3-software (Juhás et al. 2013).

Figure 7.1 shows the Rietveld-refinement of a the Si-NIST-standard substance 640d ($Fm\overline{3}m$, $a = 0.54312(3)nm$) with an Si-model. Especially around the peaks with low indexes, strong peak tails are observed. This is due to filtering the primary beam only with a Rh-filter and no further monochromator. Adequate peak tails could not be evaluated and an additional peak was inserted at the right side of the first few peaks to improve the refinement. By a refinement of the structure model to a the experimental PDF of the Si-NIST-standard, the parameters Q_{damp} and Q_{broad} (section 2.2.6) were evaluated (figure 7.2). The lattice parameters were fixed to $0.54312(3)nm$ for the Rietveld and PDF refinements.

Values for $Q_{damp} = 0.04(3)$ and $Q_{broad} = 0.02(3)$ were obtained for an R_{max} of 60 Å. Those values were used for PDF-refinements and particle size estimates from the PDF. Note that with an R_{max} of 30 Å, values for $Q_{damp} = 0.04(9)$ and $Q_{broad} = 0.03(4)$ were obtained. Figure 7.3 shows that the experimental damping is strong. In the first comparison, the PDF of a cubic particle of Si with an approximate space diagonal of 94 Å with the Si-NIST-standard is given. The second comparison contrasts this model with the experimental PDF of a synthesised substance NHMS3. The third comparison compares the PDFs of models with space diagonals of 94 and 103 Å respectively.

It can be seen from figure 7.3 that the PDFs of the NIST-standard and the experimental pattern are very similar to the 94 Å model and therefore similar to each other. It should be noted that the PDF of an arrangement of atoms with cube shape looks different than ensembles with approximate equal number of atoms with sphere- or rod-like shapes, due to their different distance-distributions. The third graph is intended to show that in theory small differences are visible. The differences in the experimental patterns to the models might be due to differences in the particles' shapes as well as to influences due to noise or instrumental effects (see section 3.3).

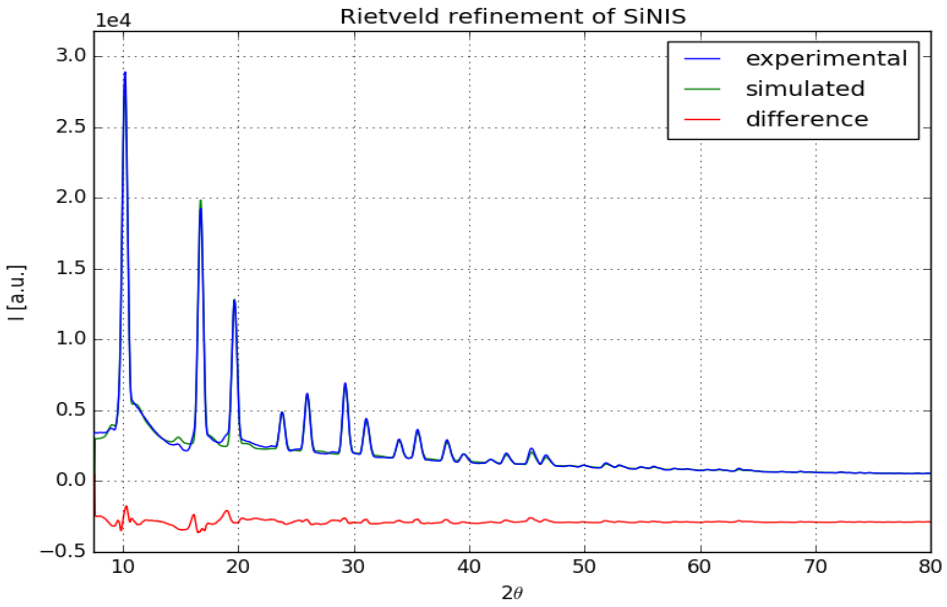

Figure 7.1: Rietveld-refinement Si-NIST 640d with TOPAS 4.2

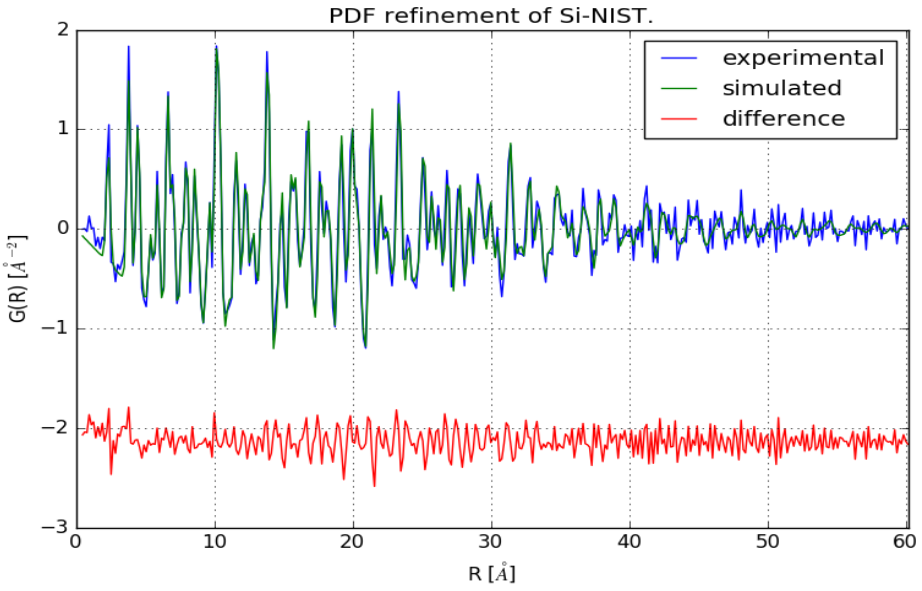

Figure 7.2: PDF-Refinement of Si-NIST 640d with pdfgui in order to obtain the instrumental parameters Q_{broad} and Q_{damp}.

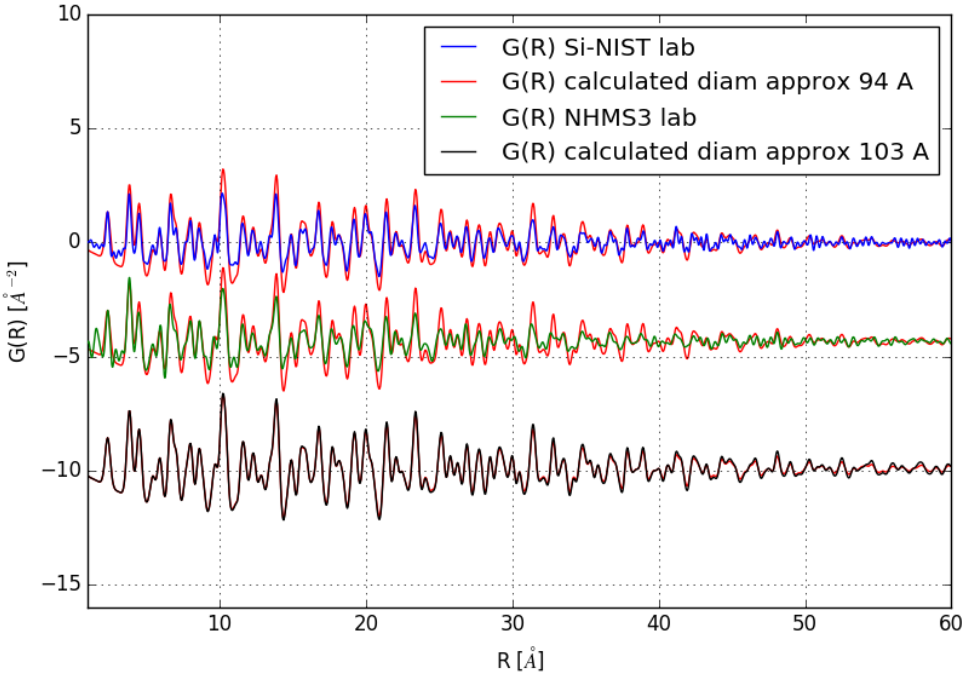

Figure 7.3: Comparison of dampening effects in lab measurements. The first curve shows the PDF of a Si-NIST standard. The second one of a synthesised sample. Curves three and four in lab and calculated Compared with a cubic supercell of Si with an extension of 10x10x10 unit cells .

7.1 A comparison of crystallite sizes from reciprocal space and real space estimates

The aim of the syntheses was the preparation of either nano-particulate material or amorphous silicon (a-Si) or both. Due to a large expertise in sol-gel chemistry for the production of SiO_2-networks PLUS (Salzburg), a large and defined variety of such networks can be produced. Those differently shaped silicas were reduced with Mg in a magnesiothermic reaction and further shaped by washing with either HCl oder HCl and HF. By this route cellular Si-networks with mean crystallite sizes of at least 20 nm can be prepared. It is asserted that by variation of the reaction parameters: temperature, stoichiometric ratio of Mg/SiO_2, and duration of the reaction, crystallite size, crosslinking of crystallites as well as specific surface area can be set specifically. A higher temperature and longer reaction time lead to larger Si-crystallites. Removal of MgO (reaction product) and remaining SiO_2 are strongly infuential on the area of the resulting specific surface. Sample preparation was done by Nastaran Hayatiroodbari at PLUS. The reaction conditions of the materials are not available. Out of this reason, the analyses here are limited to a general comparison of analytic methods and general remarks on the materials.

Figure 7.4 gives an exemplary comparison of only HCl washed (left), and HCl and HF washed (right) material. Unsurprisingly, in the HF washed material less Silica remained.

Under the assumption of collecting data from nano-particles, data suitable for PDF-creation were collected of all received samples. The corresponding PDF-refinements can be found in figures 7.38 to 7.34 in section 7.5. PDF-measurements were not only intended for a possible estimation of crystallite sizes but also for the determination of amorphous contents. Figures 7.5 and 7.6 exemplary show the refinements of the diffractogram and the PDF of a substance.

It is possible to estimate the largest extension of a coherently scattering structure from the PDF. This is meaningful only if the "experimental damping" is less strong than the decay by the structure itself and if the instrumental influence on the signal could be determined. Such a "particle or crystallite

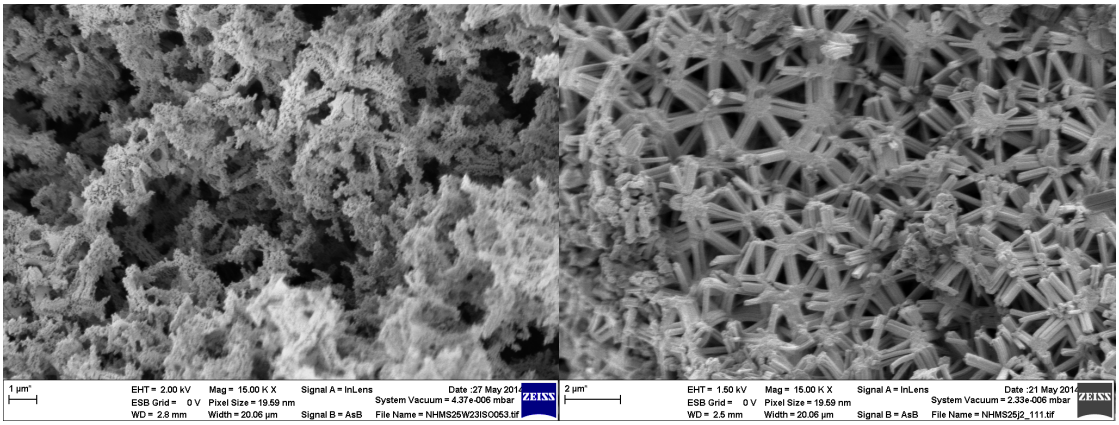

Figure 7.4: SEM-images of synthesised materials. The left image shows the material only HCl-washed (NHMS2). The right image shows the material after washing with HCl and HF (NHMS3).

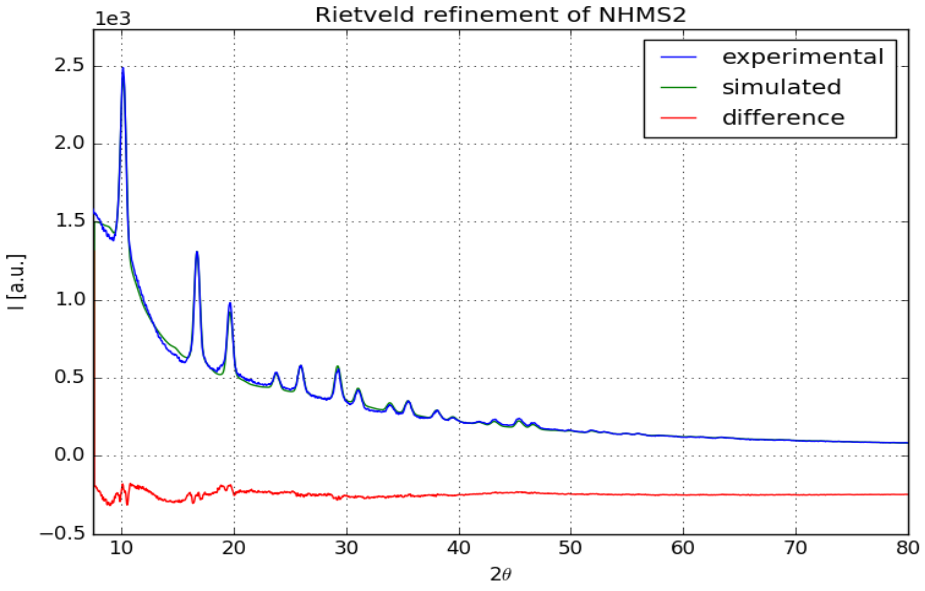

Figure 7.5: Refinement of NHMS2 with TOPAS

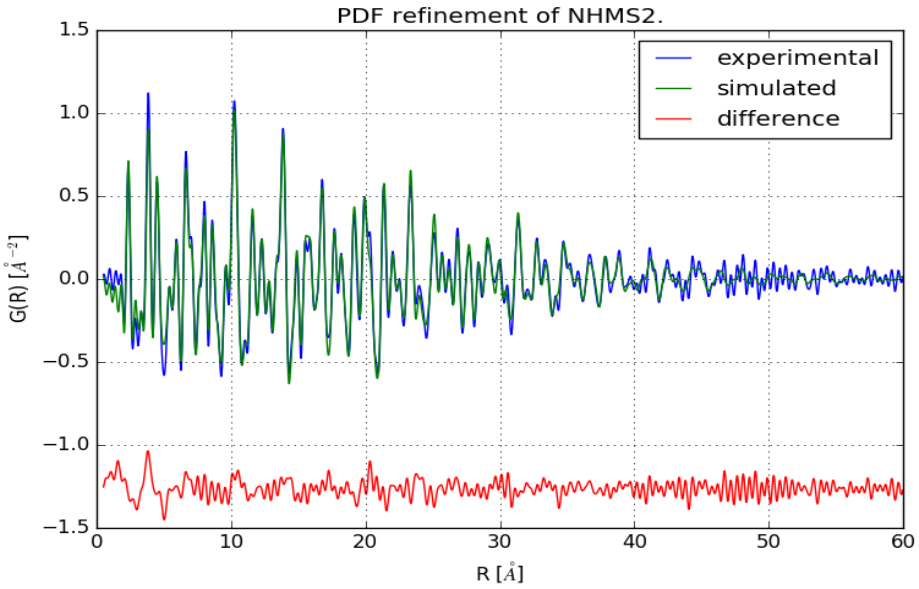

Figure 7.6: Refinement of NHMS2 with pdfgui

size analyses" can be done by looking for a cutoff in the PDF. Such a cutoff corresponds to the largest distance in a material. - It is also possible to get an estimate the decay and calculate from that where the PDF will be zero. - Another approach could be to calculate distinct structures and compare those with the PDF. The applied parameters give then an information on the particles properties. Given the availability of a shape function, the PDF of an extended structure e.g. crystalline and several unit cells in extension) can be multiplied with the corresponding shape function. Masadeh et al. (2007) did this for the case of spherical particles.

In theory, there is no advantage or disadvantage for choosing either method. The only thing that must be known is the relationship between the diffractogram and the structural properties. - What appears important to mention is that there seems to be an upper limit of 100-200nm concerning crystallite sizes analyses, at least when applying the Scherrer-equation. At higher crystallite sizes, the peak broadening cannot be "reliably" distinguished from other broadening effects (Holzwarth and Gibson 2011 and references in Masadeh et al. 2007). As a matter of principle, this limitation might be true for other approaches to analysis of

diffractograms. As a word of caution, a description of an ensemble of crystallites which underlies a distribution in sizes and structures by means of only one parameter might be insufficient and physically incorrect.

In practice, as very small nano-particles show very broad features in the diffraction image, it might be impossible to elucidate the broad "peaks" by pattern decomposition or to distinguish the signal of interest from the underground (Compton-scattering, TDS, other non-sample related signal). So no "correct" FWHM might be obtained and analysis of a PDF could be more suitable in such cases.

If, on the other hand, a highly crystalline material is to be investigated, the PDF decays to zero beyond very high values of R_{max} only. In such cases it is questionable if the PDF approach should be chosen. A large amount of data (xy-table) has to be calculated and processed and prior to FT it is not sure if a sufficient limit for R_{max} was chosen. Also, over large R-ranges, it will be questionable if the very weak (exponential?) decay of the PDF has been estimated correctly; an analysis of the peak shape in the diffractogram, which are ready at hand, might be more accurate. Another obstacle in crystallite-size analysis from the PDF might be that much information on the particles' shape-properties might be necessary prior to analysis. The particles' shapes influence the PDF differently than they influence the diffraction peaks and it seems to be less of a problem when FWHMs of the diffraction peaks in reciprocal space are estimated (besides the fact that also this is an unreliable practice).

Table 7.3 gives a comparison of crystallite sizes estimated from Rietveld- and PDF-refinement for each material that was obtained from PLUS. It can be seen that there is a strong discrepancy between the values which were estimated with TOPAS from the reciprocal space data and pdfgui from the PDFs. TOPAS applies a fundamental parameter approach and the estimated values are congruent with the values in figure 7.3 and corresponding discussion (section 7). Not only do the values between TOPAS and pdfgui differ, also the estimated standard uncertainties (ESUs) are in unacceptable ranges. It cannot be said here if this testifies against the PDF-method or the applied software.

Furthermore, a lithiated Si-compound could be prepared by Nastaran (see figure 7.7). The substance reacted in the capillary, presumably with oxygen

Table 7.3: Comparison of crystallite size estimates for spherical crystallite approximation in [nm] from reciprocal and real space Rietveld-refinements

substance	diam PDF	ESU	diam Rietveld (recip)	ESU
NHM3	36.0	38	14.6	2.8
NHM4	100.0	960	8.9	1.1
NHMS1	62.2	54	22.8	4.4
NHMS2	81.0	150	23.6	8.3
NHMS3	54.2	110	19	8.9
NHS2	50.0	400	6.3	0.6
NHS5	41.7	400	14.9	1.8
PN45	12.0	-12	13.4	2.9
RaSi2	34.8	240	19.3	3.5
Si325	1621594.3	-7.40E+10	500.3	319.6
Si50	42.2	-74	32.6	3.9

or humidity, as the capillary was not air-tight. Although no refinement was possible with pdfgui, a simple calculated PDF of $Li_{12}Si_7$ shows that the material is the intended material. The materials suitability as anode material was not tested owing to its predisposition to exothermic reaction

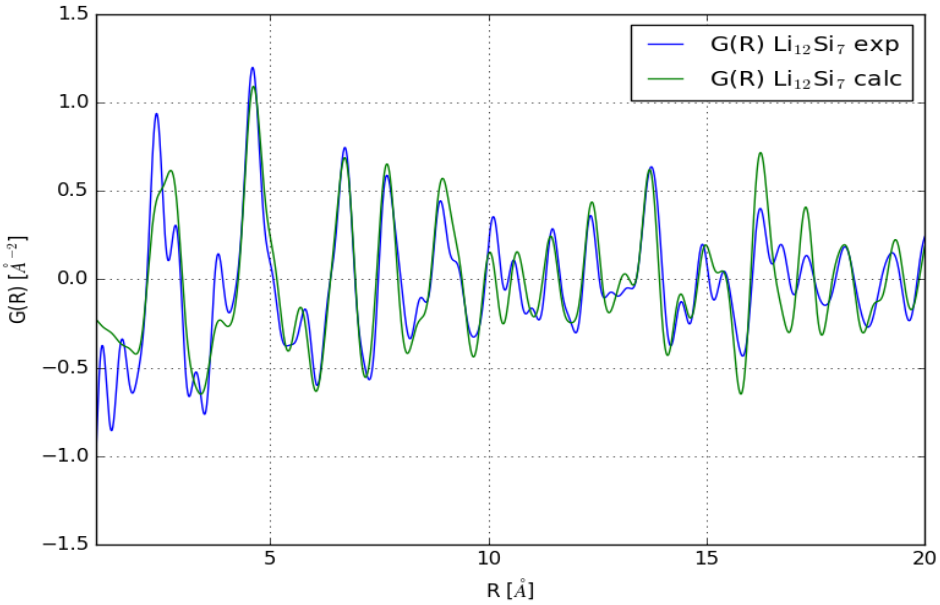

Figure 7.7: Comparison of the experimental PDF of $Li_{12}Si_7$ with a model calculation. Although oxidation occurred during the measurement, a relatively good agreement shows that the aim of synthesis has been accomplished.

7.2 No amorphous silicon via synthesis.

As far as data quality, current methodology and data corrections permit, the investigation of the PDF reveals that syntheses gave exclusively crystalline Si. The corresponding Rietveld- and PDF-refinements are documented in section 7.5. - Concerning a-Si, Mousseau and Barkema (2001) state that "*in fact, a material like a-Si cannot be formed experimentally by quenching from the melt; it is produced by vapor deposition or ion-bombardment*". Our present study might by an indication that it is also not possible via chemical reactions.

Some of the patterns exhibit distances corresponding to Si-O (Peaks at 1.6 Å) from oxides (figure 7.8). This can be observed particularly well in the difference curve. It was not possible to account for amorphous contents by corefinement of e.g. a strongly dampened PDF of a crystalline Si-O compound with pdfgui (which in general seems to be capable only of handling very simple (crystalline) structure models).

In the next section methods for quantification of amorphous contents and an attempt at doing so will be discussed.

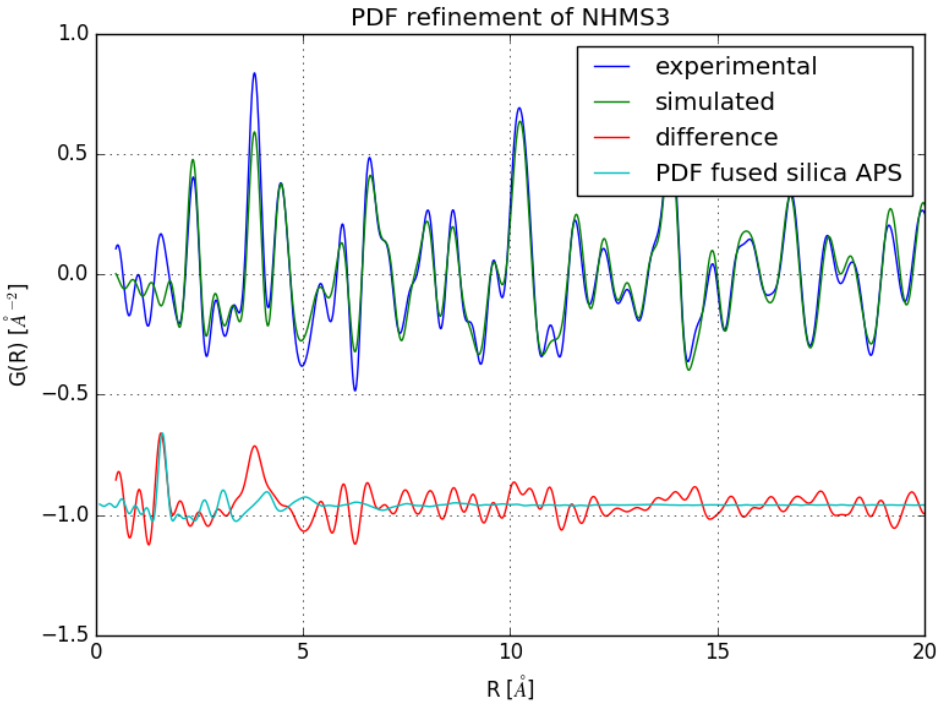

Figure 7.8: Structure refinement against the PDF of a material with remaining amorphous SiO_2 with pdfgui. It was not possible to fit a a dampened PDF of an SiO_2-compound such as quartz to the experimental PDF with the pdfgui-software. The difference curve shows similarities to a PDF of fused silica measured at APS. The second broad contribution could stem either from the differing atomic arrangement in the used kind of silica or it is a mixture of instrumental effects and termination ripples subsumed with the natural contributions of fused silica.

7.3 Quantifying amorphous parts in crystalline systems

The amount of amorphous content in a system can be an important indicator for the efficiency of a synthesis. Furthermore, amorphous content might or might not be wanted because of structural or chemical properties. It is possible that crystalline particles are covered by an amorphous shell.

A suitable definition of "amorphous" is given by Klug and Alexander (1974) so that *the term, amorphous solid, must be reserved for substances that show no crystalline nature whatsoever by any of the means available for detecting it*. Anyways, here is no definite distinction between amorphous and crystalline.

Amorphous materials don't give well defined peaks. Therefore, in contrast to crystalline compounds, no phase-identification algorithms for identification of amorphous phases are available. Furthermore, owing to its shape, scattering from amorphous structures can be hard to distinguish from peak tails. In addition, broad background intensities, which result in increased peak overlaps, make it even more difficult to distinguish its contribution to the diffractogram from other sorts of diffuse scattering (Madsen et al. 2011). Without a structure of the amorphous material, quantification and calculation of physical properties is not possible in e.g. a Rietveld-refinement. This happens especially when an intensity contribution to the diffractogram is small, e.g. at low concentrations of the amorphous phase.

To summarize, amorphous structures are hard to detect, identify and discriminate in reciprocal space, making it thereby challenging to quantify them.

7.3.1 General discussion of methods for quantification of amorphous contents and methodological problems thereof.

Quantification by help of data in the reciprocal space representation

There are numerous possibilities for the quantification of amorphous contents from a diffractogram, each with their advantages and disadvantages. Some give the proportion directly and others indirectly by means of comparison with a

well defined standard substance. Depending on the ratio of amorphous material and the amount of sample given, different methods are proposed. The effect of (micro)absorption depends on the composition of the sample and cannot be handled with every method. In other cases, calibration with a mixture of known composition has to be made in order to evaluate absorption and composition of the amorphous phase. (See Kern et al. (2012) and Madsen et al. (2011) for much more detailed information.)

Widely used methods for quantification of amorphous phases are according to Madsen et al. (2011):

- In a whole powder pattern modeling (WPPM; Scardi and Leoni 2002) approach, the diffraction pattern of the amorphous phase is decomposed into parametrized peaks. The obtained set of parametrised peaks is kept fixed then and used as a phase in a refinement. The amorphous content is determined from its refined scale factor.

- A well known standard substance (e.g. Corundum) can be added and from the overestimation of the amounts of crystalline phases calculated in a Rietveld-refinement, the amount of amorphous substance can be deduced (internal standard method).

- The peak intensities of the crystalline phase(es) can be compared with the diffraction pattern of the pure substance. This needs additional calibration methods and ideal sample-preparation (external standard method).

- The diffractogram of a crystalline structure can be convoluted with a broadening function and damped to get the shape of the signal stemming from amorphous content. The amount of amorphous content present is determined by means of a scaling factor.

- Le Bail et al. (1985) attempted simulation of amorphous phase by the distortion of an ordered supercell. A problem with this latter method could be that some for of periodicity remains, which introduces artefacts. With suitable terms to model size dependent broadening, this issue could be resolved.

Quantification by help of data in the real-space representation

Concerning investigation via PDF-analysis it appears unclear how it could unambiguously be used for quantification of amorphous phases in heterogeneous systems. For systems with compounds of the same stoichiometry - although the evaluation of the baselines of various phases due to differences in extension and varying ρ_0s of different modifications -might be possible and was approached (Davis et al. 2013). The theory is not designed for polyphasic materials. In the known ways for data extraction are developed for single-phase materials and the estimation of a mean atomic form factor as described seems not possible. So while qualitative information could be still available, the validity of quantitative information obtained could be difficult to determine. Also here, errors due to absorption might have to be taken into consideration and there is no method yet to apply this on PDF-data.

Another point is that for correct data reduction, the correct stoichiometry has to be known. If there is only one amorphous phase present, quantification in direct space appears to be unnecessary. - Conventional analysis could be done and from the mass ratios, the rest can be calculated. We don't need to transform then and we also do not need to find a structural model. - Nevertheless, determining the correct stoichiometry (eg the oxygen content in unstoichiometric oxide-compounds) by RFA, XPS or spectroscopic analysis is difficult. Either the radiation (electrons, light) does not penetrate the material or the emitted signal is absorbed by the matrix (XRF) where characteristic energies are very low. In summary, in dealing with stoichiometric Si/Si-O compounds the information about atomic ratios would suffice for quantification. And this we supposedly do not get from PDF-analysis, it has to be known beforehand.

7.3.2 Quantification of amorphous content with a method developed in this work and comparison with the standard-series approach

The common methods for quantifying amorphous contents from the diffraction pattern rely on references. Small sample-amounts, which preclude series of

mixtures or blending with a standard, are a problematic aspect. In the following, a potential solution to this problem is discussed. A method (that was not found in literature in this form) for quantification of amorphous content is proposed and compared with the internal-standard method:

internal-standard method: A series of mixtures of Si and fused-silica powder (with approximate same coarseness) have been analyzed. For the internal-standard method, corundum (Al_2O_3) was added in a defined amount. In a Rietveld-refinement, the amounts of crystalline phases are systematically overestimated, because the scattering from amorphous parts is shifted into the underground. Because the mass content of corundum is known, the overestimation of all crystalline phases can be corrected. The remainder is the amount of amorphous phases (see Westphal 2007).

proposed method (similar to the PONKCS-method mentioned in Madsen et al. (2011) but no calibration step is needed):

- The aim of the method is to identify the contribution of the scattering from the amorphous phase (fused silica) to the total intensity.
- To do so, the pure amorphous phase and a sample containing this phase of interest are measured.
- Since the signal stemming from air scattering shows strong contribution to the left part of the diffractogram (figure 7.9), it is necessary to subtract this contribution. This is accomplished via subtraction of an estimated baseline (figures 7.10 and 7.11)
- After the baseline-subtraction, a constant is added to both diffractograms in order to eliminate negative intensities (figure 7.12). It is disputable if it would be better to set all values under a threshold $|I| < \delta$, e.g. the largest negative value, to zero. The determination of such a δ is dependent on the amount of noise present in the data and the quality of the polynomial to be subtracted. Each procedure influences the areas under the corrected diffractograms.

- The diffraction pattern of the amorphous substance is scaled in order to fully overlap with the contribution in the sample of interest (figure 7.13)
- The scaled pattern of the amorphous phase is subtracted (figure 7.14)
- The areas of both curves are determined by integration and the relative contributions are calculated to obtain a scale-factor.
- The weight-fraction can be calculated according to $W_a = \frac{S_a(ZMV)_a}{\sum[S_i(ZMV)_i]}$, with Z the formula units per unit cell, V unit cell volume and M the mass of a formula unit (see e.g. Kniess et al. (2012) and Madsen et al. (2011)).
- Estimating the correct amount of atoms, which corectly arranged would give the diffraction pattern of the amorphous solid, is difficult. This is also one of the main problems of the other methods. According to the PDF of fused silica, correlation ends at approximately 8 Å. To account for this, 3 times the unit cell of alpha-quartz was chosen, weighted with the ratio of the density of fused silica and the reciprocal density alpha-quartz.

Table 7.4 gives a comparison of the amorphous contents, which are known from the initial weights, calculated with the internal-standard method and the method of directly determining the intensity contribution. - The comparison shows that given an appropriate representative structure, the second method is very capable of quantifying amorphous content. Certainly, the estimation of the underground is a crucial step. In any case, for a more reliable investigation series repeated of mixtures should be performed. Crucial questions that remain are how much intensity data must be recorded and how micro-absorption effects can be handled.

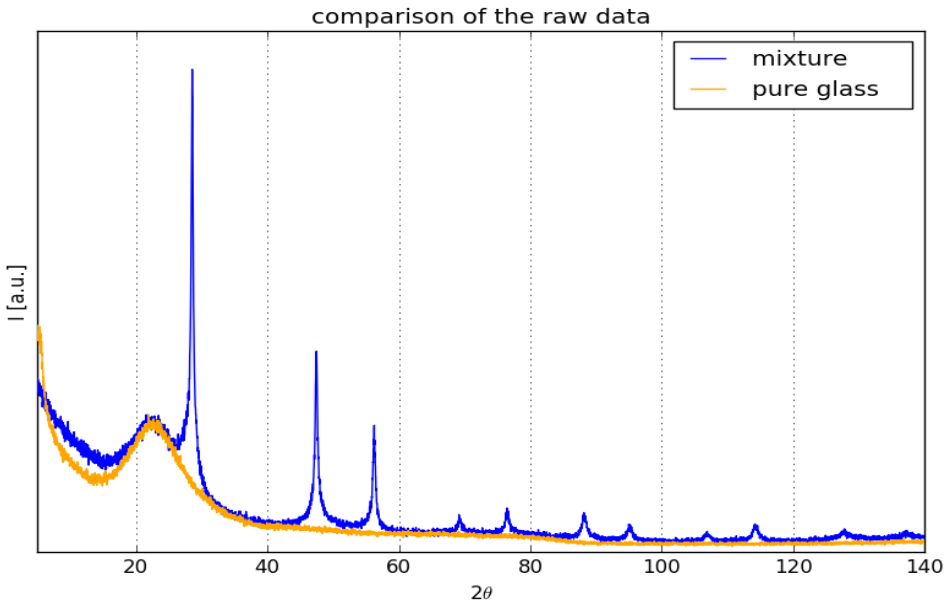

Figure 7.9: A comparison of the datasets show that the diffuse contributions do not overlap very well. This is due to an alleged contribution of air scattering.

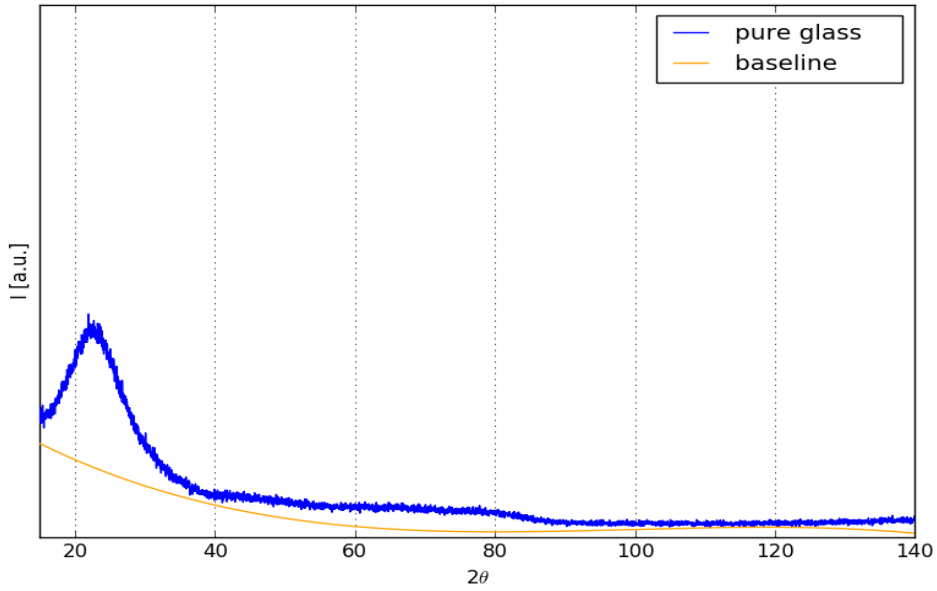

Figure 7.10: This figure shows the baseline that was fitted onto the diffractogram of the fused silica.

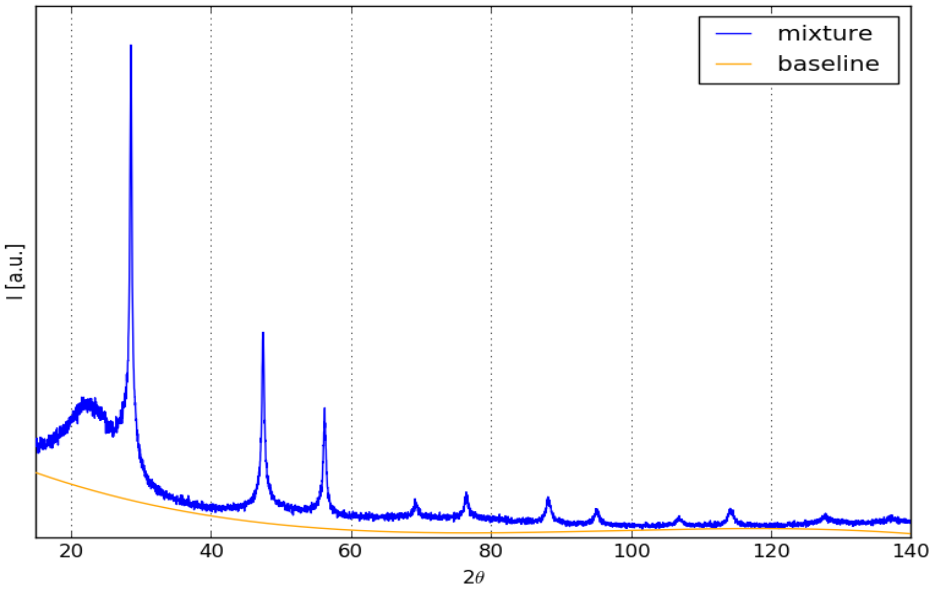

Figure 7.11: This figure shows the baseline that was fitted onto the diffractogram of a mixture.

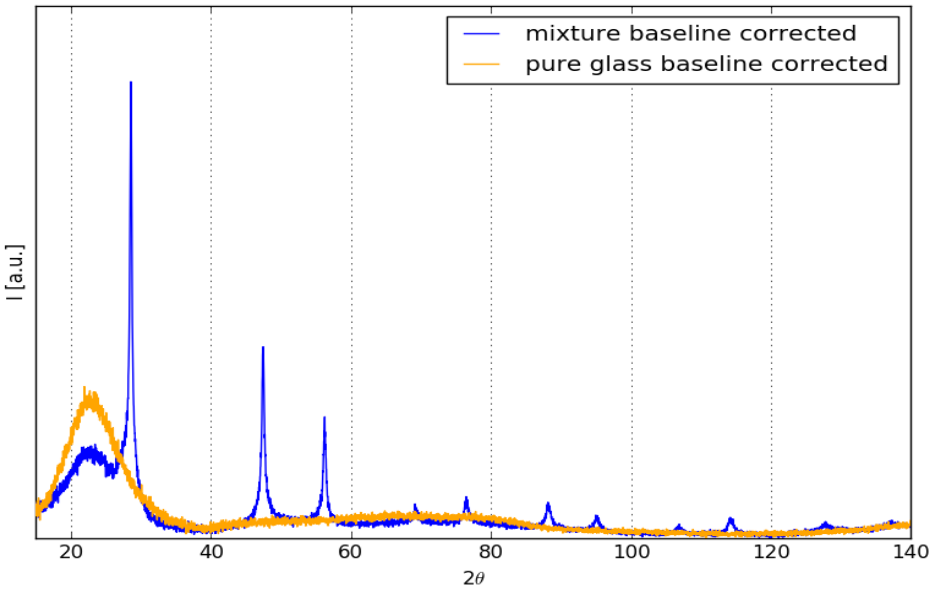

Figure 7.12: The figure shows the diffractograms after baseline subtraction.

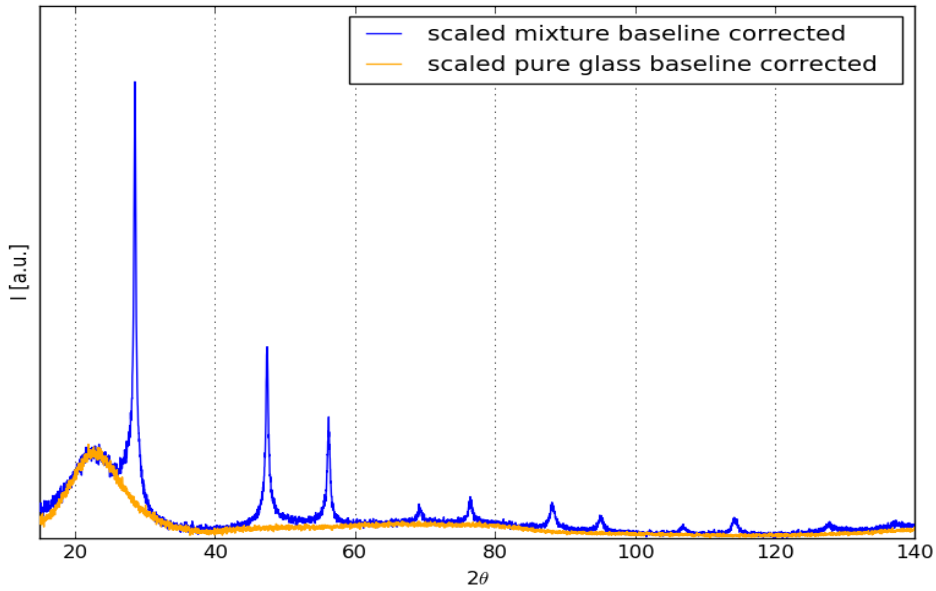

Figure 7.13: The figure shows the diffractograms from figure 7.12 scaled in a manner that the contribution due to amorphous contents are aligned.

Table 7.4: Estimation of amorphous contents

Ratio Si:Glas	wt Si[g]	wt Glas [g]	wt% Si	wt% fused silica	wt% Al2O3
9010	89.519	10.481	67.732	7.930	
7525	74.981	25.019	57.250	19.102	23.647
5050	50.006	49.994	38.051	38.041	23.908
2575	25.053	74.947	18.788	56.205	25.007
1090	11.074	88.926	8.420	67.610	23.971

	quant crystalline phases by Rietveld		recalculated from Rietveld		
	Si	corrundum	silicon	fused silica	corundum
9010	77.104	22.895	72.533	4.572	22.895
7525	74.000	26.000	67.304	6.696	26.000
5050	63.370	36.630	41.361	22.009	36.630
2575	45.440	54.560	20.827	24.613	54.560
1090	27.660	72.340	9.165	18.495	72.340

	pure Si:fused silica from Rietveld		Method examined	
	Si	fused silica	Si	fused silica
	94.070	5.930	81.406	18.594
	90.951	9.049	71.591	28.409
	65.268	34.732	50.569	49.431
	45.834	54.166	23.662	76.338
	33.136	66.864	9.135	90.865

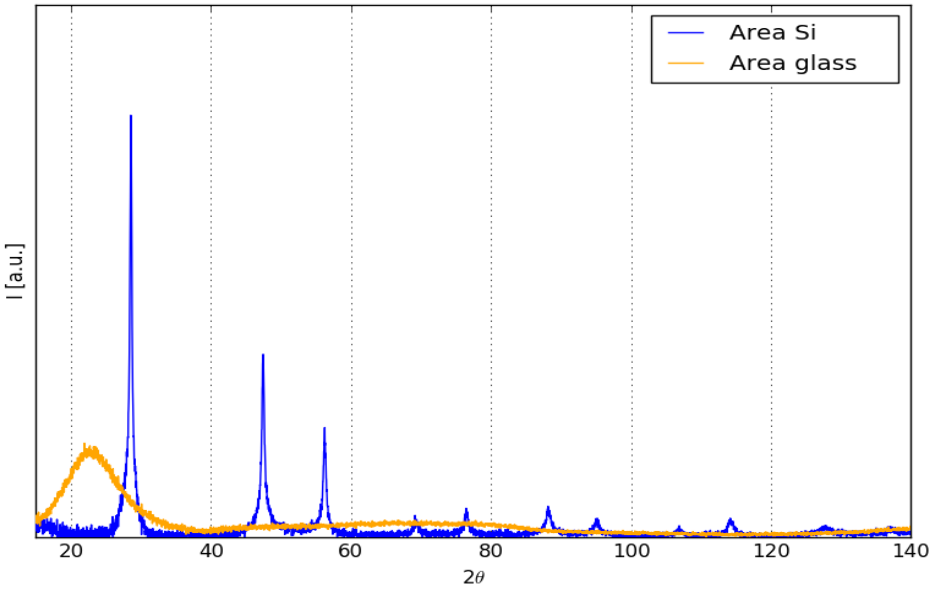

Figure 7.14: From the mixture's diffractograms of figure 7.13 the contribution from the amorphous content has been subtracted. The areas of both curves give the total scattering contributions of the phases. The advantage of this method is that instrumental contributions are the same for both phases and so no additional special correction is needed.

7.4 Conclusions

The project ended too early for finding an anode-material with the demanded properties. Synthetic silicon particles (networks) showed crystallinity independent of the synthesis-route. This is an empirical finding that strengthens (Mousseau and Barkema (2001)) skepticism towards "bulk"-approaches leading to amorphous silicon. - Crystallite size estimates which were obtained from Rietveld- and PDF-refinements differ strongly. With the pdfgui-software standard deviations that were larger than the evaluated quantities were obtained. For the evaluation of the Q_{broad} and Q_{damp}, it is possible to get different values for refinements over different R-ranges. In the optimal case, samples are characterized with highly collimated radiation from a Cu-source before the measurement in order to get an estimate for the necessity and required instrumental parameters of a PDF-measurement of the sample in a capillary.

If an amorphous phase with a stoichiometry ditinct to a crystalline phase is present, quantification by the PDF-representation is pointless. For the extraction of the PDf the correct stoichiometry must be known and this information contains the information on the mass amount of the amorphous phase. Further, it is still a subject of research, inhowfar the analysis of a PDF of multiphasic compounds is justified. In this work a method for the quantification of amorphous material without additional measurements could be defined. If the for an amorphous ensemble that would give the diffractogram is known, the quanification competes much better then the established standard-series approach. As suitable stoichiometry could be avaluated by an estimate from the PDF of fused silica.

7.5 Refinements

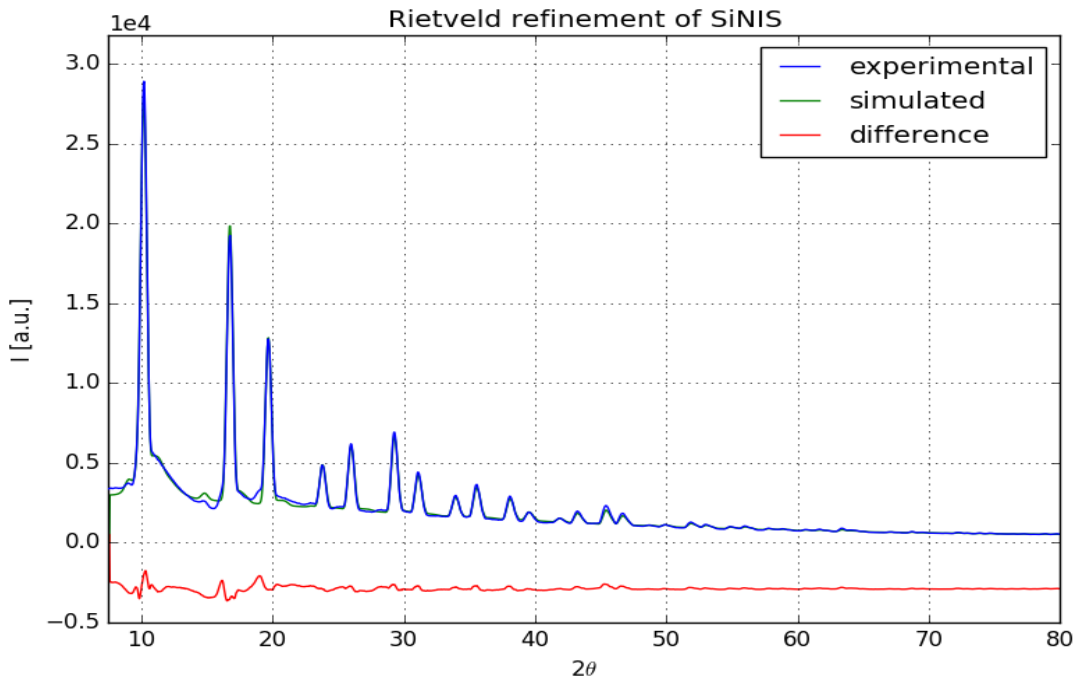

Figure 7.15: Rietveld-Refinement of Si NIST 640d with TOPAS 4.2

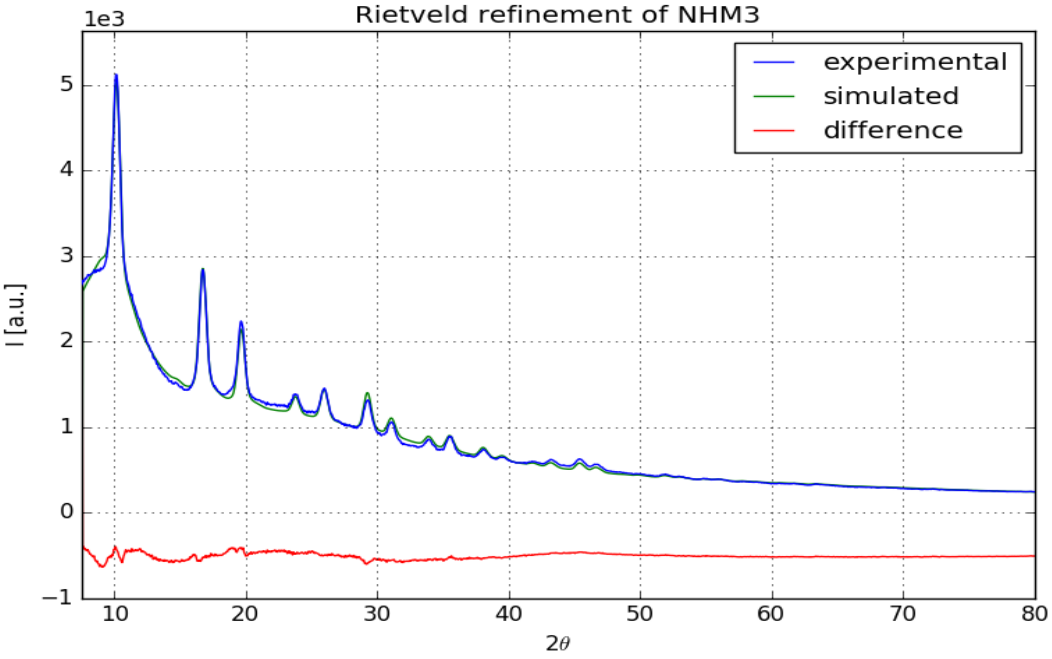

Figure 7.16: Rietveld-Refinement of NHM3 with TOPAS 4.2

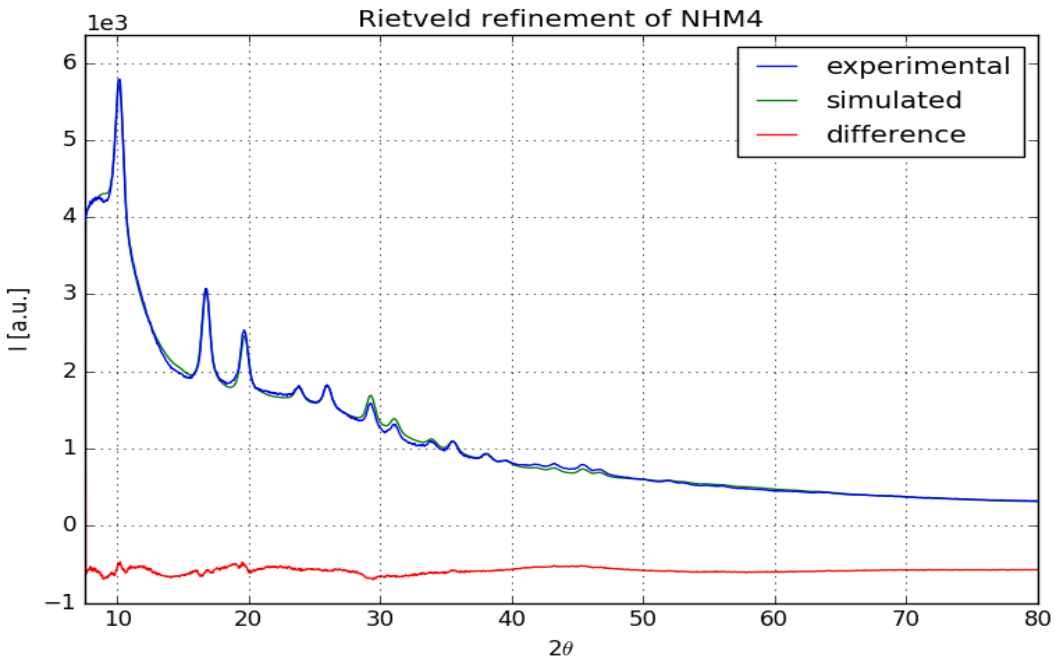

Figure 7.17: Rietveld-Refinement of NHM4 with TOPAS 4.2

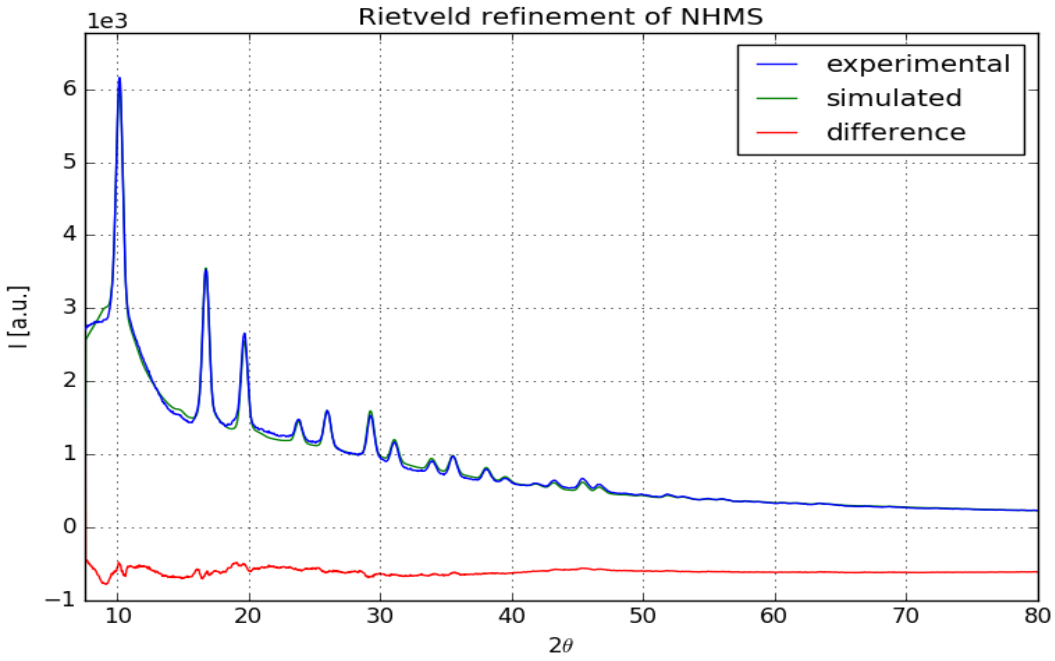

Figure 7.18: Rietveld-Refinement of NHMS1 with TOPAS 4.2

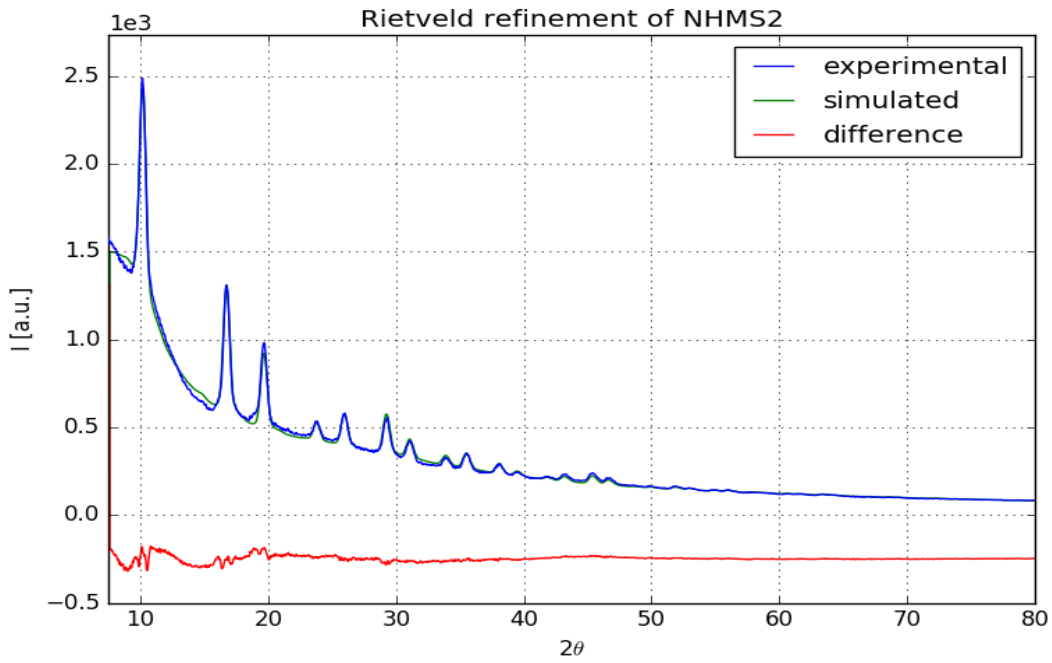

Figure 7.19: Rietveld-Refinement of NHMS2 with TOPAS 4.2

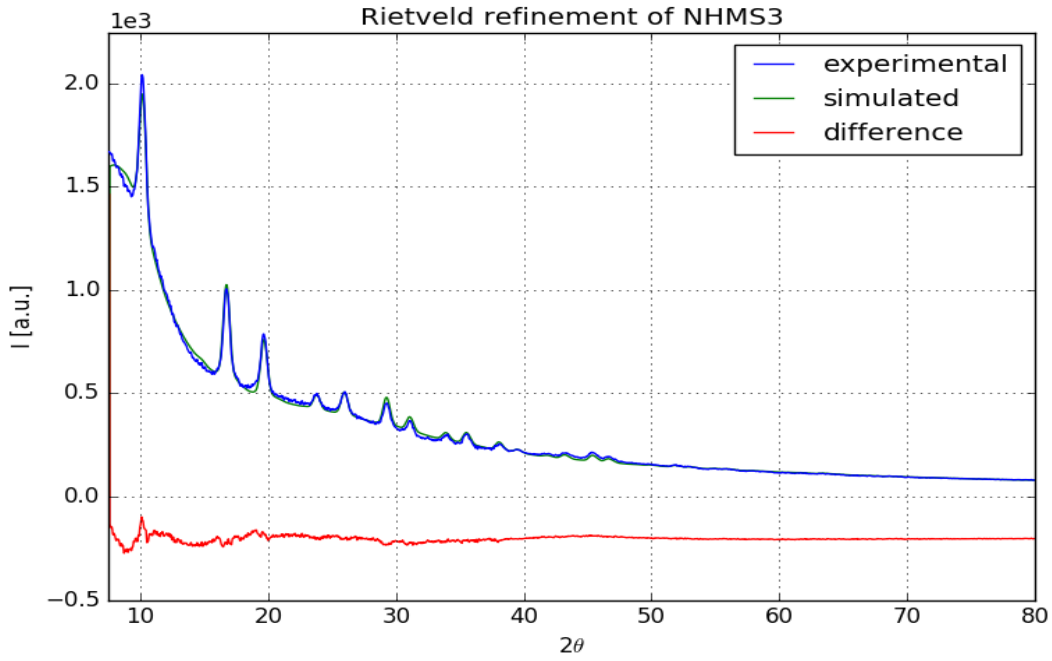

Figure 7.20: Rietveld-Refinement of NHMS3 with TOPAS 4.2

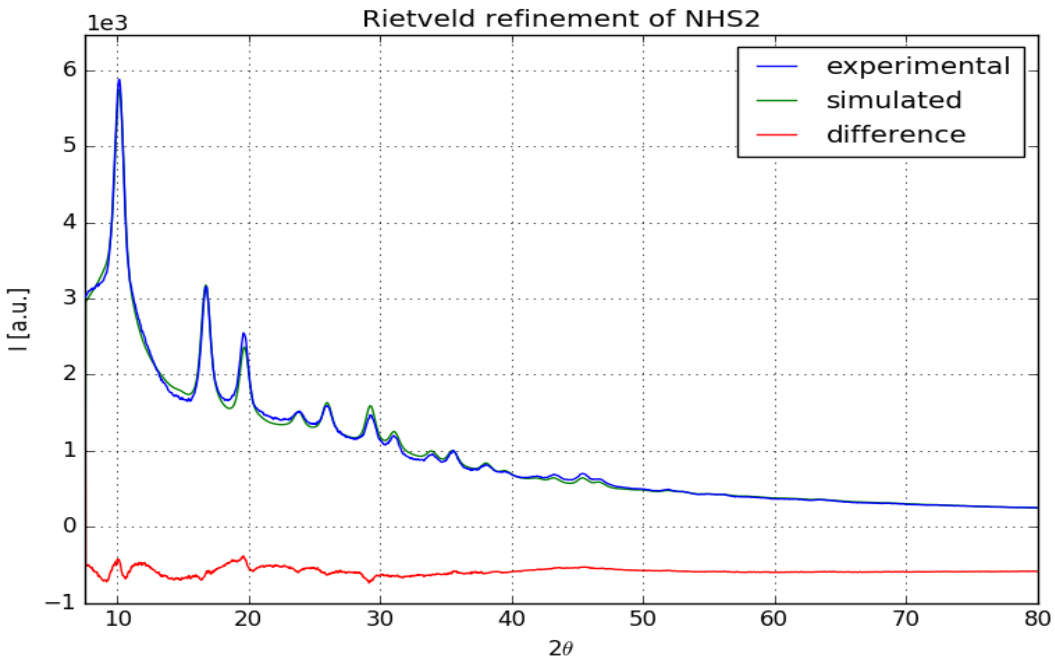

Figure 7.21: Rietveld-Refinement of NHS2 with TOPAS 4.2

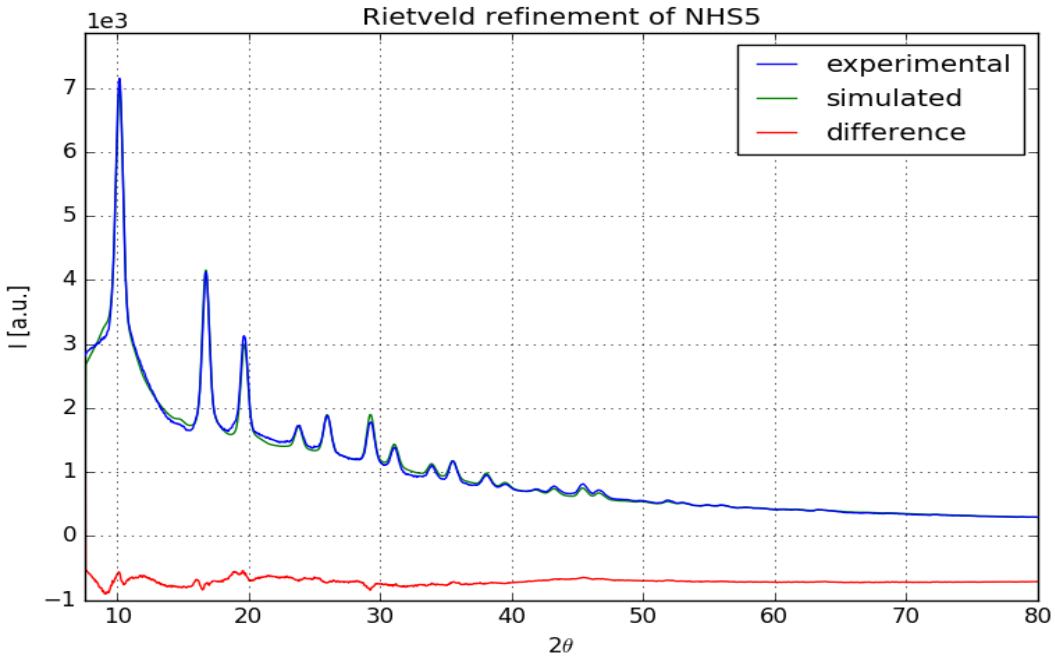

Figure 7.22: Rietveld-Refinement of NHS5 with TOPAS 4.2

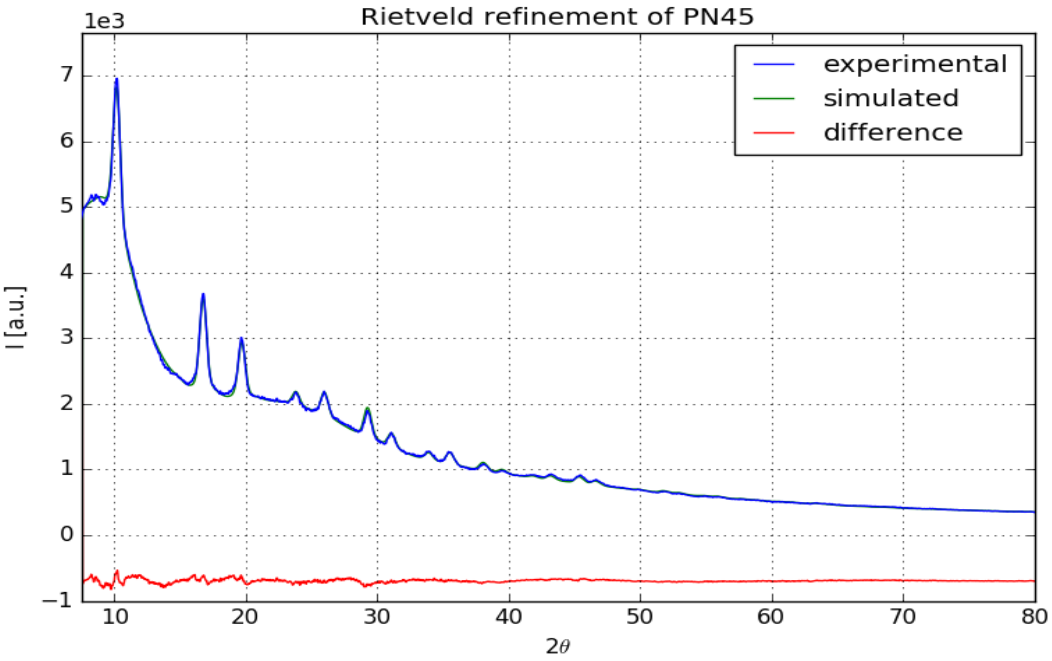

Figure 7.23: Rietveld-Refinement of PN45 with TOPAS 4.2

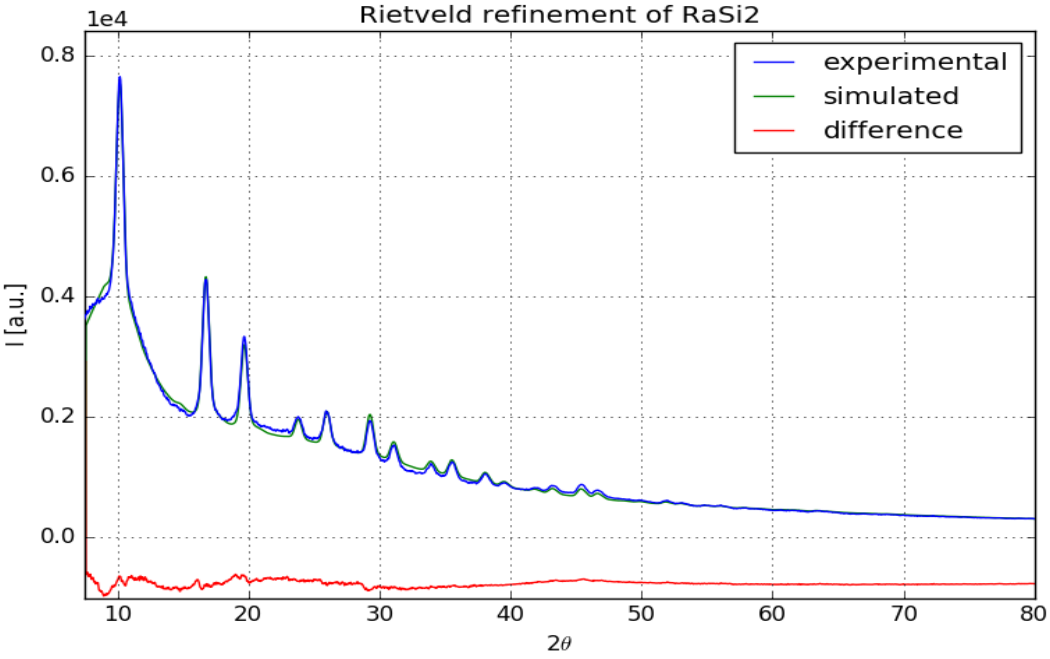

Figure 7.24: Rietveld-Refinement of RaSi2 with TOPAS 4.2

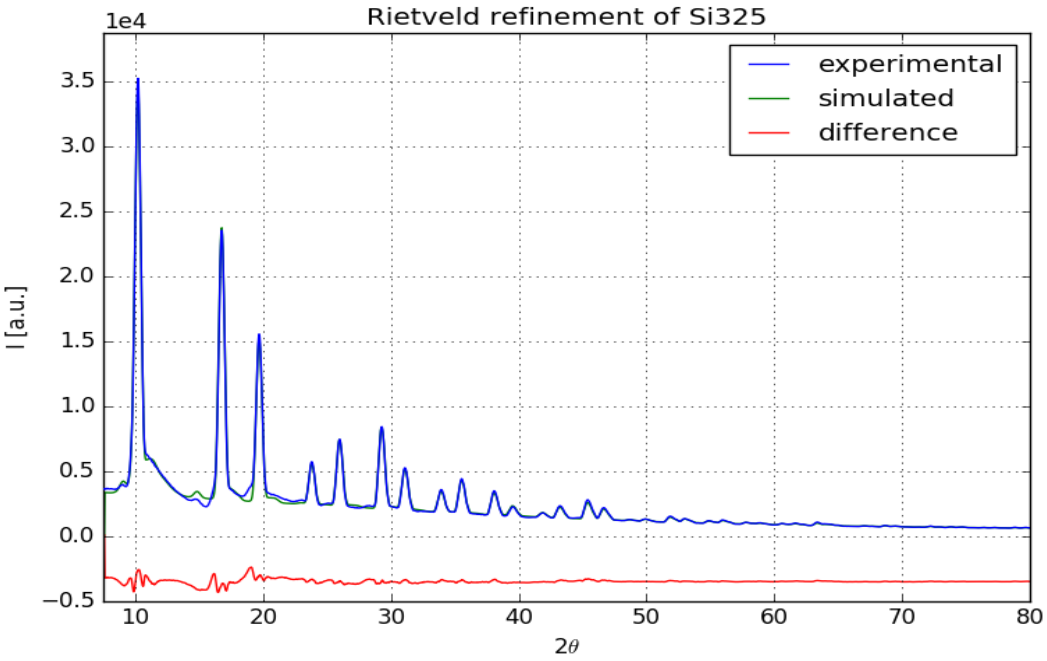

Figure 7.25: Rietveld-Refinement of Si325 with TOPAS 4.2

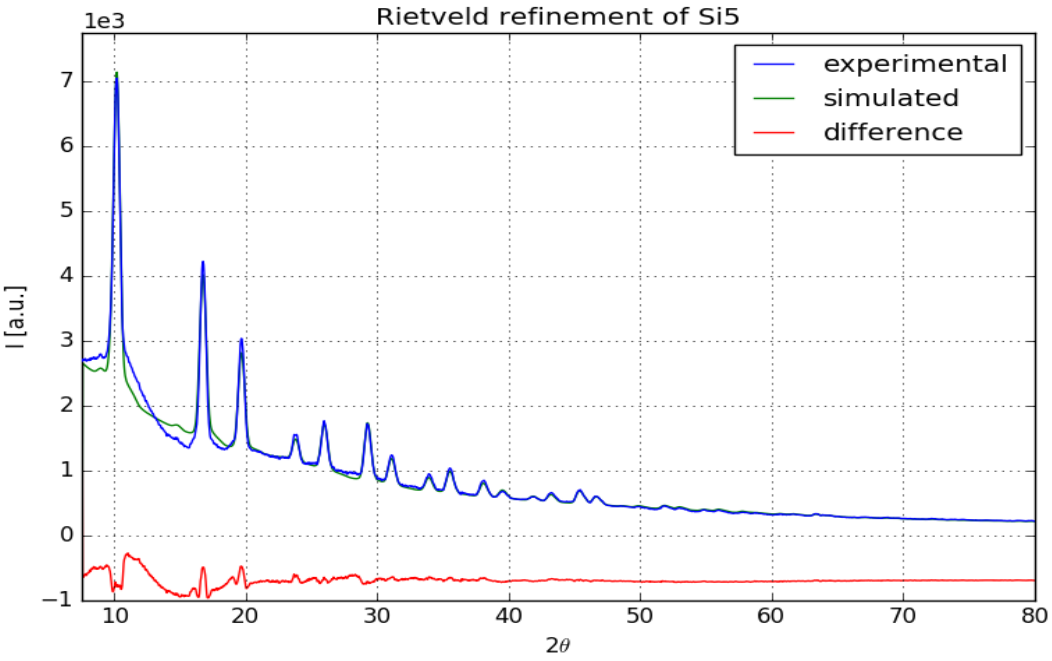

Figure 7.26: Rietveld-Refinement of Si50 with TOPAS 4.2

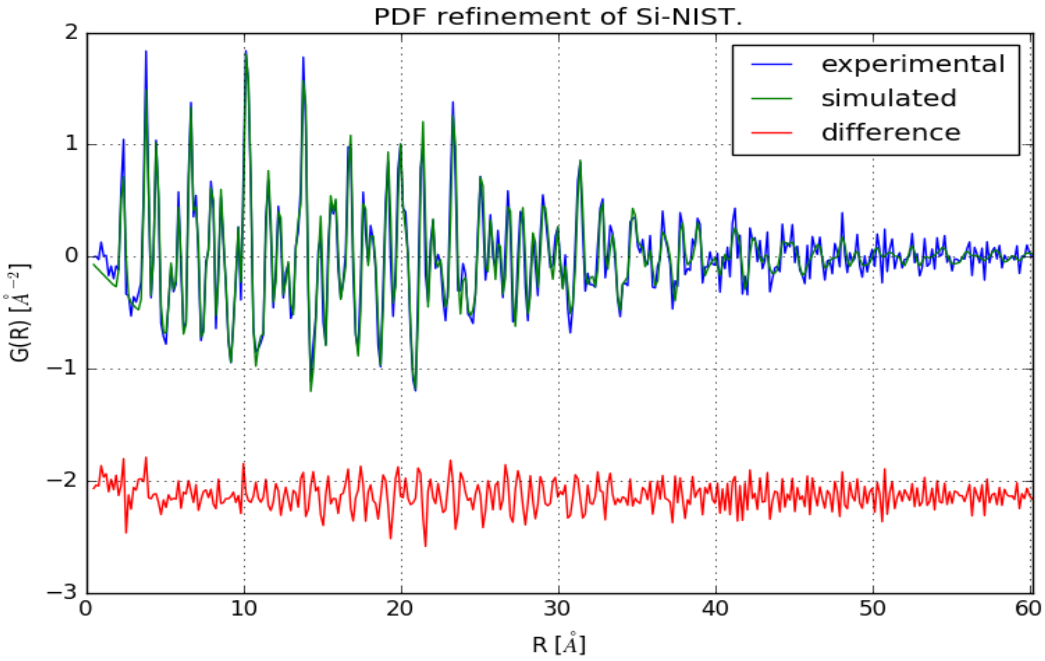

Figure 7.27: PDF-Refinement of Si-NIST 640d with pdfgui

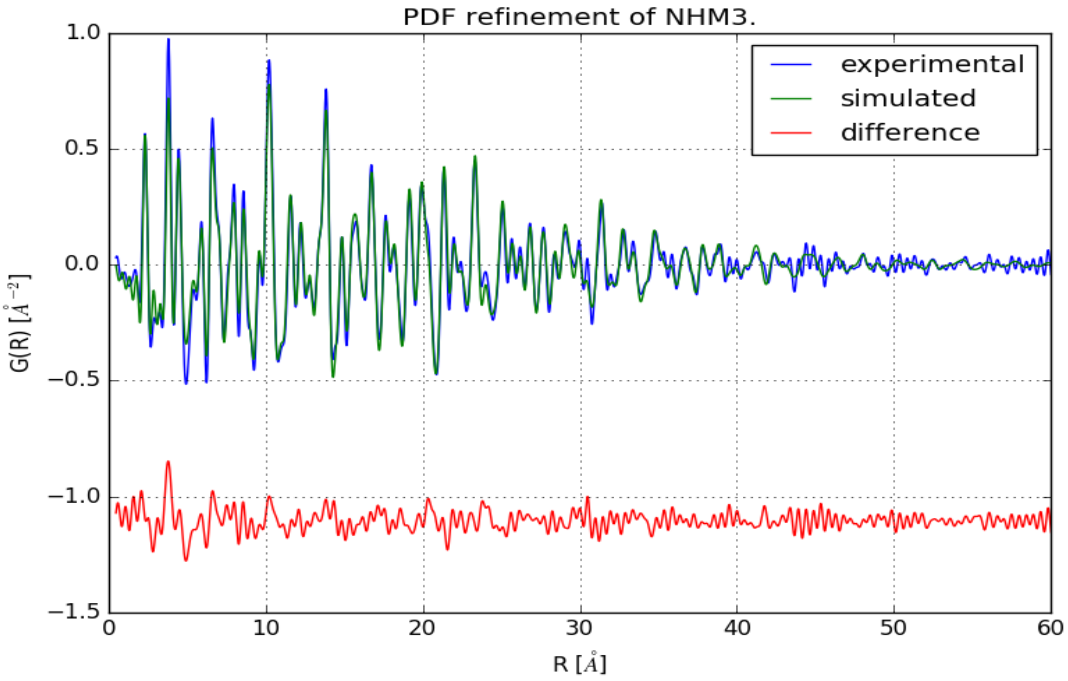

Figure 7.28: PDF-Refinement of NHM3 with pdfgui

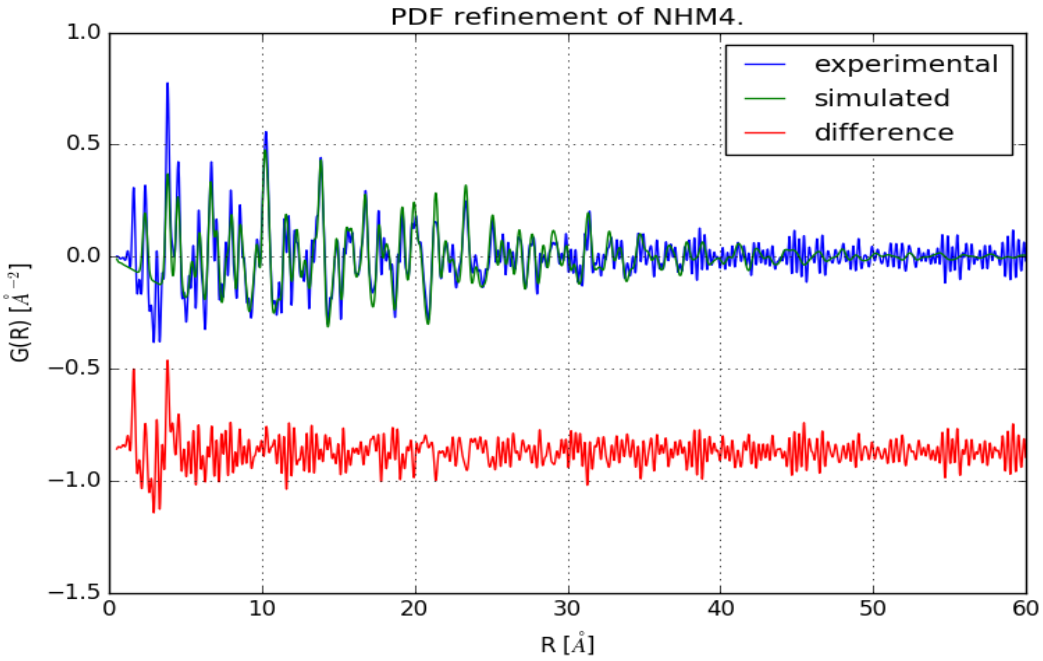

Figure 7.29: PDF-Refinement of NHM4 with pdfgui

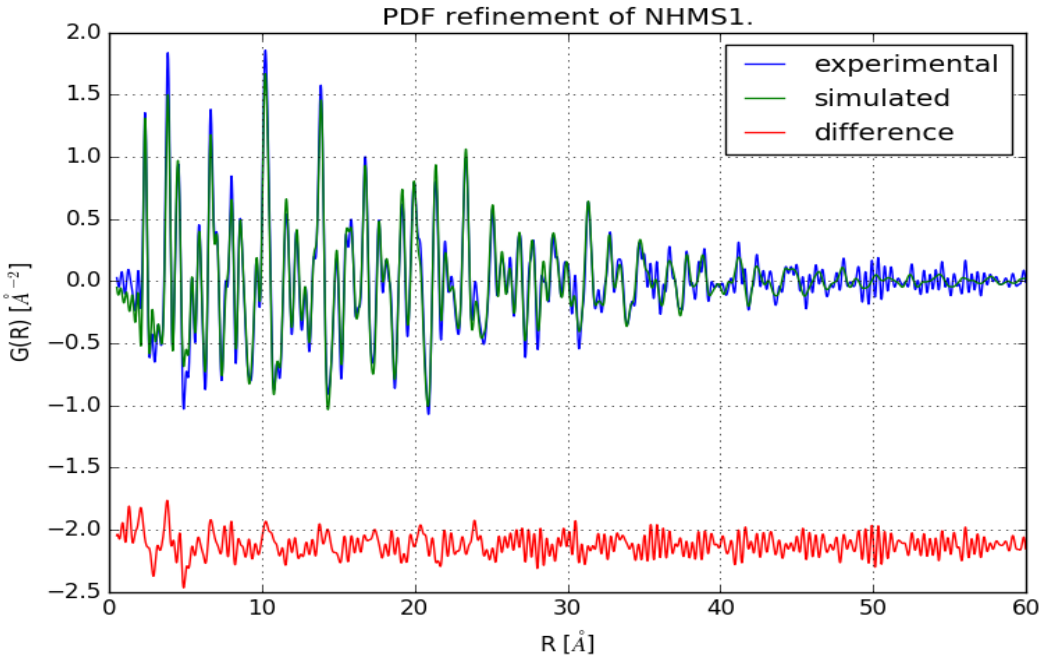

Figure 7.30: PDF-Refinement of NHMS1 with pdfgui

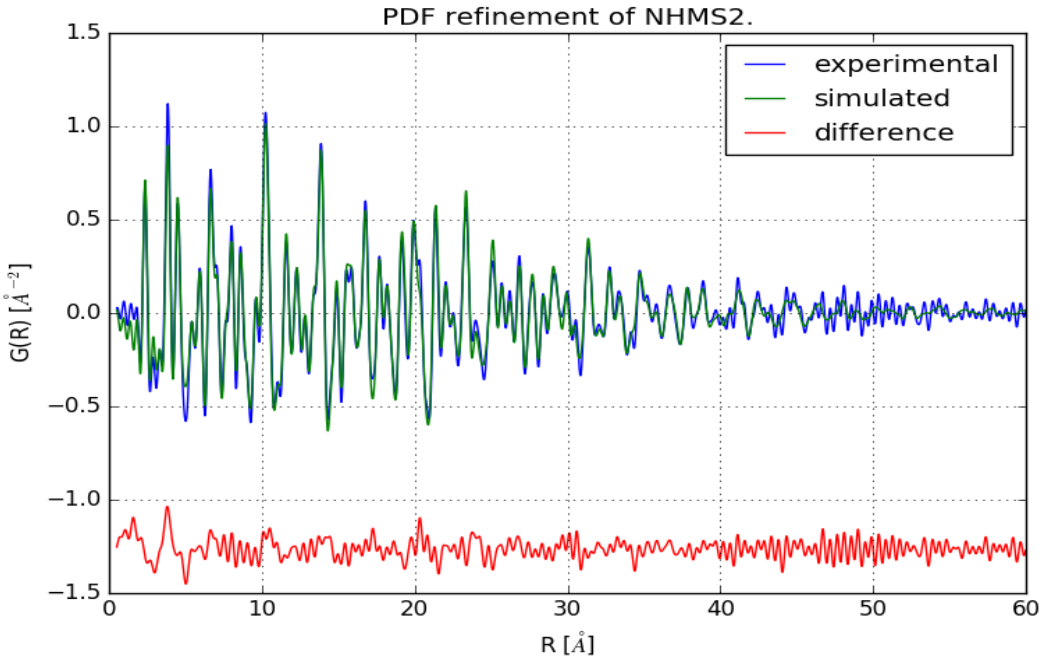

Figure 7.31: PDF-Refinement of NHMS2 with pdfgui

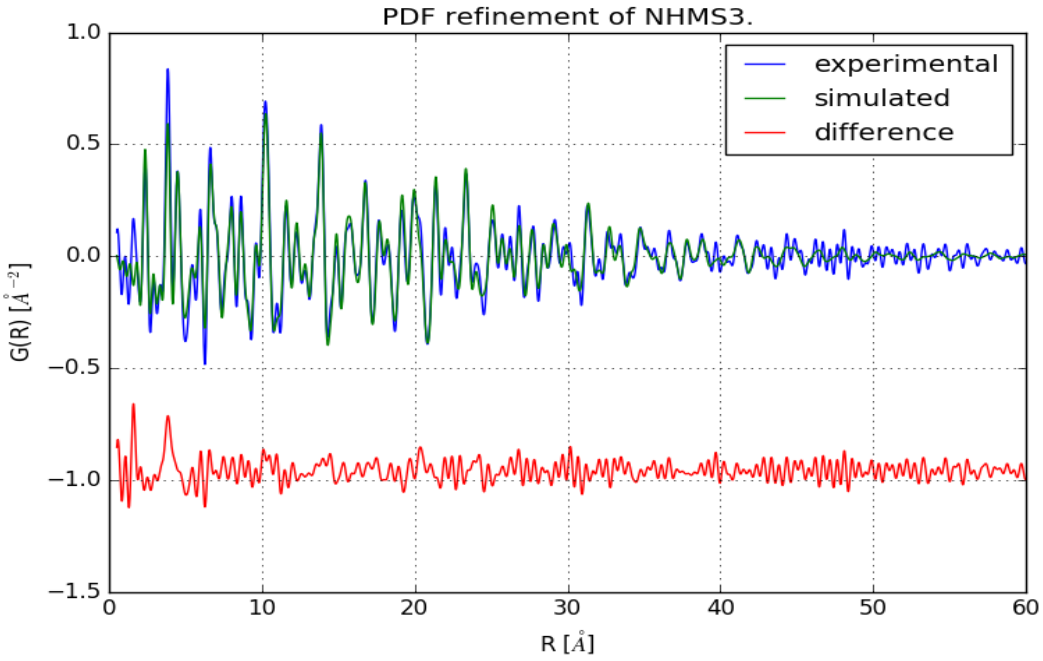

Figure 7.32: PDF-Refinement of NHMS3 with pdfgui

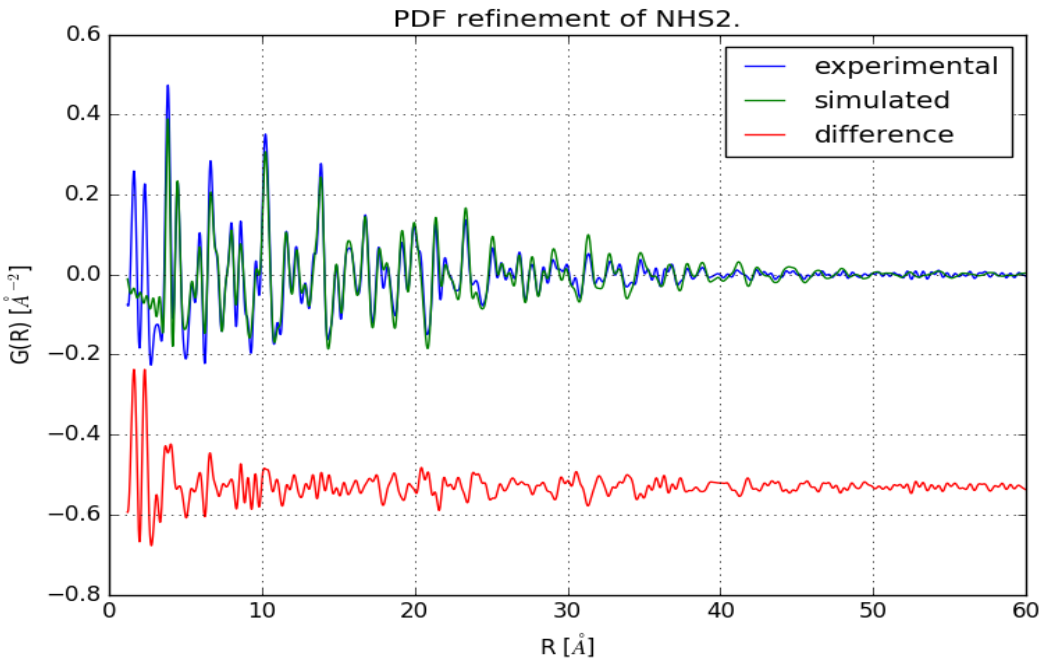

Figure 7.33: PDF-Refinement of NHS2 with pdfgui

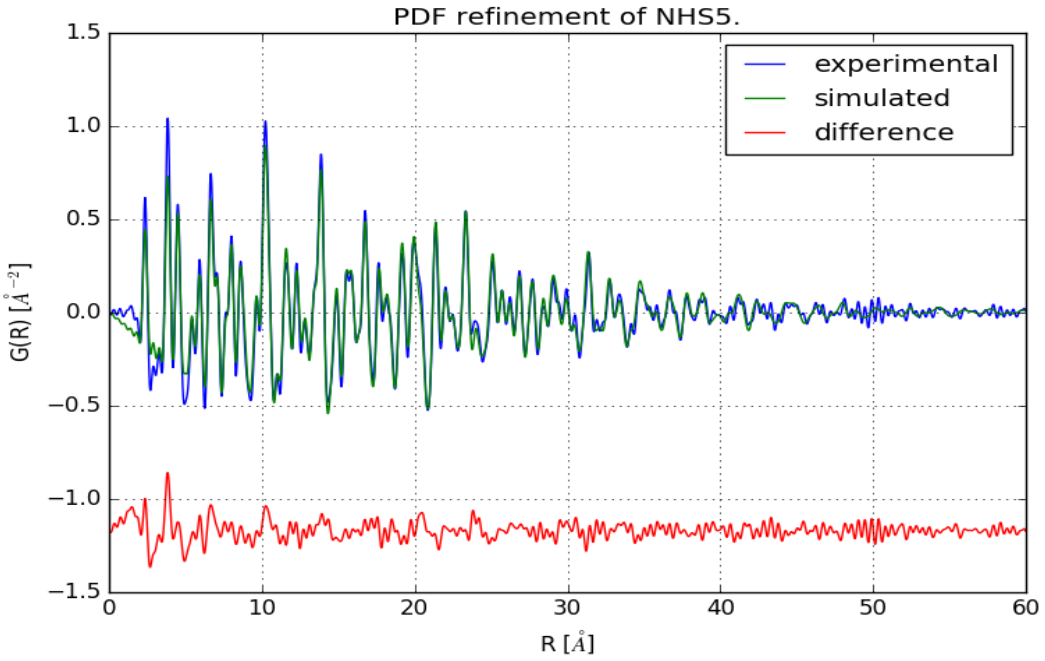

Figure 7.34: PDF-Refinement of NHS5 with pdfgui

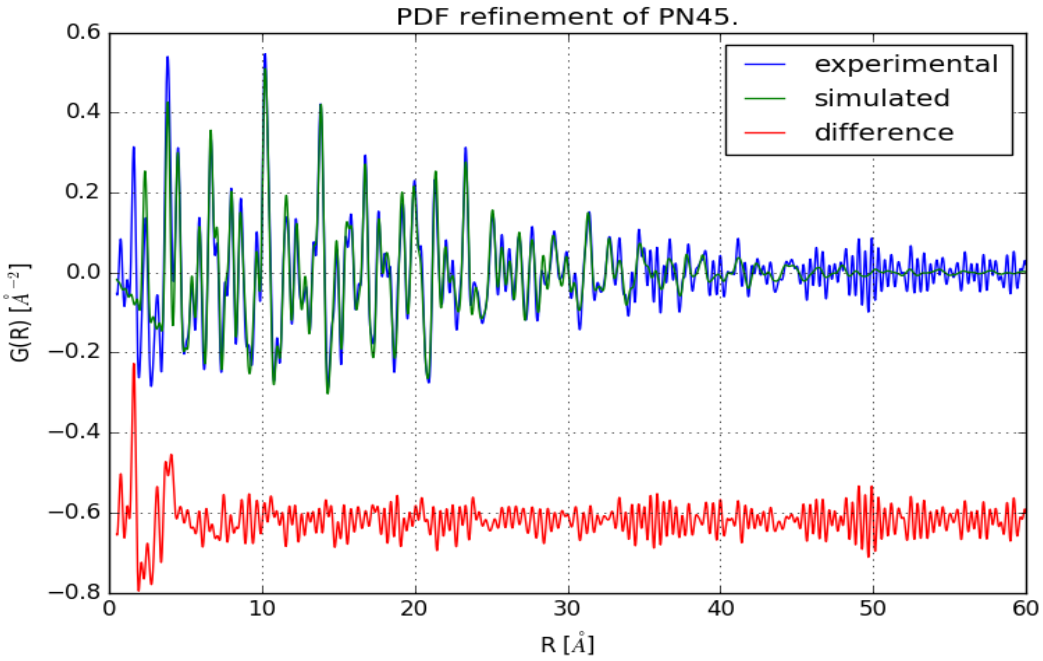

Figure 7.35: PDF-Refinement of PN45 with pdfgui

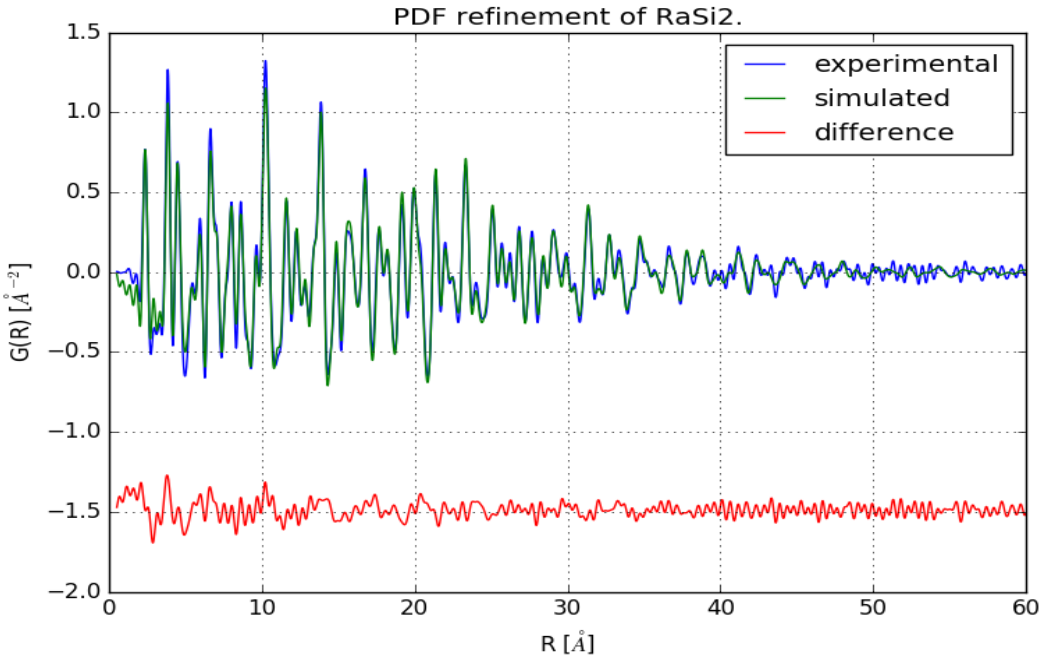

Figure 7.36: PDF-Refinement of RaSi2 with pdfgui

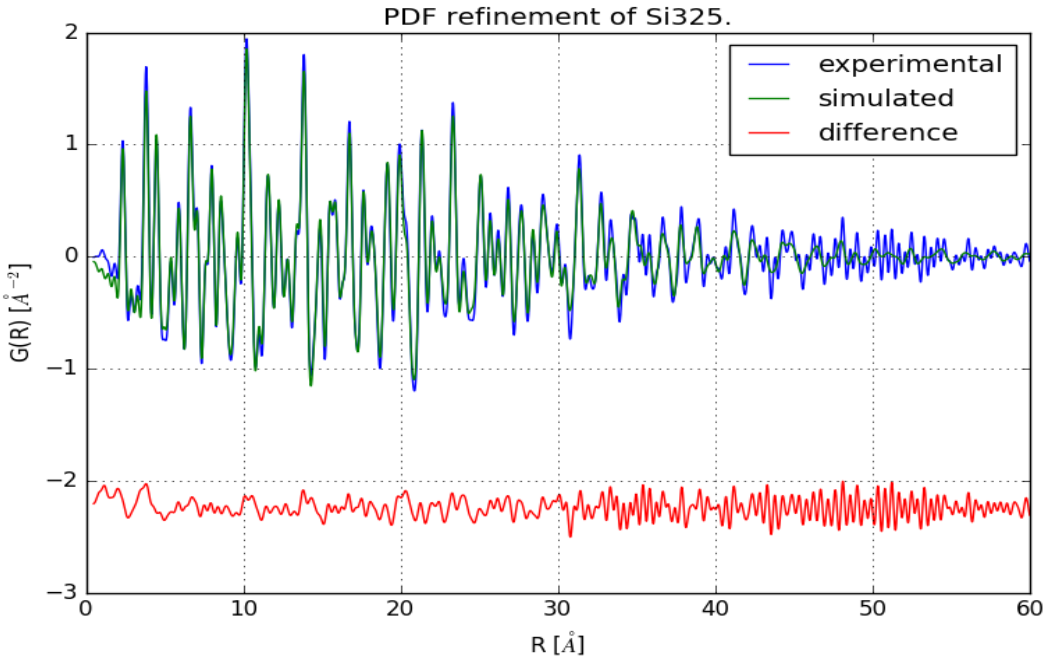

Figure 7.37: PDF-Refinement of Si325 with pdfgui

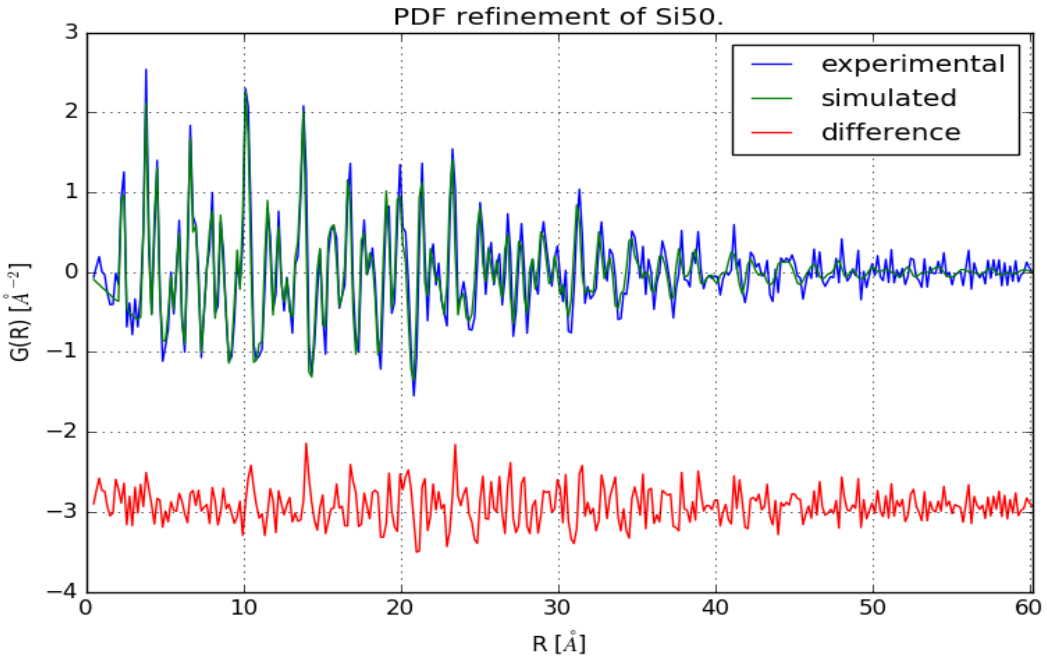

Figure 7.38: PDF-Refinement of Si50 with pdfgui

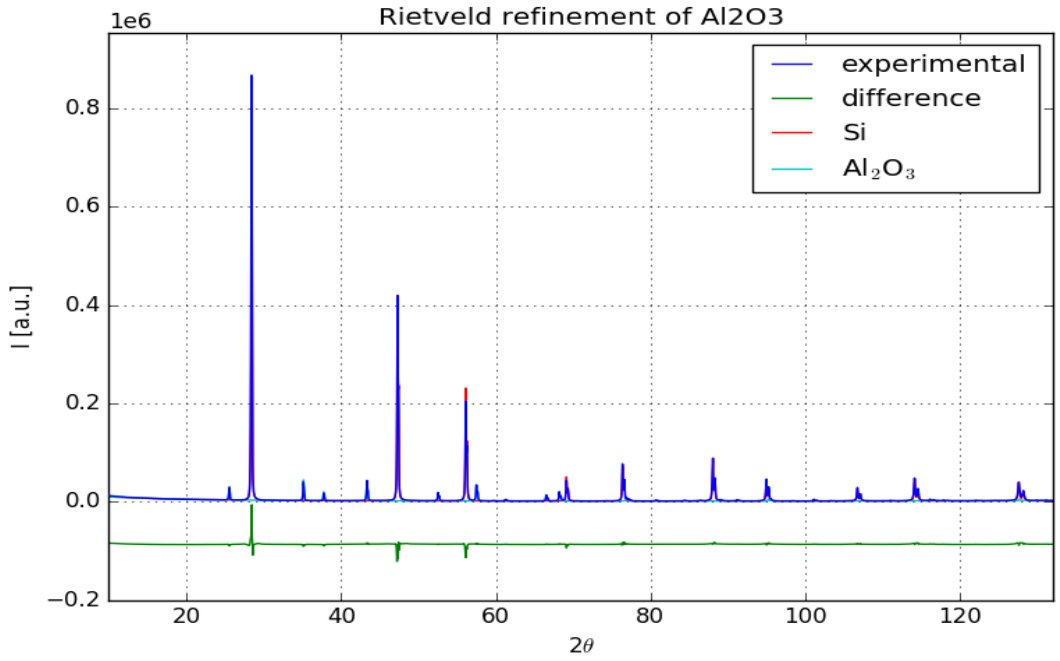

Figure 7.39: Rietveld-refinement of pure Silicon with 20wt% Al_2O_3 with Topas 4.2

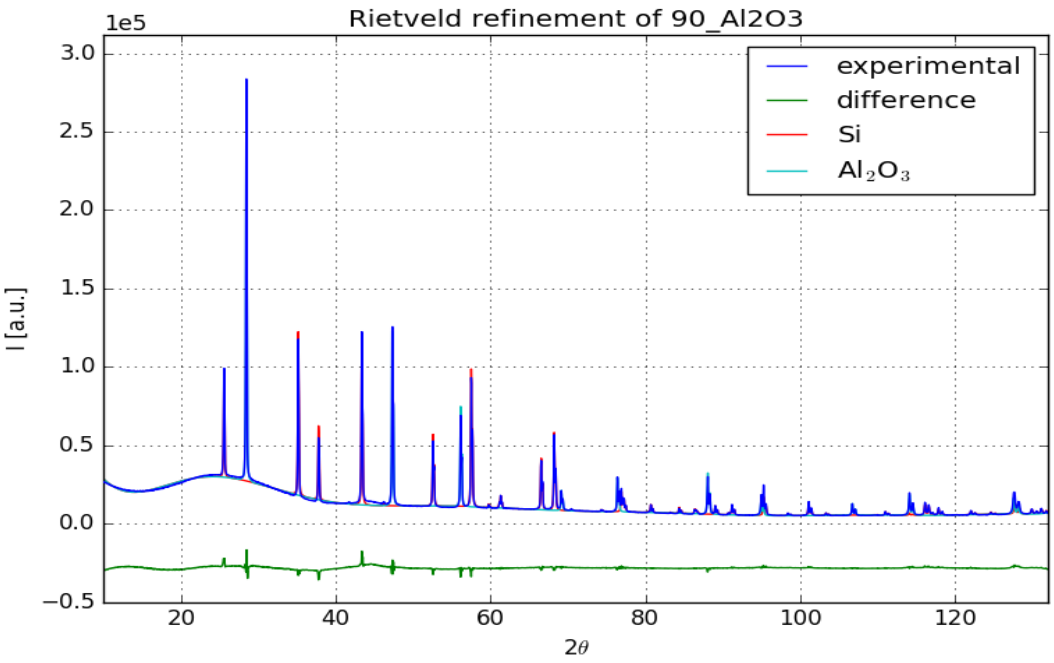

Figure 7.40: Rietveld-refinement of mixture Silicon:Glass 10:90 with 20wt% Al_2O_3 with Topas 4.2

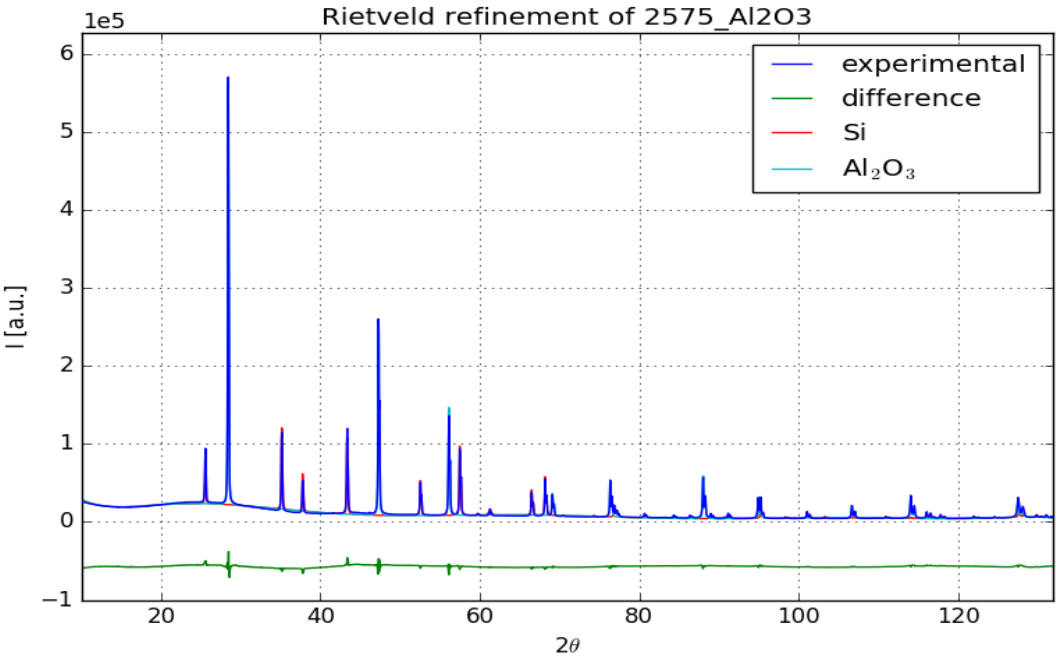

Figure 7.41: Rietveld-refinement of mixture Silicon:Glass 25:75 with 20wt% Al_2O_3 with Topas 4.2

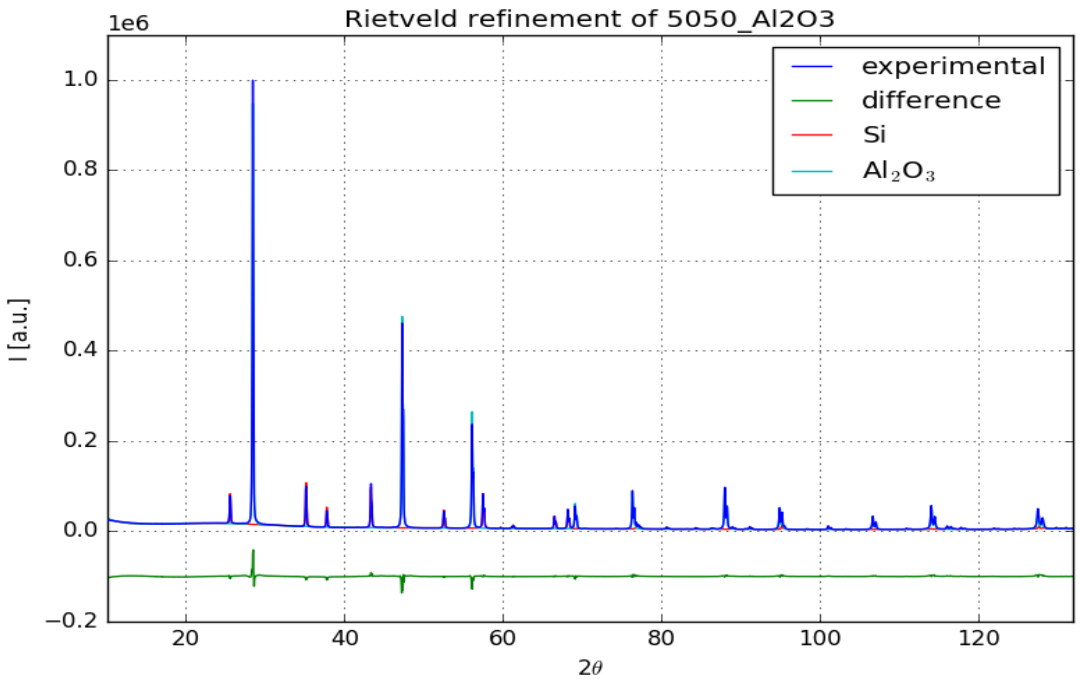

Figure 7.42: Rietveld-refinement of mixture Silicon:Glass 50:50 with 20wt% Al_2O_3 with Topas 4.2

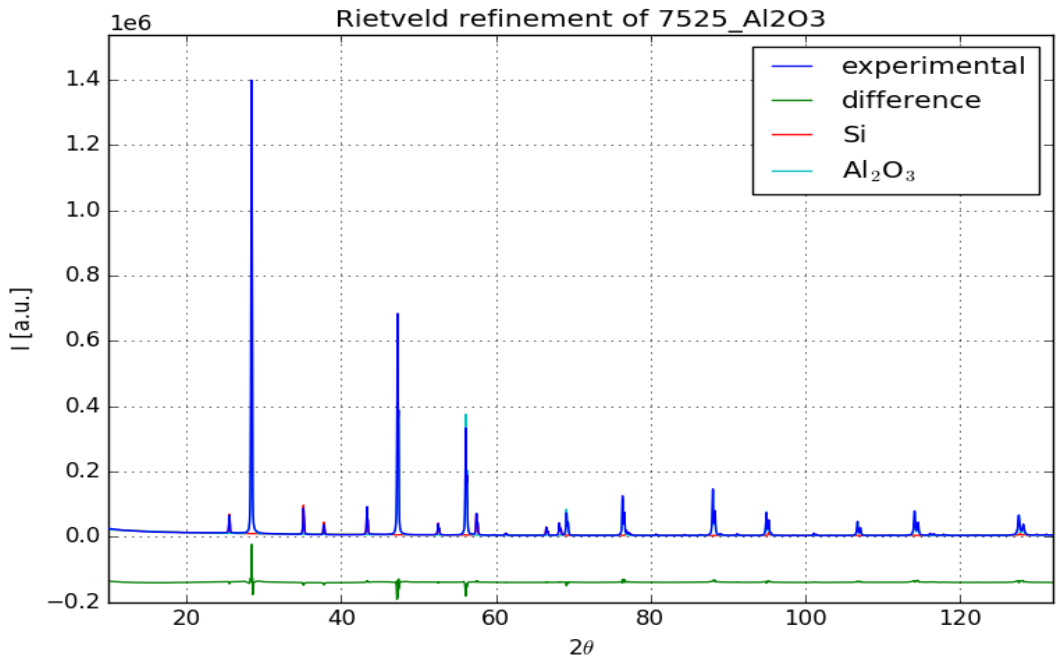

Figure 7.43: Rietveld-refinement of mixture Silicon:Glass 75:25 with 20wt% Al_2O_3 with Topas 4.2

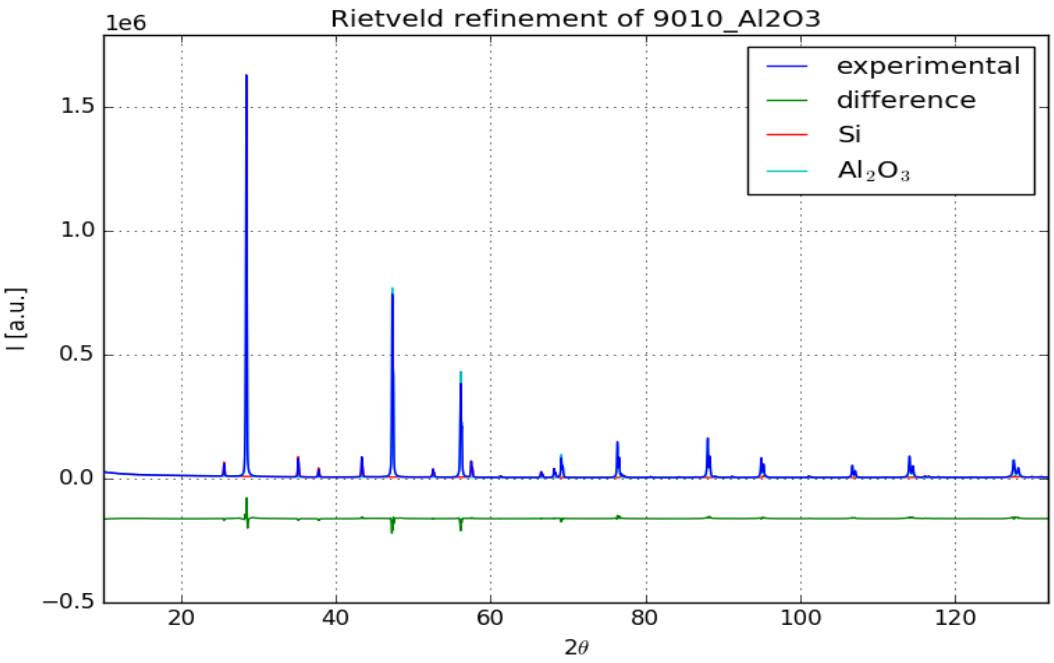

Figure 7.44: Rietveld-refinement of mixture Silicon:Glass 90:10 with 20wt% Al_2O_3 with Topas 4.2

Final conclusions and outlook

> "Relative to the potential structural information procurable, it is fair to say that the quantity and quality of the results are a direct reflection of the pains that have been exercised in measuring and processing the experimental intensities."
>
> — Klug and Alexander (1974, p. 853), *X-Ray Diffraction Procedures for Crystalline and Amorphous Solids.*

In contrast to giving striking new 'insights' into the atomic arrangement of nano-materials, this dissertation is critically assessing the PDF methodology. This means: investigating effects caused by measurement artefacts, data "correction" and applications of PDF analysis where it is not valid according to the theory.

As in today's scientific practice large amounts of data are acquired and handled, the development of convenient and fast-to-use tools is desired. Moreover, automated processing, refinements and data extraction are tempting. In the newest developments of data correction by means of user defined ad-hoc procedures, neither instrumental effects nor precise information on the sample are considered any more. The use of empirical correction procedures is justified and advantageous (e.g. empirical X-ray absorption correction), because it is partly even impossible to describe all parameters important and necessary for a physically meaningful data correction. On the flip side, procedures that are specially designed for laymen, which are fast to learn and easy to use as a black box, might have severe drawbacks - what seems easy can be treacherous. It was easily possible to create a large variety of different PDFs from a single data set by means of such an ad-hoc data correction. In addition, data collection and

treatment procedures are not unique and PDFs of different appearance could be obtained. Furthermore, it was possible to extract spurious structure information from PDF simulations, which could not be confirmed by complementary methods such as TEM.

It is crucial to understand the methods and possible error sources. Otherwise, accuracy and even reliability of analysis suffer. While it is understandable that ever increasing specialization does not leave much room for a human individual to be a specialist on a range, there seems to be no alternative to a sufficient degree of understanding even very complex systems and trends of physical quantities. It must be emphasized, especially in the light of the increasing popularity of PDF analysis, that many questions concerning the PDF methodology are still unanswered.

Some other thoughts

What I recognise is that (even) in science, there is lots of dogmatism and unwillingness to critically reflect what became dear. Anyway, retrospectively seen, staying in academia was the best and the most reasonable choice I could make. It is clear for me now that I would not want to miss it. Properly done, a PhD is an important and valuable personal accomplishment and the degree is almost indispensable for entering the next level of research.

A part of my thesis was financed by the FFG project LixSi with the number 841218. TU Wien gave me financial support in form of a scholarship for my scientific stay in Erlangen and a grant for my participation in the European Crystallographers Meeting ECM30 in Basel. Surely, many things would not have been possible without the good educational system that the state of Austria provides.

I am more than happy that Elena Nourkova convinced me to stay at university because she found the labs so interesting. It was good that she did it.

Also, I had much luck and am indebted to Hermine Peter, my grandmother, who gave me a preliminary home.

I am glad that Klaudia Hradil offered me the possibility for performing a PhD-thesis. Although appropriate communication was hard sometimes, she profoundly supported me in many ways, such as giving me scientific, financial and personal support. Without her, I would not have started a PhD in crystallography, what has crystallised to be one of the best happenings in my live, both for scientific and personal development. Without her, I likely would not have had the chance of working together with Reinhard Neder and also Matteo Leoni.

Werner Artner, very patiently, gave me uncountable and invaluable personal and scientific support in the laboratory.

Furthermore, I am glad about Berthold Stöger's supervision and the manifold help and support concerning scientific practice, argumentation etc he dedicated to me.

I am also indebted to Reinhard Neder, who gave me manifold support in many scientific issues and hope, as well as for being my scientific host for 6 months, which I am especially grateful for.

I am glad that Matteo Leoni was there for many important conversations. He was readily there to support me and showed me that I am not the only person puzzled by many scientific practices.

I think it is more than kind that Erich Halwax freely offered me his expertise and support in the stage of finishing my thesis.

I am further glad to have shared my office with Stephan Pollitt, who was a good colleague and conversation partner. Also, Stefan Diez from Erlangen, with whom I had a great time when I came to visit Reinhard Neder, won me as a friend.

I express my deep happiness about the support I received from my mother Regina Hans, when I nearly had what some would call a substantial crises. With wise and friendly words, she helped me to find a profound change of perspective, which enabled me to resume and lately, but ultimately finishing my work. Also Edmund Winkler helped me to find some insights.

In addition, I want to mention the involvement of Nastaran Hayati-Roodbari, my colleague from PLUS, and Joong-Hee Han, the project coordinator from AIT. I am convinced that both did their best in our mutual work. Herwig Peterlik from the university of Vienna measured and interpreted small angle scattering for me and kindly discussed with me. He is a great person.

Also, I am glad that Hermann Kronberger drew my attention to an open position of an X-ray scientist at my current working place CEST, to earn me a living besides finishing my thesis.

I hope that I was able to avoid the commonly used and empty standard phrases. To subsume, I am a lucky person to find myself in this situation. Thanks to everyone.

APPENDIX

A.1 Script to merge files

```
#!/usr/bin/env python3

import numpy as np
import matplotlib.pyplot as plt
from scipy.interpolate import interp1d
import bisect

def index_le(a, x):
        'Find rightmost value less than or equal to x'
        i = bisect.bisect_right(a, x)
        if i:
        return i-1
        raise ValueError

data_directory= './'
data_working1 = '1'
data_working2 = '2'
data_working3 = '3'
headerSkip = 0

# load data
d01 = np.genfromtxt(data_directory+ data_working1+'.xy',
    skip_header=headerSkip, dtype=float ,usecols=(0,1),
    comments='#')
```

```
d02 = np.genfromtxt(data_directory+ data_working2+'.xy',
    skip_header=headerSkip, dtype=float ,usecols=(0,1),
    comments='#')
d03 = np.genfromtxt(data_directory+ data_working3+'.xy',
    skip_header=headerSkip, dtype=float ,usecols=(0,1),
    comments='#')

# split data
X1 , I1 = d01.T
X2 , I2 = d02.T
X3 , I3 = d03.T

# remove overlaps with worse signal-to-noise ration
last = index_le(X1, X2[0])
X1 = X1[:last]
I1 = I1[:last]
last = index_le(X2, X3[0])
X2 = X2[:last]
I2 = I2[:last]
last = index_le(X3, 150)
X3 = X3[:last]
I3 = I3[:last]

# add and convert section
Xtot = list(X1) + list(X2) + list(X3)
Itot = np.array( list(I1/15) + list(I2/35) + list(I3/70) )/125.25

# interpolate on equidistant grid --- could be omitted
helperFunction = interp1d(Xtot, Itot)
Xtot = np.linspace(Xtot[0], Xtot[-1], num=len(Xtot), endpoint=True,
    retstep=False)
Itot = helperFunction(Xtot)

```

```
51 # save merged data set with specifications
52 outp = np.array([Xtot,Itot]).T
53 name = 'merged_wOutInt'
54 np.savetxt(name+'.xy', outp, fmt='%.3f')
```

A.2 Script for the creation of a dummy 2D-detector image

```
#!/usr/bin/python3

from PIL import Image
from numpy import exp, sqrt, sin, tan, arcsin, arctan
from math import pi
import sys
import datetime

print(datetime.datetime.now())

imgDimX = int(2048/1)      # gives img.size[0]
imgDimY = int(2048/1)      # gives img.size[1]
pixLen = 0.2               |#| µm
Lambda = 0.21140           # Angstrom
D = 161.0                  # direct distance sample-detector in [mm]
highest = 999999           # defines factor to calculate relative
    intensities

QMAX = (4*pi/Lambda*sin(0.5*arctan((sqrt((imgDimX/2*pixLen)**2
+(imgDimY/2*pixLen)**2))/D)))
QMAXedge = (4*pi/Lambda*sin(0.5*arctan((imgDimX/2*pixLen)/D)))
bckgr0 = 1.5*sqrt(QMAX)#sqrt(2)*imgDimX*pixLenX)
print('QMAX           = ', QMAX)
print('QMAXedge       = ', QMAXedge)
print('BackgroundZero = ', bckgr0)


# define parameters for function
wantedMaxQ1 = 4.0
```

```
wantedMaxQ2 = 8.2

sigma1 = 1.5
sigma2 = 3.0
sigma3 = 2.0
sigma4 = 7.0


img = Image.new('I', (imgDimX,imgDimY))
#created a new Image with dimensions X Y
pixels = img.load()
# created the pixel map


# sets a value for every pixel: We will calculate the Q that corresponds to each R-value and
# calculate the intensities found at the corresponding pixel for this Q and therefore R
for posHori in range(imgDimX):
        x = (posHori - imgDimX/2 + 0.5)             # corrected x-pixel position for centre of image
        for posVerti in range(imgDimY):
                y = (posVerti - imgDimY/2 + 0.5)    # corrected y-pixel position for centre of image

                radius = sqrt((x*pixLen)**2+(y*pixLen)**2)
                Q = 4*pi/Lambda*sin(0.5*arctan(radius/D))


                arg1 = exp(-(Q**2))

                if (Q-wantedMaxQ1) <= 0:
                    arg2 = exp(-((Q-wantedMaxQ1)/sigma1)**2)
```

```
58                  else:
59                      arg2 = exp(-((Q-wantedMaxQ1)/sigma2)**2)
60
61                  if (Q-wantedMaxQ2) <= 0:
62                      arg3 = exp(-((Q-wantedMaxQ2)/sigma3)**2)
63                  else:
64                      arg3 = exp(-((Q-wantedMaxQ2)/sigma4)**2)
65
66                  bckgr = ((bckgr0-sqrt(Q))/bckgr0)
67
68
69                  pixels[posHori,posVerti] =
    int(round(exp(-Q*0.05)*highest*(arg1+arg2+0.8*arg3+bckgr)))
70
71 outfileName = sys.argv[1]
72 img.save(outfileName)
73 print(datetime.datetime.now())
```

A.3 Script for the incorporatiin of a mask into a 2D-image

```
#!/usr/bin/python3

from PIL import Image
from numpy import exp, sqrt, sin, tan, arcsin, arctan
from math import pi
import sys
import datetime

print(datetime.datetime.now())

imgDimX = int(2048/1)      # gives img.size[0]
imgDimY = int(2048/1)      # gives img.size[1]
pixLen = 0.2               |#| µm
Lambda = 0.21140           # Angstrom
D = 161.0                  # direct distance sample-detector in [mm]
highest = 999999           # defines factor to calculate relative
    intensities

QMAX = (4*pi/Lambda*sin(0.5*arctan((sqrt((imgDimX/2*pixLen)**2
+(imgDimY/2*pixLen)**2))/D)))
QMAXedge = (4*pi/Lambda*sin(0.5*arctan((imgDimX/2*pixLen)/D)))
bckgr0 = 1.5*sqrt(QMAX)#sqrt(2)*imgDimX*pixLenX)
print('QMAX           = ', QMAX)
print('QMAXedge       = ', QMAXedge)
print('BackgroundZero = ', bckgr0)


# define parameters for function
wantedMaxQ1 = 4.0
```

```
wantedMaxQ2 = 8.2

sigma1 = 1.5
sigma2 = 3.0
sigma3 = 2.0
sigma4 = 7.0


img = Image.new('I', (imgDimX,imgDimY))
#created a new Image with dimensions X Y
pixels = img.load()
# created the pixel map


# sets a value for every pixel: We will calculate the Q that corresponds to each R-value and
# calculate the intensities found at the corresponding pixel for this Q and therefore R
for posHori in range(imgDimX):
x = (posHori - imgDimX/2 + 0.5)              # corrected x-pixel position for centre of image
for posVerti in range(imgDimY):
y = (posVerti - imgDimY/2 + 0.5)     # corrected y-pixel position for centre of image

radius = sqrt((x*pixLen)**2+(y*pixLen)**2)
Q = 4*pi/Lambda*sin(0.5*arctan(radius/D))


arg1 = exp(-(Q**2))

if (Q-wantedMaxQ1) <= 0:
arg2 = exp(-((Q-wantedMaxQ1)/sigma1)**2)
```

```
58 else:
59 arg2 = exp(-((Q-wantedMaxQ1)/sigma2)**2)
60
61 if (Q-wantedMaxQ2) <= 0:
62 arg3 = exp(-((Q-wantedMaxQ2)/sigma3)**2)
63 else:
64 arg3 = exp(-((Q-wantedMaxQ2)/sigma4)**2)
65
66 bckgr = ((bckgr0-sqrt(Q))/bckgr0)
67
68
69 pixels[posHori,posVerti] =
      int(round(exp(-Q*0.05)*highest*(arg1+arg2+0.8*arg3+bckgr)))
70
71 outfileName = sys.argv[1]
72 img.save(outfileName)
73 print(datetime.datetime.now())
```

Bibliography

Abeykoon, A.; Malliakas, C. D.; Juhás, P.; Bozin, E. S.; Kanatzidis, M. G. and Billinge, S. J. (2012). 'Quantitative nanostructure characterization using atomic pair distribution functions obtained from laboratory electron microscopes'. In: *Zeitschrift für Kristallographie Crystalline Materials* 227.5, pp. 248–256. DOI: 10.1524/zkri.2012.1510.

Abeykoon, A.; Castro-Colin, M.; Anokhina, E.; Iliev, M.; Donner, W.; Brunelli, M.; Jacobson, A. and Moss, S. (2008). 'X-Ray Scattering Studies of HgSe Nanoclusters in Zeolite'. In: *Metallurgical and Materials Transactions A* 39.13, pp. 3179–3183. DOI: 10.1007/s11661-008-9563-9.

Alexandropoulos, N. G.; Cooper, M. J.; Suortti, P. and Willis, B. T. M. (2006). 'Correction of systematic errors'. In: *International Tables for Crystallography*. International Union of Crystallography, pp. 653–665. DOI: 10.1107/97809553602060000607.

Aste, T and Weaire, D (2008). *The Pursuit of Perfect Packing*. Institute of Physics Publishing.

Barkema, G. T. and Mousseau, N. (2000). 'High-quality continuous random networks'. In: *Physical Review B* 62.8, p. 4985.

Barkema, G. and Mousseau, N. (1996). 'Event-based relaxation of continuous disordered systems'. In: *Physical review letters* 77.21, p. 4358.

Beek, W. v.; Emerich, H.; Urakawa, A.; Palin, L.; Milanesio, M.; Caliandro, R.; Viterbo, D. and Chernyshov, D. (2012). 'Untangling diffraction intensity: modulation enhanced diffraction on ZrO2 powder'. In: *Journal of Applied Crystallography* 45.4, pp. 738–747. DOI: 10.1107/s0021889812018109.

Berriot, J.; Montes, H.; Lequeux, F.; Long, D. and Sotta, P. (2002). 'Evidence for the Shift of the Glass Transition near the Particles in Silica-Filled Elastomers'. In: *Macromolecules* 35.26, pp. 9756–9762. DOI: 10.1021/ma0212700.

Beyerlein, K. R.; Leoni, M. and Scardi, P. (2012). 'Temperature diffuse scattering of nanocrystals'. In: *Acta Crystallographica Section A Foundations of Crystallography* 68.3, pp. 382–392. DOI: 10.1107/s0108767312009853.

Beyerlein, K. R. (2013). 'A review of Debye function analysis'. In: *Powder diffraction* 28.S2, S2–S10. DOI: 10.1017/s0885715613001218.

Billinge, S. (2013). 'Materials science: Nanoparticle structures served up on a tray'. In: *Nature* 495.7442, pp. 453–454. DOI: 10.1038/495453a.

Billinge, S. J. L. and Farrow, C. L. (2013). 'Towards a robust ad hoc data correction approach that yields reliable atomic pair distribution functions from powder diffraction data'. In: *Journal of Physics: Condensed Matter* 25.45, p. 454202. DOI: 10.1088/0953-8984/25/45/454202.

Billinge, S. J. (2010). 'Viewpoint: The nanostructure problem'. In: *Physics* 3, p. 25.

Billinge, S. J.; Dykhne, T.; Juhás, P.; Božin, E.; Taylor, R.; Florence, A. J. and Shankland, K. (2010). 'Characterisation of amorphous and nanocrystalline molecular materials by total scattering'. In: *CrystEngComm* 12.5, pp. 1366–1368. DOI: 10.1039/b915453a.

Billinge, S. and Kwei, G. (1996). 'Probing the short-range order and dynamics of phase transitions using neutron powder diffraction'. In: *Journal of Physics and Chemistry of Solids* 57.10, pp. 1457–1464. DOI: 10.1016/0022-3697(96)00013-3.

Billinge, S.; Gutmann, M and Bozin, E. (2000a). 'Local structure as a probe of stripes and its relation to T'. In: *Physica C: Superconductivity* 341, pp. 1795–1796.

Billinge, S.; Petkov, V and Proffen, T. (2000b). 'Structure on different length scales from powder diffraction: The real-space pair-distribution function (PDF) technique'. In: *Commission on Powder Diffraction of the International Union of Crystallography Newsletter* 24.

Bordet, P. (2015). 'Local structure studies using the pair distribution function'. In: *EPJ Web of Conferences* 104. Ed. by M. Ceretti; W. Paulus; M.-H. Mathon and C. Ritter, p. 01003. DOI: 10.1051/epjconf/201510401003.

Born, M. (1926). 'Quantenmechanik der Stoßvorgänge'. In: *Zeitschrift für Physik* 38.11-12, pp. 803–827.

Bourderau, S; Brousse, T and Schleich, D. (1999). 'Amorphous silicon as a possible anode material for Li-ion batteries'. In: *Journal of power sources* 81, pp. 233–236. DOI: 10.1016/s0378-7753(99)00194-9.

Bowron, D. (2008). 'An experimentally consistent atomistic structural model of silica glass'. In: *Materials Science and Engineering: B* 149.2, pp. 166–170. DOI: 10.1016/j.mseb.2007.11.030.

Bricogne, G. (2010). 'Fourier transforms in crystallography: theory, algorithms and applications'. In: *International Tables for Crystallography*. International Union of Crystallography, pp. 24–113. DOI: 10.1107/97809553602060000760.

Cervellino, A.; Giannini, C.; Guagliardi, A. and Ladisa, M. (2005). 'Disentangling instrumental broadening'. In: *Journal of Applied Crystallography* 38.4, pp. 685–687. DOI: 10.1107/S0021889805017206.

Cervellino, A.; Giannini, C. and Guagliardi, A. (2006). 'On the efficient evaluation of Fourier patterns for nanoparticles and clusters'. In: *Journal of Computational Chemistry* 27.9, pp. 995–1008. DOI: 10.1002/jcc.20407.

Chung, J. S. and Thorpe, M. (1997). 'Local atomic structure of semiconductor alloys using pair distribution functions'. In: *Physical Review B* 55.3, p. 1545. DOI: 10.1103/physrevb.55.1545.

Cliffe, M. J. and Goodwin, A. L. (2013). 'Nanostructure determination from the pair distribution function: a parametric study of the INVERT approach'. In: *Journal of Physics: Condensed Matter* 25.45, p. 454218.

Cliffe, M. J.; Dove, M. T.; Drabold, D. and Goodwin, A. L. (2010). 'The nanostructure problem'. In: *Physical Review Letters* 104.12. DOI: 10.1103/PhysRevLett.104.125501.

Coelho, A. (2008). 'DIFFRACplus TOPAS 4.2'. In: *BrukerAXS GmbH, Karlsruhe*.

Collins, H. M. (1994). 'A strong confirmation of the experimenters' regress'. In: *Studies in History and Philosophy of Science Part A* 25.3, pp. 493–503. DOI: 10.1016/0039-3681(94)90063-9.

Compton, A. H. (1923). 'The quantum integral and diffraction by a crystal'. In: *Proceedings of the National Academy of Sciences* 9.11, pp. 359–362.

Coppens, P. (2010). 'The structure factor'. In: *International Tables for Crystallography*. International Union of Crystallography, pp. 10–23. DOI: 10.1107/97809553602060000759.

Davis, T.; Johnson, M. and Billinge, S. J. L. (2013). 'Toward Phase Quantification at the Nanoscale Using the Total Scattering Pair Distribution Function (TSPDF) Method: Recrystallization of Cryomilled Sulfamerazine'. In: *Crystal Growth & Design* 13.10, pp. 4239–4244. DOI: 10.1021/cg400179p.

Davis, T. D. (2011). *Fingerprinting analysis of non-crystalline pharmaceutical compounds using high energy X-rays and the total scattering pair distribution function*. Columbia University.

Debye, P (1930). 'Röntgeninterferenzen und Atomgröße'. In: *Physik. Zeitschr.* 31, p. 419.

Debye, P. (1915). 'Zerstreuung von Röntgenstrahlen'. In: *Annalen der Physik* 351.6, pp. 809–823. DOI: 10.1002/andp.19153510606.

Debye, P. J. W. and Menke, H. (1931). 'Untersuchung der molekularen Ordnung in Flüssigkeiten mit Röntgenstrahlung'. In: *Ergebnisse der technischen Röntgenkunde*. Vol. 2. Akademische Verlagsgesellschaft. Chap. 1.

Detlefs, C; Rio, M. S. del and Mazzoli, C (2012). 'X-ray polarization: General formalism and polarization analysis'. In: *The European Physical Journal Special Topics* 208.1, pp. 359–371.

Djordjević, B.; Thorpe, M. and Wooten, F (1995). 'Computer model of tetrahedral amorphous diamond'. In: *Physical Review B* 52.8, p. 5685.

Durbin, S. (1995). 'Darwin spherical-wave theory of kinematic surface diffraction'. In: *Acta Crystallographica Section A: Foundations of Crystallography* 51.3, pp. 258–268.

Dykhne, T.; Taylor, R.; Florence, A. and Billinge, S. J. (2011). 'Data requirements for the reliable use of atomic pair distribution functions in amorphous pharmaceutical fingerprinting'. In: *Pharmaceutical research* 28.5, pp. 1041–1048. DOI: 10.1007/s11095-010-0350-0.

Egami, T. and Billinge, S. J. (2003). *Underneath the Bragg peaks: structural analysis of complex materials*. Vol. 16. Elsevier.

Ekstein, H (1942). 'Connection between the kinematic and dynamical theories of x-ray diffraction'. In: *Physical Review* 62.5-6, p. 255.

Enderby, J. E.; North, D. M. and Egelstaff, P. A. (1966). 'The partial structure factors of liquid Cu-Sn'. In: *Philosophical Magazine* 14.131, pp. 961–970. DOI: 10.1080/14786436608244767.

Ewald, P. (1969). 'Introduction to the dynamical theory of X-ray diffraction'. In: *Acta Crystallographica Section A: Crystal Physics, Diffraction, Theoretical and General Crystallography* 25.1, pp. 103–108.

Farrow, C. L. and Billinge, S. J. (2009). 'Relationship between the atomic pair distribution function and small-angle scattering: implications for modeling of nanoparticles'. In: *Acta Crystallographica Section A: Foundations of Crystallography* 65.3, pp. 232–239. DOI: 10.1107/s0108767309009714.

Farrow, C. L.; Ruan, C.-Y. and Billinge, S. J. L. (2010). 'Quantitative nanoparticle structures from electron crystallography data'. In: *Physical Review B* 81.13. DOI: 10.1103/physrevb.81.134104.

Farrow, C.; Juhas, P; Liu, J.; Bryndin, D; Božin, E.; Bloch, J; Proffen, T. and Billinge, S. (2007). 'PDFfit2 and PDFgui: computer programs for studying nanostructure in crystals'. In: *Journal of Physics: Condensed Matter* 19.33, p. 335219. DOI: 10.1088/0953-8984/19/33/335219.

Feil, D. (1977). 'II. Diffraction Physics'. In: *Israel Journal of Chemistry* 16.2-3, pp. 103–110.

Filik, J.; Ashton, A. W.; Chang, P. C. Y.; Chater, P. A.; Day, S. J.; Drakopoulos, M.; Gerring, M. W.; Hart, M. L.; Magdysyuk, O. V.; Michalik, S.; Smith, A.; Tang, C. C.; Terrill, N. J.; Wharmby, M. T. and Wilhelm, H. (2017). 'Processing two-dimensional X-ray diffraction and small-angle scattering data in DAWN 2'. In: *Journal of Applied Crystallography* 50.3, pp. 959–966. DOI: 10.1107/s1600576717004708.

Finbak, C.; Schwarz, B.; Melaja, A.; Kainulainen, A.; Halonen, A. and Pulkkinen, E. (1949a). 'The Structure of Liquids. I.' In: *Acta Chemica Scandinavica* 3, pp. 1279–1292. DOI: 10.3891/acta.chem.scand.03-1279.

— (1949b). 'The Structure of Liquids. II.' In: *Acta Chemica Scandinavica* 3, pp. 1293–1308. DOI: 10.3891/acta.chem.scand.03-1293.

Flaig, S.; Akbarzadeh, J.; Dolcet, P.; Gross, S.; Peterlik, H. and Hüsing, N. (2014). 'Hierarchically organized silica–titania monoliths prepared under purely

aqueous conditions'. In: *Chemistry-A European Journal* 20.52, pp. 17409–17419.

Frey, F.; Boysen, H. and Jagodzinski, H. (2010). 'Disorder diffuse scattering of X-rays and neutrons'. In: *International Tables for Crystallography*. International Union of Crystallography, pp. 492–539. DOI: 10.1107/97809553602060000774.

Gelisio, L. and Scardi, P. (2016). '100 years of Debyes scattering equation'. In: *Acta Crystallographica Section A Foundations and Advances* 72.6, pp. 608–620. DOI: 10.1107/s2053273316014881.

Gelisio, L.; Ricardo, C. L. A.; Leoni, M. and Scardi, P. (2010). 'Real-space calculation of powder diffraction patterns on graphics processing units'. In: *Journal of Applied Crystallography* 43.3, pp. 647–653. DOI: 10.1107/s0021889810005133.

Gereben, O. and Pusztai, L. (2012). 'RMC_POT: A computer code for reverse monte carlo modeling the structure of disordered systems containing molecules of arbitrary complexity'. In: *Journal of Computational Chemistry* 33.29, pp. 2285–2291. DOI: 10.1002/jcc.23058.

Gibson, J. M. (2007). 'Understanding the limits of pair-distribution functions for nanoscale correlation function measurement'. In: *Journal of Physics: Condensed Matter* 19.45, p. 455217. DOI: 10.1088/0953-8984/19/45/455217.

Gingrich, N. S. (1943). 'The diffraction of x-rays by liquid elements'. In: *Reviews of Modern Physics* 15.1, p. 90. DOI: 10.1103/revmodphys.15.90.

Gingrich, N. and Heaton, L. (1961). 'Structure of alkali metals in the liquid state'. In: *The Journal of Chemical Physics* 34.3, pp. 873–878. DOI: 10.1063/1.1731688.

Godin, B. and Gingras, Y. (2002). 'The experimenters' regress: from skepticism to argumentation'. In: *Studies in History and Philosophy of Science Part A* 33.1, pp. 133–148. DOI: 10.1016/s0039-3681(01)00032-2.

Granlund, L.; Billinge, S. J. L. and Duxbury, P. M. (2015). 'Algorithm for systematic peak extraction from atomic pair distribution functions'. In: *Acta Crystallographica Section A Foundations and Advances* 71.4, pp. 392–409. DOI: 10.1107/s2053273315005276.

Grigson, C. (1967). 'Validity of the Debye Scattering Equation in Elastic Electron Diffraction'. In: *Nature* 215.5099, p. 382.

Hamad, E. Z. and Mansoori, G. (1989). 'Mixture radial distribution functions: Are they all independent?' In: *Fluid Phase Equilibria* 51, pp. 13–21. DOI: 10.1016/0378-3812(89)80351-6.

Hammersley, A. P.; Svensson, S. O.; Hanfland, M.; Fitch, A. N. and Hausermann, D. (1996). 'Two-dimensional detector software: From real detector to idealised image or two-theta scan'. In: *High Pressure Research* 14.4-6, pp. 235–248. DOI: 10.1080/08957959608201408.

Hansen, A.-L.; Dietl, B.; Etter, M.; Kremer, R. K.; Johnson, D. C. and Bensch, W. (2018). 'Temperature-dependent synchrotron X-ray diffraction, pair distribution function and susceptibility study on the layered compound CrTe3'. In: *Zeitschrift für Kristallographie - Crystalline Materials* 233.6, pp. 361–370. DOI: 10.1515/zkri-2017-2100.

Harrington, R.; Neder, R. B. and Parise, J. B. (2012). 'The nature of x-ray scattering from geo-nanoparticles: Practical considerations of the use of the Debye equation and the pair distribution function for structure analysis'. In: *Chemical Geology* 329, pp. 3–9. DOI: 10.1016/j.chemgeo.2011.06.010.

He, B. B. (2009). *Two-Dimensional X-Ray Diffraction*. JOHN WILEY & SONS INC. 426 pp.

Henry, P. F.; Weller, M. T. and Wilson, C. C. (2001). 'Structural Investigation of TS-1: Determination of the True Nonrandom Titanium Framework Substitution and Silicon Vacancy Distribution from Powder Neutron Diffraction Studies Using Isotopes'. In: *The Journal of Physical Chemistry B* 105.31, pp. 7452–7458. DOI: 10.1021/jp0107715.

Holzwarth, U. and Gibson, N. (2011). 'The Scherrer equation versus the'Debye-Scherrer equation''. In: *Nature nanotechnology* 6.9, p. 534.

Ida, T and Toraya, H (2002). 'Deconvolution of the instrumental functions in powder X-ray diffractometry'. In: *Journal of applied crystallography* 35.1, pp. 58–68. DOI: 10.1107/s0021889801018945.

Jensen, K.; Blichfeld, A. B.; Bauers, S. R.; Wood, S. R.; Dooryhée, E.; Johnson, D. C.; Iversen, B. B. and Billinge, S. J. (2015). 'Demonstration of thin film pair distribution function analysis (tfPDF) for the study of local structure in amorphous and crystalline thin films'. In: *IUCrJ* 2.5, pp. 481–489. DOI: 10.1107/s2052252515012221.

Jeong, I.-K.; Heffner, R.; Graf, M. and Billinge, S. (2003). 'Lattice dynamics and correlated atomic motion from the atomic pair distribution function'. In: *Physical Review B* 67.10, p. 104301. DOI: 10.1103/physrevb.67.104301.

Jeong, I.-K.; Proffen, T.; Mohiuddin-Jacobs, F. and Billinge, S. J. L. (1999). 'Measuring Correlated Atomic Motion Using X-ray Diffraction'. In: *The Journal of Physical Chemistry A* 103.7, pp. 921–924. DOI: 10.1021/jp9836978.

Jeong, I.-K.; Graf, M. J. and Heffner, R. H. (2005). 'Effects of Bragg peak profiles and nanoparticle sizes on the real-space pair distribution function'. In: *Journal of Applied Crystallography* 38.1, pp. 55–61. DOI: 10.1107/s0021889804025841.

Juhás, P; Cherba, D.; Duxbury, P.; Punch, W. and Billinge, S. (2006). 'Ab initio determination of solid-state nanostructure'. In: *Nature* 440.7084, pp. 655–658.

Juhás, P; Granlund, L; Duxbury, P.; Punch, W. and Billinge, S. (2008). 'The Liga algorithm for ab initio determination of nanostructure'. In: *Acta Crystallographica Section A: Foundations of Crystallography* 64.6, pp. 631–640.

Juhas, P.; Granlund, L.; Gujarathi, S. R.; Duxbury, P. M. and Billinge, S. J. (2010). 'Crystal structure solution from experimentally determined atomic pair distribution functions'. In: *Journal of Applied Crystallography* 43.3, pp. 623–629.

Juhás, P.; Davis, T.; Farrow, C. L. and Billinge, S. J. (2013). 'PDFgetX3: a rapid and highly automatable program for processing powder diffraction data into total scattering pair distribution functions'. In: *Journal of Applied Crystallography* 46.2, pp. 560–566. DOI: 10.1107/s0021889813005190.

Kammler, D. W. (2008). *A First Course in Fourier Analysis*. Cambridge University Press.

Keen, D. A. (2001). 'A comparison of various commonly used correlation functions for describing total scattering'. In: *Journal of Applied Crystallography* 34.2, pp. 172–177. DOI: 10.1107/s0021889800019993.

Keen, D. A. and Goodwin, A. L. (2015). 'The crystallography of correlated disorder'. In: *Nature* 521.7552, p. 303. DOI: 10.1038/nature14453.

Kennefick, D. (2000). 'Star crushing: Theoretical practice and the theoreticians' regress'. In: *Social Studies of Science* 30.1, pp. 5–40. DOI: 10.1177/030631200030001001.

Kern, A.; Madsen, I. C. and Scarlett, N. V. (2012). 'Quantifying amorphous phases'. In: *Uniting Electron Crystallography and Powder Diffraction*. Springer, pp. 219–231.

Klug, H. and Alexander, L. E. (1974). *X-Ray Diffraction Procedures for Crystalline and Amorphous Solids*. Wiley-Interscience New York, NY, USA.

Kniess, C. T.; Lima, J. C. de and Prates, P. B. (2012). 'The quantification of crystalline phases in materials: Applications of rietveld method'. In: *Sintering-Methods and Products*. InTech.

Korsunskiy, V. and Neder, R. (2005). 'Exact model calculations of the total radial distribution functions for the X-ray diffraction case and systems of complicated chemical composition'. In: *Journal of applied crystallography* 38.6, pp. 1020–1027. DOI: 10.1107/s0021889805031948.

Korsunskiy, V.; Neder, R.; Hradil, K; Barglik-Chory, C.; Müller, G and Neuefeind, J (2003). 'Investigation of nanocrystalline CdS–glutathione particles by radial distribution function'. In: *Journal of applied crystallography* 36.6, pp. 1389–1396. DOI: 10.1107/s0021889803018302.

Korsunskiy, V. I.; Neder, R. B.; Hofmann, A.; Dembski, S.; Graf, C. and Rühl, E. (2007). 'Aspects of the modelling of the radial distribution function for small nanoparticles'. In: *Journal of Applied Crystallography* 40.6, pp. 975–985. DOI: 10.1107/s0021889807038174.

Lamberti, C; Bordiga, S; Zecchina, A; Carati, A; Fitch, A.; Artioli, G; Petrini, G; Salvalaggio, M and Marra, G. (1999). 'Structural characterization of Ti-silicalite-1: A synchrotron radiation X-ray powder diffraction study'. In: *Journal of Catalysis* 183.2, pp. 222–231.

Landauer, R. (1989). 'Nanostructure physics: fashion or depth'. In: *Nanostructure Physics and Fabrication*, pp. 17–30.

Le Bail, A; Jacoboni, C and De Pape, R (1985). 'REFINING STRUCTURAL MODELS FOR GLASSES: IS IT POSSIBLE? THE CASE OF'. In: *Le Journal de Physique Colloques* 46.C8, pp. C8–163.

Leadbetter, A. and Wright, A. (1972). 'Diffraction studies of glass structure III. Limitations of the fourier method for polyatomic glasses'. In: *Journal of Non-Crystalline Solids* 7.2, pp. 141–155.

Lee, B. M.; Baik, H. K.; Seong, B. S.; Munetoh, S. and Motooka, T. (2006). 'Generation of glass SiO2 structures by various cooling rates: A molecular-dynamics study'. In: *Computational Materials Science* 37.3, pp. 203–208. DOI: 10.1016/j.commatsci.2006.01.003.

Leonardi, A. and Bish, D. L. (2016). 'High-performance powder diffraction pattern simulation for large-scale atomistic modelsviafull-precision pair distribution function computation'. In: *Journal of Applied Crystallography* 49.5, pp. 1593–1608. DOI: 10.1107/s1600576716011729.

Li, G.; Wang, X.; Guo, X.; Liu, S.; Zhao, Q.; Bao, X. and Lin, L. (2001). 'Titanium species in titanium silicalite TS-1 prepared by hydrothermal method'. In: *Materials chemistry and physics* 71.2, pp. 195–201.

Lipkin, H. J. (2004). 'Physics of Debye-Waller Factors'. In: *arXiv preprint cond-mat/0405023*.

Lorch, E (1969). 'Neutron diffraction by germania, silica and radiation-damaged silica glasses'. In: *Journal of Physics C: Solid State Physics* 2.2, p. 229.

Madsen, I. C.; Scarlett, N. V. and Kern, A. (2011). 'Description and survey of methodologies for the determination of amorphous content via X-ray powder diffraction'. In: *Zeitschrift für Kristallographie Crystalline Materials* 226.12, pp. 944–955. DOI: 10.1524/zkri.2011.1437.

Mansoori, G. A. (1993). 'Radial distribution functions and their role in modeling of mixtures behavior'. In: *Fluid phase equilibria* 87.1, pp. 1–22.

Marians, C. S. and Burdett, J. K. (1990). 'Geometric constraints: a refined model for the structure of silica glass'. In: *Journal of Non-Crystalline Solids* 124.1, pp. 1–21.

Martínez, L.; Andrade, R.; Birgin, E. G. and Martínez, J. M. (2009). 'PACKMOL: a package for building initial configurations for molecular dynamics simulations'. In: *Journal of computational chemistry* 30.13, pp. 2157–2164.

Masadeh, A. S.; Božin, E. S.; Farrow, C. L.; Paglia, G.; Juhas, P.; Billinge, S. J. L.; Karkamkar, A. and Kanatzidis, M. G. (2007). 'Quantitative size-dependent structure and strain determination of CdSe nanoparticles using atomic pair distribution function analysis'. In: *Physical Review B* 76.11. DOI: 10.1103/physrevb.76.115413.

McCusker, L.; Von Dreele, R.; Cox, D.; Louër, D and Scardi, P (1999). 'Rietveld refinement guidelines'. In: *Journal of Applied Crystallography* 32.1, pp. 36–50.

Mou, Q; Benmore, C. and Yarger, J. (2015). 'X-ray Intermolecular Structure Factor (XISF): separation of intra-and intermolecular interactions from total X-ray scattering data'. In: *Journal of Applied Crystallography* 48.3, pp. 950–952. DOI: 10.1107/s1600576715005518.

Mousseau, N. and Barkema, G. (2001). 'Fast bond-transposition algorithms for generating covalent amorphous structures'. In: *Current Opinion in Solid State and Materials Science* 5.6, pp. 497–502.

Mukhopadhyay, A. and Sheldon, B. W. (2014). 'Deformation and stress in electrode materials for Li-ion batteries'. In: *Progress in Materials Science* 63, pp. 58–116. DOI: 10.1016/j.pmatsci.2014.02.001.

Neder, R. and Proffen, T. (1997). 'DISCUS: A program for diffuse scattering and defect-structure simulation'. In: *Journal of applied crystallography* 30.2, pp. 171–175. DOI: 10.1107/s002188989600934x.

Neder, R.; Frey, F and Schulz, H (1990). 'Diffraction theory for diffuse scattering by correlated microdomains in materials with several atoms per unit cell'. In: *Acta Crystallographica Section A: Foundations of Crystallography* 46.10, pp. 792–798.

Neder, R. B. and Korsunskiy, V. I. (2005). 'Structure of nanoparticles from powder diffraction data using the pair distribution function'. In: *Journal of Physics: Condensed Matter* 17.5, S125–S134. DOI: 10.1088/0953-8984/17/5/013.

Neder, R. B. and Proffen, T. (2008). *Diffuse Scattering and Defect Structure Simulations: A cook book using the program DISCUS*. Vol. 11. Oxford University Press.

Olds, D.; Wang, H.-W. and Page, K. (2015). '*DShaper*: an approach for handling missing low-Q data in pair distribution function analysis of nanostructured systems'. In: *Journal of Applied Crystallography* 48.6, pp. 1651–1659. DOI: 10.1107/S1600576715016581.

Page, K.; Hood, T. C.; Proffen, T. and Neder, R. B. (2011). 'Building and refining complete nanoparticle structures with total scattering data'. In: *Journal of Applied Crystallography* 44.2, pp. 327–336. DOI: 10.1107/s0021889811001968.

Paglia, G.; Božin, E. S. and Billinge, S. J. (2006). 'Fine-scale nanostructure in γ-Al2O3'. In: *Chemistry of Materials* 18.14, pp. 3242–3248. DOI: 10.1021/cm060277j.

Pandey, A.; Biswas, P.; Bhattarai, B. and Drabold, D. (2016). 'Realistic inversion of diffraction data for an amorphous solid: The case of amorphous silicon'. In: *Physical Review B* 94.23, p. 235208. DOI: 10.1103/physrevb.94.235208.

Patterson, A. L. (1935). 'A direct method for the determination of the components of interatomic distances in crystals'. In: *Zeitschrift für Kristallographie-Crystalline Materials* 90.1, pp. 517–542. DOI: 10.1524/zkri.1935.90.1.517.

Pedone, A.; Malavasi, G.; Menziani, M. C.; Cormack, A. N. and Segre, U. (2006). 'A new self-consistent empirical interatomic potential model for oxides, silicates, and silica-based glasses'. In: *The Journal of Physical Chemistry B* 110.24, pp. 11780–11795. DOI: 10.1021/jp0611018.

Peterson, P. F.; Božin, E. S.; Proffen, T. and Billinge, S. J. (2003). 'Improved measures of quality for the atomic pair distribution function'. In: *Journal of applied crystallography* 36.1, pp. 53–64. DOI: 10.1107/s0021889802018708.

Petkov, V.; Cozzoli, P. D.; Buonsanti, R.; Cingolani, R. and Ren, Y. (2009). 'Size, Shape, and Internal Atomic Ordering of Nanocrystals by Atomic Pair Distribution Functions: A Comparative Study of γ-Fe2O3Nanosized Spheres and Tetrapods'. In: *Journal of the American Chemical Society* 131.40, pp. 14264–14266. DOI: 10.1021/ja9067589.

Petkov, V.; Prasai, B.; Ren, Y.; Shan, S.; Luo, J.; Joseph, P. and Zhong, C.-J. (2014). 'Solving the nanostructure problem: exemplified on metallic alloy nanoparticles'. In: *Nanoscale* 6.17, pp. 10048–10061. DOI: 10.1039/c4nr01633e.

Prescher, C. and Prakapenka, V. B. (2015). 'DIOPTAS: a program for reduction of two-dimensional X-ray diffraction data and data exploration'. In: *High Pressure Research* 35.3, pp. 223–230. DOI: 10.1080/08957959.2015.1059835.

Prill, D.; Juhás, P.; Schmidt, M. U. and Billinge, S. J. (2015). 'Modelling pair distribution functions (PDFs) of organic compounds: describing both intra- and intermolecular correlation functions in calculated PDFs'. In: *Journal of Applied Crystallography* 48.1, pp. 171–178.

Proffen, T. and Billinge, S. (2002). 'Probing the local structure of doped manganites using the atomic pair distribution function'. In: *Applied Physics A: Materials Science & Processing* 74.0, s1770–s1772. DOI: 10.1007/s003390201846.

Proffen, T.; Billinge, S.; Egami, T and Louca, D (2003). 'Structural analysis of complex materials using the atomic pair distribution function—A practical guide'. In: *Zeitschrift für Kristallographie-Crystalline Materials* 218.2, pp. 132–143. DOI: 10.1524/zkri.218.2.132.20664.

Proffen, T. and Kim, H. (2009). 'Advances in total scattering analysis'. In: *Journal of Materials Chemistry* 19.29, pp. 5078–5088. DOI: 10.1039/b821178g.

Proffen, T.; Page, K. L.; McLain, S. E.; Clausen, B.; Darling, T. W.; TenCate, J. A.; Lee, S.-Y. and Ustundag, E. (2005). 'Atomic pair distribution function analysis of materials containing crystalline and amorphous phases'. In: *Zeitschrift für Kristallographie-Crystalline Materials* 220.12, pp. 1002–1008. DOI: 10.1524/zkri.2005.220.12.1002.

Pusztai, L.; Harsányi, I.; Dominguez, H. and Pizio, O. (2008). 'Assessing the level of consistency between diffraction experiments and interaction potentials: A combined molecular dynamics (MD) and Reverse Monte Carlo (RMC) approach'. In: *Chemical Physics Letters* 457.1-3, pp. 96–102. DOI: 10.1016/j.cplett.2008.03.091.

Qiu, X.; Božin, E. S.; Juhas, P.; Proffen, T. and Billinge, S. J. (2004). 'Reciprocal-space instrumental effects on the real-space neutron atomic pair distribution function'. In: *Journal of Applied Crystallography* 37.1, pp. 110–116. DOI: 10.1107/s0021889803026670.

Rademacher, N.; Daemen, L. L.; Chronister, E. L. and Proffen, T. (2012). 'Pair distribution function analysis of molecular compounds: significance and modeling approach discussed using the example of p-terphenyl'. In: *Journal of Applied Crystallography* 45.3, pp. 482–488.

Rahman, M. (2011). *Applications of Fourier Transforms to Generalized Functions*. WIT Press / Computational Mechanics.

Ravy, S. (2013). 'Homometry in the light of coherent beams'. In: *Acta Crystallographica Section A: Foundations of Crystallography* 69.6, pp. 543–548.

Saravanan, R. and Rani, M. P. (2011). 'Charge Density Analysis from X-Ray Diffraction'. In: *Metal and Alloy Bonding - An Experimental Analysis*. Springer London, pp. 31–64. DOI: 10.1007/978-1-4471-2204-3_2.

Sava, F. and Popescu, M. (2011). 'New structural features of non-crystalline tetrahedrally bonded networks'. In: *Journal of Non-Crystalline Solids* 357.14, pp. 2552–2554. DOI: 10.1016/j.jnoncrysol.2011.02.056.

Scardi, P and Leoni, M (2002). 'Whole powder pattern modelling'. In: *Acta crystallographica section A* 58.2, pp. 190–200.

Schülke, W (1989). 'Inelastic X-ray scattering'. In: *Nuclear Instruments and Methods in Physics Research Section A: Accelerators, Spectrometers, Detectors and Associated Equipment* 280.2-3, pp. 338–348.

Shan, T.-R.; Devine, B. D.; Hawkins, J. M.; Asthagiri, A.; Phillpot, S. R. and Sinnott, S. B. (2010). 'Second-generation charge-optimized many-body potential forSi/SiO2and amorphous silica'. In: *Physical Review B* 82.23. DOI: 10.1103/physrevb.82.235302.

Sinn, H; Sette, F; Bergmann, U; Halcoussis, C.; Krisch, M; Verbeni, R and Burkel, E (1997). 'Coherent dynamic structure factor of liquid lithium by inelastic X-ray scattering'. In: *Physical review letters* 78.9, p. 1715.

Skinner, L. B.; Benmore, C. J. and Parise, J. B. (2012). 'Area detector corrections for high quality synchrotron X-ray structure factor measurements'. In: *Nuclear Instruments and Methods in Physics Research Section A: Accelerators, Spectrometers, Detectors and Associated Equipment* 662.1, pp. 61–70. DOI: 10.1016/j.nima.2011.09.031.

Soper, A. K. (2007). 'On the uniqueness of structure extracted from diffraction experiments on liquids and glasses'. In: *Journal of Physics: Condensed Matter* 19.41, p. 415108. DOI: 10.1088/0953-8984/19/41/415108.

Soper, A. K. (2013). 'The radial distribution functions of water as derived from radiation total scattering experiments: is there anything we can say for sure?' In: *ISRN Physical Chemistry* 2013.

Soper, A. K. and Barney, E. R. (2011). 'Extracting the pair distribution function from white-beam X-ray total scattering data'. In: *Journal of Applied Crystallography* 44.4, pp. 714–726. DOI: 10.1107/s0021889811021455.

Soules, T. F. (1990). 'Computer simulation of glass structures'. In: *Journal of Non-Crystalline Solids* 123.1-3, pp. 48–70.

Taramasso, M.; Perego, G; Notari, B et al. (1983). *Preparation of porous crystalline synthetic material comprised of silicon and titanium oxides: US, 4410501*.

Tarascon, J.-M. and Armand, M. (2001). 'Issues and challenges facing rechargeable lithium batteries'. In: *Nature* 414.6861, pp. 359–367. DOI: 10.1038/35104644.

Temleitner, L and Pusztai, L (2013). 'The origin of diffuse scattering in crystalline carbon tetraiodide'. In: *Journal of Physics: Condensed Matter* 25.45, p. 454209. DOI: 10.1088/0953-8984/25/45/454209.

Thorpe, M. (1998). 'Advances in Pair Distribution Profile Fitting in Alloys in Local Structure from Diffraction'. In: ed. by M. Thorpe; J. Chung; S. Billinge and F Mohiuddin-Jacobs. Springer Science & Business Media. Chap. 9, pp. 157–174.

Thorpe, M.; Levashov, V.; Lei, M and Billinge, S. J. (2002). 'Notes on the analysis of data for pair distribution functions'. In: *From Semiconductors to Proteins: Beyond the Average Structure (eds Billinge, SJL & Thorpe, MF)(Kluwer|Plenum, New York, 2002)*, pp. 105–128.

Toby, B. and Egami, T (1992). 'Accuracy of pair distribution function analysis applied to crystalline and non-crystalline materials'. In: *Acta Crystallographica Section A: Foundations of Crystallography* 48.3, pp. 336–346. DOI: 10.1107/s0108767391011327.

Toby, B. H. and Billinge, S. J. L. (2004). 'Determination of standard uncertainties in fits to pair distribution functions'. In: *Acta Crystallographica Section A Foundations of Crystallography* 60.4, pp. 315–317. DOI: 10.1107/s0108767304011754.

Toby, B. H. and Von Dreele, R. B. (2013). 'GSAS-II: the genesis of a modern open-source all purpose crystallography software package'. In: *Journal of Applied Crystallography* 46.2, pp. 544–549.

Tong, L.; Rossmann, M. G. and Arnold, E. (2010). 'Patterson and molecular replacement techniques, and the use of noncrystallographic symmetry in phasing'. In: *International Tables for Crystallography*. International Union of Crystallography, pp. 244–281. DOI: 10.1107/97809553602060000765.

Treacy, M. and Borisenko, K. (2012). 'The local structure of amorphous silicon'. In: *Science* 335.6071, pp. 950–953.

Treacy, M.; Newsam, J. and Deem, M. (1991). 'A general recursion method for calculating diffracted intensities from crystals containing planar faults'. In: *Proc. R. Soc. Lond. A* 433.1889, pp. 499–520.

Trueblood, K.; Bürgi, H.-B.; Burzlaff, H; Dunitz, J.; Gramaccioli, C.; Schulz, H.; Shmueli, U and Abrahams, S. (1996). 'Atomic dispacement parameter nomenclature. Report of a subcommittee on atomic displacement parameter nomenclature'. In: *Acta Crystallographica Section A: Foundations of Crystallography* 52.5, pp. 770–781.

Tu, Y.; Tersoff, J; Grinstein, G and Vanderbilt, D. (1998). 'Properties of a continuous-random-network model for amorphous systems'. In: *Physical Review Letters* 81.22, p. 4899.

Tucker, M. G.; Keen, D. A.; Dove, M. T.; Goodwin, A. L. and Hui, Q. (2007). 'RMCProfile: reverse Monte Carlo for polycrystalline materials'. In: *Journal of Physics: Condensed Matter* 19.33, p. 335218. DOI: 10.1088/0953-8984/19/33/335218.

Van Houteghem, M.; Ghysels, A.; Verstraelen, T.; Poelmans, W.; Waroquier, M. and Van Speybroeck, V. (2014). 'Critical analysis of the accuracy of models predicting or extracting liquid structure information'. In: *The Journal of Physical Chemistry B* 118.9, pp. 2451–2470.

Van Hove, L. (1958). 'A remark on the time-dependent pair distribution'. In: *Physica* 24.1-5, pp. 404–408.

Waller, I and Hartree, D. (1929). 'On the intensity of total scattering of X-rays'. In: *Proc. R. Soc. Lond. A*. Vol. 124. 793. The Royal Society, pp. 119–142.

Warren, B. E. (1990). *X-Ray Diffraction (Dover Books on Physics)*. Dover Publications.

Warren, B.; Krutter, H and Morningstar, O (1936). 'FOURIER ANALYSIS OF X-RAY PATTERNS OF VITREOUS SiO2 AND B2O2'. In: *Journal of the American Ceramic Society* 19.1-12, pp. 202–206.

Welberry, T. R. (2010). *Diffuse x-ray scattering and models of disorder*. Vol. 16. Oxford University Press on Demand. 266 pp.

Welberry, T. and Butler, B. (1994). 'Interpretation of diffuse X-ray scattering via models of disorder'. In: *Journal of applied crystallography* 27.3, pp. 205–231. DOI: 10.1107/s0021889893011392.

Westphal, T. (2007). 'Quantitative Rietveld-Analyse von amorphen Materialien: am Beispiel von Hochofenschlacken und Flugaschen'. In: *Diss. Naturwissenschaftlichen Fakultät III der Martin-Luther-Universität Halle-Wittenberg*.

Willis, B. (1969). 'Lattice vibrations and the accurate determination of structure factors for the elastic scattering of X-rays and neutrons'. In: *Acta Crystallographica Section A: Crystal Physics, Diffraction, Theoretical and General Crystallography* 25.2, pp. 277–300.

Wooten, F and Weaire, D (1984). 'Generation of random network models with periodic boundary conditions'. In: *Journal of non-crystalline solids* 64.3, pp. 325–334.

— (1987a). 'Modeling tetrahedrally bonded random networks by computer'. In: *Solid State Physics*. Vol. 40. Elsevier, pp. 1–42.

— (1987b). 'Recent developments with the sillium model'. In: *Journal of Non-Crystalline Solids* 97, pp. 349–351.

Wooten, F; Winer, K and Weaire, D (1985). 'Computer generation of structural models of amorphous Si and Ge'. In: *Physical review letters* 54.13, p. 1392.

Wright, A.; Shakhmatkin, B. and Vedishcheva, N. (2001). 'The chemical structure of oxide glasses: A concept consistent with neutron scattering studies?' In: *Glass physics and chemistry* 27.2, pp. 97–113.

Wright, A. C. (1988). 'Neutron and X-ray amorphography'. In: *Journal of Non-Crystalline Solids* 106.1, pp. 1–16.

— (1990). 'Diffraction studies of glass structure'. In: *Journal of Non-Crystalline Solids* 123.1-3, pp. 129–148.

— (1993). 'The comparison of molecular dynamics simulations with diffraction experiments'. In: *Journal of non-crystalline solids* 159.3, pp. 264–268.

— (1994). 'Neutron scattering from vitreous silica. V. The structure of vitreous silica: What have we learned from 60 years of diffraction studies?' In: *Journal of non-crystalline solids* 179, pp. 84–115.

— (2000a). 'Defect-free vitreous networks: The idealised structure of SiO2 and related glasses'. In: *Defects in SiO2 and Related Dielectrics: Science and Technology*. Springer, pp. 1–35.

— (2000b). 'Glass Structure by Scattering Methods and Spectroscopy—A. X-RAY AND NEUTRON DIFFRACTION'. In: *Insulating and Semiconducting Glasses*. World Scientific, pp. 147–190.

Wright, A. C.; Clare, A. G.; Bachra, B.; Sinclair, R. N.; Hannon, A. C. and Vessal, B. (1991). 'Neutron diffraction studies of silicate glasses'. In: *Trans. Am. Crystallogr. Assoc* 27, pp. 239–254.

Xu, R. and Chiang, T. C. (2005). 'Determination of phonon dispersion relations by X-ray thermal diffuse scattering'. In: *Zeitschrift für Kristallographie-Crystalline Materials* 220.12, pp. 1009–1016.

Yang, G.; Lan, X.; Zhuang, J.; Ma, D.; Zhou, L.; Liu, X.; Han, X. and Bao, X. (2008). 'Acidity and defect sites in titanium silicalite catalyst'. In: *Applied Catalysis A: General* 337.1, pp. 58–65. DOI: 10.1016/j.apcata.2007.11.037.

Yang, X.; Juhás, P. and Billinge, S. J. L. (2014). 'On the estimation of statistical uncertainties on powder diffraction and small-angle scattering data from two-dimensional X-ray detectors'. In: *Journal of Applied Crystallography* 47.4, pp. 1273–1283. DOI: 10.1107/s1600576714010516.

Yang, Z. Q.; He, L. L.; Zhao, S. J. and Ye, H. Q. (2002). 'Experimental evidence of structural transition at the crystal-amorphous interphase boundary between Al and Al2O3'. In: *Journal of Physics: Condensed Matter* 14.8, pp. 1887–1893. DOI: 10.1088/0953-8984/14/8/316.

Young, C. A. and Goodwin, A. L. (2011). 'Applications of pair distribution function methods to contemporary problems in materials chemistry'. In: *Journal of Materials Chemistry* 21.18, p. 6464. DOI: 10.1039/c0jm04415f.

Zachariasen, W. (1935). 'Note on the Scattering of X-Rays from Fluids Containing Polyatomic Molecules'. In: *Physical Review* 47.4, p. 277.

Zachariasen, W. H. (1932). 'The atomic arrangement in glass'. In: *Journal of the American Chemical Society* 54.10, pp. 3841–3851.

Zallen, R. (1985). 'Models of amorphous solids'. In: *Journal of Non-Crystalline Solids* 75.1-3, pp. 3–14.

Zernike, F. t. and Prins, J. (1927). 'Die beugung von röntgenstrahlen in flüssigkeiten als effekt der molekülanordnung'. In: *Zeitschrift für Physik A Hadrons and nuclei* 41.6, pp. 184–194.

Zobel, M.; Neder, R. B. and Kimber, S. A. (2015). 'Universal solvent restructuring induced by colloidal nanoparticles'. In: *Science* 347.6219, pp. 292–294.

Zuev, A. (2006). 'Calculation of the instrumental function in X-ray powder diffraction'. In: *Journal of applied crystallography* 39.3, pp. 304–314. DOI: 10.1107/s0021889806005693.